
# Studies of the Torrefaction of Sugarcane Bagasse and Poplar Wood

**David Alejandro Granados Morales**

**Universidad Nacional de Colombia**

**Facultad de Minas, Departamento de Procesos y Energía**

**Medellín, Colombia**

**2017**

# Study of the Torrefaction of Sugarcane Bagasse and Poplar Wood

**David Alejandro Granados Morales**

Thesis submitted in partial fulfillments of requirements for the degree of
**Doctor in Enginerring – Energetic Systems**

Advisor:
Ph.D. Farid Chejne Janna

Line of Research:
Energetic Systems
Research Group:
Termodinámica Aplicada y Energías Alternativas *TAYEA*

**Universidad Nacional de Colombia**
**Facultad de Minas, Departamento de Procesos y Energía**
**Medellín, Colombia**
**2017**

# *Dedication*

*To my wife Catalina for her great love and valuable company in this important stage of my life. To my parents for their sacrifice and unconditional support. To my brother, that great voice of encouragement that always walk beside me.*

# Content

# Acknowledgments

I want to tank specially to Professor Farid Chejne, my thesis advisor, for his support, dedication, patience and for giving me the great honor of working with him and his TAYEA group for these last 8 years. To Professor Prabir Basu, for bring me the wonderfull opportunity to work whit him in Halifax, in his laboratory. To my friends Daya Nhuchhen, Anant Patel, Anand Arjunwadkar, Akash Kulshreshtha and Bharat Verma for thier support during my work in Halifax.

I am particularly grateful with my good friends Victor Borda, Alejandro Jaramillo, Esteban Largo, and Ivan Moncayo for their support and important discussions that enriched my work. To engineers and friends David Román, Leidy Vega, and Ricardo Ruiz that participated in a special way in my work whit their important and professional contributions in research and laboratory activities.

To my other friends and TAYEA group members that without their valuable support it would not be possible the culmination of this work: Carlos Gomez, Jorge Montoya, Carlos Valdés, Carlos Maya, Javier Ordoñez, Robert Macias, Diego Camargo, Adriana Blanco, Jessi Osorio, Gloria Marrugo, Daniela Vasquez, and Raiza Manrique.

I also thank COLCIENCIAS for their valuable assistance with the financial support for my doctoral studies and my international stay in Canada.

# Study of the Torrefaction of Sugarcane Bagasse and Poplar Wood

## Summary

By David Alejandro Granados Morales
Advisor: Farid Chejne Jana
Universidad Nacional de Colombia-Sede Medellin
2017

In this thesis, the main physical and chemical characteristics of sugarcane bagasse and poplar wood submitted to a thermo-chemical torrefaction process were studied. The materials were dried at a temperature of 105°C for 12 hours, to a moisture content of about 5%. The sugarcane bagasse was torrefied in TGA and in a custom designed thermogravimetric reactor for the evaluation of big particles in the temperature ranges of 200-300°C. With TGA tests, kinetic parameters representative of the material decomposition were obtained, and with large particles tests, the degradation was compared when the amount and particle size of material increases. The products of all torrefied tests were characterized and compared.

Poplar wood was torrefied in a custom thermogravimetric reactor in order to determine its kinetic parameters and in a two-stage rotary reactor by varying the operating parameters. These experimental tests with poplar were carried out in the circulating fluidized bed laboratory of Dalhousie University, Halifax, Canada. In the rotary reacctor, the biomass is dried in the first stage, and then torrefied in the second. Torrefaction process is carried out under volatiles atmosphere generated during the process, without inlet of inert gases. Fine particles, between 0.5 and 1 mm in diameter were used in this study, and characterized before and after torrefaction. A characterization of the biomass being torrefied was performed using two novel scooper devices for sample capture from inside reactor, specially designed for this research. These two devices allow to capture biomass samples being torrefied and measuring their temperatures in different axial positions of the reactor.

Two phenomenological models were constructed: a two-dimensional model for torrefaction of a biomass particle and a two-stage rotary reactor model. Both were duly validated and great information was obtained from them. A kinetic scheme involving secondary reactions to the interior of the biomass particle was used and validated with experimental information. Four phases were considered in the model: Biomass, water, char and gases, and for each of them it was possible to obtain distributions of their volumetric fractions at any time in the process. In addition, temperature distributions, velocities of volatiles generated and pressures can be obtained.

A vertical reactor was designed and built in order to evaluate the behavior of large particles in torrefaction process. With this reactor, it is possible to follow the mass and temperature of the

particle during the process. In addition, it is possible to capture volatiles and separate them into condensables and non-condensables throught a condensation unit which operates at -15°C and capture the condensable portion of the volatiles stream. With this reactor, it is possible to perform a complete characterization of all torrefation products such as liquid, gas and solid. This reactor was designed and built by the TAYEA group, specifically for the realization of this research work.

# List of Tables

# List of Figures

# General Introduction

Biomass is a promising source of solid fuel that compete with fossil fuels because of their low greenhouse gas emissions and their acceptable performance in thermal processes. Despite the benefits of biomass in thermal processes, its implementation has important limitations for projects involving high biomass flows. The high humidity and low biomass density make the feasibility of some projects drastically reduced as project size increases. The high cost associated with transport of biomass, makes the benefits obtained from it diminish. For this reason, only small and perhaps medium-scale projects become viable option for obtaining economic benefits from the thermal transformation of biomass.

Torrefaction process is defined as a thermal pre-treatment carried out in the temperature range of 200-300°C, with low heating rates (<50°C), with low residence times and in inert environments or low oxygen concentrations [1,2]. Torrefaction appears as a promising solution to the difficulties mentioned that are associated with the use of biomass as an energy agent. During torrefaction process the biomass undergoes a mass loss of around 40% and a energy loss between 10-15%, generating biomass with highest specific energy, fragile (requiring low energy consumption for crushing), low amounts of moisture absorbed after process (can be around 3%), homogeneous in quality and resistant to their decomposition by environment exposure [1,3,4].

A biomass consists mainly of hemicellulose, cellulose and lignin, which, during thermal processing, degrade differently and in turn generate volatiles and char. The hemicellulose is the most thermally unstable component and decomposes in the temperature range of 150-350°C, the cellulose decomposes in the temperature range of 275-350°C and the lignin decomposes in the temperature range of 180 -500°C [2,5]. Much of the hemicellulose and amorphous cellulose decompose during the torrefaction process, whereas the crystalline cellulose and lignin undergo less decomposition [5].

During the torrefaction process, the H/C and O/C ratios (Van-Krevelen diagram in Figure 1) decrease due to the decomposition of their three main components. This decrease is due to released volatiles from the system, mainly $CO_2$, CO and in smaller amounts $H_2$, $CH_4$, acetic acid, formic, converting the solid into a fuel with higher specific energy [6–8]. Figure 1 shows the effect of torrefaction process on a biomass where, as the H/C and O/C ratio decreases, the torrefied solid moves down in the diagram becoming in a solid fuel with high carbon and making it like low rank coals. This improved solid has been test in subsequent process such as combustion [9–15], gasification [9,16–19], palletization [4,20–24], grindability [25–28], pyrolysis [29–33], and fluidization [34,35] with excellent results.

Many researchs in torrefaction have been carried out in the experimental field, where different kind of biomass are torrefied with different operating conditions [9,16,19,29,31,36–38]. In these tests, the operating conditions are proposed intuitively in order to find those capable to generate a good solid with improved properties. As a result of the review of the state of the art, numerous variables have been evaluated in torrefaction processes, including temperature, particle size, heating rate, residence time, pressure, atmosphere, and others with less impact on the final product.

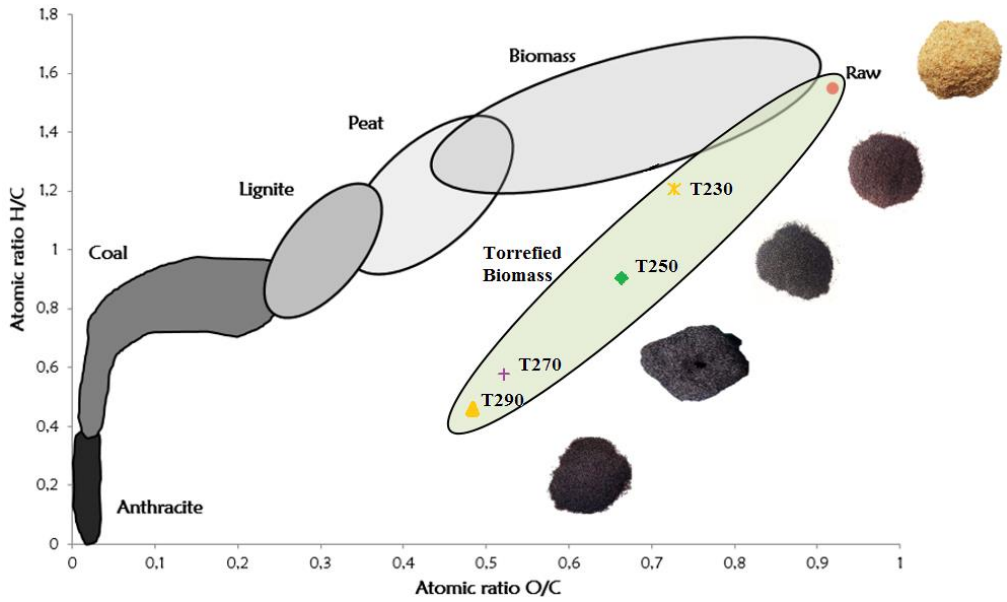


Figure 1. Van Krevelen diagram for solid fuels.

In the modelling field limited information is available [39–44]. Some models found in the literature, despite considering the influence of parameters such as heating rate, process temperature, residence times, have good adjustments with experimental data. These models consider global kinetics without secondary char formation from the generated condensable volatiles during devolatilization or from some liquid phases formed inside the solid.

In accordance with all above, it is possible contribuite in the technical knowledge about torrefaction process and predictive models, and is precisely where this thesis has a great impact. The develop of two predictive models for particle and reactor, and their respective validations generate two valuable tools for future developments in the subject. In addition, obtaining biomass kinetics, achieved under stricts prior experimental evaluations to guarantee kinetic control, and subsequent experimental tests under strict experimental designs for particle size evaluation, make this thesis a great contribution in the field of biomass torrefaction.

The main objective of this research was to advance the scientific knowledge in the biomass torrefaction area. For this, experiments were carry out in different and novel reactors, and developing phenomenological models that help to corroborate and obtain novel and useful information of the process, advancing in the knowledge of the phenomena ocurring. These phenomena were studied by means of two-stage rotary reactor, and a thermogravimetric vertical reactor specially designed for this study, in which torrefaction products (liquid, solid and gas) can be obtained to be characterized. Some objectives drawn in this research work are the following:

- To investigate the behavior of sugarcane bagasse and poplar wood in a torrefaction process.

- To propose methodologies for the appropriate selection of a biomass to be transformed into a torrefaction process.
- To investigate the distribution of the products generated in a torrefaction process and obtain kinetics of the main products in TGA ensuring the kinetic control of the material.
- To couple the main physical and chemical phenomena occurring during biomass torrefaction throught phenomenological models capable of predict the biomass behavior during torrefaction.
- To propose new methodologies for the evaluation and characterization of torrefied biomass in rotary reactors by designing new devices that allow their capture and measurement in situ.

For clarity about the sequence of this thesis, a list with a clear description of chapters with the main topic to study and experimental tools used, is shows bellow.

**First section (Chapter 1):** State of the art with a parametric study on main factors and operational parameters affecting the torrefaction products. Other topics such as reactors technology for torrefaction, kinetics of main biomass compounds and developed models were studied as well.

**Second sections (Chapter 2):** Methodology based on mass, energy and exergy balance for selection of biomass for a torrefaction process. In this chapter, five different Colombian biomasses were evaluated and sugarcane bagasse and sawdust were selected for this thesis.

**Third section (Chapter 3 - 4):** Torrefaction of sugarcane bagasse and poplar wood in TGA and QWM reactors for obtain kinetics and to characterize solid products of torrefaction with small particles sizes. In chapter 3, a complete characterization for char was done throght proximate, ultimate analysis, HHV, SEM, polymeric analysis, FTIR, and reactivity tests. In chapter 4, kinetic models were studied for sugarcane bagasse, poplar wood and the m ain compounds of biomass cellulose, hemicellulose and lignin. A study for superposition theory in the biomass from main compounds was developed.

**Fourth section (Chapter 5):** Experimental tests with poplar wood in a two-step rotary reactor performed in the circulating fluidized bed laboratory of Dalhousie University, Halifax, Canada. In this chapter correlations for properties of biomass were found, and a novel methodology for biomass sampling inside the reactor wich allows the measuring of properties of biomass being torrefied was developed.

**Fifith section (Chapter 6):** Experimetnal tests with sugarcane bagasse in a custom thermogravimetric unit were performed. In this chapter, biomass torrefaction was studied with a custom designed thermogravimetric reactor capable to measure mass, temperature and allows the capture and separation pf condensables and non-condensables volatiles during the process. Characterizations of each product in the process were developed.

**Sixth section (Chapter 7-8):** Evaluation of torrefaction process with two phenomenological models. Chapter 7 shows the develop and validation of the one-dimensional rotary reactor model with experimental tests with poplar wood. Chapter 8 shows the develop and validation of two-

dimenisonal particle model in a torrefaction process with poplar wood tests performed in the circulating fluidized bed laboratory of Dalhousie University, Halifax, Canada.

Some contributions of this work are listed below:

1. Develop of a new thermogravimetric reactor for the study of the products generated during biomass torrefaction.

2. Develop of methodology for selection of biomass in a torrefaction process through mass, energy and exergy balances.

3. Obtaining of torrefied biomass in a novel two-step rotary reactor under volatiles atmosphere without addition of inert gas, and obtaining correlations to determine the transformation and properties of biomass in rotary kiln.

4. Develop of a predictive model of a novel two-step rotary reactor with internal flights which includes kinetics of biomass, experimental correlations for energy transfer and residence times especially developed for this reactor.

5. Develop of a 2D phenomenological particle model that couples the chemical and physical behavior of the biomass in a torrefaction process. It includes kinetics of two stages considering secondary reactions to the interior of the particle

**Scientific publications, software and patents**

**Papers published**

- **D. A. Granados**, H. I. Velásquez, and F. Chejne, "Energetic and exergetic evaluation of residual biomass in a torrefaction process". Energy, vol. 74, pp. 181–189, Jun. 2014.

- **D. A. Granados**, F. Chejne, and P. Basu, "A two dimensional model for torrefaction of large biomass particles". *J. Anal. Appl. Pyrolysis*, 2016..

- **D. A. Granados**, P. Basu, F. Chejne, and D. R. Nhuchhen, "Detailed Investigation into Torrefaction of Wood in a Two-Stage Inclined Rotary Torrefier". *Energy & Fuels*, p. acs.energyfuels.6b02524, 2016.

- **D. A. Granados**, P. Basu, and F. Chejne, "Biomass Torrefaction in a Two-Stage Rotary Reactor: Modeling and Experimental Validation". *Energy & Fuels*, p. acs.energyfuels.7b00653, 2017.

**Papers Submitted**

- **D.A. Granados**, R.A. Ruiz, L.Y. Vega, F. Chejne. "Study of Reactivity Reduction in Sugarcane Bagasse as consequence of a Torrefaction Process". Submitted to Energy Journal 2017.

**Papers in preparation**

- **D.A. Granados**, D. Nhuchhen, P. Basu and F. Chejne. "Devolatilization Kinetics of Biomass, Cellulose, Xylan, and Lignin in Torrefaction Temperature Range: Validation of Superposition Theory". To be submitted to JAAP 2017.

- **D.A. Granados**, F. Chejne and P. Basu. "Torrefaction of Large Biomass Particles in a Custom Designed Thermo-gravimetric Unit: Modeling and Experimental Validation". To be submitted to JAAP 2017.

- **D. A. Granados**, L.Y Vega, R. A. Ruiz, and F. Chejne. "Kinetic Study of Sugarcane Bagasse in a Torrefaction Process". To be submitted to JAAP 2017.

**Software registration**

- **D. A. Granados**, J.M Mejía, F. Chjene. "Rotary Kiln Simulator". Ministry of Interior. National Direction of Copyright. Special Administrative Unit. Registration 13-50-212 of November 12, 2015.

**Software registration in preparation**

- **D. A. Granados**, F. Chjene. "2D Simulator of the torrefaction process of a large biomass particle".
- **D. A. Granados**, P. Basu, F. Chjene. "Two-step rotary kiln simulator".

**Patents in process**

- **D. A. Granados,** V.H. Borda, F. Chjene. "Vertical thermogravimetric reactor with volatiles capture (VTR)"

**Scientific events**

- **D. A. Granados**, H. I. Velásquez, and F. Chejne. "Energetic evaluation of residual biomass in a torrefaction process," Proceedings of the 26th International Conference on Efficiency, Cost, Optimization, Simulation and Environmental Impact of Energy Systems, ECOS 2013, 2013

- **D. A. Granados**, R. J. Macías, and F. Chjene. "Evaluación Energética y Exergética de biomasas residuales en un proceso de torrefacción," XXVII Congr. Interam. y Colomb. Ing. Química, pp. 809–816, 2014.

**References**

[1] Pentananunt R, Rahman ANMM, Bhattacharya SC. Upgrading of biomass by means of torrefaction. Energy 1990;15:1175–9. doi:10.1016/0360-5442(90)90109-F.

[2] Basu P. Biomass Gasification, Pyrolysis and Torrefaction. Elsevier; 2013. doi:10.1016/B978-0-12-396488-5.00004-6.

[3] Medic D, Darr M, Shah a., Potter B, Zimmerman J. Effects of torrefaction process parameters on biomass feedstock upgrading. Fuel 2012;91:147–54. doi:10.1016/j.fuel.2011.07.019.

[4] Wattananoi W, Khumsak O, Worasuwannarak N. Upgrading of biomass by torrefaction and densification process. 2011 IEEE Conf Clean Energy Technol 2011:209–12. doi:10.1109/CET.2011.6041465.

[5] Shafizadeh F. Pyrolytic Reactions and Products of Biomass. Fundam. Thermochem. Bimoass Convers., 1985, p. 183–217.

[6] Prins MJ, Ptasinski KJ, Janssen FJJ. Torrefaction of wood. Part 2. Analysis of products. J Anal Appl Pyrolysis 2006;77:35–40. doi:10.1016/j.jaap.2006.01.001.

[7] Liaw SS, Zhou S, Wu H, Garcia-Perez M. Effect of pretreatment temperature on the yield and properties of bio-oils obtained from the auger pyrolysis of Douglas fir wood. Fuel 2013;103:672–82. doi:10.1016/j.fuel.2012.08.016.

[8] Wang Z, McDonald AG, Westerhof RJM, Kersten SR a, Cuba-Torres CM, Ha S, et al. Effect of cellulose crystallinity on the formation of a liquid intermediate and on product distribution during pyrolysis. J Anal Appl Pyrolysis 2013;100:56–66. doi:10.1016/j.jaap.2012.11.017.

[9] Fisher EM, Dupont C, Darvell LI, Commandré J-M, Saddawi a, Jones JM, et al. Combustion and gasification characteristics of chars from raw and torrefied biomass. Bioresour Technol 2012;119:157–65. doi:10.1016/j.biortech.2012.05.109.

[10] Bridgeman TG, Jones JM, Shield I, Williams PT. Torrefaction of reed canary grass, wheat straw and willow to enhance solid fuel qualities and combustion properties. Fuel 2008;87:844–56. doi:10.1016/j.fuel.2007.05.041.

[11] Jones JM, Bridgeman TG, Darvell LI, Gudka B, Saddawi a., Williams a. Combustion properties of torrefied willow compared with bituminous coals. Fuel Process Technol 2012;101:1–9. doi:10.1016/j.fuproc.2012.03.010.

[12] Fang MX, Shen DK, Li YX, Yu CJ, Luo ZY, Cen KF. Kinetic study on pyrolysis and combustion of wood under different oxygen concentrations by using TG-FTIR analysis. J Anal Appl Pyrolysis 2006;77:22–7. doi:10.1016/j.jaap.2005.12.010.

[13] Costa FF, Wang G, Costa M. Combustion kinetics and particle fragmentation of raw and torrified pine shells and olive stones in a drop tube furnace. Proc Combust Inst 2014;35:3591–9. doi:10.1016/j.proci.2014.06.024.

[14] Liu Z, Hu W, Jiang Z, Mi B, Fei B. Investigating combustion behaviors of bamboo, torrefied bamboo, coal and their respective blends by thermogravimetric analysis. Renew Energy 2016;87:346–52. doi:10.1016/j.renene.2015.10.039.

[15] Ramajo-Escalera B, Espina A, García JR, Sosa-Arnao JH, Nebra SA. Model-free kinetics applied to sugarcane bagasse combustion. Thermochim Acta 2006;448:111–6. doi:10.1016/j.tca.2006.07.001.

[16] Berrueco C, Recari J, Güell BM, Alamo G Del. Pressurized gasification of torrefied woody biomass in a lab scale fluidized bed. Energy 2014;70:68–78. doi:10.1016/j.energy.2014.03.087.

[17] Xue G, Kwapinska M, Kwapinski W, Czajka KM, Kennedy J, Leahy JJ. Impact of

torrefaction on properties of Miscanthus×giganteus relevant to gasification. Fuel 2014;121:189–97. doi:10.1016/j.fuel.2013.12.022.

[18] Couhert C, Salvador S, Commandré J-M. Impact of torrefaction on syngas production from wood. Fuel 2009;88:2286–90. doi:10.1016/j.fuel.2009.05.003.

[19] Deng J, Wang G, Kuang J, Zhang Y, Luo Y. Pretreatment of agricultural residues for co-gasification via torrefaction. J Anal Appl Pyrolysis 2009;86:331–7. doi:10.1016/j.jaap.2009.08.006.

[20] Ghiasi B, Kumar L, Furubayashi T, Lim CJ, Bi X, Soo C. Densified biocoal from woodchips : Is it better to do torrefaction before or after densification ? Appl Energy 2014;134:133–42. doi:10.1016/j.apenergy.2014.07.076.

[21] Agar D, Gil J, Sanchez D, Echeverria I, Wihersaari M. Torrefied versus conventional pellet production - A comparative study on energy and emission balance based on pilot-plant data and EU sustainability criteria. Appl Energy 2015;138:621–30. doi:10.1016/j.apenergy.2014.08.017.

[22] Wang C, Peng J, Li H, Bi XT, Legros R, Lim CJ, et al. Oxidative torrefaction of biomass residues and densification of torrefied sawdust to pellets. Bioresour Technol 2013;127:318–25. doi:10.1016/j.biortech.2012.09.092.

[23] Peng JH, Bi XT, Sokhansanj S, Lim CJ. Torrefaction and densification of different species of softwood residues. Fuel 2013;111:411–21. doi:10.1016/j.fuel.2013.04.048.

[24] Bergman P. Combined torrefaction and pelletisation. The TOP process. 2005.

[25] Repellin V, Govin A, Rolland M, Guyonnet R. Energy requirement for fine grinding of torrefied wood. Biomass and Bioenergy 2010;34:923–30. doi:10.1016/j.biombioe.2010.01.039.

[26] Phanphanich M, Mani S. Impact of torrefaction on the grindability and fuel characteristics of forest biomass. Bioresour Technol 2011;102:1246–53. doi:10.1016/j.biortech.2010.08.028.

[27] Bridgeman TG, Jones JM, Williams a., Waldron DJ. An investigation of the grindability of two torrefied energy crops. Fuel 2010;89:3911–8. doi:10.1016/j.fuel.2010.06.043.

[28] Arias B, Pevida C, Fermoso J, Plaza MG, Rubiera F, Pis JJ. Influence of torrefaction on the grindability and reactivity of woody biomass. Fuel Process Technol 2008;89:169–75. doi:10.1016/j.fuproc.2007.09.002.

[29] Hassan E, Steele P, Ingram L. Characterization of fast pyrolysis bio-oils produced from pretreated pine wood. Appl Biochem Biotechnol 2009;154:182–92. doi:10.1007/s12010-008-8445-3.

[30] Meng J, Park J, Tilotta D, Park S. The effect of torrefaction on the chemistry of fast-pyrolysis bio-oil. Bioresour Technol 2012;111:439–46. doi:10.1016/j.biortech.2012.01.159.

[31] Zheng A, Zhao Z, Chang S, Huang Z, Wang X, He F, et al. Effect of torrefaction on structure and fast pyrolysis behavior of corncobs. Bioresour Technol 2013;128:370–7. doi:10.1016/j.biortech.2012.10.067.

[32] Zheng A, Zhao Z, Chang S, Huang Z, He F, Li H. Effect of Torrefaction Temperature on

Product Distribution from Two-Staged Pyrolysis of Biomass. Energy & Fuels 2012;26:2968–74.

[33] Wannapeera J, Fungtammasan B, Worasuwannarak N. Effects of temperature and holding time during torrefaction on the pyrolysis behaviors of woody biomass. J Anal Appl Pyrolysis 2011;92:99–105. doi:10.1016/j.jaap.2011.04.010.

[34] Bergman P, Boersma A, Kiel J, Prins MJ, Ptasinski K, Janssen FJ. Torrefaction for entrained-flow gasification of biomass. 2nd World Conf. Technol. Exhib. Biomass Energy, Ind. Clim. Prot., Rome: 2005, p. 78–82.

[35] Li H, Liu X, Legros R, Bi XT, Lim CJ, Sokhansanj S. Torrefaction of sawdust in a fluidized bed reactor. Bioresour Technol 2012;103:453–8. doi:10.1016/j.biortech.2011.10.009.

[36] Li J, Brzdekiewicz A, Yang W, Blasiak W. Co-firing based on biomass torrefaction in a pulverized coal boiler with aim of 100% fuel switching. Appl Energy 2012;99:344–54. doi:10.1016/j.apenergy.2012.05.046.

[37] Broström M, Nordin A, Pommer L, Branca C, Di Blasi C. Influence of torrefaction on the devolatilization and oxidation kinetics of wood. J Anal Appl Pyrolysis 2012;96:100–9. doi:10.1016/j.jaap.2012.03.011.

[38] Granados DA, Velásquez HI, Chejne F. Energetic and exergetic evaluation of residual biomass in a torrefaction process. Energy 2014;74:181–9. doi:10.1016/j.energy.2014.05.046.

[39] Ratte J, Marias F, Vaxelaire J, Bernada P. Mathematical modelling of slow pyrolysis of a particle of treated wood waste. J Hazard Mater 2009;170:1023–40. doi:10.1016/j.jhazmat.2009.05.077.

[40] Bates RB, Ghoniem AF. Biomass torrefaction: modeling of volatile and solid product evolution kinetics. Bioresour Technol 2012;124:460–9. doi:10.1016/j.biortech.2012.07.018.

[41] Basu P, Sadhukhan AK, Gupta P, Rao S, Dhungana A, Acharya B. An experimental and theoretical investigation on torrefaction of a large wet wood particle. Bioresour Technol 2014;159:215–22. doi:10.1016/j.biortech.2014.02.105.

[42] Felfli F, Luengo C, Soler P, Rocha J. Mathematical modelling of wood and briquettes torrefaction. Procedings 5th Encontro Energ. no Meio Rural, Campinas: 2004, p. 1–9.

[43] Perré P, Rémond R, Turner I. A comprehensive dual-scale wood torrefaction model: Application to the analysis of thermal run-away in industrial heat treatment processes. Int J Heat Mass Transf 2013;64:838–49. doi:10.1016/j.ijheatmasstransfer.2013.03.066.

[44] Ratte J, Fardet E, Mateos D, Héry J-S. Mathematical modelling of a continuous biomass torrefaction reactor: TORSPYD$^{TM}$ column. Biomass and Bioenergy 2011;35:3481–95. doi:10.1016/j.biombioe.2011.04.045.

# Chapter 1. State of the Art

This revision of state of the art was divided in sections considered as fundamentals for this doctoral work. In the first section, an introduction to the biomass structure and torrefaction process is developed. In second section, call “process parameters” the different conditions which torrefaction processes is developed in literature such as temperature, pressure, heating rate, residence time, particle size, and atmosphere are described to identify those that represent greater incidence in the process. In third section, some uses for torrefied biomass such as combustion, gasification, pyrolysis, crushing, fluidization, and palletization were described. In fourth section, some works where the torrefaction process is evaluated by mass, energy and exergy balance are mentioned. In fifth section, the common reactors used for torrefaction process are described to determine the feasibility of our experimental tests are mentioned. In the sixth section, the different kinetic models proposed for biomass and its main components to predict the thermal decomposition of them in a torrefaction process are analyzed. In the last section, called "Models", the different models developed to explain physical and chemical phenomena during torrefaction process are mentioned.

## 1.1. Lignocellulosic structure

The biomass constituents include cellulose, hemicellulose, lignin, organic extractives and inorganic minerals called ashes. The first three constituents are predominant in biomass and their percentages depend on the biomass species, ranging from 42-45% for cellulose, 27-30% for hemicellulose, 28-45% for lignin, and 3-5% organic extractives for softwoods and hardwoods respectively. The ashes in these types of biomass are approximately less than 1% [1].

Table 1-1. Properties of cellulose, hemicellulose and lignin

| | Cellulose | Hemicellulose | Lignin |
|---|---|---|---|
| Structure | Linear | Branched | Three-dimensional |
| Formula | $(C_6H_{10}O_5)_m$ | $(C_5H_8O_4)_m$ | $[C_9H_{10}O_3{\cdot}(OCH_3)_{0.9\text{-}1.7}]_m$ |
| Atomic O/C | 0.83 | 0.8 | 0.47-0.36 |
| Atomic H/C | 1.67 | 1.6 | 1.19-1.53 |
| Decomposition Temperature | 315-400 | 220-315 | 160-900 |
| Component | Glucose | Xylose, glucose, mannose, galactose, arabinose and glucoronic acid | Phenylpropane |
| Thermal behavior | Endothermic (exothermic if char is significant) | Exothermic | Exothermic |

Cellulose is a linear polysaccharide composed of glucopyranose units linked by glycosidic bonds [2]. It contains amorphous and crystalline structures, and can be expressed as $(C_6H_{10}O_5)_m$, where the subscript m is the degree of polymerization. Hemicellulose is a mixture of several branched polymerized polysaccharides such as xylose, glucose, mannose, galactose, arabinose and glucuronic acid [3]. Its base structure can be expressed as $(C_5H_8O_4)_m$. Lignin is a highly branched three-dimensional polyphenolic substance consisting of an irregular arrangement of hydroxy and

methoxy substituted phenylpropane units [4]. Its chemical formula is represented as $[C_9H_{10}O_3 \cdot (OCH_3)_{0.9\text{-}1.7}]_m$ [5].

Based on its chemical formulas, the atomic ratio O/C are 0.83, 0.80 and 0.47-0.36, and H/C are 1.67, 1.6, and 1.19-1.53 for cellulose, hemicellulose and lignin respectively. Due to the different structures, their thermal decompositions are very different. Hemicellulose decomposes in the range of 220-315°C, cellulose between 315-400°C, and lignin decomposes in a wider range of 160-900°C [6], but at low temperatures its decomposition is very slow. Some properties of each structure can be seen in Table 1-1.

## 1.2. Torrefaction process

Torrefaction has been defined as a thermal pretreatment where the biomass is heated in an inert atmosphere to temperatures of 200-300°C for improving biomass as a solid fuel [7]. To generate the inert atmosphere, nitrogen has usually been used. Torrefaction process has been known as a mild pyrolysis process, as it is performed under conditions similar to those of pyrolysis, but at lower temperatures. Raw biomass is characterized by its high moisture content, low HHV, high volume and low energy density. After the torrefaction process, the biomass properties are considerably improved [8,9],and some of these improvements include high HHV, lower O/C and H/C, lower moisture absorption, better grindability and reactivity, and uniform properties, as is shown in Figure 1-1.

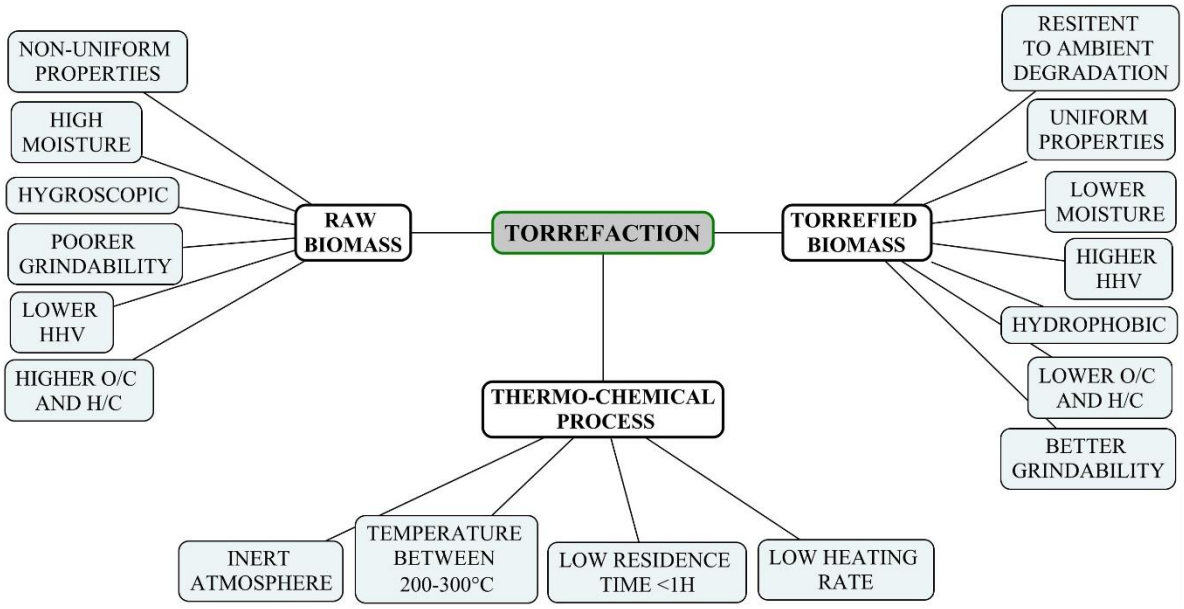


Figure 1-1. Property variation of biomass undergoing torrefaction.

The torrefaction process is classified into three different intensities according to the temperature at which it is carried out. Between 200 and 235°C the torrefaction is classified as slight, between 235-275°C as mild, and between 275-300°C as severe [4]. A summary of the different torrefaction conditions can be seen in Table 1-2.

Table 1-2. Torrefaction classification

| | Classification | | |
|---|---|---|---|
| | Light | Mild | Severe |
| Temperature (°C) | 200-235 | 235-275 | 275-300 |
| Consumption | | | |
| Hemicellulose | Mild | Mild to severe | Severe |
| Cellulose | Slight | Slight to mild | Mild to severe |
| Lignin | Slight | Slight | slight |
| Liquid color | Brown | Brown dark | Black |

In slight torrefaction, only hemicellulose is affected, while lignin and cellulose are poorly affected or unaffected. In this process, the biomass properties do not improve significantly. In the mild torrefaction, the hemicellulose decomposition is intensified and the volatile release is intensified. The cellulose is also decomposed in some part, and the properties of the final biomass begin to improve in comparison with initial properties. In severe torrefaction the hemicellulose is completely decomposed while the cellulose is mostly degraded. Lignin is difficult to thermally degrade so it hardly decomposes a small proportion, achieving a final material with high lignin content which improves its properties as a solid fuel. As product of the torrefaction process and polymers decomposition, $H_2$, CO, $CO_2$, $CH_4$, toluene, benzene and $C_xH_y$ can be obtained in non-condensable volatiles, $H_2O$, acetic acids, alcohols, aldehydes and ketones in the condensable volatiles, and char and ash in the solid.

## 1.3. Process parameters

Many investigations in torrefaction field have been carried out in the experimental field, where different types of biomass were torrefied under different operating conditions. In these experiments, operating conditions are evaluated in order to find those optimum conditions which generate the best final properties of the solids after process.

It was observed from this review of literature that numerous variables have been evaluated in torrefaction processes, including temperature, particle size, heating rate, residence time, pressure, and process atmosphere. The objective of this section is to identify those variables that present more incidence on the process in order to consider them in the model that will be developed in this doctoral thesis.

### *1.3.1. Atmosphere*

One of the parameters studied in torrefaction process is the atmosphere during the process [6,10–19]. Originally the process must be carried out in an inert atmosphere, but due to the high costs that this requires, recently has been studied other atmospheres with air or with low oxygen concentrations, carbon dioxide concentrations and mixtures of these species in order to be able to use or recycle flue gases generated in other processes.

Torrefaction in oxidative atmospheres have been evaluated in the literature [6,15,16], the performance of fibrous and ligneous biomasses were evaluated in torrefaction when air or high oxygen concentration was used as atmosphere. Authors found that the components in the biomass have different reactivities depend on the kind of biomass and therefore degrade differently. At low

temperatures (<240°C), the high oxygen concentration in atmosphere does not have a significant effect over the properties of the final solid. At higher temperatures (> 240 ° C) the effect over final product is evident since a partial combustion of volatiles may occur locally increasing the temperature and generating heterogeneous structures in the solid. An important conclusion from these works is that ligneous biomass, unlike fibrous biomass, can be torrefied in oxidative environments at low oxygen concentrations to reduce the operating cost.

Other authors [10–14,17,19] evaluated low oxygen and carbon dioxide levels, or flue gases in the working atmosphere focusing to using gas streams generated in combustion processes. When the oxygen concentration is low, no significant impact is observed on the properties of the solid in all torrefaction range. This suggest that the process can be performed with flue gases as working atmosphere to reduce the operating cost.

### *1.3.2. Particle size*

Particle size is another parameters evaluated during torrefaction tests [20–23]. This parameter has been varied in order to find ranges of dimensions in which the final product can be found homogeneous when other parameters such as temperature, or residence time also vary in the process. Particle size is linked to heating rate, the latter detected as a fundamental parameter in the decomposition process in torrefaction [24–26], because it directly influences the decomposition and char formation of the components of biomass (hemicellulose, cellulose and lignin).

Interesting results were found in the work developed by Bridgeman et al. [21], where same analysis for the same kind of biomass with different particle sizes were found diferents. It was found that the crushing process is not homogeneous in the components of the biomass and a separation of organic and inorganic matter in particles of different sizes was evidenced. Larger particle sizes have greater carbon content, greater volatile content, cellulose content and, ultimately, a larger calorific value, while smaller particles have grater ash content. In this work was found that the particles smaller than 90μm have lower mass loss than the larger ones during a thermal process, due to mentioned differences.

Peng et al. [23] evaluated the effect of particle size on the thermal phenomena involved in torrefaction process and pelletization from torrefied biomass. Densification tests showed that the energy consumption for making torrefied pellets increased with increasing the particle size and the degree of torrefaction, and the quality of torrefied pellets (hydro phobicity and hardness) could be improved with decreasing the particle size and increasing the severity of torrefaction. The thermal process inside the particle was analyzed throught characteristic dimensionless numbers for this type of process such as Biot, Pirólisis, Weitz-Protes, Knudsen, and it was found that the diffusivity of the volatiles generated during the biomass decomposition considerably affects the kinetics of the process for greater particles. This could be verified experimentally when tests were carried out in TGA and the larger particles presented smaller mass losses in contrast with results found by Bridgeman et al. [21] but in bigger particle size ranges.

Basú et al. [20] studied the effect of particle size in torrefaction with large particles (pellets) with dimensions up to 25 mm in diameter and 65 mm in length. In this study, interesting results were found when the internal temperatures of the pellets were measured during the process. Pellets with

larger diameter required longer preheating and heating times up to process temperature since they had to be heated at lower speeds than those with smaller diameters. In addition to this increase in processing time, their internal temperatures were increased to almost 20°C above oven temperature (also verified by Pierré et al. [27]), suggesting exothermic reactions within the biomass in the early states of the process. In addition, it was found that the mass yield and energy yield parameters decrease with the pellet diameter, but an opposite behavior presents the calorific value, which increases with the diameter of the pellet.

### *1.3.3. Temperature and residence time*

Residence time and process temperature are perhaps the most experimentally analyzed parameters in the literature. The common approach of found works is to evaluate the impact of these two parameters on the properties of final solid by analyzing the decomposition of torrefied biomass and products yield [26,28–36], behavior of solid in subsequent thermal processes such as gasification [37–41], pyrolysis [33,42–45], combustion [22,37,46–50], and in mechanical processes such as pelletizing [11,51–55], crushing [56–59] and fluidization [60,61].

Early in 80's Bourgois et al [62,63], analyzed separately the effect of residence time [62] and temperature [63] of torrefaction process in a biomass. The residence times of the biomass were varied between 15 min and 4 hours and temperature between 240-290°C. Results about impact of residence time and temperature over properties of final solid were similar, having more impact the temperature. The torrefied solid was analyzed by monitoring its weight during torrefaction and by elemental and proximate analysis and polymeric composition. In these analyzes it was found that when residence time increases, mass loss, oxygen, and hydrogen decrease, but carbon content and lignin increase. Similar results were found later by other authors when same parameters were varied with different biomasses [30,36,46,51,64–72].

Subsequent investigations of these parameters over biomass torrefaction have been focused to the formation and characterization of generated products. For the capture of the condensable products of the volatiles, common condensation methods were used then analyzed by HPLC (High-performance liquid chromatography), GC-MS, FTIR methods. Main detected species are $CO_2$, CO, $CH_4$, acetic acid, formic, methanol, water, and others [41,46,73]. Mass balances for products generated during torrefaction have been conducted [36,41,62]. A maximum liquid formation of up to 12% and gas formation of up to 6% with errors in the mass balances around 5% [36,74].

After this review, it is clear that the parameters that have the greatest influence on the final properties of torrefied solid are temperature and residence time. These two parameters are further evaluated and investigated in literature in order to find the best combinations that generate torrefied biomass suitable for incorporation into subsequent thermal or mechanical processes such as combustion, gasification, pyrolysis, and pelletizing.

### *1.3.4. Pressure*

Few studies have been found in literature evaluating the effect of pressure on torrefied biomass [75–77]. In general, in these investigations has been found that with higher pressures than atmospheric, the boiling points of species increase making it difficult to volatilize and favor some

reactions of secondary formation of solids. On the other hand, when torrefaction is carried out with vacuum, lower than atmospheric pressure, it is possible to favor the generation of volatiles.

## 1.4. Torrefied solid in subsequent process.

The solid obtained in torrefaction, have been studied in later thermal and mechanical processes such as combustion, pyrolysis, gasification, pelletization, crushing, and other. These studies have found promising results in the combination of torrefaction with subsequent thermal processes. In addition, studies on the densification or pelletizing of the torrefied solid have yielded good results for transport, storage, conservation and final disposal of these elements.

### *1.4.1. Combustion*

The most studied thermal processes for torrefied solids is combustion [22,37,46–50,78–85]. These evaluations of solids in combustion have been carried out with a view to their smokes generation, incandescence, comparisons of ignition and burnout temperatures, comparisons of reaction time with raw material and coals, and behavior with biomass and coal blends. In these works, it was found that the smoke generation and flame time are considerably reduced and the incandescence time increases with respect to the untreated wood. Kinetics were obtained for the combustion of torrefied biomass by means of TGA analysis, where it was found that the combustion reactivity for torrefied biomass decreases and raw biomass generates an additional shoulder of mass loss due to the decomposition of the hemicellulose.

Some authors [22,78] also evaluated torrefied biomasses in combustion process in order to analyze the generation of nitrogen compounds and others gaseous pollutants. It was verified in this work that the low temperature and short residence times favor nitrogen retention in the solid while high temperatures and long residence times favor nitrogen elimination in the volatiles. This elimination can occur by two routes: formation of $NH_3$ or volatile cyclic amides. The first route way leads simultaneously to char formation, whereas second route leads to the formation of HCN or HNCO by cracking reactions.

### *1.4.2. Gasification*

Gasification has been studied for torrefied biomass [86–93] in order to evaluate the syngas generation, reactivity, tar generation, and other important properties in the process.

Fisher et al. [37] evaluated the reactivity of torrefied biomass, and found to decrease with the severity of process. In addition, the handling of this material in equipments improves ostensibly due to the facility to crush it and obtain the desired particle sizes, and to fluidize the material due to the new more rounded forms of the particles. Deng, et al. [41] proposed a configuration in which the torrefaction is linked to a gasification process of torrefied biomass with coal (co-gasification). One of the advantages of biomass torrefaction is that it generates coal-like properties for grinding, fluidization, handling, and the above plant configuration contemplates the introduction of torrefied solid together with coal in a mill to be subsequently fed into the reactor. Generated volatiles during torrefaction (formed mainly of $CO_2$) enters the gasifier like gasifying agent, and the those generated in the gasification dry the material before torrefaction. Couhert et al. [40] evaluated the generation of gaseous species during gasification of torrefied biomass. It was found that torrefied biomass has

a similar generation of $CO_2$ than raw biomass but it exceeds it by 7% in the generation of hydrogen and in 20% in the CO.

### *1.4.3. Pyrolysis*

Torrefied biomasses have also been analyzed in pyrolysis processes [42–45]. In these works, fast pyrolysis was analyzed and interesting conclusions were found about the quality of the bio-oils obtained with torrefied biomasses. In torrefaction, the biomass is deoxygenated and lose acids (acetic, lactic), which indicate a low presence of oxygen and acids in the bio-oil. This result in a higher heating value and higher pHs. During torrefaction at high temperatures, the cross-linking and charring reactions are promoted in cellulose, which generates more final char and decreases the final amount of bio-oil obtained in fast pyrolysis. For this reason, authors recommend mild torrefaction process prior to fast pyrolysis in order to maximize the production of bio-oil.

### *1.4.4. Crushing and fluidization*

Crushing and fluidization processes have also been studied for torrefied biomasses in order to evaluate performance in subsequent processes such as combustion, gasification or pyrolysis. Different authors [29,57–61,85,94–96] have studied the performance of torrefied wood in a crushing and fluidization process. As results of these investigations it was found that torrefied biomass can reduce the energy consumptions for crushing between 50-85% of energy necessary for raw biomass. Depending of torrefaction severity, can generate smaller particles size with smaller amount of fibers. After torrefaction, the biomass loses its fibrous structure, causing it to disappear or reduce the needle shapes, this improves the pneumatic feed to reactor, which would be unthinkable for untreated biomass. These changes in torrefied biomass ostensibly improves the fluidization, achieving bubbling fluidizations for particles of 160-170μm and soft fluidizations with particles of approximately 100μm.

### *1.4.5. Pelletization*

Biomass palletization has also been studied with torrefied biomass [52,97–106]. Wang et al. [11] evaluated the wood torrefaction in fluidized bed with small amounts of oxygen in working atmosphere with variations of temperature and residence time. The pelletizing of the torrefied biomass was compared to that of untreated biomass in terms of the energy consumed to manufacture the pellet by two different processes: Compression and extrusion. An increase in energy consumption for palletization by compression and extrusion was found as the torrefaction was performed with higher temperature. Peng et al. [23] found results similar to those found by Wang in terms of energy consumption in the pelletizing process. In addition, the energy consumed in the pellet increases up to 40% as the particle sizes increase (going from 0.2mm to 0.8mm) and up to 200% compared to raw biomass. Wattananoi, et al. [51] evaluated the densification of biomass when pellets were generated from torrefied biomass. In this work, it was found that the oellet density from torrefied biomass reaches up to 340% compared to that from raw biomass. The energy densification carried out by this process is up to 400% of the volumetric energy value of raw biomass ($GJ/m^3$). These results were obtained for torrefaction at 275°C for 30 minutes.

## 1.5. Balances

Some authors have approached the torrefaction by performing mass, energy, and exergy balances, trying to add to the evidenced benefits of the process, an energetic, and exergetic viability [88,90,107–110]. Authors evaluated torrefaction process linked to a gasification process. Different configurations were evaluated in which torrefaction and gasification are combined. After analyzing exergetically the different configurations, it was concluded that is possible to improve the performance of the biomass in the gasification process and the overall efficiency of the process when torrefaction is linked to gasification. This happens when volatiles produced in torrefaction is supplied as an energetic part to the gasification. These analyzes were performed theoretically, so the authors suggest experimental verification.

## 1.6. Technologies

This section describes the equipment used in torrefaction in experimental works. Different kind of reactors such as fixed bed, fluidized, horizontal reactor, rotary reactor, screw reactor, and thermo-gravimetric balances were found in this review. The use of thermo-balances and fixed bed reactors prevail because their easy operation, control, and reliability of results.

### *1.6.1. Thermo-gravimetric balance (TGA)*

Majority of found studies found in the literature that experimentally studies biomass torrefaction, do so by means of thermo-gravimetric (TGA) reactors [1,11,21,23,24,26,46,59,60,69,108,111–123]. This equipment is widely used because its easy control over operating parameters such as temperature, residence time, and heating rate. In addition, the fast and reliable results that can be obtained in relatively short times and with a very small sample, with the possibility of varying particle sizes, become it a suitable reactor for preliminary testing.

Obtaining kinetics in this reactor is facilitated due to continuous temperature and mass recording developed during test. It also allows the possibility of connection with analysis equipment with real-time species registration such as FTIR or GC-MS, which also allows obtaining kinetics of products. This obtainment of kinetics is facilitated mainly by the small amount of sample in which eliminates thermal gradients for solid in the bed, and small volatiles residence times, avoiding the occurrence of secondary reactions that can distort the results.

### *1.6.2. Fix bed reactor*

This kind of reactor has been widely used for torrefaction due to easy operation and reliable results [6,10,20,23,24,28,31,36,37,40,41,51,60,62–64,67,71–73,124–129]. Have been widely used for the study of other thermal processes such as gasification, combustion, and pyrolysis. The operation of this reactors allows flexibility to evaluate a wide range of particle sizes, beds with very fine particles to very large particles and pellets with operation in batch, although could be performed in continuous mode. One of the main benefits of torrefaction is the destruction of the fibrous structure which generates a fragile material that allows to have energetic benefits in later crushing processes. It is for this reason that torrefaction must to be carried out with large particles to later crush it and fed with coal in combustion processes or to compact it for pellet generation, and fix bed reactor is ideal for this purpose.

Most configurations for the operation with a fixed bed are basically similar, although sometimes the feeding technique of material to the reactor, the reactor heating system, and subsequent gas cleaning may vary. During process with fixed bed, the bed porosity and its height do not vary, as no great decomposition of the material or expansion of the bed is obtained and the pressure of the working gas is increased in this zone of the reactor. In these reactors, secondary reactions are usually potentiated due to the high residence times of volatiles. In the case of torrefaction, homogenous secondary reactions are not so important because the main interest is focused in solid, contrary to gasification and pyrolysis where the secondary reactions are of great interest.

### *1.6.3. Fluidized bed reactor*

The operation of torrefaction in a fluidized bed is not very common in the scientific literature [11,20,61,130–132]. As mentioned earlier, large particles are more convenient to perform the torrefaction process, thinking about the advantages it generates in later processes. This restricts the use of fluidized beds, since to fluidize particles of relatively large sizes would be impractical and would lead to large equipment that guarantee the supply of gases to be able to carry out the fluidization.

One of the main advantages of fluidized beds is the excellent heat transfer conditions between biomass particles and gases, which makes the process take place in less time. Operating a fluidized bed reactor requires a perfect match between particle sizes and gas flow, since for each particle size there will be a minimum fluidization velocity, increasing with particle size. In addition to the relationship between particle size and gas velocity, it is necessary the operational knowledge of the temperature profile in the bed, in order to make corrections by temperature and to maintain fluidization conditions. The above demonstrates that the operation under fluidization conditions is of special care and precision, which is not convenient for exploration stage since results are not obtained relatively quickly. This makes the options of experimentation in TGA or in fixed bed conditions much more attractive.

### *1.6.4. Horizontal reactor*

Horizontal reactors have been widely used in experimental field for torrefaction [22,30,59,68,133–135]. Are usually used for preliminary tests due to very simple, and easily operation. Can be easily coupled with additional equipment such as gas analyzers or precision balances. Samples used are relatively small, but larger than those used in TGA. Continuous operation becomes difficult in this type of configuration, and this is why its operation is performed in batch. It allows great flexibility in particle sizes, since it offers the possibility of processing from very fine to very large particles or pellets.

### *1.6.5. Other reactors*

In addition to mentioned reactors, other less conventional reactors, with which biomass torrefaction has been carried out, have been found in the scientific literature. Among these types of reactors are rotary reactor, microwave, and screw reactors.

From latter, rotary reactors are an excellent alternative for thermal processes with biomass because it provides a great facility to operate continuously making a permanent mixture of the material in the interior [25,74,136,137]. This type of reactor is not very used because it requires extra

equipment to generate the movement of the furnace which implies in additional energy consumptions. The above is not very suitable for experimental stages as is the case of torrefaction where the working atmosphere must be inert or with low oxygen concentrations to ensure no combustion of the material is generated.

Another type of reactor not widely used in the experimentation for biomass torrefaction is the screw reactor [44,45,96,138,139]. Few studies have been found in the literature, where use it to perform continuous torrefaction of biomass. In this type of reactor, it is possible to process a wide range of particle sizes with restrictions on large particles, and is possible modify easily the biomass residence time by varying the RPM of screw. One of the advantages of this type of reactor is that it can be coupled to another subsequent thermal process such as combustion, pyrolysis, or gasification acting as a feed system without incurring additional costs.

Microwave reactors have been not widely used in biomass torrefaction processes, but lately work has been published with this type of reactor [140–148]. One of the main complications in its use is the temperature control in the material, since only power is controlled in them. Some results show that mass and energy yield parameters decrease considerably compared to conventional torrefaction. In recent works temperatures have been measured in the samples, which is necessary due to the increase in temperature in the center of the particle which causes non-homogeneous solids.

## 1.7. Kinetics

In this section, the different kinetic models proposed in the literature to explain the thermal decomposition of the biomass in the roasting and pyrolysis processes were investigated. Pyrolysis models were included in this review because actual torrefaction models have been based in published for pyrolysis. In addition to the kinetics of biomass, the main components (cellulose, hemicellulose and lignin) will also be presented.

Cellulose, hemicellulose and lignin are the three main components of the biomass, and in a small amount ash and extractives, mainly composed of alkaloids, waxes, fats, proteins, phenolic compounds, simple sugars, gums, resins, starches, and essential oils. As products of thermal decomposition of cellulose, hemicellulose and lignin, three products are obtained: permanent gases (consisting mainly of CO, $CO_2$, $CH_4$ and small amounts of $H_2$ and $C_2$ hydrocarbons), condensable gases and char. The kinetics proposed in the literature attempt to describe and predict the formation of each of these phases or species present in them by real-time monitoring or by measuring the total production of each product.

### *1.7.1. Cellulose*

Cellulose is the most abundant component in wood (most studied biomass in thermal processes such as pyrolysis, gasification, and torrefaction). It consists mainly of polymers of six carbons that form large linear chains of glucose molecules (usually 8.000-10.000) with high molecular weights, ranging from 300.000–500.000, with general formula $(C_6H_{10}O_5)_n$. Cellulose is the most studied component of biomass in the field of kinetics.

The simplest model to describe the decomposition of cellulose found in the literature was proposed by Antal et al. [149], which describes the decomposition of cellulose in a pyrolysis process such as the formation of volatiles (formed by condensable compounds and permanent gases) and char, according to the kinetic scheme shown in equation (1-1).

$$\text{Cellulose} \rightarrow \text{Volatiles} + \text{Char} \tag{1-1}$$

Different authors have experimented on cellulose pyrolysis in order to obtain the kinetic parameters of this kinetic scheme [150–153]. Large differences have been found in the values obtained for these parameters due to differences in heating rates, TGA equipment, sample type and mathematical procedure to adjust the TGA data.

Prior to this simple model, some authors investigated the cellulose decomposition in a pyrolysis process in order to propose a kinetic model from pseudo-components. One of the first known models was the proposed by Broido et al. [154], in which the cellulose decomposes into two endothermic competitive reactions. At low temperatures, between 220-280°C, there is an endothermic dehydration that produces anhydrocellulose, tars and water. Above 280°C, a depolymerization of the anhydrocellulose is shown generating char and gases. This kinetic scheme is shown in equation (1-2).

$$\begin{array}{l} \text{Cellulose} \rightarrow \text{Anhidrocellulose} + H_2O \rightarrow 0.35\text{Char} + 0.65\text{Gases} \\ \qquad\qquad\quad \downarrow \\ \qquad\qquad\quad \text{Tars} \end{array} \tag{1-2}$$

This model was modified several times later by Broido himself [133,155]. In its first modification proposed a model without taking into account the anhydrocellulose as shown in equation (1-3), where tested with large particles of cellulose oriented towards the analysis of char formation, between temperatures of 230-370°C. In his second modification added a reaction step (see equation (1-4)) in order to adjust its data to an experimental curve.

This model was modified several times later by Broido himself [133,155]. In its first modification, where it tested with large particles of cellulose oriented towards the analysis of char formation, between temperatures of 230-370°C, proposed a model without taking into account the anhydrocellulose as shown in equation (1-3), and in its second modification added an additional reaction step (see equation (1-4)) in order to adjust its data to an experimental curve.

$$\begin{array}{l} \text{Cellulose} \rightarrow \text{Char} + \text{Gases} \\ \quad\downarrow \\ \text{Tar} \end{array} \tag{1-3}$$

$$\begin{array}{l} \text{Cellulose} \rightarrow \text{Precursor} \rightarrow \text{Anhidrocellulose} + H_2O \rightarrow \text{Char} + \text{Gases} \\ \qquad\qquad\qquad\qquad\qquad\qquad\qquad\qquad \downarrow \\ \qquad\qquad\qquad\qquad\qquad\qquad\qquad\qquad \text{Tar} \end{array} \tag{1-4}$$

Bradbury et al. [156] proposed a model called "Broido-Shafizadeh" in which it is assumed an initiation stage that generates an active cellulose which later decomposes through two competitive reactions, into volatiles, char and gases. This kinetics were obtained with tests between 259-341°C, and this initiation stage is linked to the decomposition of the cellulose at low temperatures 259-295°C because of depolymerization, as shown in equation (1-5).

$$\begin{array}{l} \text{Cellulose} \rightarrow \text{Active cellulose} \rightarrow \text{Volatiles} \\ \qquad\qquad\qquad\qquad\qquad\qquad \downarrow \\ \qquad\qquad\qquad\qquad\qquad\qquad \text{Gas} + \text{Char} \end{array} \tag{1-5}$$

Varhegyi et al. [157] refuted Bradbury's approach to the generation of an active cellulose as an initiation step. He argued that at low temperatures (250-370°C), this initiation step is superfluous and for high temperatures is not representative, so he proposed a new model without active cellulose generation but includes a high temperature decomposition step (see Equation (1-6)).

$$\begin{array}{l} \text{Cellulose} \rightarrow \text{Char} + \text{Gases} \\ \qquad\qquad \downarrow \\ \qquad\qquad \text{Tar} \end{array} \tag{1-6}$$

After this model, Banyasz et al. [158] proposed a kinetic model for cellulose decomposition where active cellulose was not included, confirming the work presented by Varhegyi (see equation (1-7)).

$$\begin{array}{l} \text{Cellulose} \rightarrow \text{Tar}/\text{Levoglucosan} + \text{Char} + CO_2 \\ \qquad\qquad \downarrow \\ \text{Gas}/(\text{HAA} + \text{FA} + \text{CO}) \end{array} \tag{1-7}$$

With technological development of advanced analytical equipment in which different species can be monitored, the depolymerization of cellulose at low temperatures and rapid pyrolysis has been evidenced [159,160]. In these evidences, the existence of liquid intermediary species and solids can be verified, which, although formed in the process, are destroyed after considerable residence times. The authors have associated each of these superfluous species with the formation of active cellulose, mentioned in Broido and Shafizadeh models. From these new evidences, and with identifications of some main species in the phases, similar models have been proposed to those already presented, considering the active cellulose and some species formation. In equation (1-8), is shown the model proposed by Piskorz et al. [161] for fast pyrolysis, and in equation (1-9) a kinetic model proposed by Diebold et al. [162] and subsequently confirmed by Wooten et al. [159] to represent the decomposition of cellulose at low temperatures is shown. Both models consider intermediate species in the decomposition process as "active cellulose".

$$\begin{array}{c} \text{Cellulose} \rightarrow \text{Active cellulose} \rightarrow \text{HAA} + H_2O + CO_2 + \text{CO...} \\ \downarrow \qquad\qquad \downarrow \\ H_2O + CO_2 + \text{CO} + \text{Char} \qquad \text{Tars} \end{array} \tag{1-8}$$

$$\begin{array}{c} \qquad\qquad\qquad\quad \text{Secundary gas} \\ \qquad\qquad\qquad\quad \uparrow \qquad\qquad \uparrow \\ \text{Cellulose} \rightarrow \text{Active cellulose} \rightarrow \text{Primary vapors} \rightarrow \text{Secondary tar} \\ \quad \downarrow \qquad\quad \downarrow \\ \text{Char} + H_2O \qquad \text{Char} + H_2O \end{array} \tag{1-9}$$

The difference between these two kinetic models is that the second one considers char formation from the active cellulose. This char formation had been mentioned in previous years by Bradbury et al. [156] and Antal et al. [157], where they suggested that char formation was a consequence of the repolymerization of volatile compounds such as levoglucosan. This reaction from the active cellulose was included in the model proposed by Mamleev et al. [163] presented in equation (1-10).

$$\begin{array}{c} \qquad\qquad\qquad\quad \text{Gas}_1(\text{HAA} + \text{FA} + \text{CO...}) \\ \qquad\qquad\qquad\quad \uparrow \\ \qquad\qquad \text{Cellulose} \rightarrow \text{Intermediate} \rightarrow \text{Char}_1 \\ \qquad\qquad \downarrow \\ H_2O + CO_2 + \text{LG} + \text{Cellobiosan} \rightarrow \text{Gas}_2 \\ \qquad\qquad\qquad\quad \downarrow \\ \qquad\qquad\qquad\quad \text{Char}_2 \end{array} \tag{1-10}$$

Evidence of the existence of these components is not complicated with the help of advanced analytical equipment, but the chemical reaction mechanisms remain ambiguous.

In this section, is clear that the kinetic models proposed to describe cellulose decomposition are based on the need to fit a model with experimental data. As part of these adjustments, pseudo-components have been established as the "active cellulose" in order to justify behaviors evidenced in the experimentation and of which it is not yet clear its cause.

### *1.7.2. Hemicellulose*

Hemicellulose is one of the most important compound in biomass. This compound consists mainly of 5-carbon polymers but also includes 6-carbon species such as glucose, mannose, galactose, xylose, arabinose, glucuronic acids of the general formula $(C_5H_8O_4)_n$. The most abundant compound in hemicellulose is xylan and it is for this reason that some studies found in the literature are made with xylan as a representative compound of hemicellulose.

The simplest model to represent the decomposition of hemicellulose is a single step as shown in equation (1-11).

$$\text{Hemicellulose} \rightarrow \text{Volatiles} + \text{Char} \qquad (1\text{-}11)$$

Different authors have also worked on obtaining the kinetic parameters for this model [150,164–167], but large differences have been reported due to the same causes mentioned above (differences in heating rates, TGA equipment, sample, and mathematical procedure).

Di Blasi et al. [135] proposed a model for the decomposition of xylan by means of two reactions in which an intermediate compound is generated, which yields later volatiles and char (see equation (1-12)).

$$\begin{array}{l} \text{Hemicellulose} \rightarrow \text{Intermediate} \rightarrow \text{Char} + \text{Volatiles}_2 \\ \quad\downarrow \\ \quad\text{Volatiles}_1 \end{array} \qquad (1\text{-}12)$$

In this model, the intermediate compound is consequence of depolymerization of the hemicellulose at low temperature (<150°C), leading to the formation of altered and rearranged structures of poly-sugars. Above this temperature, the oligosaccharides and monosaccharides decomposition generate char, water and permanent gases such as CO and $CO_2$.

Koufopanos et al. [168] proposed a model for the decomposition of hemicellulose, which included a zero-order reaction in which a rapid depolymerization without mass loss was described where an intermediate compound was generated which subsequently formed gases, volatiles and char (see Equation (1-13)). This model is similar to that proposed by Shafizadeh et al. [169,170] but without considering mass loss in the initial reaction.

$$\begin{array}{l} \text{Hemicellulose} \rightarrow \text{Intermediate} \rightarrow \text{Gas} + \text{Volatiles} \\ \qquad\qquad\downarrow \\ \qquad\qquad\text{Char} \end{array} \qquad (1\text{-}13)$$

Ward et al. [171] represented the decomposition of a wood as the sum of the decomposition of each of its components (cellulose, hemicellulose and lignin). In this work, they proposed a kinetic model formed of three order one reactions in which two consecutive intermediate solids were generated and at the end only char is generated. This model considers a formation of volatiles after the formation of each intermediate solid as is shown in equation (1-14).

$$\begin{array}{l} \text{Hemicellulose} \rightarrow \text{Intermediate}_1 \rightarrow \text{Intermediate}_2 \rightarrow \text{Char} \\ \qquad\qquad\downarrow \qquad\qquad\qquad\downarrow \\ \qquad\qquad\text{Volatiles}_1 \qquad\qquad \text{Volatiles}_2 \end{array} \qquad (1\text{-}14)$$

In the current literature, little kinetic information is found for hemicellulose, since, as mentioned earlier, cellulose has been the most studied component in biomass. In addition, the kinetics found only take into account pseudo-components, without reaching the detail to which the cellulose kinetics have reached in terms of the generation of some representative species.

It is questionable whether the kinetic models proposed for a reaction can similarly predict the decomposition of the same component under similar operating conditions as two-reaction or multiple-reaction models. This subject has been addressed by some authors [172], and they conclude that this model adjustment depends directly on the operating conditions of the experimental tests.

### *1.7.3. Lignin*

Lignin is the third component in importance in biomass for torrefaction process; it is composed of aromatic polymer complexes in an irregular matrix of several highly branched "hydroxy" and "methoxy" groups. It is more stable and resistant to thermal decomposition than cellulose and hemicellulose.

Tang [173] proposed a single-reaction model for the decomposition of lignin as a result of experimental tests on vacuum TGA (equation (1-15)). Subsequently different authors studied the decomposition of biomass and its components and found kinetic parameters to describe the decomposition of lignin in a single reaction [151,153,173–175]. These parameters differ in values, but are a little more concordant compared to those found for cellulose and hemicellulose.

$$\text{Lignina} \rightarrow \text{Volátiles} + \text{Char} \tag{1-15}$$

In their research, Koufopanos et al. [168] and Ward, et al. [171] proposed models for biomass decomposition that also applied to lignin, in which it is decomposed thermally by mechanisms of multiple reactions in which the formation of an intermediate solid [168] and two intermediate solid are considered [171]. These models can be observed in equations (1-16) and (1-17).

$$\begin{array}{l} \text{Lignina} \rightarrow \text{Producto intermedio} \rightarrow \text{Gas} + \text{Volátiles} \\ \qquad\qquad\quad \downarrow \\ \qquad\qquad\quad \text{Char} \end{array} \tag{1-16}$$

$$\begin{array}{l} \text{Lignina} \rightarrow \text{Sólido intermedio}_1 \rightarrow \text{Sólido intermedio}_2 \rightarrow \text{Char} \\ \qquad\qquad\quad \downarrow \qquad\qquad\quad \downarrow \\ \qquad\qquad\quad \text{Volátiles}_1 \qquad\quad \text{Volátiles}_2 \end{array} \tag{1-17}$$

Authors such as Liu et al. [176] evaluated the pyrolysis of lignin over a wide temperature range (20-800°C) with different heating rates and observed that lignin throughout its decomposition process has three regions of mass loss. To explain this behavior, they proposed a simple three-stage model where they explain each zone and the kinetic parameters were found for them.

### *1.7.4. Biomass*

As already mentioned, the complexity of the reactions occurring in biomass in a thermal process makes it difficult to generate or propose an acceptable chemical model that describes this process. Different global kinetic models have been proposed and used. The simplest model to describe the decomposition of a wood is that shown in equation (1-18).

$$\text{Biomasa} \rightarrow \text{Volátiles} + \text{Char} \qquad (1\text{-}18)$$

Similar to previous models applied to biomass components, numerous studies have also been carried out to try to find the values of the kinetic parameters [171,177–179].

Shafizadeh et al. [180], proposed a model for the decomposition of wood, where three simultaneous reactions are considered, each forming a different product (solid, liquid and gas) as observed in equation (1-19).

$$\begin{array}{c} \text{Char} \\ \uparrow \\ \text{Biomasa} \rightarrow \text{Tar} \\ \downarrow \\ \text{Gas} \end{array} \qquad (1\text{-}19)$$

This model of three reactions has been used by different authors to study wood decomposition and find the kinetic parameters for the formation of each product in the process [178,179,181,182].

Branca et al. [183] performed the pyrolysis of wood in the temperature range of 275-435°C and proposed a reaction mechanism of 3 consecutive stages presented in equation (1-20), since the thermograms had three zones of different velocities of mass loss, which are assumed to correspond to the decomposition of hemicellulose, cellulose and lignin respectively. In each stage volatiles generation is considered. In this kinetic study, the parameters were found for each region observed.

$$\begin{array}{ccccc} \text{Biomasa} & \rightarrow & \text{Intermedios de reacción}_1 & \rightarrow & \text{Intermedios de reacción}_2 \rightarrow \text{Char} \\ \downarrow & & \downarrow & & \downarrow \\ \text{Volátiles}_1 & & \text{Volátiles}_2 & & \text{Volátiles}_3 \end{array} \qquad (1\text{-}20)$$

Di Blasi [184], studied secondary char formation from volatiles in a combustion process (equation (1-21)), later Park et al. [185] studied these kinetics proposed by Di Blasi but coupled to a process of biomass pyrolysis, being the only kinetic proposal for this type of secondary reactions (equation (1-22)).

$$\begin{array}{ccc} \text{Gas} & & \text{Gas} \\ \uparrow & & \uparrow \\ \text{Biomasa} & \rightarrow & \text{Tar} \\ \downarrow & & \downarrow \\ \text{Char} & & \text{Char} \end{array} \qquad (1\text{-}21)$$

$$\begin{array}{c} \text{Gas} \\ \uparrow \\ \text{Biomasa} \rightarrow \text{Tar} \rightarrow \text{Char} \\ \downarrow \\ \text{Solido intermedio} \rightarrow \text{Char} \end{array} \qquad (1\text{-}22)$$

Some authors in this topic of biomass kinetics consider that the decomposition of a biomass can be expressed as the sum of the individual decompositions of each of its main components (cellulose, hemicellulose and lignin) [26,153,171,186]. This position does not consider synergistic behaviors between the components, nor catalytic effects due to the ashes contained in the biomass. This hypothesis has been debated by some authors who experimentally verify the synergy of the components and the catalytic effect of the ashes on the products obtained and on the decomposition rate of the main components [129,187–189].

## 1.8. Models

The need to explain theoretically and predict the phenomena involved in thermal processes has led to the development of phenomenological models with which a complete description of chemical and physical process occurring during the process can be done. In this section, a review of literature was carried out to identify the proposed models, global, one-dimensional, in two or three dimensions, that predict or describe the behavior of a biomass in a torrefaction process.

Currently in the literature the information about predictive models in the field of torrefaction is limited [65,137,190–194]. These models, consider the influence of parameters such as heating rate, process temperature, residence times, etc, having good adjustments with experimental data, but, some models have considerable simplifications respect to energy transfer between phases inside particle, or global kinetics without consider secondary char formation.

The first models for thermal process were developed in the field of the combustion and pyrolysis of coal and biomass. In these, very precise kinetics and more complete models have been developed for the prediction of the phenomena occurring in the different types of fuels. Torrefaction, as a study area post-pyrolysis and gasification (as it aroused great interest beginning 1990s) has taken much of the knowledge and advances in the field of pyrolysis [149,181,185,195–201] to structure the models that describe the process in a biomass.

Chan et al. [181] developed a model for a biomass particle subjected to heating under inert atmosphere. This model considered the drying of the particles, the exit of volatiles and cracking. Conduction and convection inside the particle were considered and thermal properties as conductivity and heat capacity vary with process temperature. A biomass decomposition model considering solid, gas and tar formation and subsequent secondary decomposition of tar into volatiles and tar was included in the model.

Di Blasi et al. [202] modeled a two-dimensional biomass particle which is heated under inert atmosphere at controlled heating rates. The particle was considered as isotropic and with properties varying in the thermal process. In this model, physical phenomena such as conduction and

convection of heat inside the particle, and convection and radiation in the particle surface were considered. The kinetic model of decomposition of biomass proposed by Broido [156] was used in this model without taking into account secondary reactions between volatile and solid. In this model they obtained temperature contours, gas velocity and char production. The results were compared with one-dimensional models with comparable results.

Felfi et al. [203] developed an one-dimensional phenomenological model in a transient state applied to torrefaction process of a wood pellet. In this model it was considered that volatiles and steam generated are in thermal equilibrium with the solid. Geometric changes of the solid during the process and pressure gradients were negligible due to the high permeability of the solid. Diffusive transport of the gaseous species in the solid was negligible as well. Kinetics model used in this model was proposed by Shafizadeh et al. [180] which considers that the biomass is decomposed by three competitive reactions to gas, tar and char. This model reproduced the drying process, particle heating and volatiles generation. This model is not sufficiently explanatory to the phenomena that occur within the particle.

Ratte et al. [204] proposed a one-dimensional phenomenological model in a transient state for slow pyrolysis of a spherical wood particle. In this model they used the average volume simplification (Volume averaging) proposed by Withaker [205]. Mass and energy balances were performed for wood particle, considering the kinetic model proposed by Shafizadeh et al. [180]. With this model it is possible to reproduce the distribution of temperatures inside the particle, moisture content, increase of pressure as a consequence of the generation of volatiles. This model considered more physical phenomena than those considered by Felfli et al. [203], but the kinetics responsible for explaining the chemical phenomena during the process were the same.

Turner et al. [206] modeled wood torrefaction process using a transient two-dimensional phenomenological model, which coupled chemical and physical phenomena using the transpore model previously developed by Perré et al. [207], which describes the drying of a porous medium. The kinetic model used is based on the hypothesis that biomass decomposition can be described as the decomposition of each of its main components (cellulose, hemicellulose and lignin) and kinetics available in the literature are used to model the decomposition of each one.

Pétrissanset al. [208] modeled the thermal degradation of a wood particle by phenomenological equations in a one-dimensional transient state model. They did not consider convective energy transfer between volatiles and solid, and used a kinetic model that describes the decomposition of the wood as two simultaneous reactions that generate gases and char. His main focus was on primary char yield so no information was shown about field of other products.

Ratte et al. [190] developed one of the few models found for a torrefaction reactor. In this model two phases were considered inside the reactor: A particulate phase formed by the biomass and a continuous phase formed by 11 species present in the gases that enter to the reactor and those generated in the process. The kinetic model only considers the formation of volatiles and char, without considering secondary reactions in heterogeneous phase. The modeling process is continuous and eight reactions were considered to represent the homogeneous phase reactions during the torrefaction process.

According to presented in this section of models, the field of investigation about models for torrefaction process is increasing and is an area for exploration, which can be improved with more detailed kinetic models.

**Referencias**

[1] Peng J, Bi XT, Lim J, Sokhansanj S. Development of Torrefaction Kinetics for British Columbia Softwoods. Int J Chem React Eng 2012;10. doi:10.1515/1542-6580.2878.

[2] Balat M, Balat H, ??z C. Progress in bioethanol processing. Prog Energy Combust Sci 2008;34:551–73. doi:10.1016/j.pecs.2007.11.001.

[3] Mohan D, Pittman CU, Steele PH. Pyrolysis of Wood / Biomass for Bio-oil : A Critical Review. Energy & Fuesl 2006;20:848–89. doi:10.1021/ef0502397.

[4] Chen WH, Kuo PC. Torrefaction and co-torrefaction characterization of hemicellulose, cellulose and lignin as well as torrefaction of some basic constituents in biomass. Energy 2011;36:803–11. doi:10.1016/j.energy.2010.12.036.

[5] Chen WH, Cheng WY, Lu KM, Huang YP. An evaluation on improvement of pulverized biomass property for solid fuel through torrefaction. Appl Energy 2011;88:3636–44. doi:10.1016/j.apenergy.2011.03.040.

[6] Lu K-M, Lee W-J, Chen W-H, Liu S-H, Lin T-C. Torrefaction and low temperature carbonization of oil palm fiber and Eucalyptus in nitrogen and air atmospheres. Bioresour Technol 2012;123:98–105. doi:10.1016/j.biortech.2012.07.096.

[7] Tran KQ, Luo X, Seisenbaeva G, Jirjis R. Stump torrefaction for bioenergy application. Appl Energy 2013;112:539–46. doi:10.1016/j.apenergy.2012.12.053.

[8] van der Stelt MJC, Gerhauser H, Kiel JH a., Ptasinski KJ. Biomass upgrading by torrefaction for the production of biofuels: A review. Biomass and Bioenergy 2011;5. doi:10.1016/j.biombioe.2011.06.023.

[9] Chew JJ, Doshi V. Recent advances in biomass pretreatment – Torrefaction fundamentals and technology. Renew Sustain Energy Rev 2011;15:4212–22. doi:10.1016/j.rser.2011.09.017.

[10] Rousset P, Macedo L, Commandré J, Moreira A. Biomass torrefaction under different oxygen concentration and its effect on the composition of the solid by-product. J Anal Appl Pyrolysis 2012;96:86–91.

[11] Wang C, Peng J, Li H, Bi XT, Legros R, Lim CJ, et al. Oxidative torrefaction of biomass residues and densification of torrefied sawdust to pellets. Bioresour Technol 2013;127:318–25. doi:10.1016/j.biortech.2012.09.092.

[12] Sellappah V, Uemura Y, Hassan S, Sulaiman MH, Lam MK. Torrefaction of Empty Fruit Bunch in the Presence of Combustion Gas. Procedia Eng 2016;148:750–7. doi:10.1016/j.proeng.2016.06.608.

[13] Li M-F, Li X, Bian J, Xu J-K, Yang S, Sun R-C. Influence of temperature on bamboo torrefaction under carbon dioxide atmosphere. Ind Crops Prod 2015;76:149–57. doi:10.1016/j.indcrop.2015.04.060.

[14] Mei Y, Liu R, Yang Q, Yang H, Shao J, Draper C, et al. Torrefaction of cedarwood in a pilot scale rotary kiln and the influence of industrial flue gas. Bioresour Technol 2015;177:355–60.

doi:10.1016/j.biortech.2014.10.113.

[15] Uemura Y, Saadon S, Osman N, Mansor N, Tanoue KI. Torrefaction of oil palm kernel shell in the presence of oxygen and carbon dioxide. Fuel 2015;144:171–9. doi:10.1016/j.fuel.2014.12.050.

[16] Chen WH, Lu KM, Lee WJ, Liu SH, Lin TC. Non-oxidative and oxidative torrefaction characterization and SEM observations of fibrous and ligneous biomass. Appl Energy 2014;114:104–13. doi:10.1016/j.apenergy.2013.09.045.

[17] Saadon S, Uemura Y, Mansor N. Torrefaction in the Presence of Oxygen and Carbon Dioxide: The Effect on Yield of Oil Palm Kernel Shell. Procedia Chem 2014;9:194–201. doi:10.1016/j.proche.2014.05.023.

[18] Chen WH, Lu KM, Liu SH, Tsai CM, Lee WJ, Lin TC. Biomass torrefaction characteristics in inert and oxidative atmospheres at various superficial velocities. Bioresour Technol 2013;146:152–60. doi:10.1016/j.biortech.2013.07.064.

[19] Chen WH, Zhuang YQ, Liu SH, Juang TT, Tsai CM. Product characteristics from the torrefaction of oil palm fiber pellets in inert and oxidative atmospheres. Bioresour Technol 2016;199:367–74. doi:10.1016/j.biortech.2015.08.066.

[20] Basu P, Rao S, Dhungana A. An investigation into the effect of biomass particle size on its torrefaction. Can J Chem Eng 2013;91:466–74. doi:10.1002/cjce.21710.

[21] Bridgeman TG, Darvell LI, Jones JM, Williams PT, Fahmi R, Bridgwater a. V, et al. Influence of particle size on the analytical and chemical properties of two energy crops. Fuel 2007;86:60–72. doi:10.1016/j.fuel.2006.06.022.

[22] Jones JM, Bridgeman TG, Darvell LI, Gudka B, Saddawi a., Williams a. Combustion properties of torrefied willow compared with bituminous coals. Fuel Process Technol 2012;101:1–9. doi:10.1016/j.fuproc.2012.03.010.

[23] Peng JH, Bi HT, Sokhansanj S, Lim JC. A Study of Particle Size Effect on Biomass Torrefaction and Densification. Energy & Fuels 2012;26:3826–39. doi:10.1021/ef3004027.

[24] Shang L, Ahrenfeldt J, Holm JK, Barsberg S, Zhang R, Luo Y, et al. Intrinsic kinetics and devolatilization of wheat straw during torrefaction. J Anal Appl Pyrolysis 2013;100:145–52. doi:10.1016/j.jaap.2012.12.010.

[25] Broström M, Nordin A, Pommer L, Branca C, Di Blasi C. Influence of torrefaction on the devolatilization and oxidation kinetics of wood. J Anal Appl Pyrolysis 2012;96:100–9. doi:10.1016/j.jaap.2012.03.011.

[26] Prins MJ, Ptasinski KJ, Janssen FJJ. Torrefaction of wood. Part 1. Weight loss kinetics. J Anal Appl Pyrolysis 2006;77:28–34. doi:10.1016/j.jaap.2006.01.002.

[27] Pierre F, Almeida G, Brito J, Perré P. Influence of torrefaction on some chemical and energy properties of maritime pine and pedunculate oak. Bioresources 2011;6:1204–18.

[28] Melkior T, Jacob S, Gerbaud G, Hediger S, Le Pape L, Bonnefois L, et al. NMR analysis of the transformation of wood constituents by torrefaction. Fuel 2012;92:271–80. doi:10.1016/j.fuel.2011.06.042.

[29] Shang L, Ahrenfeldt J, Holm JK, Sanadi AR, Barsberg S, Thomsen T, et al. Changes of chemical

and mechanical behavior of torrefied wheat straw. Biomass and Bioenergy 2012;40:63–70. doi:10.1016/j.biombioe.2012.01.049.

[30] Chen W-H, Lu K-M, Tsai C-M. An experimental analysis on property and structure variations of agricultural wastes undergoing torrefaction. Appl Energy 2012;100:318–25. doi:10.1016/j.apenergy.2012.05.056.

[31] Lee J-W, Kim Y-H, Lee S-M, Lee H-W. Optimizing the torrefaction of mixed softwood by response surface methodology for biomass upgrading to high energy density. Bioresour Technol 2012;116:471–6. doi:10.1016/j.biortech.2012.03.122.

[32] Demirbas A. The influence of temperature on the yields of compounds existing in bio-oils obtained from biomass samples via pyrolysis. Fuel Process Technol 2007;88:591–7. doi:10.1016/j.fuproc.2007.01.010.

[33] Wannapeera J, Fungtammasan B, Worasuwannarak N. Effects of temperature and holding time during torrefaction on the pyrolysis behaviors of woody biomass. J Anal Appl Pyrolysis 2011;92:99–105. doi:10.1016/j.jaap.2011.04.010.

[34] Pelaez-Samaniego MR, Yadama V, Garcia-Perez M, Lowell E, McDonald AG. Effect of temperature during wood torrefaction on the formation of lignin liquid intermediates. J Anal Appl Pyrolysis 2014;109:222–33. doi:10.1016/j.jaap.2014.06.008.

[35] Strandberg M, Olofsson I, Pommer L, Wiklund-Lindström S, Åberg K, Nordin A. Effects of temperature and residence time on continuous torrefaction of spruce wood. Fuel Process Technol 2015;134:387–98. doi:10.1016/j.fuproc.2015.02.021.

[36] Prins MJ, Ptasinski KJ, Janssen FJJ. Torrefaction of wood. Part 2. Analysis of products. J Anal Appl Pyrolysis 2006;77:35–40. doi:10.1016/j.jaap.2006.01.001.

[37] Fisher EM, Dupont C, Darvell LI, Commandré J-M, Saddawi a, Jones JM, et al. Combustion and gasification characteristics of chars from raw and torrefied biomass. Bioresour Technol 2012;119:157–65. doi:10.1016/j.biortech.2012.05.109.

[38] Berrueco C, Recari J, Güell BM, Alamo G Del. Pressurized gasification of torrefied woody biomass in a lab scale fluidized bed. Energy 2014;70:68–78. doi:10.1016/j.energy.2014.03.087.

[39] Xue G, Kwapinska M, Kwapinski W, Czajka KM, Kennedy J, Leahy JJ. Impact of torrefaction on properties of Miscanthus×giganteus relevant to gasification. Fuel 2014;121:189–97. doi:10.1016/j.fuel.2013.12.022.

[40] Couhert C, Salvador S, Commandré J-M. Impact of torrefaction on syngas production from wood. Fuel 2009;88:2286–90. doi:10.1016/j.fuel.2009.05.003.

[41] Deng J, Wang G, Kuang J, Zhang Y, Luo Y. Pretreatment of agricultural residues for co-gasification via torrefaction. J Anal Appl Pyrolysis 2009;86:331–7. doi:10.1016/j.jaap.2009.08.006.

[42] Hassan E, Steele P, Ingram L. Characterization of fast pyrolysis bio-oils produced from pretreated pine wood. Appl Biochem Biotechnol 2009;154:182–92. doi:10.1007/s12010-008-8445-3.

[43] Meng J, Park J, Tilotta D, Park S. The effect of torrefaction on the chemistry of fast-pyrolysis bio-oil. Bioresour Technol 2012;111:439–46. doi:10.1016/j.biortech.2012.01.159.

[44] Zheng A, Zhao Z, Chang S, Huang Z, Wang X, He F, et al. Effect of torrefaction on structure and

fast pyrolysis behavior of corncobs. Bioresour Technol 2013;128:370–7. doi:10.1016/j.biortech.2012.10.067.

[45] Zheng A, Zhao Z, Chang S, Huang Z, He F, Li H. Effect of Torrefaction Temperature on Product Distribution from Two-Staged Pyrolysis of Biomass. Energy & Fuels 2012;26:2968–74.

[46] Bridgeman TG, Jones JM, Shield I, Williams PT. Torrefaction of reed canary grass, wheat straw and willow to enhance solid fuel qualities and combustion properties. Fuel 2008;87:844–56. doi:10.1016/j.fuel.2007.05.041.

[47] Fang MX, Shen DK, Li YX, Yu CJ, Luo ZY, Cen KF. Kinetic study on pyrolysis and combustion of wood under different oxygen concentrations by using TG-FTIR analysis. J Anal Appl Pyrolysis 2006;77:22–7. doi:10.1016/j.jaap.2005.12.010.

[48] Costa FF, Wang G, Costa M. Combustion kinetics and particle fragmentation of raw and torrified pine shells and olive stones in a drop tube furnace. Proc Combust Inst 2014;35:3591–9. doi:10.1016/j.proci.2014.06.024.

[49] Liu Z, Hu W, Jiang Z, Mi B, Fei B. Investigating combustion behaviors of bamboo, torrefied bamboo, coal and their respective blends by thermogravimetric analysis. Renew Energy 2016;87:346–52. doi:10.1016/j.renene.2015.10.039.

[50] Ramajo-Escalera B, Espina A, García JR, Sosa-Arnao JH, Nebra SA. Model-free kinetics applied to sugarcane bagasse combustion. Thermochim Acta 2006;448:111–6. doi:10.1016/j.tca.2006.07.001.

[51] Wattananoi W, Khumsak O, Worasuwannarak N. Upgrading of biomass by torrefaction and densification process. 2011 IEEE Conf Clean Energy Technol 2011:209–12. doi:10.1109/CET.2011.6041465.

[52] Ghiasi B, Kumar L, Furubayashi T, Lim CJ, Bi X, Soo C. Densified biocoal from woodchips : Is it better to do torrefaction before or after densification ? Appl Energy 2014;134:133–42. doi:10.1016/j.apenergy.2014.07.076.

[53] Agar D, Gil J, Sanchez D, Echeverria I, Wihersaari M. Torrefied versus conventional pellet production - A comparative study on energy and emission balance based on pilot-plant data and EU sustainability criteria. Appl Energy 2015;138:621–30. doi:10.1016/j.apenergy.2014.08.017.

[54] Peng JH, Bi XT, Sokhansanj S, Lim CJ. Torrefaction and densification of different species of softwood residues. Fuel 2013;111:411–21. doi:10.1016/j.fuel.2013.04.048.

[55] Bergman P. Combined torrefaction and pelletisation. The TOP process. 2005.

[56] Repellin V, Govin A, Rolland M, Guyonnet R. Energy requirement for fine grinding of torrefied wood. Biomass and Bioenergy 2010;34:923–30. doi:10.1016/j.biombioe.2010.01.039.

[57] Phanphanich M, Mani S. Impact of torrefaction on the grindability and fuel characteristics of forest biomass. Bioresour Technol 2011;102:1246–53. doi:10.1016/j.biortech.2010.08.028.

[58] Bridgeman TG, Jones JM, Williams a., Waldron DJ. An investigation of the grindability of two torrefied energy crops. Fuel 2010;89:3911–8. doi:10.1016/j.fuel.2010.06.043.

[59] Arias B, Pevida C, Fermoso J, Plaza MG, Rubiera F, Pis JJ. Influence of torrefaction on the grindability and reactivity of woody biomass. Fuel Process Technol 2008;89:169–75. doi:10.1016/j.fuproc.2007.09.002.

[60] Bergman P, Boersma A, Kiel J, Prins MJ, Ptasinski K, Janssen FJ. Torrefaction for entrained-flow gasification of biomass. 2nd World Conf. Technol. Exhib. Biomass Energy, Ind. Clim. Prot., Rome: 2005, p. 78–82.

[61] Li H, Liu X, Legros R, Bi XT, Lim CJ, Sokhansanj S. Torrefaction of sawdust in a fluidized bed reactor. Bioresour Technol 2012;103:453–8. doi:10.1016/j.biortech.2011.10.009.

[62] Bourgois J, Guyonnet R. Characterization and analysis of torrefied wood. Wood Sci Technol 1988;22:143–55. doi:10.1007/BF00355850.

[63] Bourgois J, Bartholin MC, Guyonnet R. Thermal treatment of wood: analysis of the obtained product. Wood Sci Technol 1989;23:303–10. doi:10.1007/BF00353246.

[64] Pentananunt R, Rahman ANMM, Bhattacharya SC. Upgrading of biomass by means of torrefaction. Energy 1990;15:1175–9. doi:10.1016/0360-5442(90)90109-F.

[65] Felfli FF, Luengo CA, Suárez JA, Beatón PA. Wood briquette torrefaction. Energy Sustain Dev 2005;9:19–22. doi:10.1016/S0973-0826(08)60519-0.

[66] Prins MJ, Ptasinski KJ, Janssen FJJG. Torrefaction of wood. Part 1. Weight loss kinetics. J Anal Appl Pyrolysis 2006;77:28–34. doi:10.1016/j.jaap.2006.01.002.

[67] Yan W, Acharjee T, Coronella C, Vásquez V. Thermal pretreatment of lignocellulosic biomass. Environ Prog Sustain Energy 2009;28:435–40. doi:10.1002/ep.

[68] Sadaka S, Negi S. Improvements of biomass physical and thermochemical characteristics via torrefaction process. Environ Prog Sustain Energy 2009;28:427–34. doi:10.1002/ep.

[69] Chen W-H, Kuo P-C. A study on torrefaction of various biomass materials and its impact on lignocellulosic structure simulated by a thermogravimetry. Energy 2010;35:2580–6. doi:10.1016/j.energy.2010.02.054.

[70] Almeida G, Brito JO, Perré P. Alterations in energy properties of eucalyptus wood and bark subjected to torrefaction: the potential of mass loss as a synthetic indicator. Bioresour Technol 2010;101:9778–84. doi:10.1016/j.biortech.2010.07.026.

[71] Wang G, Luo Y, Deng J, Kuang J, Zhang Y. Pretreatment of biomass by torrefaction. Chinese Sci Bull 2011;56:1442–8. doi:10.1007/s11434-010-4143-y.

[72] Medic D, Darr M, Shah a., Potter B, Zimmerman J. Effects of torrefaction process parameters on biomass feedstock upgrading. Fuel 2012;91:147–54. doi:10.1016/j.fuel.2011.07.019.

[73] Khazraie Shoulaifar T, Demartini N, Ivaska A, Fardim P, Hupa M. Measuring the concentration of carboxylic acid groups in torrefied spruce wood. Bioresour Technol 2012;123:338–43. doi:10.1016/j.biortech.2012.07.069.

[74] Nhuchhen DR, Basu P, Acharya B. Torrefaction of poplar in continuous two- stage indirectly heated rotary torrefier. Energy & Fuels 2016;30:1027–38. doi:10.1021/acs.energyfuels.5b02288.

[75] Carrier M, Hugo T, Gorgens J, Knoetze H. Comparison of slow and vacuum pyrolysis of sugar cane bagasse. J Anal Appl Pyrolysis 2011;90:18–26. doi:10.1016/j.jaap.2010.10.001.

[76] Carrier M, Hardie AG, Uras Ü, Görgens J, Knoetze J. Production of char from vacuum pyrolysis of South-African sugar cane bagasse and its characterization as activated carbon and biochar. J Anal

Appl Pyrolysis 2012;96:24–32. doi:10.1016/j.jaap.2012.02.016.

[77] Wannapeera J, Worasuwannarak N. Upgrading of woody biomass by torrefaction under pressure. J Anal Appl Pyrolysis 2012;96:173–80. doi:10.1016/j.jaap.2012.04.002.

[78] Lasek JA, Kopczyński M, Janusz M, Iluk A, Zuwała J. Combustion properties of torrefied biomass obtained from flue gas-enhanced reactor. Energy 2017;119:362–8. doi:10.1016/j.energy.2016.12.079.

[79] Kopczyński M, Lasek JA, Iluk A, Zuwała J. The co-combustion of hard coal with raw and torrefied biomasses (willow (Salix viminalis), olive oil residue and waste wood from furniture manufacturing). Energy 2017:1–10. doi:10.1016/j.energy.2017.04.036.

[80] Valix M, Katyal S, Cheung WH. Combustion of thermochemically torrefied sugar cane bagasse. Bioresour Technol 2017;223:202–9. doi:10.1016/j.biortech.2016.10.053.

[81] Zhang S, Chen T, Li W, Dong Q, Xiong Y. Physicochemical properties and combustion behavior of duckweed during wet torrefaction. Bioresour Technol 2016;218:1157–62. doi:10.1016/j.biortech.2016.07.086.

[82] Muizniece I, Klavina K, Blumberga D. The Impact of Torrefaction on Coniferous Forest Residue Fuel. Energy Procedia 2016;95:319–23. doi:10.1016/j.egypro.2016.09.013.

[83] Guizani C, Haddad K, Jeguirim M, Colin B, Limousy L. Combustion characteristics and kinetics of torrefied olive pomace. Energy 2016;107:453–63. doi:10.1016/j.energy.2016.04.034.

[84] Toptas A, Yildirim Y, Duman G, Yanik J. Combustion behavior of different kinds of torrefied biomass and their blends with lignite. Bioresour Technol 2015;177:328–36. doi:10.1016/j.biortech.2014.11.072.

[85] Gil M V., García R, Pevida C, Rubiera F. Grindability and combustion behavior of coal and torrefied biomass blends. Bioresour Technol 2015;191:205–12. doi:10.1016/j.biortech.2015.04.117.

[86] Ku X, Jin H, Lin J. Comparison of gasification performances between raw and torrefied biomasses in an air-blown fluidized-bed gasifier. Chem Eng Sci 2017. doi:10.1016/j.ces.2017.04.050.

[87] Woytiuk K, Campbell W, Gerspacher R, Evitts RW, Phoenix A. The effect of torrefaction on syngas quality metrics from fluidized bed gasification of SRC willow. Renew Energy 2017;101:409–16. doi:10.1016/j.renene.2016.08.071.

[88] Manatura K, Lu JH, Wu KT, Hsu H Te. Exergy analysis on torrefied rice husk pellet in fluidized bed gasification. Appl Therm Eng 2017;111:1016–24. doi:10.1016/j.applthermaleng.2016.09.135.

[89] Tran KQ, Bui HH, Luengnaruemitchai A, Wang L, Skreiberg ??yvind. Isothermal and non-isothermal kinetic study on CO2 gasification of torrefied forest residues. Biomass and Bioenergy 2016;91:175–85. doi:10.1016/j.biombioe.2016.05.024.

[90] Tapasvi D, Kempegowda RS, Tran KQ, Skreiberg Ø, Grønli M. A simulation study on the torrefied biomass gasification. Energy Convers Manag 2015;90:446–57. doi:10.1016/j.enconman.2014.11.027.

[91] Clausen LR. Maximizing biofuel production in a thermochemical biorefinery by adding electrolytic hydrogen and by integrating torrefaction with entrained flow gasification. Energy 2015;85:94–104. doi:10.1016/j.energy.2015.03.089.

[92] Dudyński M, Van Dyk JC, Kwiatkowski K, Sosnowska M. Biomass gasification: Influence of torrefaction on syngas production and tar formation. Fuel Process Technol 2015;131:203–12. doi:10.1016/j.fuproc.2014.11.018.

[93] Daniyanto, Sutidjan, Deendarlianto, Budiman A. Torrefaction of Indonesian sugar-cane bagasse to improve bio-syngas quality for gasification process. Energy Procedia 2015;68:157–66. doi:10.1016/j.egypro.2015.03.244.

[94] Repellin V, Govin A, Rolland M, Guyonnet R. Energy requirement for fine grinding of torrefied wood. Biomass and Bioenergy 2010;34:923–30. doi:10.1016/j.biombioe.2010.01.039.

[95] Colin B, Dirion J-L, Arlabosse P, Salvador S. Quantification of the torrefaction effects on the grindability and the hygroscopicity of wood chips. Fuel 2017;197:232–9. doi:10.1016/j.fuel.2017.02.028.

[96] Nachenius RW, van de Wardt TA, Ronsse F, Prins W. Torrefaction of pine in a bench-scale screw conveyor reactor. Biomass and Bioenergy 2014;79:96–104. doi:10.1016/j.biombioe.2015.03.027.

[97] Rudolfsson M, Borén E, Pommer L, Nordin A, Lestander TA. Combined effects of torrefaction and pelletization parameters on the quality of pellets produced from torrefied biomass. Appl Energy 2017;191:414–24. doi:10.1016/j.apenergy.2017.01.035.

[98] Bai X, Wang G, Gong C, Yu Y, Liu W, Wang D. Co-pelletizing characteristics of torrefied wheat straw with peanut shell. Bioresour Technol 2017;233:373–81. doi:10.1016/j.biortech.2017.02.091.

[99] Arteaga-Pérez LE, Grandón H, Flores M, Segura C, Kelley SS. Steam torrefaction of Eucalyptus globulus for producing black pellets: A pilot-scale experience. Bioresour Technol 2017;238:194–204. doi:10.1016/j.biortech.2017.04.037.

[100] Chai L, Saffron CM. Comparing pelletization and torrefaction depots: Optimization of depot capacity and biomass moisture to determine the minimum production cost. Appl Energy 2016;163:387–95. doi:10.1016/j.apenergy.2015.11.018.

[101] Araújo S, Boas MAV, Neiva DM, de Cassia Carneiro A, Vital B, Breguez M, et al. Effect of a mild torrefaction for production of eucalypt wood briquettes under different compression pressures. Biomass and Bioenergy 2016;90:181–6. doi:10.1016/j.biombioe.2016.04.007.

[102] Rudolfsson M, Stelte W, Lestander TA. Process optimization of combined biomass torrefaction and pelletization for fuel pellet production - A parametric study. Appl Energy 2015;140:378–84. doi:10.1016/j.apenergy.2014.11.041.

[103] Cao L, Yuan X, Li H, Li C, Xiao Z, Jiang L, et al. Complementary effects of torrefaction and co-pelletization: Energy consumption and characteristics of pellets. Bioresour Technol 2015;185:254–62. doi:10.1016/j.biortech.2015.02.045.

[104] Reza MT, Uddin MH, Lynam JG, Coronella CJ. Engineered pellets from dry torrefied and HTC biochar blends. Biomass and Bioenergy 2014;63:229–38. doi:10.1016/j.biombioe.2014.01.038.

[105] Nicksy D, Pollard A, Strong D, Hendry J. In-situ torrefaction and spherical pelletization of partially pre-torrefied hybrid poplar. Biomass and Bioenergy 2014;70:452–60. doi:10.1016/j.biombioe.2014.08.011.

[106] Peng J, Bi XT, Lim CJ, Peng H, Kim CS, Jia D, et al. Sawdust as an effective binder for making torrefied pellets. Appl Energy 2014;157:491–8. doi:10.1016/j.apenergy.2015.06.024.

[107] Prins MJ, Ptasinski KJ, Janssen FJJ. More efficient biomass gasification via torrefaction. Energy 2006;31:3458–70. doi:10.1016/j.energy.2006.03.008.

[108] Granados DA, Velásquez HI, Chejne F. Energetic and exergetic evaluation of residual biomass in a torrefaction process. Energy 2014;74:181–9. doi:10.1016/j.energy.2014.05.046.

[109] Nanou P, Carbo MC, Kiel JHA. Detailed mapping of the mass and energy balance of a continuous biomass torrefaction plant. Biomass and Bioenergy 2016. doi:10.1016/j.biombioe.2016.02.012.

[110] Yan W, Hastings JT, Acharjee TC, Coronella CJ, Vásquez VR. Mass and Energy Balances of Wet Torrefaction of Lignocellulosic Biomass †. Energy & Fuels 2010;24:4738–42. doi:10.1021/ef901273n.

[111] Chen YC, Chen WH, Lin BJ, Chang JS, Ong HC. Impact of torrefaction on the composition, structure and reactivity of a microalga residue. Appl Energy 2016;181:110–9. doi:10.1016/j.apenergy.2016.07.130.

[112] Zhang S, Dong Q, Zhang L, Xiong Y. Effects of water washing and torrefaction on the pyrolysis behavior and kinetics of rice husk through TGA and Py-GC/MS. Bioresour Technol 2016;199:352–61. doi:10.1016/j.biortech.2015.08.110.

[113] Rodriguez Alonso E, Dupont C, Heux L, Da Silva Perez D, Commandre JM, Gourdon C. Study of solid chemical evolution in torrefaction of different biomasses through solid-state 13C cross-polarization/magic angle spinning NMR (nuclear magnetic resonance) and TGA (thermogravimetric analysis). Energy 2016;97:381–90. doi:10.1016/j.energy.2015.12.120.

[114] Kihedu J. Torrefaction and Combustion of Ligno-Cellulosic Biomass. Energy Procedia 2015;75:162–7. doi:10.1016/j.egypro.2015.07.273.

[115] Wilk M, Magdziarz A, Kalemba I. Characterisation of renewable fuels' torrefaction process with different instrumental techniques. Energy 2015;87:259–69. doi:10.1016/j.energy.2015.04.073.

[116] Pushkin SA, Kozlova L V., Makarov AA, Grachev AN, Gorshkova TA. Cell wall components in torrefied softwood and hardwood samples. J Anal Appl Pyrolysis 2015;116:102–13. doi:10.1016/j.jaap.2015.09.020.

[117] Ren S, Lei H, Wang L, Bu Q, Chen S, Wu J. Thermal behaviour and kinetic study for woody biomass torrefaction and torrefied biomass pyrolysis by TGA. Biosyst Eng 2013;116:420–6. doi:10.1016/j.biosystemseng.2013.10.003.

[118] Ma F, Zeng Y, Wang J, Yang Y, Yang X, Zhang X. Thermogravimetric study and kinetic analysis of fungal pretreated corn stover using the distributed activation energy model. Bioresour Technol 2013;128:417–22. doi:10.1016/j.biortech.2012.10.144.

[119] Burhenne L, Messmer J, Aicher T, Laborie M-P. The effect of the biomass components lignin, cellulose and hemicellulose on TGA and fixed bed pyrolysis. J Anal Appl Pyrolysis 2013:1–8. doi:10.1016/j.jaap.2013.01.012.

[120] Gao W, Chen K, Xiang Z, Yang F, Zeng J, Li J, et al. Kinetic study on pyrolysis of tobacco residues from the cigarette industry. Ind Crops Prod 2013;44:152–7. doi:10.1016/j.indcrop.2012.10.032.

[121] Kebelmann K, Hornung A, Karsten U, Griffiths G. Intermediate pyrolysis and product identification by TGA and Py-GC/MS of green microalgae and their extracted protein and lipid components. Biomass and Bioenergy 2013;49:38–48. doi:10.1016/j.biombioe.2012.12.006.

[122] Amutio M, Lopez G, Aguado R, Artetxe M, Bilbao J, Olazar M. Kinetic study of lignocellulosic biomass oxidative pyrolysis. Fuel 2012;95:305–11. doi:10.1016/j.fuel.2011.10.008.

[123] Worasuwannarak N, Wannapeera J, Fungtammasan B. Pyrolysis behaviors of woody biomass torrefied at temperatures below 300°C. 2011 IEEE Conf Clean Energy Technol 2011:287–90. doi:10.1109/CET.2011.6041498.

[124] Zanzi R, Ferro D, Torres A, Beaton P, Björnbom E. Biomass torerfaction n.d.:1–4.

[125] Bjorck–c C. Mini-project report Torrefaction of Biomass. 2012.

[126] Chen W-H, Du S-W, Tsai C-H, Wang Z-Y. Torrefied biomasses in a drop tube furnace to evaluate their utility in blast furnaces. Bioresour Technol 2012;111:433–8. doi:10.1016/j.biortech.2012.01.163.

[127] Jaafar A, Ahmad M. Torrefaction of Malaysian Palm Kernel Shell into Value-Added Solid Fuels. World Acad Sci Eng Technol 2011;60:554–7.

[128] Dhungana A, Dutta A, Basu P. Torrefaction of non -lignocellulose biomass waste. Can J Chem Eng 2012;90:186–95. doi:10.1002/cjce.20527.

[129] Wang S, Guo X, Wang K, Luo Z. Influence of the interaction of components on the pyrolysis behavior of biomass. J Anal Appl Pyrolysis 2011;91:183–9. doi:10.1016/j.jaap.2011.02.006.

[130] Patwardhan PR, Dalluge DL, Shanks BH, Brown RC. Distinguishing primary and secondary reactions of cellulose pyrolysis. Bioresour Technol 2011;102:5265–9. doi:10.1016/j.biortech.2011.02.018.

[131] Shen DK, Gu S, Bridgwater AV. Study on the pyrolytic behaviour of xylan-based hemicellulose using TG–FTIR and Py–GC–FTIR. J Anal Appl Pyrolysis 2010;87:199–206. doi:10.1016/j.jaap.2009.12.001.

[132] Shen DK, Gu S, Bridgwater a. V. The thermal performance of the polysaccharides extracted from hardwood: Cellulose and hemicellulose. Carbohydr Polym 2010;82:39–45. doi:10.1016/j.carbpol.2010.04.018.

[133] Broido a., Nelson M a. Char yield on pyrolysis of cellulose. Combust Flame 1975;24:263–8. doi:10.1016/0010-2180(75)90156-X.

[134] Shafizadeh F, Fu Y. Pyrolysis of cellulose. Carbohydr Res 1973;29:113–22.

[135] Di Blasi C, Lanzetta M. Intrinsic kinetics of isothermal xylan degradation in inert atmosphere. J Anal Appl Pyrolysis 1997;40–41:287–303. doi:10.1016/S0165-2370(97)00028-4.

[136] Granados DA, Basu P, Chejne F, Nhuchhen DR. Detailed Investigation into Torrefaction of Wood in a Two-Stage Inclined Rotary Torrefier. Energy & Fuels 2016:acs.energyfuels.6b02524. doi:10.1021/acs.energyfuels.6b02524.

[137] Granados DA, Basu P, Chejne F. Biomass Torrefaction in a Two-Stage Rotary Reactor: Modeling and Experimental Validation. Energy & Fuels 2017:acs.energyfuels.7b00653. doi:10.1021/acs.energyfuels.7b00653.

[138] Nachenius RW, Van De Wardt TA, Ronsse F, Prins W. Residence time distributions of coarse biomass particles in a screw conveyor reactor. Fuel Process Technol 2015;130:87–95.

doi:10.1016/j.fuproc.2014.09.039.

[139] Chang S, Zhao Z, Zheng A, He F, Huang Z, Li H. Characterization of products from torrefaction of sprucewood and bagasse in an auger reactor. Energy and Fuels, vol. 26, American Chemical Society; 2012, p. 7009–17. doi:10.1021/ef301048a.

[140] Huang Y-F, Cheng P-H, Chiueh P-T, Lo S-L. Leucaena biochar produced by microwave torrefaction: Fuel properties and energy efficiency. Appl Energy 2017. doi:10.1016/j.apenergy.2017.03.007.

[141] Huang YF, Chen WR, Chiueh PT, Kuan WH, Lo SL. Microwave torrefaction of rice straw and Pennisetum. Bioresour Technol 2012;123:1–7. doi:10.1016/j.biortech.2012.08.006.

[142] Huang Y-F, Sung H-T, Chiueh P-T, Lo S-L. Microwave torrefaction of sewage sludge and leucaena. J Taiwan Inst Chem Eng 2017;70:236–43. doi:10.1016/j.jtice.2016.10.056.

[143] Wang MJ, Huang YF, Chiueh PT, Kuan WH, Lo SL. Microwave-induced torrefaction of rice husk and sugarcane residues. Energy 2012;37:177–84. doi:10.1016/j.energy.2011.11.053.

[144] Bach QV, Chen WH, Lin SC, Sheen HK, Chang JS. Wet torrefaction of microalga Chlorella vulgaris ESP-31 with microwave-assisted heating. Energy Convers Manag 2016. doi:10.1016/j.enconman.2016.07.035.

[145] Ren S, Lei H, Wang L, Yadavalli G, Liu Y, Julson J. The integrated process of microwave torrefaction and pyrolysis of corn stover for biofuel production. J Anal Appl Pyrolysis 2014;108:248–53. doi:10.1016/j.jaap.2014.04.008.

[146] Satpathy SK, Tabil LG, Meda V, Naik SN, Prasad R. Torrefaction of wheat and barley straw after microwave heating. Fuel 2014;124:269–78. doi:10.1016/j.fuel.2014.01.102.

[147] Chen WH, Ye SC, Sheen HK. Hydrothermal carbonization of sugarcane bagasse via wet torrefaction in association with microwave heating. Bioresour Technol 2012;118:195–203. doi:10.1016/j.biortech.2012.04.101.

[148] Ren S, Lei H, Wang L, Bu Q, Wei Y, Liang J, et al. Microwave Torrefaction of Douglas Fir Sawdust Pellets. Energy & Fuels 2012;26:5936–43. doi:10.1021/ef300633c.

[149] Antal J. Mathematical modelling of biomass pyrolysis phenomena. Fuel 1985;64:1483–6.

[150] Bilbao R, Millera A, Arauzo J. Kinetics of weight loss by thermal decomposition of xylan and lignin. Influence of experimental conditions. Thermochim Acta 1989;143:137–48.

[151] Williams P., Besler S. Thermogravimetric Analysis of the Components of Biomass. Adv Thermochem Biomass Convers 1993:771–83.

[152] Órfao J, Figueiredo J. A simplified method for determination of lignocellulosic materials pyrolysis kinetics from isothermal thermogravimetric experiments. Thermochim Acta 2001;380:67–78.

[153] Chen W-H, Kuo P-C. Isothermal torrefaction kinetics of hemicellulose, cellulose, lignin and xylan using thermogravimetric analysis. Energy 2011;36:6451–60. doi:10.1016/j.energy.2011.09.022.

[154] Kilzer F, Broido A. Speculations on the Nature of Cellulose Pyrolysis. Pyrodynamics 1965;2:151–63.

[155] Broido A, Weinstein M. kinetocs of Solid-phase Cellulose. Proc 3rd Int Conf Therm Anal 1972:285–96.

[156] Bradbury AGW, Sakai Y, Shafizadeh F. A kinetic model for Pyrolysis of Cellulose. J Appl Polym Sci 1979;23:3271–80. doi:10.1002/app.1979.070231112.

[157] Varhegyi G, Jakab E, Antal M. Is the Broido-Shafizadeh Model for Cellulose Pyrolysis True?? Energy & Fuels 1994;8:1345–52.

[158] Banyasz JL, Li S, Lyons-Hart JL, Shafer KH. Cellulose pyrolysis: the kinetics of hydroxyacetaldehyde evolution. J Anal Appl Pyrolysis 2001;57:223–48. doi:10.1016/S0165-2370(00)00135-2.

[159] Wooten JB, Seeman JI, Hajaligol MR. Observation and Characterization of Cellulose Pyrolysis Intermediates by 13C CPMAS NMR. A New Mechanistic Model. Energy & Fuels 2004;18:1–15.

[160] Lédé J, Blanchard F, Boutin O. Radiant Flash pyrolysis of cellulose pellets : products and mechanisms involved in transient and steady state conditions. Fuel 2002;81:1269–79.

[161] Piskorz J, Radlein D, Scott DS. On the mechanism of the rapid pyrolysis of cellulose. J Anal Appl Pyrolysis 1986;9:121–37. doi:10.1016/0165-2370(86)85003-3.

[162] Diebold JP. A unified, global model for the pyrolysis of cellulose. Biomass and Bioenergy 1994;7:75–85. doi:10.1016/0961-9534(94)00039-V.

[163] Mamleev V, Bourbigot S, Yvon J. Kinetic analysis of the thermal decomposition of cellulose: The main step of mass loss. J Anal Appl Pyrolysis 2007;80:151–65. doi:10.1016/j.jaap.2007.01.013.

[164] Stamm A. Thermal degradation of wood and cellulose. Ind Eng Chem 1956;48:413–7.

[165] Ramiah M. Thermogravimetric and Differential Thermal Analysis of. J Appl Polym Sci 1970;14:1323–37.

[166] Min K. Vapor-phase thermal analysis of pyrolysis products from cellulosic materials. Combust Flame 1977;30:285–94. doi:10.1016/0010-2180(77)90077-3.

[167] Williams PT, Besler S. The pyrolysis of rice husks in a thermogravimetric analyser and static batch reactor. Fuel 1993;72:151–9. doi:10.1016/0016-2361(93)90391-E.

[168] Koufopanos C., Maschio G, Lucchesi A. Kinetic modelling of the pyrolysis of biomass and biomass components. Can J Chem Eng 1989;67:75–84.

[169] Shafizadeh F. Introduction to pyrolysis of biomass. J Anal Appl Pyrolysis 1982;3:283–305.

[170] Shafizadeh F, Bradbury G. Thermal degradation od cellulose and air and nitrogen at low temperatures. J Appl Polym Sci 1979;23:1431–42.

[171] Ward SM, Braslaw J. Experimental weight loss kinetics of wood pyrolysis under vacuum. Combust Flame 1985;61:261–9. doi:10.1016/0010-2180(85)90107-5.

[172] Varhegyi G, Antal J, Szekely T, Szabo P. Kinetics of the thermal decomposition of cellulose, hemicellulose, and sugarcane bagasse. Energy & Fuels 1989;3:329–35.

[173] Tang W. Effect of Inorganic Salts o n Pyrolysis of Wood , Alpha-Cellulose and Lignin Determined by Dynamic Thermogravimetry. Madison, Wisconsin: 1967.

[174] Nunn TR, Howard JB, Longwell JP, Peters WA. Product Compositions and Kinetics in the Rapid Pyrolysis of MiHed Wood Lignin. Ind Eng Chem Process Des Dev 1985;24:844–52.

[175] Domínguez JC, Oliet M, Alonso MV, Gilarranz MA, Rodríguez F. Thermal stability and pyrolysis kinetics of organosolv lignins obtained from Eucalyptus globulus. Ind Crops Prod 2008;27:150–6. doi:10.1016/j.indcrop.2007.07.006.

[176] Liu Q, Wang S, Zheng Y, Luo Z, Cen K. Mechanism study of wood lignin pyrolysis by using TG–FTIR analysis. J Anal Appl Pyrolysis 2008;82:170–7. doi:10.1016/j.jaap.2008.03.007.

[177] Rogers F., Ohlemiller T. Cellulosic Insulation Material I. Overall Degradation Kinetics and Reaction Heats. Combust Sci Technol 1980;24:129–37.

[178] Thurner F, Mann U. Kinetic Investigation of Wood Pyrolysis. Ind Eng Chem Process Des Dev 1981;20:482–8.

[179] Di Blasi C, Branca C. Kinetics of Primary Product Formation from Wood Pyrolysis. Ind Eng Chem Res 2001;40:5547–56. doi:10.1021/ie000997e.

[180] Shafizadeh F, Chin PPS. Thermal Deterioration of Wood. ACS Symp. Ser., Washington: 1977, p. 57–81.

[181] Chan WC., Kelbon M, Krieger BB. Modelling and experimental verification of physical and chemical processes during pyrolysis of a large biomass particle. Fuel 1985;64:1505–13.

[182] Wagenaar B., Prins W, Swaaij W. Flash Pyrolysis Kinetics of Pine Wood. Fuel Process Technol 1993;36:291–8.

[183] Branca C, Di Blasi C. Kinetics of the isothermal degradation of wood in the temperature range 528–708 K. J Anal Appl Pyrolysis 2003;67:207–19. doi:10.1016/S0165-2370(02)00062-1.

[184] Di Blasi C. Modeling and Simulation of Combustion Processes of Charring and Non-charring Solid Fuels. Prog Energy Combust Sci 1993;19:71–104.

[185] Park WC, Atreya A, Baum HR. Experimental and theoretical investigation of heat and mass transfer processes during wood pyrolysis. Combust Flame 2010;157:481–94. doi:10.1016/j.combustflame.2009.10.006.

[186] Rousset P, Turner I, Donnot A, Perré P. Choix d'un modèle de pyrolyse ménagée du bois à l'échelle de la microparticule en vue de la modélisation macroscopique. Ann For Sci 2006;63:213–29. doi:10.1051/forest.

[187] Wang G, Li W, Li B, Chen H. TG study on pyrolysis of biomass and its three components under syngas. Fuel 2008;87:552–8. doi:10.1016/j.fuel.2007.02.032.

[188] Hosoya T, Kawamoto H, Saka S. Pyrolysis behaviors of wood and its constituent polymers at gasification temperature. J Anal Appl Pyrolysis 2007;78:328–36. doi:10.1016/j.jaap.2006.08.008.

[189] Shen D. The pyrolytic mechanism of the main components in woody biomass and their interactions. University of Southampton, 2011.

[190] Ratte J, Fardet E, Mateos D, Héry J-S. Mathematical modelling of a continuous biomass torrefaction reactor: TORSPYD$^{TM}$ column. Biomass and Bioenergy 2011;35:3481–95. doi:10.1016/j.biombioe.2011.04.045.

[191] Bates RB, Ghoniem AF. Biomass torrefaction: modeling of volatile and solid product evolution kinetics. Bioresour Technol 2012;124:460–9. doi:10.1016/j.biortech.2012.07.018.

[192] Shi X, Ronsse F, Pieters JG. Space-time integral method for simplifying the modeling of torrefaction of a centimeter-sized biomass particle. J Anal Appl Pyrolysis 2017;124:486–98. doi:10.1016/j.jaap.2017.02.009.

[193] Park C, Zahid U, Lee S, Han C. Effect of process operating conditions in the biomass torrefaction: A simulation study using one-dimensional reactor and process model. Energy 2015;79:127–39. doi:10.1016/j.energy.2014.10.085.

[194] Granados DA, Chejne F, Basu P. A two dimensional model for torrefaction of large biomass particles. J Anal Appl Pyrolysis 2016. doi:10.1016/j.jaap.2016.02.016.

[195] Koufopanos C., Papayannakos N, Maschio G, Lucchesi A. Modelling of the pyrolysis of biomass particles. Studies on kinetics, thermal and heat transfer effects. Can J Chem Eng 1991;69:907–15. doi:10.1002/cjce.5450690413.

[196] Mousquès P, Dirion J, Grouset D. Modeling of solid particles pyrolysis. J Anal Appl Pyrolysis 2001;59:733–45.

[197] Dufour A, Ouartassi B, Bounaceur R, Zoulalian A. Modelling intra-particle phenomena of biomass pyrolysis. Chem Eng Res Des 2011;89:2136–46. doi:10.1016/j.cherd.2011.01.005.

[198] Peters B. Validation of a numerical approach to model pyrolysis of biomass and assessment of kinetic data. Fuel 2011;90:2301–14. doi:10.1016/j.fuel.2011.02.003.

[199] Haseli Y, van Oijen J a., de Goey LPH. Modeling biomass particle pyrolysis with temperature-dependent heat of reactions. J Anal Appl Pyrolysis 2011;90:140–54. doi:10.1016/j.jaap.2010.11.006.

[200] Lam KL, Oyedun AO, Hui CW. Experimental and Modelling Studies of Biomass Pyrolysis. Chinese J Chem Eng 2012;20:543–50. doi:10.1016/S1004-9541(11)60217-6.

[201] Mehrabian R, Scharler R, Obernberger I. Effects of pyrolysis conditions on the heating rate in biomass particles and applicability of TGA kinetic parameters in particle thermal conversion modelling. Fuel 2012;93:567–75. doi:10.1016/j.fuel.2011.09.054.

[202] Blasi C Di. Physico-chemical processes occurring inside a degrading two-dimensional anisotropic porous medium. Int J Heat Mass Transf 1998;41:4139–50. doi:10.1016/S0017-9310(98)00142-2.

[203] Felfli F, Luengo C, Soler P, Rocha J. Mathematical modelling of wood and briquettes torrefaction. Procedings 5th Encontro Energ. no Meio Rural, Campinas: 2004, p. 1–9.

[204] Ratte J, Marias F, Vaxelaire J, Bernada P. Mathematical modelling of slow pyrolysis of a particle of treated wood waste. J Hazard Mater 2009;170:1023–40. doi:10.1016/j.jhazmat.2009.05.077.

[205] Withaker S. Simultaneous heat, mass and momentum transfer in porous media. A theory of drying porous media. Adv Heat Transf 1977;13:119–203.

[206] Turner I, Rousset P, Rémond R, Perré P. An experimental and theoretical investigation of the thermal treatment of wood (Fagus sylvatica L.) in the range 200–260°C. Int J Heat Mass Transf 2010;53:715–25. doi:10.1016/j.ijheatmasstransfer.2009.10.020.

[207] Perré P, Turner I. A 3-D version of TransPore: a comprehensive heat and mass transfer

computational model for simulating the drying of porous media. Int J Heat Mass Transf 1999;42:4501–21.

[208] Pétrissans a., Younsi R, Chaouch M, Gérardin P, Pétrissans M. Experimental and numerical analysis of wood thermodegradation. J Therm Anal Calorim 2011;109:907–14. doi:10.1007/s10973-011-1805-1.

# Chapter 2. Energetic and Exergetic Evaluation of Residual Biomass in a Torrefaction Process

**(Paper published in Energy Journal)**


## Abstract

Torrefaction test in a TGA (Termo-gravimeter analyzer) for six different types of residual biomass (sugarcane bagasse, banana rachis, rice husk, palm oil fiber, sawdust and coffee waste) was developed in this work. These six materials were evaluated before and after torrefaction process through HHV (High Heating Value), and energetic and exergetic balances to find a promising solid fuel biomass for a torrefaction process. Torrefaction is a thermal process performed in an inert atmosphere at temperatures between 200 and 300°C, with residence times lower than 60min and heating rates lower than 20°C/min. Its aim is to improve a biomass as a solid fuel. In this processing, the lignocellulosic components are degraded (hemicellulose and cellulose are more degraded than lignin), having as result a biomass with a predominant amount of lignin. In this work, the torrefaction process was carried out at a temperature of 250°C in an inert atmosphere with 10°C/min of heating rate and a residence time of 30 min. As a result, it was found that the biggest and lowest increases in HHV for torrefied biomass were14.5% and 5.2% for sawdust and palm oil fiber, respectively. Sawdust was found to have the best performance in the torrefaction process evaluated from the energy yield parameter but rice husk was the best biomass in the energetic balances of the process. Energy and exergy balances show that palm oil fiber and banana rachis are the least efficient biomass in the torrefaction process.


**Keywords:** Torrefaction, energy balances, residual biomass, exergy balances, energy yield, HHV.

## 2.1. Introduction

Biomass is a promising source of solid fuels that compete with fossil fuels like oil and coal because of its low emission of greenhouse gases and its acceptable performance in thermal processes. Despite the benefits of using biomass in thermal processes, its implementation has a major limitation for projects involving high biomass flows. High humidity and low biomass density reduces the feasibility of the projects as the projects' size increases. This is due to the high cost associated with the transport of large amounts of biomass. It is for this reason that only small and medium scale projects may become the only option for obtaining economic benefits from the transformation of thermal biomass.

The torrefaction process is carried out in inert atmospheres or low amounts of oxygen at temperatures in the range of 200-300 °C and low heating rates (<20 °C/min) [1]. During the torrefaction process a mass loss of up to 40% and an energy loss between 5-10% are registered for the biomass and a HHV is generated [2–4]. Different authors in the literature have experimentally evaluated the performance of biomass when it is subjected to a torrefaction process with variations in operating parameters [5,6], have evaluated the kinetics to suggest reaction mechanisms [7], and have evaluated the torrefied biomass in a combustion process[8–10], gasification[10–12]and

crushing [13–15] to improve the process or the performance of the biomass. In addition to the above experimental studies, other approaches such as developing process models [16,17], mass and energy balances that provide information on process feasibility [18–20] and some cost analysis can be found in the literature [21,22].

Bourgois et al. [5] examined the effect of a thermal process at 260°C in an inert atmosphere on a pine biomass. Residence times were varied between 15 min and 4 hours. The gases generated in the process were examined by chromatography, finding the dominant presence of non-condensable components such as CO, $CO_2$, $O_2$ and $N_2$.. The authors concluded that CO generation is instantaneous, so that $CO_2$ generation is not a product of CO combustion. The torrefied solid was analyzed by monitoring its weight during torrefaction and by ultimate and proximate analysis. In these tests, it was found that when the residence time varies between 15 minutes and 4 hours, the mass (20 - 50%), the amount of hydrogen (0.2 - 19%) and the amount of oxygen of the biomass (5 - 40%) decrease. In contrast, the amount of carbon in the torrefied material (4 - 33%) and lignin (30 - 200%) increase when the residence time increases. In general, the torrefaction process produces an increase in the biomass HHV of up to 44% and improves hydrophobic characteristics that directly impact the lifetime of the material. These tests were performed only at a process temperature, and the heating rate of the biomass or the particle size used is not mentioned in the article, leaving unrevealed much of the behavior of the material when the temperature and other parameters, such as the fraction of oxygen in the process, are modified. These tests were not conducted under experimental design so they only evaluated the impact of a parameter in the process and, therefore, the effect of the other variables in the results cannot be concluded with certainty.

In a later work, Bourgois et al. [6] performed experimental tests similar to those of previous work [5], with the same operating parameters unspecified such as particle size and heating rates and with the difference that the residence time was kept constant and the temperature varied in the range of 240 to 290°C. The trends found in the behavior of parameters, such as mass loss, oxygen, hydrogen and lignin, were very similar to those found in previous work. It is noteworthy that the same shortcomings noted in previous work were evidenced again.

Pentananunt et al. [2] evaluated the final characteristics of the torrefied biomass such as proximate and ultimate analysis, and density, but with an additional component corresponding to the performance analysis of the material roasted in a combustion process. In the torrefaction tests, the temperature and residence times were varied from 250 to 270°C and 2 to 3 hours, respectively. This study found similar results to those found in the works of Bourgois et al. [5], [6] in terms of the reduction of hydrogen and oxygen, and increased carbon when the process temperature and the residence time increase. In the combustion tests conducted with torrefied wood and charcoal, the findings were that torrefied biomass shows better performance because it generates less dense smoke, less soot and higher speeds in combustion than virgin biomass. The study does not mention the type of wood used for the torrefaction process.

W-H Chen et al. [23,24] evaluated the torrefaction process in a TGA with four kinds of biomasses with the aim to study the behavior of lignocellulosic structure after thermal process. In this work it was found that hemicellulose is almost completely decomposed, but cellulose and lignin are

partially decomposed. They also studied the kinetics of cellulose, hemicelluloses and lignin for different temperatures in an isothermal torrefaction process [23]. They found the kinetic parameter for different ranges of temperature and proposed a reaction order for each reaction in the components. Additionally, they propose a model to predict biomass decomposition from the decomposition of each component. This model has been controverted by different authors because neither synergic effects nor the catalytic effect of ash are considered.

Fisher et al. [10] performed torrefaction tests with willow wood with sizes ranging between 5.6 and 9.5 mm in order to evaluate its performance during the combustion and gasification process. The torrefaction is carried out with heating rates of 5°C/min from room temperature to 150°C and maintained there for 45 minutes. Subsequently, the heating continues with the same heating rate until reaching the process temperature which varies between 270 and 290°C and it is maintained at this temperature for between 38 and 41 minutes. Differences in reactivity during the combustion and gasification between torrefied biomass and virgin biomass have been found. The difference in reactivities between these biomasses with longer residence times and higher processing temperatures was evident.

S-W Park et al. [25] evaluated the performance of a torrefied biomass with different operational conditions in a torrefaction process, and in a co-combustion process with coal. In this work low-temperature and several torrefaction processes were developed and blended later with coal for co-combustion tests. The biomass with several torrefaction processes was more reactive than the low-torrefied biomass. This behavior is due to the complete decomposition of some components like hemicelluloses and cellulose in the pre-treatment process because, during combustion process, some shoulders are seen for low-temperature torrefied biomass due to the components that were not decomposed in the torrefaction process.

Repellin et al. [14] evaluated the performance of torrefied biomass in terms of energy consumption in a shredding process. The torrefaction process was carried out with biomass pellets, varying residence time (5 - 60min) and process temperatures (180 - 260 °C), and subsequently crushing the pellets in a ball mill to a particle size of less than 200μm. Once this particle size was reached, the energy consumed in the grinding process was measured and compared with other virgin and torrefied biomasses with different operating conditions. It was found that with biomass torrefied at higher temperatures significant reductions (93%) in energy consumption can be obtained.

Some authors have addressed the issue of biomass torrefaction by performing mass, energy and exergy balances, trying to add its energy and exergy viability to the obvious benefits of the process.

Prins et al. [18] evaluated the torrefaction process bound to a gasification process. To carry out the analysis of torrefied biomass performance under different operating conditions, different configurations were evaluated combining the torrefaction processes and gasification. One of the tested combinations considers the use of volatiles produced in the torrefaction as an energy part of the gasification. After an exergetic analysis of the different configurations, the authors concluded that when a torrefaction pretreatment is linked to the gasification process, where part of the energy of the process is provided by the exhaust gases and volatiles from the gasification process and torrefaction, respectively, it is possible to improve the performance of the biomass in the

gasification process as well as the overall efficiency of the process. These analyses were conducted theoretically and, therefore, the authors suggest experimental verification.

Yan et al. [20] performed mass and energy balances for biomass torrefaction process under two different operating conditions and the same residence time. The torrefied biomass (pine) showed the trends highlighted by different authors in their experimental work when the temperatures increase. In these balances, the heats of reaction in each solid biomass were calculated and the authors concluded that these were totally independent from process temperatures.

Models have been developed trying to describe the torrefaction process. Ratte et al. [17] developed one of the most complete models found so far in the literature for biomass torrefaction process. This model considered two phases inside the reactor: a phase composed by biomass particles and a continuous phase composed of 11 species for the gas entering the reactor and generated in the process. The modeling process is for a continuous process and eight reactions were considered during the torrefaction process. Although the validations performed with experimental data have acceptable agreement with the results of the model, some simplifications in the simulations limited the accuracy of the results and forced the authors to improve them to increase the model's performance. One of the phenomena that occurs during the torrefaction process and which is not considered in the model is the condensation of condensable volatiles or tar generated in the process.

This work was focused on finding a potentially promising solid fuel from residual biomasses when they are treated thermally in a torrefaction process in TGA. For this purpose, the residual biomasses were torrefied at 250°C and 30 minutes of residence time and evaluated with energy and exergy analysis and energy experimental parameters.

## 2.2. Experimental Setup

Six biomasses were torrefied in a APT STA 1600 LINSEIS TGA located in the Energy Laboratory of the National University of Colombia of Medellín. All biomasses were dried at ambient temperature with an average temperature of 23°C and 400 $W/m^2$ of average solar radiation for 12 hours, and crushed to obtain a particle size of 150 µm (mesh 100). Two experimental runs were done for each biomass with 10 mg aproximately. The torrefaction process was developed in an inert atmosphere, and nitrogen was supplied at a rate of 50 ml/min. An initial heating until 110°C for 10 minutes, followed by heating until the process temperature of 250°C were developed. The material was kept for 30 minutes in this condition. The torrefaction tests were developed in a mild range according to Prins et al. [26,27] who found this condition as optimal for biomass. Both heatings were done with a heating rate of 10°C/min. A natural cooling was achieved until reaching ambient temperature for each biomass.

Two runs for each biomass were done and during the experimental runs the mass was monitored. An initial run without material was done with the aim to correct and eliminate errors by external effects in the thermo-gravimetric analysis. The experimental setup used for the thermal process is shown in Figure 2-1.

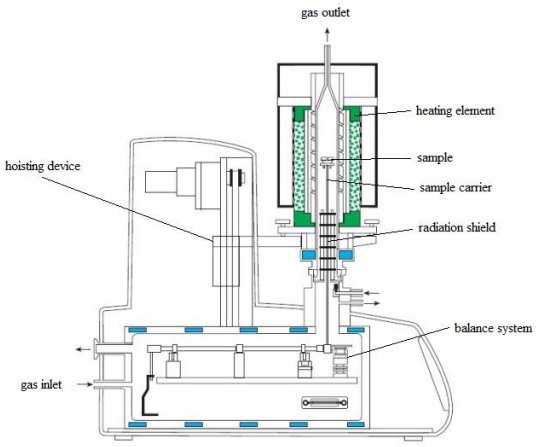


Figure 2-1. TGA scheme used in the experimental torrefaction process of biomass (250°C, 30 min)

All biomasses were characterized before thermal process by ultimate and proximate analysis, and HHV (Table 2-1 and Table 2-2). After the thermal process, all biomasses were characterized only by ultimate analysis (Table 2-2) because with the reduced amount of material the proximate analysis could not be done. All the information shown in the analysis is the average of three analyses done for each biomass. The HHV was obtained from ultimate analysis information through the empirical correlations for biomass suggested by Fried et al. [28]. This correlation is shown in equation (2-1) in which elemental amounts from ultimate analysis are used.

$$HHV(kJ/kg) = 3.55C^2 - 232C - 2230H + 51.2C*H + 131N + 20600 \quad (2\text{-}1)$$

Table 2-1.Ultimate analysis and theoretical HHV of raw biomass (% w/w)

| Biomass | C | H | N | O | Theoretical HHV (kJ/kg) |
|---|---|---|---|---|---|
| Palm oil fiber | 42.5±0.4 | 6.4±0.3 | 1.0±0.1 | 42.6±0.7 | 16953±899 |
| Banana rachis | 32.5±0.3 | 4.6±0.3 | 1.6±0.5 | 36.4±1.1 | 14388±969 |
| Sugarcane bagasse | 42.5±1.1 | 5.4±0.4 | 0.4±0.1 | 47.6±1.7 | 16267±1616 |
| Rice husk | 33.6±1.0 | 4.0±0.9 | 2.2±0.4 | 38.5±2.3 | 15047±2471 |
| Sawdust | 45.2±0.1 | 5.7±0.2 | 0.4±0.2 | 45.7±0.5 | 17936±590 |
| Coffee waste | 44.6±0.6 | 6.3±0.5 | 2.7±0.4 | 41.8±1.6 | 18012±1577 |

Table 2-2.Proximate analysis and experimental HHV of raw biomass (% w/w)

| Biomass | Moisture | Ash | Fixed Carbon | Volatiles | Experimental HHV (kJ/kg) |
|---|---|---|---|---|---|
| Palm oil fiber | 4.2±0.2 | 7.3±0.1 | 9.9±0.6 | 78.3±0.6 | 18448±172 |
| Banana rachis | 5.1±0.1 | 24.7±0.4 | 11.6±0.5 | 58.4±0.8 | 13479±92 |
| Sugarcane bagasse | 5.2±0.2 | 3.9±0.6 | 8.3±0.3 | 82.5±0.5 | 16920±340 |
| Rice husk | 5.1±0.1 | 21.5±0.2 | 17.1±0.4 | 56.5±0.4 | 14627±408 |
| Sawdust | 6.5±0.2 | 2.8±0.3 | 2.2±0.2 | 88.3±0.3 | 18503±660 |
| Coffee waste | 4.4±0.2 | 5.3±0.2 | 11.6±0.5 | 78.6±0.2 | 16412±537 |

As shown in Table 2-1 and Table 2-2, the differences between HHV calculated with correlation and experimental HHV are in a range of 420 – 1600 kJ/kg (2.8 to 9.7%). These differences will be considered to analyze the results after the thermal process.

## 2.3. Results

As mentioned in the previous chapter, the biomasses were heated at 10°C/min until a temperature of 110°C for 10 minutes and then heated again at 10°C/min until torrefaction process temperature of 250ºC and maintained at this temperature for 30 minutes. After process, the kiln was turned off and a natural cooling until room temperature was done for the biomass and, after this, the biomass was extracted. Ultimate analysis was done for the torrefied biomasses and the HHV was calculated according to the correlation mentioned above [28].

The mass loss in all runs was monitored and recorded with maximum errors of 5% between runs of the same material. The representative results of each run in the process are shown in Figure 2-2. In this figure, can be observed that 10 minutes for dry process is enough to remove the water in the biomass. All biomasses starts decomposition around 180-190ºC in the second heating process, which is in accordance with literature about decomposition temperatures of biomass components [29]. In this temperature range (180-190ºC) the hemicelluloses start their decomposition producing volatiles like $CO_2$, CO and low fractions of liquids like acetic acid [27]. In this decomposition, banana rachis, coffee waste and palm oil fiber present a fast mass loss probably due to a high amount of hemicellulose.

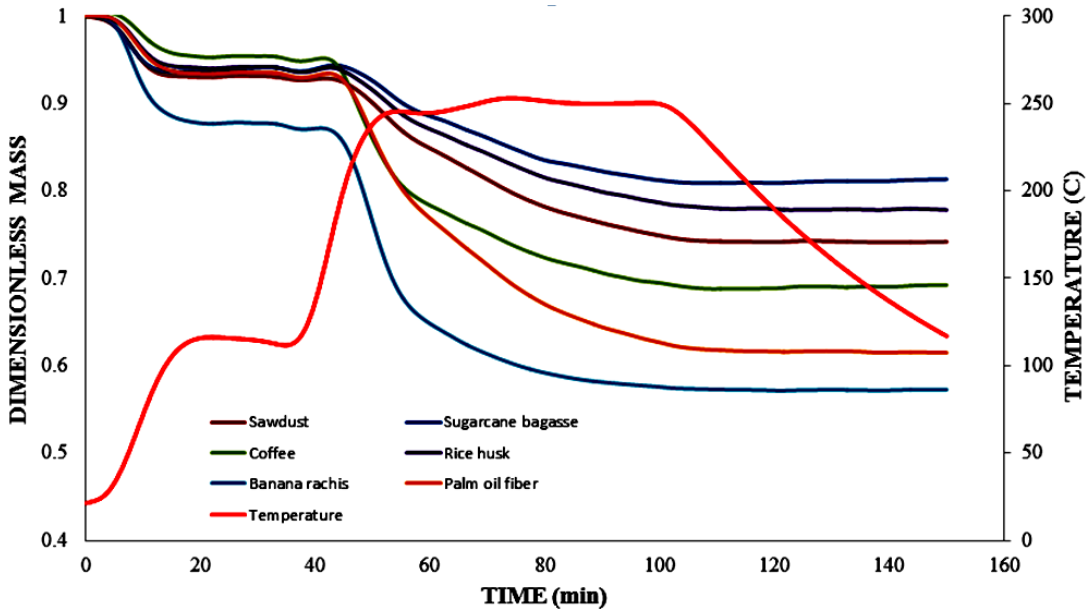


Figure 2-2. Mass loss during torrefaction process of biomass (250°C, 30 min)

The banana rachis was also dried at ambient temperature, but its moisture was higher than others (12% approximately) resulting in a larger mass loss in this material. As results of these experimental runs, sugarcane bagasse was the material that exhibited the least mass loss with around 13.5%, followed by rice husk and sawdust with 17% and 20%, respectively, neglecting the initial moisture. Coffee wastes, palm oil fiber and banana rachis were the materials with a high

mass loss of 27, 34 and 35%, respectively, neglecting the initial moisture. Figure 2-2 shows some slope changes during the process as result of the start of decomposition of cellulose and lignin, which are decomposed into smaller quantities than hemicelluloses. This fact is observed in the different slopes that are present in all the thermal process.

One of the main features in the torrefaction process is that mass loss is higher than energy loss, leading to a densification of biomass and increasing the HHV. Results of ultimate analyses for all torrefied biomasses (Table 2-3) are shown and their new HHVs were obtained using the above correlation (2-1) [28]. The values shown in Table 2-3 are the average of three analyses.

Table 2-3.Ultimate analysis for biomass torrefied at 250°C for 30 min (% w/w)

| Biomass | C | H | N | O | Theoretical HHV (kJ/kg) |
|---|---|---|---|---|---|
| Palm oil fiber | 44.3±3.7 | 4.1±0.3 | 2.9±0.3 | 41.1±1.5 | 17843±1216 |
| Banana rachis | 36.2±1.5 | 3.3±0.8 | 3.0±0.3 | 32.6±1.9 | 15970±2160 |
| Sugarcane bagasse | 44.0±2.4 | 4.1±0.5 | 1.1±0.2 | 46.7±1.7 | 17519±1735 |
| Rice husk | 40.0±0.9 | 4.3±0.1 | 1.3±0.1 | 32.7±1.1 | 16422±853 |
| Sawdust | 47.8±0.9 | 4.6±0.1 | 1.1±0.1 | 39.3±1.1 | 20534±706 |
| Coffee waste | 51.7±0.6 | 4. 8±0.3 | 3.2±0.4 | 35.6±1.3 | 20560±1138 |

A comparison between mass before and after the torrefaction process was developed to clarify the effect that the thermal process produces over lingocellulosic materials (Table 2-4). The HHV comparison was done with the theoretical ones to reduce the margin of error.

Table 2-4.Mass and HHV of biomass before and after the torrefaction process.

| Biomass | Solid HHV (KJ/kg) | | | Solid mass (mg) | | |
|---|---|---|---|---|---|---|
| | Inlet | Outlet | Increase (%) | Inlet | Outlet | Mass loss (%) |
| Palm oil fiber | 16953±899 | 17843±1216 | 5.2 | 10.83±0.01 | 6.6±0.01 | 38 |
| Banana rachis | 14388±969 | 15970±2160 | 11.0 | 10.58±0.01 | 6.0±0.01 | 42 |
| Sugarcane bagasse | 16267±1616 | 17519±1735 | 7.7 | 11.07±0.01 | 9.0±0.01 | 18 |
| Rice husk | 15047±2471 | 16422±853 | 9.1 | 10.63±0.01 | 8.2±0.01 | 22 |
| Sawdust | 17936±590 | 20534±706 | 14.5 | 10.43±0.01 | 7.7±0.01 | 25 |
| Coffee waste | 18012±1577 | 20560±1138 | 14.1 | 10.60±0.01 | 7.3±0.01 | 30 |

To clarify the effect generated by the torrefaction process, a bar graph illustrates the change in the HHV of the biomass before and after the process (Figure 2-3), and is clear that the thermal process generates better solids with higher HHV.

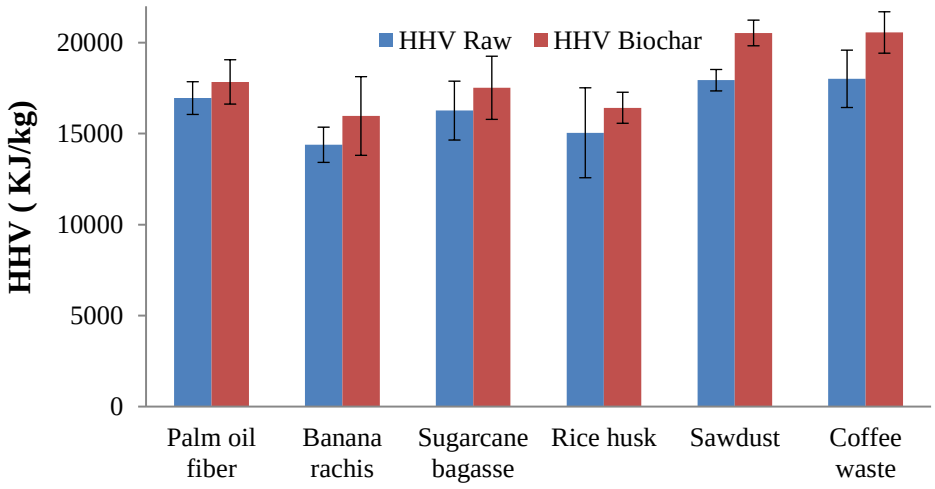


Figure 2-3. HHV of biomass before and after the torrefaction process

The biggest increase in the HHV of the biomasses evaluated was shown by sawdust with 14.5%, followed by coffee waste with 14.1%. The lowest increase in HHV was presented by the palm oil fiber with only 5.2%. Besides observing HHV increases, the loss of mass must be related to the analysis, to generate a parameter that relates HHV with mass and to obtain the energy available in the torrefied solid. This parameter is known as "*energy yield*" and is shown in equation (2-2). A graphical result is shown in Figure 2-4.

$$EnergyYield = \frac{Total\,Energy\,of\ torrefied\ biomass}{Total\,Energy\,of\ raw\,biomass} = \frac{HHV_{torrefied\,biomass} * Weight\,of\ torrefied\ biomass}{HHV_{raw\,biomass} * Weight\,of\ raw\,biomass} \quad (2\text{-}2)$$

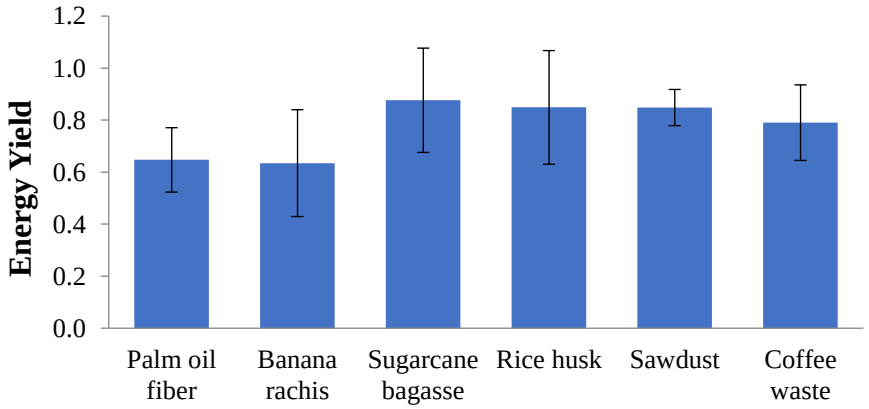


Figure 2-4. Energy yield for torrefaction process at temperature of 250°C for 30 min

The energy yield represents the available energy ratio between raw and torrefied biomass, and indicates a promissory biomass to be transformed in a torrefaction process. In this case, sugarcane

bagasse and sawdust are the promising biomasses to be transformed by a torrefaction process and obtain a solid fuel with better characteristics. Banana rachis had the lowest performance in the torrefaction process, showing only 0.63 in the energy yield parameter.

## 2.4. Mass and Energy balances

In a torrefaction process of biomass, gases, liquids and solids are obtained as main products. The main species in these products are $CO_2$ and CO, acid acetic and a torrefied solid, respectively [30]. To develop the mass and energy balances, the initial moisture in the biomass was separated, taken in separately as liquid water, and expelled of the process as steam water. The inert gas necessary for the process was considered in the process as additional specie in the balances. In order to simplify the mass and energy balances, the condensable and non-condensable gases were grouped into global specie called volatiles (Figure 2-5).

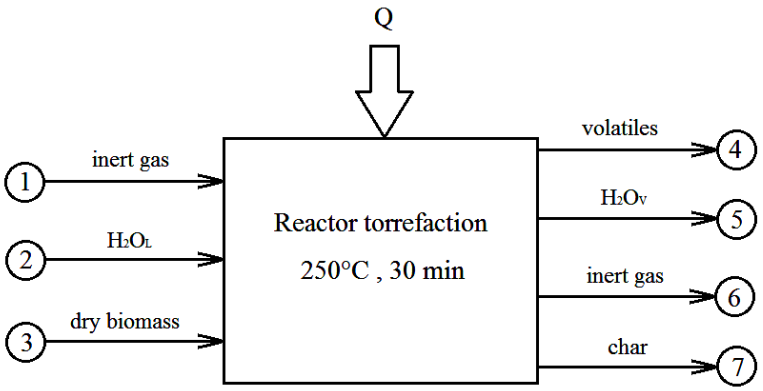


Figure 2-5. Mass and energy balance for torrefaction process at a temperature of 250°C for 30 min

With these products and flows known, the mass and energy balances can be performed. The HHV [28] and heat capacities [31]of raw and torrefied biomass were obtained from empirical correlations. The heat capacity of each biomass was found from the heat capacities of the elemental species in the solid state according to equation (2-3). It was necessary to express the biomass with a chemical expression of the elemental species ($C_xH_yO_z$).

$$c_p(J/mol*K) = (7.524*x) + (9.614*y) + (16.720*z) \quad (2\text{-}3)$$

The enthalpy of formation of raw and torrefied biomass for energy balances are calculated through the Hess law, having the calculated HHV (enthalpy of reaction) in a fictitious combustion reaction and the enthalpy of formation of products in this reaction according to equation (2-4). These enthalpies of formation, heats capacities and chemical formulas for all biomasses are shown in

Table 2-5 and Table 2-6. This methodology has also been used in some published works such as Wei Yan [20].

$$C_xH_yO_z(s) + \left(1 + \frac{y}{4} - \frac{z}{2}\right)O_2(g) \xrightarrow{\Delta H_R} CO_2(g) + \left(\frac{y}{2}\right)H_2O(L) \quad (2\text{-}4)$$

Table 2-5.Chemical formula, enthalpy capacity and enthalpy of formation for raw biomasses.

| Biomass | Raw biomass | | | | |
|---|---|---|---|---|---|
| | $C_xH_yO_z$ | | | Heat capacity | Enthalpy of formation |
| | x | y | z | kJ/kg K | kJ/kg |
| Palm oil fiber | 1.00±0.02 | 1.80±0.01 | 0.90±0.01 | 1.45±0.11 | -8257±899 |
| Banana rachis | 1.00±0.02 | 1.70±0.01 | 1.40±0.01 | 1.41±0.12 | -9189±969 |
| Sugarcane bagasse | 1.00±0.06 | 1.50±0.01 | 0.90±0.01 | 1.41±0.29 | -6786±1617 |
| Rice husk | 1.00±0.05 | 2.50±0.02 | 4.40±0.01 | 1.32±0.27 | -7030±2471 |
| Sawdust | 1.00±0.01 | 1.50±0.01 | 0.80±0.01 | 1.36±0.04 | -5868±589 |
| Coffee waste | 1.00±0.03 | 1.71±0.01 | 0.70±0.01 | 1.43±0.18 | -7544±1576 |

Table 2-6.Chemical formula, enthalpy capacity and enthalpy of formation for torrefied biomasses.

| Biomass | Torrefied Biomass | | | | |
|---|---|---|---|---|---|
| | $C_xH_yO_z$ | | | Heat capacity | Enthalpy of formation |
| | x | y | z | kJ/kg K | kJ/kg |
| Palm oil fiber | 1.00±0.17 | 1.10±0.01 | 0.80±0.01 | 1.24±0.23 | -5004±1216 |
| Banana rachis | 1.00±0.08 | 1.10±0.03 | 1.20±0.01 | 1.24±0.28 | -7165±2161 |
| Sugarcane bagasse | 1.00±0.13 | 1.10±0.02 | 0.90±0.01 | 1.22±0.32 | -3890±1735 |
| Rice husk | 1.00±0.03 | 1.30±0.01 | 1.00±0.01 | 1.31±0.20 | -8592±852 |
| Sawdust | 1.00±0.04 | 1.20±0.01 | 0.70±0.01 | 1.31±0.27 | -5229±706 |
| Coffee waste | 1.00±0.02 | 1.12±0.01 | 0.52±0.01 | 1.26±0.16 | -5304±1137 |

From the above information, energy balances were performed and the enthalpy of reaction for each torrefaction reaction of each biomass was found as is shown in equation (2-5), and the heat request for the torrefaction process was also found, as shown in equation (2-6). For energy balance calculations, it was assumed that input streams consist of raw biomass, nitrogen and liquid moisture, and outlet streams consist of volatiles, nitrogen, steam and a torrefied biomass. It was assumed that volatiles are composed of $CO_2$ and acetic acid according with previous experimental works [20,32]. The $CO_2$ and acetic acid are presented in proportions of 74% and 26%, respectively, in the volatiles [20,32]. This has been verified experimentally by Yan et al. [20] for temperatures of 260°C.

$$C_xH_yO_z(s_1) \xrightarrow{\Delta H_R} C_xH_yO_z(s_2) + CO_2 + Acetic\ Acid + H_2O \tag{2-5}$$

$$\left(m_{s_2}\Delta H^{\circ}_{f_{s_2}}\right)_{out} + \sum_{i=1}^{n} m_i(\Delta H^{\circ}_{f_i} + c_p\Delta T) - \left(m_{s_1}\Delta H^{\circ}_{f_{s_1}}\right)_{in} = Q \tag{2-6}$$

Table 2-7. Mass and energy balance for torrefaction process

| Biomass | Mass in (kg) | Energy (kJ) | Solid mass out (kg) | Energy (kJ) | Heat (Q) (kJ/kg) |
|---|---|---|---|---|---|
| Palm oil fiber | 1.00±0.01 | 16953±930 | 0.61±0.01 | 10884±1752 | 2320±2091 |
| Banana rachis | 1.00±0.01 | 14388±996 | 0.57±0.01 | 9102±1482 | 1944±3111 |
| Sugarcane bagasse | 1.00±0.01 | 15471±1646 | 0.81±0.01 | 14190±2029 | 2525±3321 |
| Rice husk | 1.00±0.01 | 15047±2500 | 0.77±0.01 | 12644±703 | -2043±3321 |
| Sawdust | 1.00±0.01 | 17935±624 | 0.74±0.01 | 15195±577 | 392±1260 |
| Coffee waste | 1.00±0.01 | 18012±1611 | 0.69±0.01 | 14186±844 | 1680±2600 |

The results of the energy balances are presented in Table 2-7. A summary of the mass and energy balances for the wood torrefaction process is presented in Figure 2-6. This graph shows that the volatile gases contain 8% of the initial energy of the biomass. This energy could be used later in a biomass pre-heater or in the gas recirculation to the reactor and provide a portion of the energy required in the system.

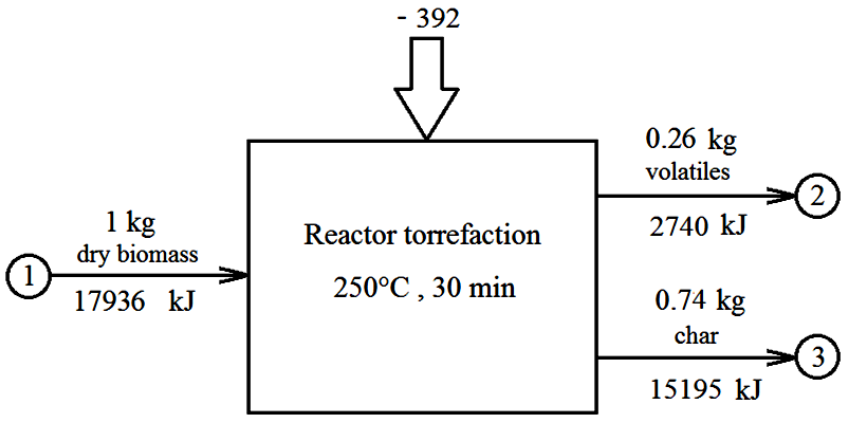


Figure 2-6. Mass and energy balance for the torrefaction process of sawdust at a temperature of 250°C for 30 min

Future assessments quantifying the species in the gas outlet and involving the amounts of hemicellulose, cellulose and lignin are under development.

## 2.5. Exergy balances

Exergy is defined as the maximum potential work that can be obtained from a material flow, heat transfer or work to bring this stream or system to environmental conditions; conditions that are associated with the dead state where the currents are in chemical, thermal and mechanical equilibrium with the atmosphere. Among the different forms of exergy, for this process, only those relevant, such as thermal, work and material exergies, are quantified, and smaller amounts, such as the kinetic and potential exergy, are neglected. According to the above, the specific exergy (J/mol) was calculated from equation(2-7) for each stream [33]:

$$b^t = b^{ch} + b^{ph} \tag{2-7}$$

Where $b^{ch}$ and $b^{ph}$ are the chemical and physical exergy, respectively. The chemical exergy for a gas mixture or non-combustible solids is obtained from equation (2-8) and for a fuel ($b_F^{ch}$) is calculated by equation (2-9) [33]:

$$b^{ch} = \sum x_i b_i^{ch} + \sum x_i \ln(x_i) \tag{2-8}$$

$$\begin{aligned} b_F^{ch} = {} & \overline{HHV}(T_0, P_0) - T_0 \left[ s_{DAF} + v_{O_2} s_{O_2} - v_{CO_2} s_{CO_2} - v_{H_2O} s_{H_2O} - v_{SO_2} S_{SO_2} - v_{N_2} s_{N_2} \right] \\ & + \left[ v_{O_2} b_{O_2}^{ch} + v_{CO_2} b_{CO_2}^{ch} + v_{H_2O} b_{H_2O}^{ch} + v_{SO_2} b_{SO_2}^{ch} + v_{N_2} b_{N_2}^{ch} \right] \end{aligned} \tag{2-9}$$

Where $x_i$ and $b_i^{ch}$ in equation (2-8) are the molar fraction of the *i* specie in the gas stream and the chemical exergy of the *i* specie in the stream. In equation (2-9), the chemical exergy of a solid fuel is obtained considering the products of a combustion reaction of this fuel. In this equation, $v_i$ is the molar fraction of the *i* specie, $s_i$ is the entropy of the *i* specie, $T_0$ and $P_0$ are the temperature and pressure of the reference state, $\overline{HHV}$ is the highest heating value of the biomass, and $b_i^{ch}$ is the chemical exergy of the *i* specie. The term $s_{DAF}$ is defined as follows:

$$s_{DAF} = c \left[ \begin{array}{l} 37.1653 - 31.4767 \exp\left( -0.564682 \dfrac{h}{c+n} \right) + 20.1145 \dfrac{o}{c+n} + 54.3111 \dfrac{n}{c+n} \\ + 44.6712 \dfrac{s}{c+n} \end{array} \right] \tag{2-10}$$

Where *h*, *n*, *c* and *o* are the amounts of hydrogen, nitrogen, carbon and oxygen in the elemental analysis. Physical exergy of a gas stream or solid was calculated with equation (2-11):

$$b_{ph} = (h_i - h_{0_i}) - T_0 (s_i - s_{0_i}) \tag{2-11}$$

Where $h_i$ and $s_i$ are the enthalpy and entropy of the specie *i* in the stream and $h_{0_i}$ and $s_{0_i}$ are the enthalpy and entropy of the specie *i* in the stream in the reference state.

With these expressions, the total exergy for each process can be obtained considering the inlet and outlet streams shown in Figure 2-5. The chemical exergy of the biomass and biochar were calculated in agreement with equation (2-9). The irreversibilities and efficiency in all processes were found in accordance with equations (2-12) and (2-13):

$$I = b_{in} - b_{out} \tag{2-12}$$

$$\Psi = \frac{b_{out}}{b_{in}} \tag{2-13}$$

Where $b_{in}$ is represented by the exergy of the biomass, moisture and inert gas, and $b_{out}$ is represented by the exergy of the biochar, volatiles (condensable and non-condensable) and the inert gas. The exergy related with heat input to realize the torrefaction process is expressed by equation (2-14):

$$b_Q = \left(1 - \frac{T_0}{T_p}\right) Q_r \tag{2-14}$$

Where $T_p$ is the process temperature and $Q_r$ is the heat of reaction shown in Table 2-7. The exergy balances were done from mass and energy balances, and the exergies of all streams can be seen in Table 2-8. The values shown in Table 2-8 are obtained in relation to the amount of raw biomass and the units shown are kJ / kg raw biomass.

Table 2-8. Total exergy of inlet and outlet streams in the process

| | IN (kJ / kg) | | | OUT (kJ / kg) | | | |
|---|---|---|---|---|---|---|---|
| | Biomass | $H_2O_L$ | Q | Biochar | $H_2O_V$ | Acetic Acid | $CO_2$ |
| Palm oil fiber | 17696±959 | 23±0.1 | 1906±1725 | 12806±880 | 27±0.2 | 1043±4 | 110±1 |
| Banana rachis | 14326±1106 | 27±0.1 | 1281±2054 | 8829±1392 | 33±0.1 | 1320±4 | 139±1 |
| Sugarcane bagasse | 16913±1676 | 94±0.3 | 1697±2238 | 15069±1664 | 100±0.3 | 621±2 | 133±1 |
| Rice husk | 13454±2528 | 92±0.3 | -1387±2250 | 12066±751 | 98±0.4 | 768±3 | 164±1 |
| Sawdust | 18620±652 | 116±0.4 | -165±531 | 16381±607 | 123±0.3 | 634±2 | 135±1 |
| Coffee waste | 18528±1641 | 80±0.3 | 742±1188 | 11993±893 | 85±0.3 | 1488±5 | 318±1 |

In this table, it is clear that the contribution of $H_2O$ in the inlet stream is negligible, and the greatest contribution is given by the chemical exergy of the raw biomass. In the outlet stream, something similar happens with $H_2O$, acetic acid and $CO_2$, which have low contribution to the total exergy in the stream. The exergy input and output of the biomass are shown in Figure 2-7 for the purpose of observing the loss availability in the biochar obtained in the torrefaction process.

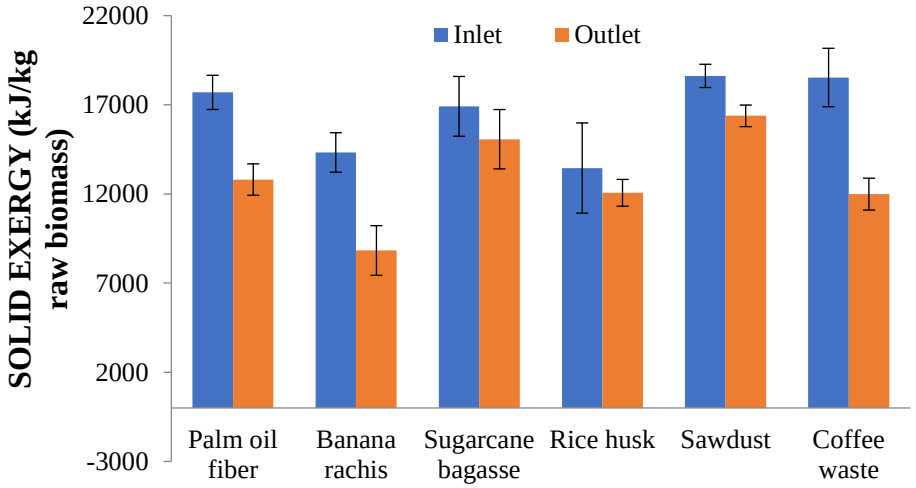


Figure 2-7.Solid exergy for biomass torrefaction at a temperature of 250°C for 30 min

The total inlet and outlet exergies in all the process are shown in Figure 2-7. In this picture, it can be seen that the irreversibility for the torrefaction of palm oil fiber, banana rachis and coffee waste are bigger than in the other processes. The big amounts of volatiles yielded in these processes cause the irreversibility to increase and a great amount of exergy to be lost in these streams. The energy loss in the exhaust gases can be used either in preheating the inlet biomass or by recirculation directly to the kiln in order to reduce the irreversibilities in the process.

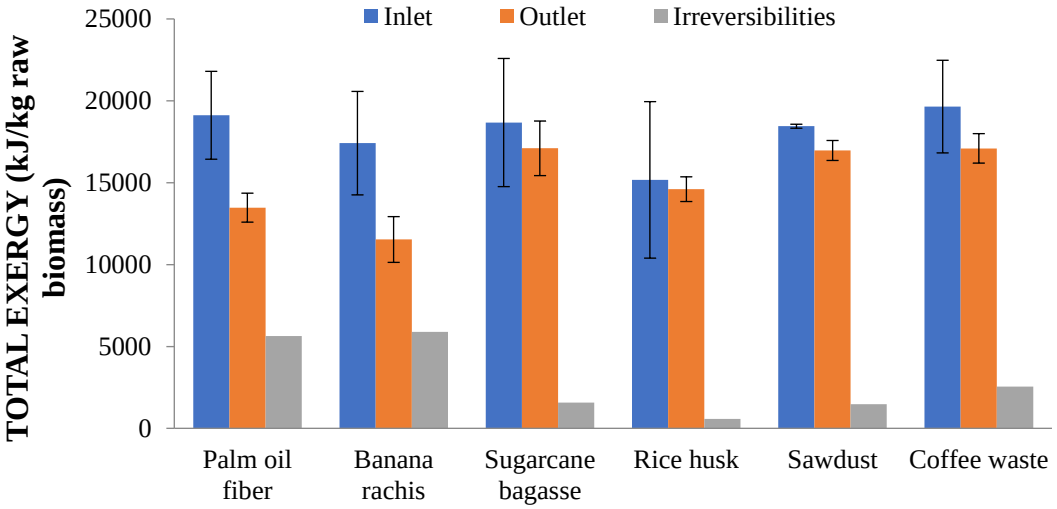


Figure 2-8. Total exergy of input and output streams in biomass torrefaction at 250°C for 30 min

The exergetic efficiency for biomass torrefaction is shown in Figure 2-9. This figure shows that torrefaction of sugarcane bagasse, rice husk and sawdust are the most efficient processes. It was expected that when the irreversibility increased, the process efficiency decreased, according to the definition of exergetic efficiency in equation (2-13). This is the reason why the highest efficiencies are found for sugarcane bagasse, rice husk and sawdust, due to their lower irreversibility present in the process.

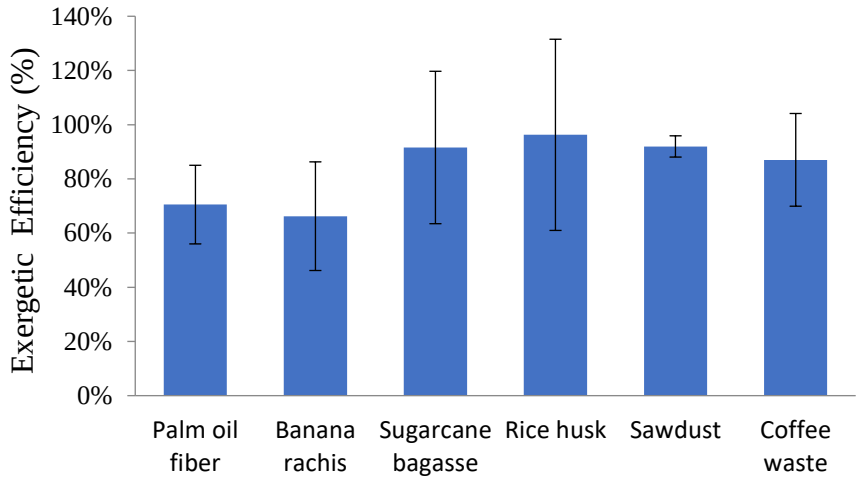


Figure 2-9.Exergetic efficiency for biomass torrefaction at 250°C for 30 min

A dynamic analysis with respect to the input and output exergy depending on a cost ratio *R*, defined by equation (2-15), was performed in order to find an optimum operating condition regarding the mass lost in the torrefaction process. This dynamic analysis was done in agreement with equations (2-16) and (2-17) and suggests an optimum value for a mass loss in a torrefaction process to obtain a profitable solid fuel from the standpoint of costs of biomass before and after the process.

$$R = \frac{Cost\ of\ biochar(\$/kg\ biochar)}{Cost\ of\ rawbiomass(\$/kg\ rawbiomass)} \tag{2-15}$$

$$E_1 = R*(M_{tb} * HHV_{rb}) \tag{2-16}$$

$$E_2 = R*(M_{tb} * HHV_{tb}) \tag{2-17}$$

$M_{tb}$ represents the mass of the biomass at any time, $HHV_{rb}$ and $HHV_{tb}$ represent the HHV of raw biomass and torrefied biomass obtained for any $M_{tb}$. This latter value was obtained by interpolation between the HHV of raw biomass and the final torrefied biomass. In Figure 2-10, $E_1$ parameter is shown in blue lines and $E_2$ parameter is shown in the green line. The intercept point of each blue line with the green line represents the mass loss optimum for a profitable process. R was set to 1.02, 1.05 and 1.08%, which means an increase in the torrefied biomass cost of 2, 5 and 8% in relation with raw biomass.

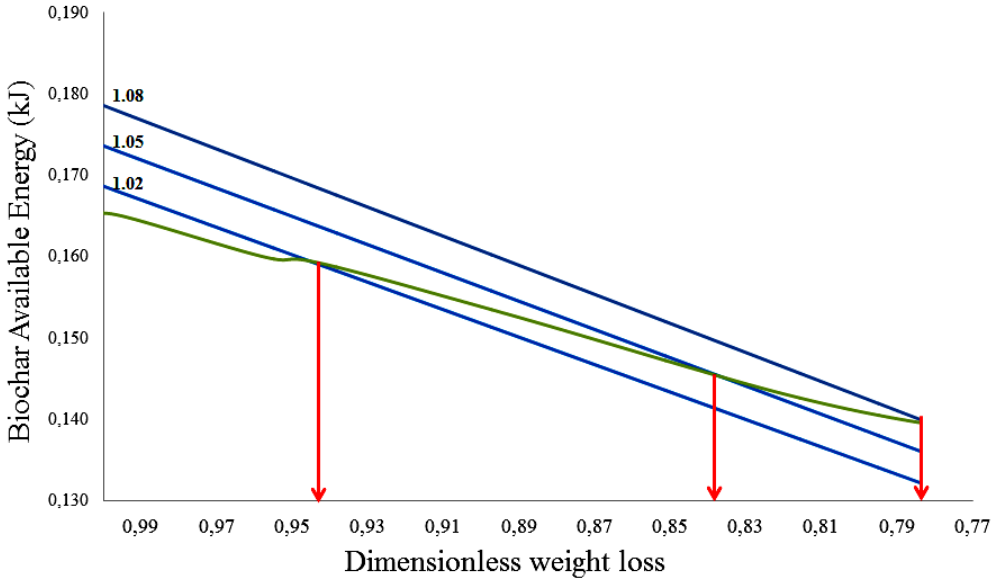


Figure 2-10.Optimal operational condition for a cost ratio of 1.02, 1.05 and 1.08 for bagasse torrefaction at 250°C for 30 min

The graph was analyzed for the case of sugarcane bagasse, in which it was found that for a ratio of 2, it should have a mass loss of about 5% for a profitable process; for a 1.08 ratio, the mass loss should be approximately 22%. The latter means that the optimum operational conditions depend on the torrefied biomass cost with respect to the biomass cost.

## 2.6. Conclusions

In this work, mass and energy balances were performed in order to find a residual agricultural biomass promising for use as a solid fuel in thermal processes. The most promising biomass was sawdust, which had an increase of 14.5%in HHV, from 17.9 MJ/kg in its raw state to 20.5 MJ/kg after processing. In addition to this increase in energy, less energy intake was required for the thermal decomposition of its structure due to exothermic reactions that took place during the torrefaction process. Rice husk presented an exothermic heat of reaction of 1541 kJ during the torrefaction process, but performing the analysis by means of the "energy yield" indicator does not have as good results compared with sawdust.

Exergy balances for the torrefaction process of all the biomass evaluated were performed. As was expected, energy availability of the biochar obtained is less than that of raw biomass, leading to losses during the process. In addition, the irreversibility present in the torrefaction of sugarcane bagasse, rice husk and sawdust is lower than for the other processes, the irreversibility of torrefaction of rice husk being the lowest and the most efficient.

Analyses of optimal operating conditions were performed using cost ratio between the biochar obtained and the untreated biomass in order to find the optimal biomass mass loss for a viable torrefaction process. We found that for a cost ratio of 1.08, the biomass mass loss can be of up to 22%. It was found experimentally that the torrefaction process is a way to transform the residual biomass and improve moisture content, biomass density and other properties in order to use it in thermal processes.

### Acknowledgments

The authors wish to thank the Colombian Administrative Department of Science, Technology and Innovation (COLCIENCIAS) for financial support.

### References

[1] Basu P. Biomass Gasification and Pyrolysis. 2010.

[2] Pentananunt R, Rahman ANMM, Bhattacharya SC. Upgrading of biomass by means of torrefaction. Energy 1990;15:1175–9.

[3] Wattananoi W, Khumsak O, Worasuwannarak N. Upgrading of biomass by torrefaction and densification process. 2011 IEEE Conference on Clean Energy and Technology 2011:209–12.

[4] Medic D, Darr M, Shah a., Potter B, Zimmerman J. Effects of torrefaction process parameters on biomass feedstock upgrading. Fuel 2012;91:147–54.

[5] Bourgois J, Guyonnet R. Characterization and analysis of torrefied wood. Wood Science and Technology 1988;22:143–55.

[6] Bourgois J, Bartholin MC, Guyonnet R. Thermal treatment of wood: analysis of the obtained product. Wood Science and Technology 1989;23:303–10.

[7] Broido a., Nelson M a. Char yield on pyrolysis of cellulose. Combustion and Flame 1975;24:263–8.

[8] Bridgeman TG, Jones JM, Shield I, Williams PT. Torrefaction of reed canary grass, wheat straw and willow to enhance solid fuel qualities and combustion properties. Fuel 2008;87:844–56.

[9] Jones JM, Bridgeman TG, Darvell LI, Gudka B, Saddawi a., Williams a. Combustion properties of torrefied willow compared with bituminous coals. Fuel Processing Technology 2012;101:1–9.

[10] Fisher EM, Dupont C, Darvell LI, Commandré J-M, Saddawi a, Jones JM, et al. Combustion and gasification characteristics of chars from raw and torrefied biomass. Bioresourse Technology 2012;119:157–65.

[11] Couhert C, Salvador S, Commandré J-M. Impact of torrefaction on syngas production from wood. Fuel 2009;88:2286–90.

[12] Deng J, Wang G, Kuang J, Zhang Y, Luo Y. Pretreatment of agricultural residues for co-gasification via torrefaction. Journal of Analytical and Applied Pyrolysis 2009;86:331–7.

[13] Bridgeman TG, Jones JM, Williams a., Waldron DJ. An investigation of the grindability of two torrefied energy crops. Fuel 2010;89:3911–8.

[14] Repellin V, Govin A, Rolland M, Guyonnet R. Energy requirement for fine grinding of torrefied wood. Biomass and Bioenergy 2010;34:923–30.

[15] Phanphanich M, Mani S. Impact of torrefaction on the grindability and fuel characteristics of forest biomass. Bioresourse Technology 2011;102:1246–53.

[16] Bates R, Ghoniem A. Biomass Torrefaction: Modeling of Volatile and Solid Product Evolution Kinetics. Bioresourse Technology 2012; 124:460-469.

[17] Ratte J, Fardet E, Mateos D, Héry J-S. Mathematical modelling of a continuous biomass torrefaction reactor: TORSPYD$^{TM}$ column. Biomass and Bioenergy 2011;35:3481–95.

[18] Prins MJ, Ptasinski KJ, Janssen FJJ. More efficient biomass gasification via torrefaction. Energy 2006;31:3458–70.

[19] Park WC, Atreya A, Baum HR. Experimental and theoretical investigation of heat and mass transfer processes during wood pyrolysis. Combustion and Flame 2010;157:481–94.

[20] Yan W, Hastings JT, Acharjee TC, Coronella CJ, Vásquez VR. Mass and Energy Balances of Wet Torrefaction of Lignocellulosic Biomass †. Energy & Fuels 2010;24:4738–42.

[21] Bergman PC., Kiel JHA. Torrefaction for biomass upgrading. 14th European Biomass Conference & Exhibition 2005:17–21.

[22] Chiueh P-T, Lee K-C, Syu F-S, Lo S-L. Implications of biomass pretreatment to cost and carbon emissions: case study of rice straw and Pennisetum in Taiwan. Bioresourse Technology 2012;108:285–94.

[23] Chen W-H, Kuo P-C. Isothermal torrefaction kinetics of hemicellulose, cellulose, lignin and xylan using thermogravimetric analysis. Energy 2011;36:6451–60.

[24] Chen W-H, Kuo P-C. A study on torrefaction of various biomass materials and its impact on lignocellulosic structure simulated by a thermogravimetry. Energy 2010;35:2580–6.

[25] Park S-W, Jang C-H, Baek K-R, Yang J-K. Torrefaction and low-temperature carbonization of woody biomass: Evaluation of fuel characteristics of the products. Energy 2012;45:676–85.

[26] Prins MJ, Ptasinski KJ, Janssen FJJ. Torrefaction of wood. Part 1. Weight loss kinetics. Journal of Analytical and Applied Pyrolysis 2006;77:28–34.

[27] Prins MJ, Ptasinski KJ, Janssen FJJG. Torrefaction of wood. Journal of Analytical and Applied Pyrolysis 2006;77:28–34.

[28] Friedl A, Padouvas E, Rotter H, Varmuza K. Prediction of heating values of biomass fuel from elemental composition. Analytica Chimica Acta 2005;544:191–8.

[29] Basu P. Biomass gasification and pyrolysis: practical design and theory. Elsevier Inc; 2010.

[30] Prins MJ. Thermodynamic analysis of biomass gasification and torrefaction. Technische Universiteit Eindhoven, 2005.

[31] Hougen O, Watson K. Chemical Process Principles. Jhon Wiley. USA: 2005.

[32] Prins MJ, Ptasinski KJ, Janssen FJJ. Torrefaction of wood. Part 2. Analysis of products. Journal of Analytical and Applied Pyrolysis 2006;77:35–40.

[33] Bejan A. Advanced Engineering Thermodynamics. Third Edit. New Jersey: 2006.

# Chapter 3. Study of Reactivity Reduction in Sugarcane Bagasse as consequence of a Torrefaction Process

**(Paper submitted to Energy Journal)**


## Abstract

A complete study of sugarcane bagasse torrefied under different operating conditions and then burned in oxidizing atmosphere is presented in this work. The torrefied biomass was characterized through chemical and physical analysis such as proximate and elemental analyses, lignocellulosic composition, HHV, FTIR and observations in scanning electron microscopy SEM. The torrefied biomass was also evaluated in oxidizing conditions in order to analyze the impact of torrefaction process over biomass. Remarkable changes of the main functional groups were observed as the severity of the torrefaction process increased. The main structural carbohydrates affected in the process were hemicellulose and cellulose, which break down largely as a result of decarboxylation reactions, and breakage of links with methyl and acetyl groups. This was evidenced qualitatively when the material was observed in SEM, and it was noted an increase in the decomposition of the cell wall structures as the process temperature increased. These changes in the material were also verified with FTIR tests, and lignified matrix with higher content of aromatic groups and greater thermal stability is yielded with temperature increases.


***Keywords***: Biomass torrefaction, sugarcane bagasse, combustion reactivity, SEM, FTIR.

## 3.1. Introduction

In Colombia, the residual biomass comes from agricultural holding, such as rice husks, banana rachis, coffee wastes, sugarcane bagasse, fiber, and palm oil shell. According to their energy content and availability, the sugarcane bagasse has one of the highest LHV with around 18 MJ/kg [1]. Therefore, there is a growing interest in bagasse as a precursor of both energetic ways and there is a need to have a better understanding of their chemical and physical properties, with the aim of optimizing its use in the energy sector. It has some drawbacks such as its high moisture content, low energy content, hygroscopic nature, low density, and heterogeneous properties, resulting in low conversion efficiency and difficulty in the collection, crushing, storage and transport [2,3]. Torrefaction, meanwhile, appears as a good alternative for thermal pre-treatment for biomass because it attacks the big drawbacks raised previously [4].

Torrefaction, as a thermochemical treatment driven in an inert atmosphere at temperatures between 200-300°C and low heating rates [3,5,6], is a good alternative to give residual biomass a better use with energy purposes. Multiple technical and scientific reports reveal that torrefaction improves biomass properties such as hydrophobicity, milling properties, increases energy density reducing H/C and O/C ratios, and it acquires properties very similar to low rank coals, peats and lignites [7].

Because of these new properties in the solid, the torrefied biomass is seen as an alternative solid fuel with possible use in other thermochemical processes such as combustion or gasification according to previous studies [8–12].

Among the wide information on biomass torrefaction processes, it stands out the research carried out by Wilk et al. [13], where wood and torrefied wood were characterized by instrumental techniques such as SEM, FTIR, and the changes in the morphology of the biomass and microstructure were studied. These analyses were supplemented with TGA analysis, elemental and proximate characterization. A primary characterization revealed changes in the properties of the biomass, which tended to be close to those for coal. It was also found that the moisture content decreased and the mechanical properties were improved. On the other hand, authors like Nocquet et al. [14] worked with thermogravimetry coupled to a system for measuring gases, which managed to characterize the gaseous species that are released in the torrefaction of beech logs. They proposed a mechanism to explain certain interactions between the constituents of the biomass, which relates some process variables such as temperature and residence time with the changes in the material. Chen et al. [15,16] studied the impact of torrefaction on the lignocellulosic structure of bamboo and willow, and characterized the transformation of hemicellulose, cellulose and lignin by thermogravimetry.

The FTIR technique has been useful in the characterization of biomasses since it allows to elucidate significant changes in the microstructure of materials after thermal processes, showing how the absorption of certain functional groups is changing as the process occurs. This performs the transformation of the chemical structure and the change in concentration of some functional groups in the material. These changes were mainly attributed to the devolatilization, carbonization and depolymerization [17,18] of the polymer chains that are organized in an amorphous way, whose thermal resistance is very weak [19].

Werner et al. [20], studied the thermal decomposition of seven different hemicelluloses, the behavior of these components was analyzed by thermogravimetric analysis, infrared spectroscopy (FTIR), differential scanning calorimetry (DSC) and gas chromatography-mass spectrometry (Py-GC / MS). It was found that temperatures near 300 °C, lead to the breakdown of most inter and intramolecular hydrogen links and, C-C and C-O bonds, resulting in the formation of hydrophilic extractives, carboxylic acids, alcohols, aldehydes, ethers, and gases such as CO, $CO_2$, and $CH_4$. At these temperatures, the cellular structure is substantially destroyed, the biomass loses its fibrous nature and becomes brittle. Similarly, Chang et al. [21] showed that the products distribution is significantly influenced by the temperature and chemical composition of biomass. These products were analyzed by different analytical techniques such as FTIR, TGA, XRD, Py-GC/MS. This allowed them to validate that the thermal decomposition of hemicellulose carbohydrates predominates on the decomposition of lignin and cellulose, generating a significant removal of water and organic components of low molecular weight. This suggests the existence of crosslinks and carbohydrates carbonization due to the formation of insoluble fibers acid.

Hoi and Martincigh [22] made the detailed characterization of four species of sugarcane from Mauritania, including leaves, fodder, and torrefied sugarcane by TGA, FTIR, SEM techniques and

proximate and ultimate analysis. They found that most components of bagasse are thermally stable at temperatures below 200 °C, as it had been stated by Tumuluru et al. [19]. Hemicellulose is the constituent whose decomposition takes place from 180°C and with a high degradation rate, it is followed by the cellulose in the range between 240 and 350 °C, and the lignin is extensively decomposed at temperatures even above 500 ° C [23,24]. The product release plays an important role in the final composition of torrefied biomass in their carbon content, volatile matter and heat value, because it defines the feasibility of torrefied biomass as an applicable solid fuel in other thermochemical processes [25,26]. Collard et al. [17] studied the mechanisms and composition of the products obtained from the decomposition of the three main components of biomass (hemicellulose, cellulose and lignin) in a pyrolysis process. They analyzed the mechanisms for each polymer decomposition in different thermal conditions.

Combustion reactivity for torrefied biomass has been studied by different authors [8,11,27–31] in order to know the impact that torrefaction generates on the material. In these studies, torrefied biomasses are subjected to burning process to study their behavior during the process, and parameters such as reaction velocity, activation energies and other kinetic parameters are obtained in the tests.

The main interest of this research, besides obtaining the traditional parameters obtained in the combustion reactivity evaluation of torrefied biomass, was to approach the characterization of torrefied biomass from chemical and physical point of view, in order to give explanations to the behavior of these materials during combustion tests. For the latter, the sugarcane bagasse was torrefied at three different temperatures, while physical and chemical characterizations were performed for raw and torrefied biomass through proximate and ultimate analysis, HHV, FTIR and char reactivity in oxidative environment. In addition, a qualitative morphological study using SEM techniques allowed to contrast the information obtained by all different characterization techniques.

## 3.2. Methods

### *3.2.1. Materials*

Samples of a lingo-cellulosic residue from sugarcane industry was used in this study. The biomass was dried at room temperature with an average temperature of 23 °C and 400 W/m$^2$ of solar average radiation for 12 h. Then, it was first crushed in a conventional ball mill and then in a micro mill IKA MF-10 for fine particles. All material was sieved for obtaining particle sizes ranging between 0.09 – 0.075 mm, and stored in sealed bags for protection.

### *3.2.2. Torrefaction process*

Torrefaction tests were performed in a thermo-gravimetric analyzer Navas Instruments TGA-2000A, where 12 samples are processed simultaneously. The torrefaction process was performed in two stages. Biomass drying was developed from room temperature until 105°C with a heating rate of 10 °C/min during 1 hour. Then, a second heating until the process temperature was between 230 and 290 °C, with the same heating rate during 3 hours. A nitrogen flow of 100 ml/min was introduced to the system to ensure the required inert atmosphere in the process. The amount of

sample used in each test was 1 g, thus, 12 g of torrefied biomass was obtained after each test and stored in air-tight containers before the analyses for protection.

### *3.2.3. Elemental, proximate and torrefaction yields*

Raw and torrefied biomass were characterized by proximate and elemental analysis. HHV, fuel ratio (FR), Mass Yield (MY), and Energy Yield (EY). FR, MY, and EY are defined as follows:

$$FR = \frac{FC}{VM} \tag{3-1}$$

$$MY = \frac{M_{T,daf}}{M_{R,daf}} \tag{3-2}$$

$$EY = \frac{M_{T,daf}\ x\, HHV_T}{M_{R,daf}\ x\, HHV_R} \tag{3-3}$$

Proximate analyses for raw and torrefied biomass were carried out in a muffle furnace according to ASTM D1762-84 aiming at obtaining volatile material, fixed carbon, ash, and moisture in all samples. This analysis was carried out twice for repeatability. Elemental analyses were measured using an Exeter Analytical Organic Elemental Analyzer, Model EA1110. Tests were conducted in triplicate according to ASTM D5373-02. These tests determined the amount of carbon, hydrogen, and nitrogen of the material, while the oxygen content was calculated by difference. Higher Heating Value (HHV) was also measured in duplicate by calorimeter bomb Parr 6100 according to ASTM D5865-04.

### *3.2.4. Lignocellulosic and SEM analysis*

The lignocellulosic analysis for lignin, cellulose and hemicellulose was carried out by implementing NREL/TP-510-42618 regulatory approach, which implies the ASTM E1721-01 (2009) standards for the determination of acid insoluble material in the biomass, and E1758 ASTM - 01 (2007) for carbohydrate determination by high performance liquid chromatography (HPLC). These analyses were developed for raw and torrefied biomasses in order to obtain information about the biomass degradation during the process. The study of morphology of raw and torrefied biomass was carried out using a scanning electron microscope (SEM) JEOL JSM-5910LV with a SEI detector and a theoretical resolution 300.000X, enabling observations until 50nm.

### *3.2.5. FT-IR*

A characterization by FT-IR technique was performed in a Spectrometer Spectrum Two, with an MIR source and Universal ATR Perkin Elmer accessory with diamond crystal. With these equipment, spectra in the infrared region between 8300 $cm^{-1}$ and 350 $cm^{-1}$ can be obtained, but in our particular case it was set for the 4000 $cm^{-1}$ to 450 $cm^{-1}$ region. This spectrometer has a spectral resolution of 0.5 $cm^{-1}$ standard with an accuracy in their higher wavelength of 0.01 $cm^{-1}$ to 3000

$cm^{-1}$. The resulting spectrum represents the sample absorption, resulting in creating a molecular fingerprint of the same, due to their own functional groups.

### *3.2.6. Combustion tests*

Raw and torrefied material were subjected to combustion in a thermo-gravimetric balance in order to assess the reactivities. Approximately 10 mg of material was burned under 4 different thermal conditions with heating rates of 5, 10, 15 and 20°C/min. Prior to the combustion process, a soft heating at a temperature of 105°C for around 30 minutes was developed in order to obtain a complete drying process of the sample. A second heating ramp was made from this temperature to 900°C with the considered heating rate. DTG curves were obtained in order to find some differences between tested materials and to compare them. The torrefied sample T230 was not evaluated in the reactivity testing, because its decomposition in the torrefaction process was relatively low. For this reactivity testing, only samples T250, T270 and T290 were tested. Kinetic parameters for combustion process were obtained following Ozawa's iso-conversional method [32], in which a distribution of activation energies was obtained for the entire combustion process. In addition, a reactivity index was used in order to measure the reactivity of each sample. This index was chosen to measure the temperature for a conversion of 25% of the sample.

## 3.3. Results and discussion

### *3.3.1. Mass and Energy yield*

Mass and energy yields and HHV are shown in Figure 3-1. In the range of temperature between 230 and 250 °C, it can be noted that the magnitude of the HHV remains in very close values, in the range of 270 and 290 °C this behavior is also observed. This has already been observed in the literature [3], because the low temperature range is within the medium severity zone and the second range is in high severity [15]. This indicates that reactions occurring in each are substantially different.

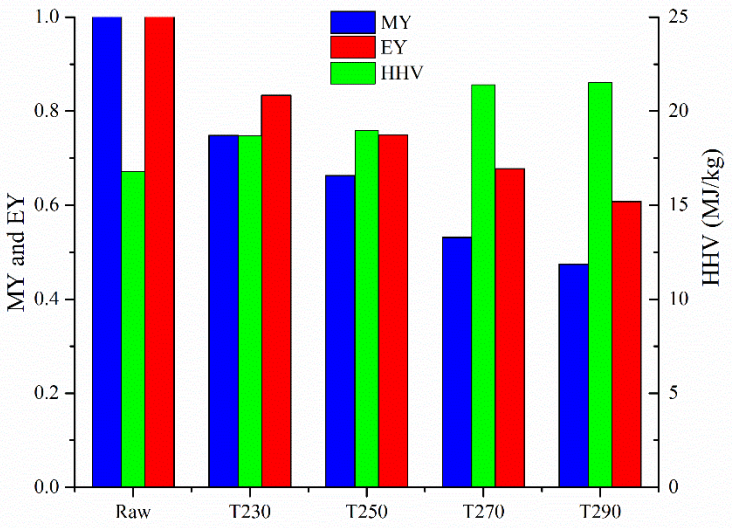


Figure 3-1. Mass and Energy yield and HHV for all torrefied samples.

In Figure 3-1, the effect of the temperature over MY and EY parameters is evident. Minimum parameter values were found in several conditions. For 290°C, MY and EY were reduced until values of 47% and 60% respectively. In soft conditions only values for MY and EY of 74% and 83% were found. An inverse behavior is observed for HHV, which increased with process severity. This takes values of 18.7 MJ/kg for soft conditions and 21.5 MJ/kg for severe conditions, increasing 11% and 28% in comparison with raw material. The above-mentioned argument is another plus for confirming that the torrefaction process increases the amount of energy available in the biomass with temperatures [33]. However, this process at more severe conditions also compromises the carbonaceous structure and mass loss becomes more extensive, harming the mass yield. Moving the process to values very close to 300 °C involves a high energy consumption and a significant mass loss. In this way, torrefaction process is a precise combination of its variables, in order to obtain not significant mass loss and to retain as much energy as possible in the product.

### *3.3.2. Proximate and elemental analysis*

Proximate and elemental analyses of raw and torrefied bagasse are shown in Figure 3-2. From Figure 3-2(a) it can be noted that the content of volatile material decreases significantly with an increase in fixed carbon. This is subjected to the severity of the process and the chemical nature of the biomass. Bagasse, as a lignocellulosic material type, consists mainly of organic components (hemicellulose, cellulose and lignin) which, when subjected to high temperatures, decompose into volatile products such as water, hydrogen, carbon dioxide, carbon monoxide, acetic acid, formic acid, furfural, levoglucosan, methanol, formaldehyde, etc. [17,20,34–37]. Therefore, it becomes a devolatilized material, with only 47% from its initial mass, but with densified fixed carbon. As carbon from ultimate and proximate analysis increases, the final biomass has a significant increase in the calorific value, making it an attractive material for subsequent thermal processes [33].

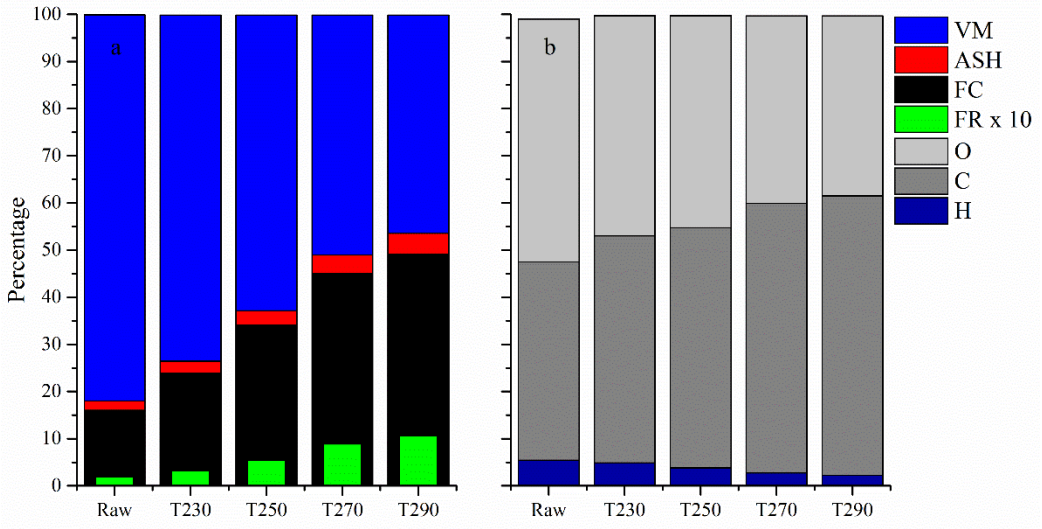


Figure 3-2. Proximate and elemental analysis for raw and torrefied bagasse (both analysis in dry basis).

The ash content was kept constant through all the process, so its fraction slightly increases. Figure 3-2(b) shows the elemental composition for raw and torrefied bagasse. Nitrogen content, which in this case is unrepresentative, is not shown. With these results, it is verified that carbon present in

the samples increases with the process severity. The fixed carbon fraction increases from 15.98% for raw material, to 49.16% when the material is torrefied at 290 °C, and the carbon from the elemental analysis increases from 42.09% to 59.27% when torrefied at the same conditions. Moreover, oxygen and hydrogen also decrease during the process to values of 25.88% and 58.49% respectively when the process is performed at the highest temperature. This is due to the increased release of volatile compounds with high oxygen and hydrogen content, which has little contribution to the HHV. On the other hand, a slight increase of 72.22% in nitrogen from 0.18 to 0.31 was observed. The magnitude of this component is very low, which does not generate concerns about the formation of nitrogen oxides ($NO_X$) emitted to the environment.

FR was also evaluated, as well as an increase from 0.19 for raw material to 1.06 for torrefied biomass at severe conditions (290°C). This parameter has big importance when the torrefied material is evaluated in a combustion process, because it indicates the combustion type that could occur in the process. Combustions of torrefied biomass with low FR may generate more emissions of $CO_2$, for CO and hydrocarbons the blending ratio is higher. In contrast, combustion of torrefied biomass with high FR, reduces greenhouse gases emission and thus it encourages a mixing of higher amounts of biomass with coal in a co-firing process.

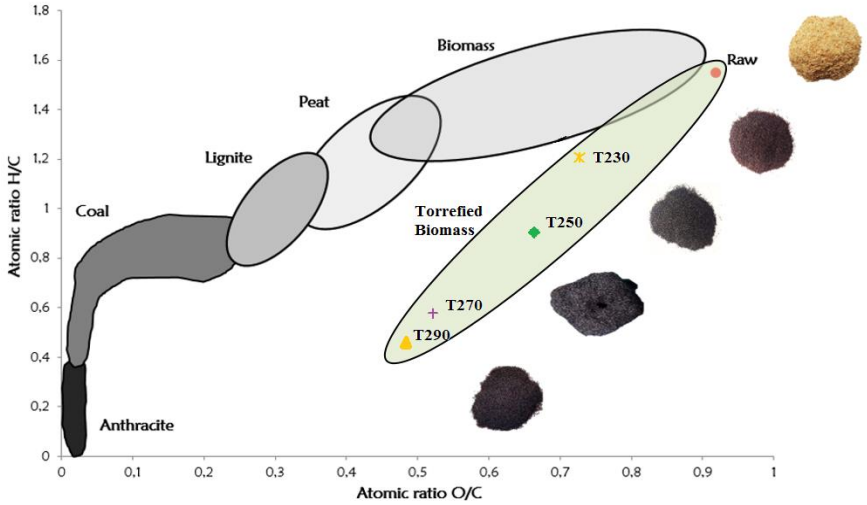


Figure 3-3. Van krevelen diagram for raw and torrefied biomass.

Solid fuels are usually classified by their degree of carbonization with the help of diagrams such as ternary, Van Krevelen or Seyler, through ratios such as O/C and H/C from their elemental composition. The Van Krevelen diagram in Figure 3-3 shows that, after the torrefaction process for sugarcane bagasse, a good carbonization degree in the material is achieved, according to photographs for each torrefied sample shown in same figure. According to Seyler classification, the torrefied bagasse at 290 °C can be classified as a lignite type. In this diagram, it is possible to appreciate that during torrefaction process, the biomass loses some oxygenate and hydrogenate compounds, which densifies the carbon content. In certain cases, the torrefied biomass is also called 'charcoal' owing to its similarities to conventional coal, shown in Van Krevelen diagram [6,7,38,39].

The change in color of the biomass during the torrefaction process is a good indicator of the severity of the process. As shown in Figure 3-3, brown color intensifies as the process temperature increases, but at high temperature, the biomass is dark brown or black color. The color is uniform in each sample, indicating that the torrefaction process was performed homogeneously throughout the sample. This change in color can be attributed to many factors such as the lignocellulosic composition, changes in the surface of the biomass that could affect the absorption properties, reflection and diffraction of light. Some formation of some chromophoric groups and displacement of some sugar molecules of low molecular weight towards the surface of the particle can affect the color in the material after being torrefied [40–43].

Some authors attribute the color change in biomass to the result of non-enzymatic browning reactions caused by condensation between carbonyl compounds and amino, or degradation of compounds with conjugated double bonds to carbonyl groups. There are four main routes to non-enzymatic browning, although chemistry of these reactions is related to the Maillard reaction: Maillard reaction, oxidation of ascorbic acid, lipid peroxidation, and caramelization at high temperatures [44–46].

### *3.3.3. Lignocellulosic analysis*

The analysis of the structure of lignocellulosic composition for raw and torrefied material was conducted according to international standards. This analysis makes it possible to determine the degree of decomposition that material suffers because of the torrefaction process in function of its polymeric composition. The results shown in Table 3-1 correspond to the standardization of quantities based on these three components.

Table 3-1. Lignocellulosic composition for raw and torrefied bagasse at 230, 250, 270, and 290 °C (dry and ash free basis)

| Sample | Hemicellulose (wt.%) | Cellulose (wt.%) | Lignin (wt.%) |
|---|---|---|---|
| Raw | 26.46±1.74 | 28.25±0.43 | 20.44±0.15 |
| T230 | 13.13±0.03 | 31.09±0.94 | 46.20±0.49 |
| T250 | 6.39±0.85 | 23.74±0.78 | 62.71±1.20 |
| T270 | 2.80±0.14 | 4.97±0.09 | 80.39±1.98 |
| T290 | 1.44±0.14 | 0.23±3.22 | 94.51±1.51 |

As shown in Table 3-1, the decomposition of the hemicellulose is evident as the temperature increases in the process. At low temperatures (230°C), the decomposition becomes considerable; it degraded about 60% of its initial amount. At higher temperatures, the destruction of this polymer is about 100% when the temperature reaches 290°C. In the case of cellulose, its degradation effect is not considerable at low temperatures, only when the temperature of 250°C is reached a strong degradation of this polymer initiates, consistent with that found by different authors [47,48]. At low temperatures, the main component that devolatilizes is hemicellulose [17,20,34–37]; while cellulose and lignin are more thermostable in these conditions and are less devolatilized. In severe thermal conditions higher than 250°C, considerable mass losses were obtained because, in addition to hemicellulose, cellulose takes greater participation in the devolatilization [15], mainly its amorphous part.

Temperature has a very noticeable effect on the biomass components, especially hemicellulose. Bergman et al. [49], associated the changes in the treated biomass to certain temperature ranges as follows: (1) 100 to 150°C, this stage is known as a nonreactive drying where the chemical components of the biomass remain almost intact and it only causes the removal of surface moisture. This reduces porosity and small structural ruptures appear; (2) from 150 to 200 °C, it is known as a stage of reactive drying and at this point, lignin begins a soft decomposition. At these temperatures, structural distortions change the original structure of the biomass, by breaking hydrogen bonds and carbon, resulting in emissions of extracts and lipophilic compounds; (3) 200 to 300 °C, it is the destructive drying zone, resulting in charring and devolatilization of the sample. At these temperatures, the cell structure is largely destroyed losing its fibrous nature, so it becomes more fragile. Below 250 °C, the mass loss is mainly attributed to the hemicellulose. Above 250 °C, the hemicellulose and cellulose decomposition occurs in volatile and char as a solid. Lignin has a small devolatilization in this condition. [15–17,19,20,39,48,50,51]

### *3.3.4. FTIR analysis*

The FTIR technique was used in order to investigate the effect of the torrefaction process on the chemical structure of bagasse. IR spectra of raw and torrefied bagasse are presented in Figure 3-4, where it is possible to observe that the changes in the bands occur in the proximity of the 4000 and 600 $cm^{-1}$, since organic components have fundamental vibration bands in the infrared middle region of 4000 and 200 $cm^{-1}$. The changes are mainly due to degradation of the polymer components of bagasse such as hemicellulose, consisting mostly of xylan, and to a lesser extent cellulose and lignin. During torrefaction these polymers can melt, vaporize, re-polymerize, char or either react [52]. This causes changes in the biomass properties and structure depending on their composition.

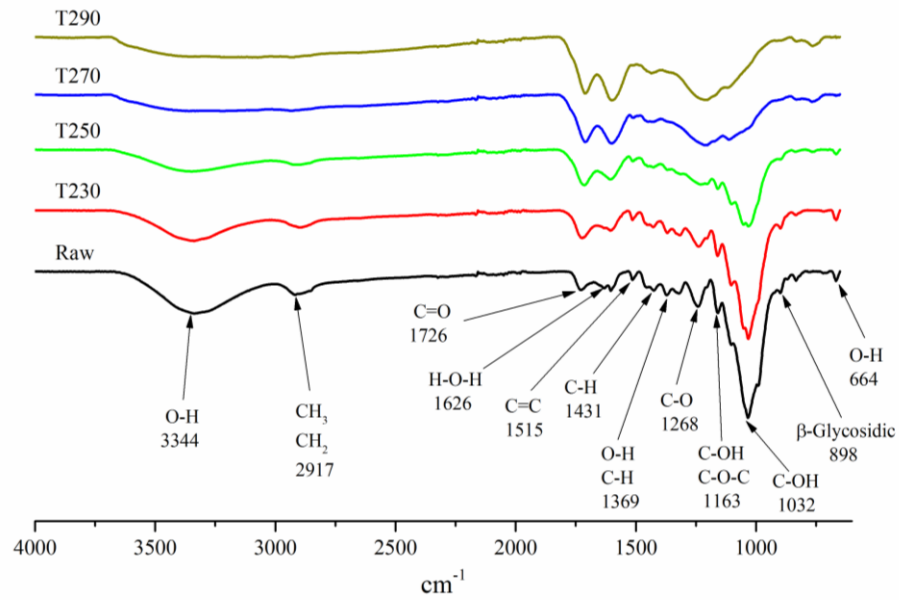


Figure 3-4. IR spectra for raw and torrefied biomass at 230, 250, 270, and 290°C.

The peaks in the IR spectrum correspond directly to the functional groups characteristic of the sample and its magnitude is indicative of the formation or disappearance of them as a result of

devolatilization, transformations, or chemical reactions. The allocation of bands in the IR spectrum for raw and torrefied bagasse is made based on a literature review where different species of bagasse were characterized by FTIR [22,34,53–59]. A more detailed description of the FTIR peaks obtained based on the main polymer components constituting the biomass (hemicellulose, cellulose and lignin) is shown in Table 3-2.

In Figure 3-4 it is possible to observe the spectrum of raw and torrefied biomass, and a wide band is displayed on 3334 $cm^{-1}$ approximately for all samples, and it is attributed to the vibration of O-H bonds [60]. This band is caused by the presence of alcoholic, hydroxyl, and phenolic groups involved in hydrogen bonds of the lignin and certain carbohydrates. Its intensity decreases by methylation reactions, but increases with demethylation reactions [61]. This indicates that methylation occurs in the sample due to the process. In addition, the loss of this functional group in the material during the torrefaction process improves hydrophobicity because of the formation of nonpolar and unsaturated compounds.

Table 3-2. Main band assignments of the FTIR spectra of the raw and torrefied bagasse [22,34,53–59].

| Wave Number ($cm^{-1}$) | Assignment/functional group | Polymer |
|---|---|---|
| 3400 | O-H Stretching bonds | Lignin |
| 2800 - 2900 | C-H Stretching of Methyl (-$CH_3$) and Methylene groups (-$CH_2$-) | Lignin |
| 1735 - 1739 | Stretching of C=O (C=O) of oxygenated functionalities in conjugated and unconjugated systems (carbonyl / carboxyl groups) | Hemicellulose |
| 1632 | H-O-H inflections of adsorbed water, C=C | Lignin |
| 1600 and 1506 - 1510 | Vibrations aromatic lignin skeletons (C=C) and vibrations of C=O | Lignin |
| 1424 - 1428 | Deformations of C-H and carbohydrates (δCHal) | Lignin |
| 1370 | Deformations of C-H | Cellulose, hemicellulose, lignin |
| 1310 | Movements (Wagging) in CH2 | Cellulose, hemicellulose |
| 1280 | Flection in C-H | Crystalline cellulose |
| 1271 | Aromatic rings stretching (C-O) | Guaiacyl lignin |
| 1159 | Asymmetrical stretching C-O-C and C-OH | Cellulose, hemicellulose |
| 1031 - 1034 | C-O, C=C, and C-C-O Stretching | Cellulose, hemicellulose, lignin |
| 898 | Deformation of C-H in amorphous cellulose xyloglucan | Cellulose, hemicellulose |
| 800 – 900 | Glucosidic linkage | Hemicellulose |
| 664 | O-H groups stretching outside of the plane | Cellulose, hemicellulose |

A small band is observed in 2917 $cm^{-1}$ attributed to the C-H stretching of aliphatic groups methyl, methylene, or methane (CHal) in the lignin. The peak at 1726 $cm^{-1}$ is associated to the stretching of the links C=O conjugated and unconjugated (carbonyl / carboxyl) of carboxylic acids in hemicellulose. Combined with this peak, there can appear structures generated by the dehydration

of cellulose (C=O), which can also be observed around 1620 cm-1 (C=C), and which increase with the severity of the process. Previous work [21,55] suggests that the torrefaction removes this signal by decreasing the amount of acetyl groups, which leads to new products that appear in low wavenumbers (1700 $cm^{-1}$) as evidenced in this work. As reported by Chang et al. [21], at values close to 1632 $cm^{-1}$ a peak for absorbed water should appear, but in our work it was not detected probably due to some overlap with another nearby peak.

Peaks located between 1600 and 1506 to 1514 $cm^{-1}$ are assigned to vibrations in aromatic skeletons of lignin (C=C) and they are maintained with an increasing tendency as temperature increases. The latter occurs, firstly because lignin does not suffer significant modifications and secondly, due to the fact that cellulose and hemicellulose degrade to form primary char rich in aromatic groups, which are more thermostable. This leads to a greater uniformity in the structure of the torrefied.

Peaks from deflections and deformations in the C-H bonds, correspondent to some amorphous polysaccharides of lignin and cellulose are observed around 1456 and 1431 $cm^{-1}$. Soft vibrations can be seen in values close to 1370 $cm^{-1}$, which are smoothed due to deformation in amorphous cellulose (C-H). Vibrations between 1268 and 1163 $cm^{-1}$ are due to the stretching of the aromatic rings of guaiacyl lignin (C-O) and stretching in the antisymmetric oxygen bridge C-OH and C-O-C of the cellulose and hemicellulose. The intensity of these bands in this region tends to disappear because of torrefaction, while a deformation of syringyl rings and a decomposition of xylan hemicellulose occurs.

One of the most pronounced bands in the region close to 1031 and 1034 $cm^{-1}$ occurs due to vibrations in C-O, C=C and C-C-O form groups of cellulose, hemicellulose and lignin. The intensity of these peaks is stable below 230°C, but as the sample was heated above 250°C, the signal intensity of these groups decreased. Lignin is an aromatic compound in its chemical nature, so it degrades much less than hemicellulose and cellulose, and decomposes producing phenols due to the breaking of the ether linkages. A very smooth peak near 898 $cm^{-1}$ is assigned to beta-glycosidic type links in glucose from cellulose and hemicellulose. This signal decreases with process temperature. Finally, it has a small band at 664 $cm^{-1}$ attributed to the vibration of O-H groups out of the plane, and degraded as temperature increase.

For all these peaks located below 1726 $cm^{-1}$, it is possible to observe that for the temperature of 230°C their intensities do not change, remaining approximately constant. The main change that was observed for the temperature of 230°C was a slight decrease in the intensity of the peaks located at 3344 $cm^{-1}$ and 2917 $cm^{-1}$, corresponding to light volatile molecules that are expelled at low process temperatures. Above 230°C, changes in all functional groups of the biomass become considerable.

### *3.3.5. SEM analysis*

The SEM micrographs obtained from raw and torrefied bagasse for different thermal conditions are summarized in Figure 3-5. In general, physical changes are observed in the morphology of the samples by alterations in structure and cellular tissue. From images, it was possible to identify that torrefaction leads to degradation of the bagasse due to devolatilization, depolymerization, and

carbonization reactions of hemicellulose, cellulose and lignin [19], which increases when the process temperature rises.

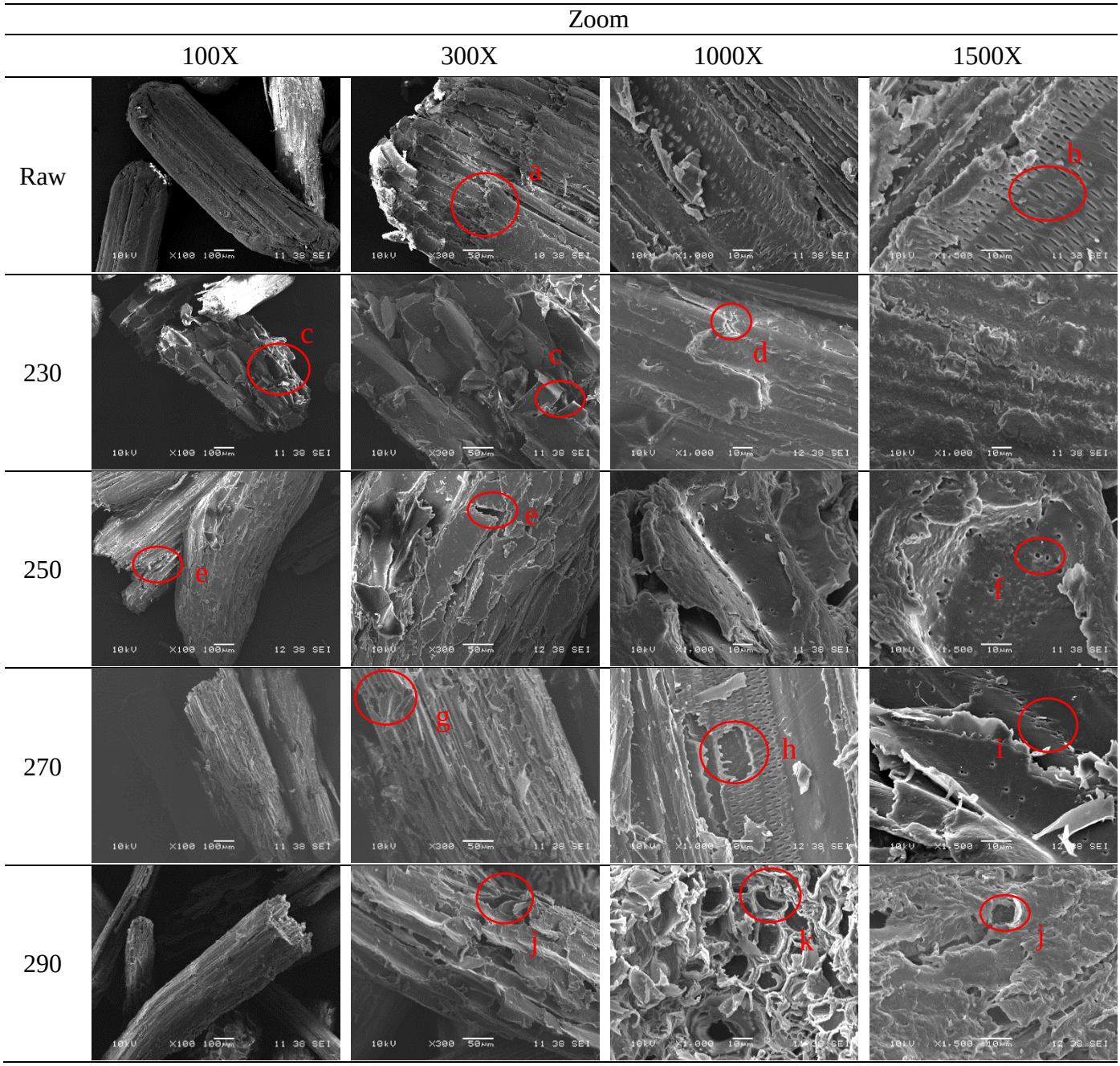


Figure 3-5. SEM micrographs for raw and torrefied bagasse at 230, 250, 270, and 290°C.

In the micrographs for raw material, it is possible to notice that the particle structure is compact and the biomass has a fibrillary organization of smooth, homogeneous parts and some rough ones in its external surface. As the zoom is increased, it is possible to notice some damage to the material at the end of some particles (a), perhaps due to the grinding pre-treatment carried out prior to heat treatment. Increasing the zoom to 1000X and 1500X, it is possible to capture some of the internal

structure, which is seen in a sheet-like form with some well-defined porous ovals (b) interconnecting in a radial direction to form a complete particle.

In the torrefied sample at 230 °C it is possible to observe, even with the smallest zoom, some visible damages to their external structure (c). Partial warps are appreciated (d), but not very strong at this low severity of the process. When the bagasse is torrefied at 250 °C, some cracks in the outer walls of the torrefied bagasse are displayed (e), and some appearances of pores (f), possibly generated by the devolatilization of less thermostable polymers. These new pores are visibly different from those observed in the micrographs of raw material, since these latter are rounded

When those particles treated with higher thermal conditions, i.e., 270 and 290 °C, are observed, it is possible to observe much more marked and deeper cracks in the torrefied particles (g, j). It is also noticeable that those outer surfaces of the particles, originally flat, are now presented with some deteriorated parts, large material detachments, and merging of some pores in these sections (h, i). A special micrograph was obtained for a torrefied sample at 290°C, where the cell structure is observed with considerable damage, and some obvious deformations (k) which confirm the severity of the torrefaction process all over the biomass structure.

It is noteworthy to mention that pores, cracks and crater formation is a direct consequence of pronounced volatile material release, and it is enhanced when increasing the process temperature. This is consistent with the information found in the proximate analysis (Figure 3-2(a)), where the volatile matter content decreases as torrefaction occurs in more severe conditions. Similarly, the cell structure appears to be melted, shrunk and almost entirely destroyed, due to the degradation of hemicellulose and amorphous cellulose portion [22].

### *3.3.6. Combustion tests*

Reactivity tests were performed on raw and torrefied biomass at 250, 270 and 290°C. These tests, as described in previous sections, were carried out for two temperature ramps. The first ramp at 105°C with 30 minutes of residence time, and the second ramp from 105°C to 900°C with heating rates of 5, 10, 15, 20°C/min. In Figure 3-6, the TGA and DTG for reactivity testing performed on all samples for a heating rate of 5°C/min are shown. The mass loss of raw material starts earlier than in the other samples, as consequence of its untreated polymeric structure. This structure contains weak functional groups, such as C-H and O-H (see Figure 3-4**)** which are responsible for volatile material generation when the biomass is heated by increasing the material reactivity.

On other hand, for the torrefied samples, the weak functional groups (e.g. C-H and O-H) were partially removed, causing mass loss to begin later than raw material. For the torrefied sample at 250°C, hemicellulose and cellulose decompose partially and only 6.88 and 25.57% respectively remain in the sample (see Table 3-1). This can be ratified in Figure 3-4 for sample T250, where unstable functional groups like CH3, O-H, and C-OH are present in the sample. In addition, some stable groups formed during the torrefaction process from primary reactions like some aromatic compounds (shown in Figure 3-4) around 700-750$cm^{-1}$ and 1515-1626$cm^{-1}$, contribute to decrease the reactivity in comparison with raw biomass. The last material to begin its mass loss was that torrefied at 290°C, because it does not have unstable polymers such as hemicellulose and cellulose

in its structure (see Table 3-1), and has a lignified structure result of primary reactions and aromatic groups formed during the process.

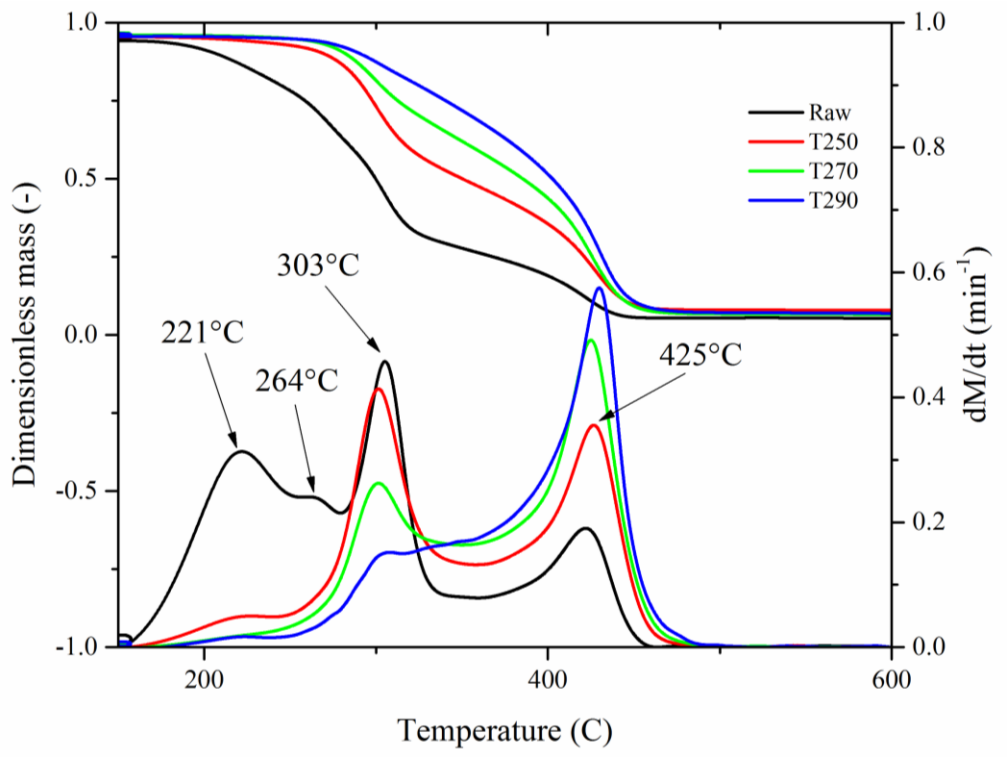


Figure 3-6. TGA and DTG for raw and torrefied samples for a heating rate of 5°C/min.

In Figure 3-6, the DTG for raw biomass shows a large initial peak around 221°C, because of the large amount of hemicellulose in its structure compared to torrefied samples. This peak decrease in the other samples, indicating that the amount of hemicellulose in the torrefied materials decreased significantly, to the point of almost fading in the T290 sample. An unexpected behavior was presented in this curve at about 264°C because a small additional peak was observed in the torrefaction process. This could be attributed to the amorphous structure of the cellulose, less thermally stable than the crystalline cellulose, which begins its decomposition at this lower temperature and can be observed separated at a peak due to the low heating rate at which the process was conducted, in accordance with results from Jiang et al. [62]. At higher heating rates, this small peak was not observed.

A peak presented at temperature around 303°C corresponds to the breakdown of cellulose. In the untreated material sample, this peak is shown as larger because, as it was previously mentioned and shown in Table 3-1, the amount of cellulose material is 100% of the original amount. An interesting behavior in this cellulose peak is that the treatment does not generate great impact therein at temperatures below 250°C, as the peak for the T250 material is just below of that for raw material. When the material is treated at higher temperatures, i.e., samples T270 and T290, the amount of cellulose is affected, as it is evidenced at the peak of these two samples, which decreases considerably.

The final peak in DTG curves is attributed to lignin and other carbonaceous materials produced in primary reactions of cellulose and hemicellulose. In the untreated material, this peak is lower than those presented in the other samples. Due to decomposition of the less thermally stable polymers such as cellulose and hemicellulose, the proportion of lignin in the material increases considerably, which is clearly observed in the peaks of the torrefied materials at higher temperatures. In addition, this is consistent with the aforementioned and claimed by different authors [63,64], who found that the hemicellulose polymers and cellulose, because of their primary decomposition, yield a char primarily formed by aromatic structures that provide and increase the aromatic structures in the material.

This behavior in the peak separation for each of the polymers in the material is possible to be observed at low heating rates because at high heating rates this behavior was avoided, the peaks of the cellulose and hemicellulose tend to overlap, such as it is shown in Figure 3-7. In this graph, it is possible to observe how for the T290 material with a heating rate of 20°C/min, only a broad peak appears where the decomposition of each component in the process is impossible to differentiate.

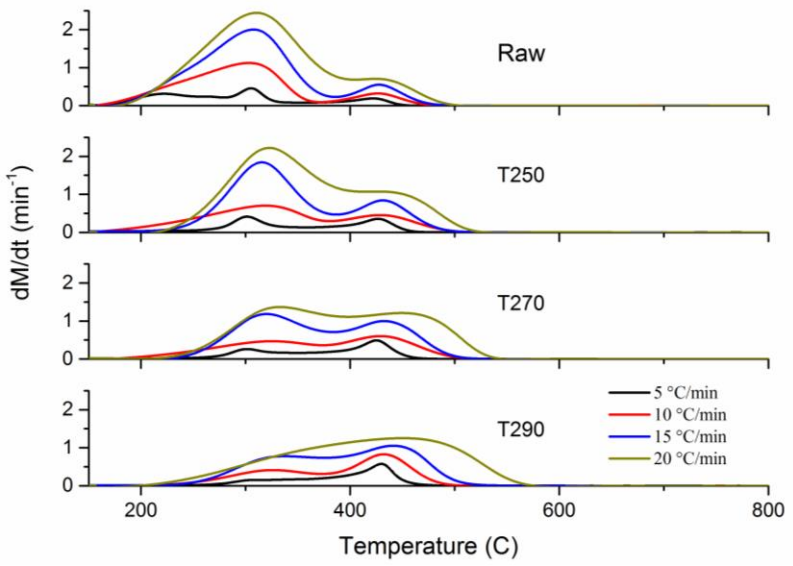


Figure 3-7. DTG for raw and torrefied samples for all heating rates.

The results presented in this study of reactivity can be compared with those obtained in the FTIR analysis, where increases are observed in the number of those peaks that reflect aromatic compounds, evidenced by peaks 1600 $cm^{-1}$, 1506-1510 $cm^{-1}$, and 1271 $cm^{-1}$. These peaks clearly rise with increases in the temperature of the process, and evidently, a decrease is observed for groups of those less thermally stable polymers as the ones present at 3400 $cm^{-1}$ and 2800-2900 $cm^{-1}$. These results shown in Figure 3-4, match with the obtained in these reactivity testing, volatiles directly reflect the reactivity of the material, but when the aromaticity of the material increases the reactivity decreases.

Activation energies that describe the behavior of each material in the combustion process were obtained and are shown in Figure 3-8(a). The procedure was performed by the Ozawa iso-

conversional method [32], by means of which a distribution of activation energies for the entire spectrum of conversion in the material can be obtained from the material conversion in each thermal condition of the tests. Kinetic parameters are shown in Table 3-3 for a conversion level of 50% in the process and order reaction one.

Table 3-3. kinetic parameters for torrefied sugarcane bagasse.

| Sample | Ea (kJ/kmol) | A ($s^{-1}$) |
|---|---|---|
| Raw | 171,00 | 1,05E+17 |
| T250 | 218,55 | 8,35E+17 |
| T270 | 166,29 | 3,42E+12 |
| T290 | 143,53 | 2,80E+10 |

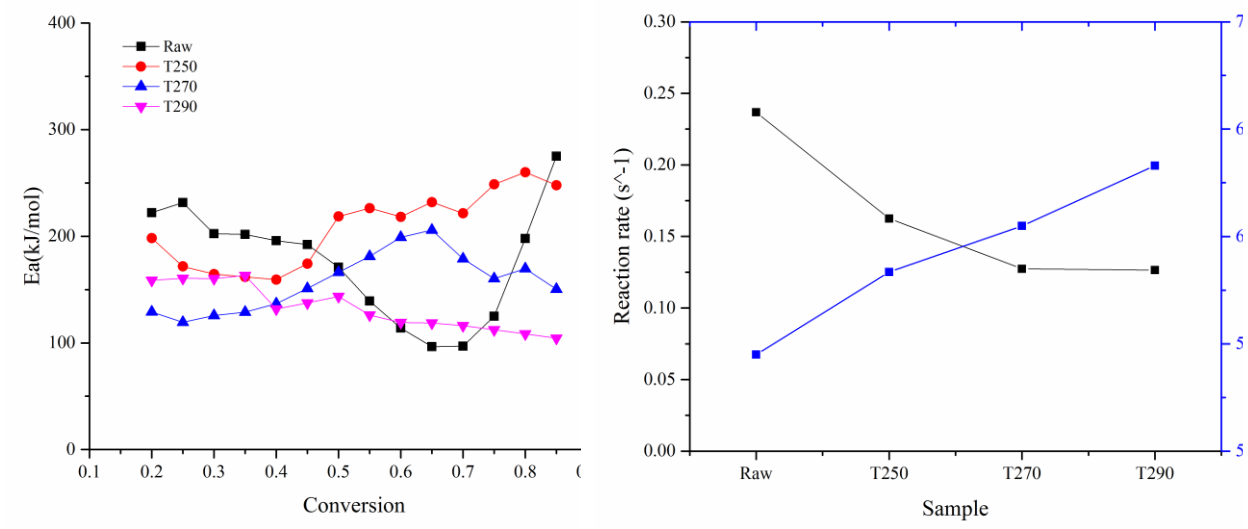


(a) (b)

Figure 3-8. Activation energy distribution from Ozawa iso-conversional method (a), and reaction rate and reactivity index (b), for raw and torrefied bagasse in a combustion process.

Although many authors measure the reactivity of a material when the maximum speed of mass loss is reached in the process, in this work it was chosen to measure it at 25% of the conversion. In Figure 3-8(b), the variation of reactivity with the pre-treatment can be observed. This tendency was consistent with the above discussion, where the reactivity of the treated material decreases with the torrefaction temperature due to the lower presence of thermally unstable compounds after the process and more energy requirements for obtaining a conversion level in comparison with other samples. The reactivity index indicated in Figure 3-8(b) corresponds to a temperature value where the decomposition reaches the value of 25%. While the reactivity index is higher, the evaluated material presents a lower reactivity. This result was expected according to the results presented in the lignocellulosic analysis, and in the results of the FTIR analyses of the torrefied biomass.

## 3.4. Conclusions

An important Colombian agricultural residue such as sugarcane bagasse was subjected to torrefaction and then to a combustion process. Kinetic parameters that give information about the

reactivity or thermal behavior of the raw and torrefied sugarcane bagasse in combustion process were obtained. A complete physical and chemical characterization of torrefied sugarcane bagasse was performed in order to explain the decrease in reactivity when is subjected to a combustion process.

From the analysis of torrefied sugarcane bagasse, it was observed that the torrefaction produces a carbon enrichment, accompanied by a decrease on the functionalities of hydrogen and oxygen in the char, and increases in HHV of about 30%. However, the mass loss becomes considerable when temperature increases, making the mass yield parameter to decrease considerably. In addition, the reactivity of raw biomass is high because of volatile material in its structure. Torrefaction severity decreases the biomass reactivity because of volatiles deployed in the process and char formation from polymers. This shows that the solid product of torrefaction (char) has good properties when being considered as a solid fuel because of the properties similar to those of coal, with great potential for the energy industry.

The changes in the main functional groups (O-H, C=O, C=C, C-H and C-O-C) shown in the FTIR spectrum, are indicative of structural changes in hemicellulose, cellulose and lignin. By increasing the severity of the process, the two main structural carbohydrates (hemicellulose and cellulose) have been mostly affected in the sugarcane bagasse. Thus, the char produced has been enriched in aromatic compounds, with the almost complete disappearance of aliphatic compounds, which is interpreted as an increase in lignified material by degradation of cellulose and hemicellulose.

## Acknowledgments

D.A Granados wish to thank the Colombian Administrative Department of Science, Technology and Innovation (COLCIENCIAS) (Departamento Administrativo de Ciencia, Tecnología e Innovacion) for financial support.

## References

[1] Unidad de Planeación Minero Energética (UPME). Atlas del Potencial Energético de la Biomasa Residual en Colombia. 1st ed. UPME; 2010.

[2] van der Stelt MJC, Gerhauser H, Kiel JH a., Ptasinski KJ. Biomass upgrading by torrefaction for the production of biofuels: A review. Biomass and Bioenergy 2011;5. doi:10.1016/j.biombioe.2011.06.023.

[3] Chen W, Peng J, Bi XT. A state-of-the-art review of biomass torrefaction , densi fi cation and applications. Renew Sustain Energy Rev 2015;44:847–66. doi:10.1016/j.rser.2014.12.039.

[4] Michael Stöcker RSAPTB. Advances in Thermochemical Conversion of Biomass - Introduction. Recent Adv. Thermo-Chemical Convers. Biomass, vol. 1. 1st ed., Elsevier B.V.; 2015, p. 3–29. doi:10.1016/B978-0-444-63289-0.00015-6.

[5] Chen W-H. Torrefaction. Elsevier B.V.; 2015. doi:10.1016/B978-0-12-800080-9.00010-4.

[6] Chew JJ, Doshi V. Recent advances in biomass pretreatment – Torrefaction fundamentals and technology. Renew Sustain Energy Rev 2011;15:4212–22.

doi:10.1016/j.rser.2011.09.017.

[7] Batidzirai B, Mignot a. PR, Schakel WB, Junginger HM, Faaij a. PC. Biomass torrefaction technology: Techno-economic status and future prospects. Energy 2013;62:196–214. doi:10.1016/j.energy.2013.09.035.

[8] Fisher EM, Dupont C, Darvell LI, Commandré J-M, Saddawi a, Jones JM, et al. Combustion and gasification characteristics of chars from raw and torrefied biomass. Bioresour Technol 2012;119:157–65. doi:10.1016/j.biortech.2012.05.109.

[9] Chen WH, Chen CJ, Hung CI, Shen CH, Hsu HW. A comparison of gasification phenomena among raw biomass, torrefied biomass and coal in an entrained-flow reactor. Appl Energy 2013;112:421–30. doi:10.1016/j.apenergy.2013.01.034.

[10] Mi B, Liu Z, Hu W, Wei P, Jiang Z, Fei B. Bioresource Technology Investigating pyrolysis and combustion characteristics of torrefied bamboo , torrefied wood and their blends. Bioresour Technol 2016;209:50–5. doi:10.1016/j.biortech.2016.02.087.

[11] Liu Z, Hu W, Jiang Z, Mi B, Fei B. Investigating combustion behaviors of bamboo, torrefied bamboo, coal and their respective blends by thermogravimetric analysis. Renew Energy 2016;87:346–52. doi:10.1016/j.renene.2015.10.039.

[12] Antonio Bizzo W, Lenço PC, Carvalho DJ, Veiga JPS. The generation of residual biomass during the production of bio-ethanol from sugarcane, its characterization and its use in energy production. Renew Sustain Energy Rev 2014;29:589–603. doi:10.1016/j.rser.2013.08.056.

[13] Wilk M, Magdziarz A, Kalemba I. Characterisation of renewable fuels' torrefaction process with different instrumental techniques. Energy 2015;87:259–69. doi:10.1016/j.energy.2015.04.073.

[14] Nocquet T, Dupont C, Commandre JM, Grateau M, Thiery S, Salvador S. Volatile species release during torrefaction of wood and its macromolecular constituents: Part 1 - Experimental study. Energy 2014;72:180–7. doi:10.1016/j.energy.2014.02.061.

[15] Chen W-H, Kuo P-C. A study on torrefaction of various biomass materials and its impact on lignocellulosic structure simulated by a thermogravimetry. Energy 2010;35:2580–6. doi:10.1016/j.energy.2010.02.054.

[16] Chen W-H, Kuo P-C. Torrefaction and co-torrefaction characterization of hemicellulose, cellulose and lignin as well as torrefaction of some basic constituents in biomass. Energy 2011;36:803–11. doi:10.1016/j.energy.2010.12.036.

[17] Collard FX, Blin J. A review on pyrolysis of biomass constituents: Mechanisms and composition of the products obtained from the conversion of cellulose, hemicelluloses and lignin. Renew Sustain Energy Rev 2014;38:594–608. doi:10.1016/j.rser.2014.06.013.

[18] Joshi Y, Di Marcello M, De Jong W. Torrefaction: Mechanistic study of constituent transformations in herbaceous biomass. J Anal Appl Pyrolysis 2015;115:353–61. doi:10.1016/j.jaap.2015.08.014.

[19] Tumuluru JS, Sokhansanj S, Hess JR, Wright CT, Boardman RD. A review on biomass torrefaction process and product properties for energy applications. Ind Biotechnol 2011;7:384–401. doi:10.1089/ind.2011.0014.

[20] Werner K, Pommer L, Broström M. Thermal decomposition of hemicelluloses. J Anal Appl Pyrolysis 2014;110:130–7. doi:10.1016/j.jaap.2014.08.013.

[21] Chang S, Zhao Z, Zheng A, He F, Huang Z, Li H. Characterization of Products from Torrefaction of Sprucewood and Bagasse in an Auger Reactor. Energy & Fuels 2012;26:7009–17. doi:10.1021/ef301048a.

[22] Wong Sak Hoi L, Martincigh BS. Sugar cane plant fibres: Separation and characterisation. Ind Crops Prod 2013;47:1–12. doi:10.1016/j.indcrop.2013.02.017.

[23] Acharya B, Sule I, Dutta A. A review on advances of torrefaction technologies for biomass processing. Biomass Convers Biorefinery 2012:349–69. doi:10.1007/s13399-012-0058-y.

[24] Mohan D, Pittman CU, Steele PH. Pyrolysis of Wood / Biomass for Bio-oil : A Critical Review. Energy & Fuesl 2006;20:848–89. doi:10.1021/ef0502397.

[25] Basu P. Biomass Gasification, Pyrolysis and Torrefaction. Elsevier; 2013. doi:10.1016/B978-0-12-396488-5.00004-6.

[26] Toptas A, Yildirim Y, Duman G, Yanik J. Combustion behavior of different kinds of torrefied biomass and their blends with lignite. Bioresour Technol 2015;177:328–36. doi:10.1016/j.biortech.2014.11.072.

[27] Bridgeman TG, Jones JM, Shield I, Williams PT. Torrefaction of reed canary grass, wheat straw and willow to enhance solid fuel qualities and combustion properties. Fuel 2008;87:844–56. doi:10.1016/j.fuel.2007.05.041.

[28] Costa FF, Wang G, Costa M. Combustion kinetics and particle fragmentation of raw and torrified pine shells and olive stones in a drop tube furnace. Proc Combust Inst 2014;35:3591–9. doi:10.1016/j.proci.2014.06.024.

[29] Fang MX, Shen DK, Li YX, Yu CJ, Luo ZY, Cen KF. Kinetic study on pyrolysis and combustion of wood under different oxygen concentrations by using TG-FTIR analysis. J Anal Appl Pyrolysis 2006;77:22–7. doi:10.1016/j.jaap.2005.12.010.

[30] Jones JM, Bridgeman TG, Darvell LI, Gudka B, Saddawi a., Williams a. Combustion properties of torrefied willow compared with bituminous coals. Fuel Process Technol 2012;101:1–9. doi:10.1016/j.fuproc.2012.03.010.

[31] Ramajo-Escalera B, Espina A, García JR, Sosa-Arnao JH, Nebra SA. Model-free kinetics applied to sugarcane bagasse combustion. Thermochim Acta 2006;448:111–6. doi:10.1016/j.tca.2006.07.001.

[32] Ozawa T. A New Method of Analyzing Thermogravimetric Data. Bull Chem Soc Jpn 1965;38:1881–6. doi:10.1246/bcsj.38.1881.

[33] Khan AA, de Jong W, Jansens PJ, Spliethoff H. Biomass combustion in fluidized bed boilers: Potential problems and remedies. Fuel Process Technol 2009;90:21–50. doi:10.1016/j.fuproc.2008.07.012.

[34] Yang H, Yan R, Chen H, Lee DH, Zheng C. Characteristics of hemicellulose, cellulose and lignin pyrolysis. Fuel 2007;86:1781–8. doi:10.1016/j.fuel.2006.12.013.

[35] Wang G, Luo Y, Deng J, Kuang J, Zhang Y. Pretreatment of biomass by torrefaction. Chinese Sci Bull 2011;56:1442–8. doi:10.1007/s11434-010-4143-y.

[36] Deng J, Wang G, Kuang J, Zhang Y, Luo Y. Pretreatment of agricultural residues for co-gasification via torrefaction. J Anal Appl Pyrolysis 2009;86:331–7. doi:10.1016/j.jaap.2009.08.006.

[37] Shen DK, Gu S, Bridgwater a. V. The thermal performance of the polysaccharides extracted from hardwood: Cellulose and hemicellulose. Carbohydr Polym 2010;82:39–45. doi:10.1016/j.carbpol.2010.04.018.

[38] Sule I. Torrefaction Behaviour of Agricultural Biomass. The University of Guelph, 2012.

[39] Bergman PC a, Boersma a R, Zwart RWR, Kiel JH a. Torrefaction for biomass co-firing in existing coal-fired power stations. Energy Res Cent Netherlands ECN ECNC05013 2005:71.

[40] Sandoval-Torres S, Jomaa W, Marc F, Puiggali J-R. Causes of color changes in wood during drying. For Stud China 2010;12:167–75. doi:10.1007/s11632-010-0404-8.

[41] Sundqvist B. Colour changes and acid formation in wood during heating. Lulea University of Technology, 2004.

[42] Dietenberger MA, Hasburgh LE. Wood Products: Thermal Degradation and Fire. Elsevier Ltd.; 2016. doi:10.1016/B978-0-12-803581-8.03338-5.

[43] Aydemir D, Gunduz G, Ozden S. The influence of thermal treatment on color response of wood materials. Color Res Appl 2012;37:148–53. doi:10.1002/col.20655.

[44] Willits C., Underwood J., Lento H., Ricciuti C. BROWNING OF SUGAR SOLUTIONS. I. Effect of pH and Type of Amino Acid in Dilute Sugar Solutions. J Food Sci 1958;23:61–7.

[45] Lento H., Underwood JC, Willits C. BROWNING OF SUGAR SOLUTIONS. II. Effect of the Position of Amino Group in the Acid Molecule in Dilute Gluscose Solutions. J Food Sci 1958;23:68–71.

[46] Underwood J., Lento H., Willits C. BROWNING OF SUGAR SOLUTIONS. 3. Effect of pH on the Color Preduced in Dilute Gluscose Solutions Containing Amino Acids with the Amino Group in Different Positions in the Molecule. J Food Sci 1958;24:181–4.

[47] Chen W-H, Kuo P-C. Isothermal torrefaction kinetics of hemicellulose, cellulose, lignin and xylan using thermogravimetric analysis. Energy 2011;36:6451–60. doi:10.1016/j.energy.2011.09.022.

[48] Stefanidis SD, Kalogiannis KG, Iliopoulou EF, Michailof CM, Pilavachi PA, Lappas AA. A study of lignocellulosic biomass pyrolysis via the pyrolysis of cellulose, hemicellulose and lignin. J Anal Appl Pyrolysis 2014;105:143–50. doi:10.1016/j.jaap.2013.10.013.

[49] Bergman P, Kiel J. Torrefaction for biomass upgrading. 14th Eur Biomass Conf Exhib Paris, Fr 17-21 Oct 2005:3–8.

[50] García R, Pizarro C, Lavín AG, Bueno JL. Biomass proximate analysis using thermogravimetry. Bioresour Technol 2013;139:1–4. doi:10.1016/j.biortech.2013.03.197.

[51] Saldarriaga JF, Aguado R, Pablos A, Amutio M, Olazar M, Bilbao J. Fast characterization of biomass fuels by thermogravimetric analysis (TGA). Fuel 2015;140:744–51. doi:10.1016/j.fuel.2014.10.024.

[52] Tumuluru JS, Sokhansanj S, Wright CT, Kremer T. GC Analysis of Volatiles and Other

Products from Biomass Torrefaction Process. Adv Gas Chromatogr Agric Biomed Indistrial Appl 2012:211–34. doi:10.5772/33488.

[53] Pohlmann JG, Osório E, Vilela ACF, Diez MA, Borrego AG. Integrating physicochemical information to follow the transformations of biomass upon torrefaction and low-temperature carbonization. Fuel 2014;131:17–27. doi:10.1016/j.fuel.2014.04.067.

[54] Li M-F, Chen C-Z, Li X, Shen Y, Bian J, Sun R-C. Torrefaction of bamboo under nitrogen atmosphere: Influence of temperature and time on the structure and properties of the solid product. Fuel 2015;161:193–6. doi:10.1016/j.fuel.2015.08.052.

[55] Ibrahim RHH, Darvell LI, Jones JM, Williams A. Physicochemical characterisation of torrefied biomass. J Anal Appl Pyrolysis 2013;103:21–30. doi:10.1016/j.jaap.2012.10.004.

[56] Na B Il, Ahn BJ, Lee JW. Changes in chemical and physical properties of yellow poplar (Liriodendron tulipifera) during torrefaction. Wood Sci Technol 2014;49:257–72. doi:10.1007/s00226-014-0697-1.

[57] Toscano G, Pizzi A, Foppa Pedretti E, Rossini G, Ciceri G, Martignon G, et al. Torrefaction of tomato industry residues. Fuel 2015;143:89–97. doi:10.1016/j.fuel.2014.11.039.

[58] Xu F, Yu J, Tesso T, Dowell F, Wang D. Qualitative and quantitative analysis of lignocellulosic biomass using infrared techniques : A mini-review. Appl Energy 2013;104:801–9. doi:10.1016/j.apenergy.2012.12.019.

[59] Pereira SC, Maehara L, Machado CMM, Farinas CS. Physical-chemical-morphological characterization of the whole sugarcane lignocellulosic biomass used for 2G ethanol production by spectroscopy and microscopy techniques. Renew Energy 2016;87:607–17. doi:10.1016/j.renene.2015.10.054.

[60] Liu Q, Wang S, Zheng Y, Luo Z, Cen K. Mechanism study of wood lignin pyrolysis by using TG–FTIR analysis. J Anal Appl Pyrolysis 2008;82:170–7. doi:10.1016/j.jaap.2008.03.007.

[61] Ghaffar SH, Fan M. Structural analysis for lignin characteristics in biomass straw. Biomass and Bioenergy 2013;57:264–79. doi:10.1016/j.biombioe.2013.07.015.

[62] Jiang Z, Liu Z, Fei B, Cai Z, Yu Y, Liu X. The pyrolysis characteristics of moso bamboo. J Anal Appl Pyrolysis 2012;94:48–52. doi:10.1016/j.jaap.2011.10.010.

[63] Pastorova I, Botto RE, Arisz PW, Boon JJ. Cellulose char structure: a combined analytical Py-GC-MS, FTIR, and NMR study. Carbohydr Res 1994;262:27–47. doi:10.1016/0008-6215(94)84003-2.

[64] McGrath TE, Chan WG, Hajaligol MR. Low temperature mechanism for the formation of polycyclic aromatic hydrocarbons from the pyrolysis of cellulose. J Anal Appl Pyrolysis 2003;66:51–70. doi:10.1016/S0165-2370(02)00105-5.

# Chapter 4. Devolatilization Kinetics of Biomass, Cellulose, Xylan, and Lignin in Torrefaction Temperature Range: Validation of Superposition Theory

**(Paper to be submitted to JAAP)**


## Abstract

A kinetic study of sugarcane bagasse (SCB), yellow poplar (YP), xylan, cellulose and lignin in torrefaction conditions is presented in this work. Thermal decomposition of materials was evaluated under isothermal conditions using a thermogravimetric analyzer in the temperature range 240- 300°C. Using the kinetic parameter of the main polymers of biomass, the superposition theory was deployed and then validated with good accuracy. This method is capable to predict a biomass behavior in a torrefaction process with deviations of only 10% for YP and 7% for SCB in all range evaluated. Modified expression for the superposition approach to predict the thermal degradation of biomass, which is validated for SCB and YP, was also suggested for the future use. Combustion reactivity kinetics was also developed for the torrefied SCB and for the torrefied and pyrolyzed YP in order to evaluate the impact of torrefaction in the reactivity. Activation energies were estimated as a function of conversion in accordance with the Ozawa's method for the non-isothermal events associated to different reaction steps. A reactivity index was determined for each sample when 25% of decomposition was reached. Results showed that a high index was obtained for all samples when torrefaction process was developed at high temperatures. Different stages according to the thermal degradation of each polymer in the material were identified in these combustion process.


***Keywords:*** Kinetics, superposition theory, reactivity, reaction rate.

## 4.1. Introduction

Biomass resources are defined as all organic matters, including plants and animals that do not take millions of years to form. The biomass resources include wood and wood wastes, agricultural crops and their waste by-products, municipal solid waste, animal wastes, waste from food processing industries, and aquatic plants and algae [1]. Biomass resources can also be classified into lignocellulosic and non-lignocellulosic materials. The lignocellulosic biomass consists of cellulose (a polymer glucosan), hemicelluloses (known as polyose), lignin (a complex phenolic polymer), organic extractives, and inorganic minerals (also called ash content) [2]. The first three compositions are collectively described as the polymeric constituents of biomass. While hemicellulose is a very reactive part of biomass, lignin shows a thermal stability over a wide temperature range [3]. Therefore, the degradation of biomass during a pyrolysis process depends highly on the behavior of the polymeric constituents of the biomass.

Despite of a huge potential of biomass energy resources, different limitations of biomass such as low heating value, low bulk density, high oxygen content, high moisture content, hygroscopic behavior, and fibrous nature decrease the use of biomass for energy generation [3]. To eliminate

these limitations, torrefaction process is introduced as a thermal pretreatment method that enhances the fuel qualities of biomass. Torrefaction is a mild pyrolysis process that is usually carried out in an inert atmospheric pressure condition and in a narrow temperature range of 200-300˚C [3–17]. The kinetics of a torrefaction process are, therefore, like a pyrolysis process. Devolatilization kinetics of torrefaction provide a good insight into the degree and rate at which mass loss will occur during the process. Torrefaction being a relatively slow process, it is governed primarily by kinetic rates of reaction rather than the mass transfer rate that occurs during the combustion process. So, any simulation or predictive model of the overall process needs to have an accurate data on its kinetic parameters.

Lignocellulosic biomass -a complex composite material made up of three main components - is a complex topic to analyze the thermal degradation [18]. So, the mass loss during the process depends on how these polymeric compositions behave at the given operating condition. Thermogravimetric mass loss curve shows three distinct zones, representing the decompositions of hemicellulose, cellulose, and lignin contents. Degradation temperature ranges of hemicellulose, cellulose, and lignin are 200-400 ˚C, 275-430 ˚C, and 127-900 ˚C, respectively [3]. Hemicellulose is the most reactive polymeric composition in the temperature range (200-300 ˚C) of torrefaction process. Breakdown of other two polymers is relatively small in this temperature range.

Different kinetic models have been examined for predicting the solid mass loss during the pyrolysis process. Global, three parallel, and competitive reaction models three primary approaches of kinetic studies of pyrolysis of biomass [19]. The competitive reactions model was further modified by adding secondary tar cracking reaction mechanism [20]. Shafizadeh and Bradbury model is also introduced to represent reaction kinetics in the fast pyrolysis in which the feedstock initially produces an activated intermediate biomass that then undergoes competitive and cracking reactions [19]. A more detailed review of kinetic modeling of biomass pyrolysis is presented in Di Blasi [21].

As the torrefaction process mainly decomposes hemicelluloses and partially degrades cellulose and lignin, Prins et al. [18] have examined two-stage reaction kinetics to predict the weight loss of willow biomass. They have represented the first step as the hemicellulose degradation and a second step as a cellulose decomposition that is relatively slow. Turner et al. [22] have used the approach of thermal degradation of individual polymeric compositions to predict the decomposition of wood (Fagus sylvatica L.). Similar assumptions have also reported on Rousset model to predict the anhydrous mass loss during the torrefaction process [23]. Chen and Kuo [4] have also concluded that the individual kinetics of polymeric compositions could be used to determine the kinetics of biomass. Such attempts for simplification would be valid only if there is no interaction synergy between the polymeric compositions when they are treated together. Repellin et al. [23] they tested this only for the spruce and beech. So, more studies for different biomass materials are necessary to support superposition theory of reaction kinetics. This study, therefore presents torrefaction kinetics of raw, hemicellulose, cellulose, and lignin and validates superposition approach using two new biomass materials (yellow poplar and sugarcane bagasse).

Replacing fossil fuels with biomass is generally considered both efficient and cost-effective [7]. Biomass co-firing is one of the promising techniques of converting biomass materials into energy. However, the amount of biomass used in co-firing plants are typically less than 20% of the fuel

supply [24]. Despite one of the most favorable alternatives to coal in energy generation, biomass possesses different limitations such as hydrophilic nature, low heating value, high fibrous, and high biological decay [3,25]. Pretreatment of biomass via torrefaction process has reduced such limitation significantly. Torrefied biomass materials have a high fuel ratio (Volatile/ fixed carbon ratio) [26,27] and low H/C and O/C ratios, making them more suitable for co-combustion. However, only a few studies have been reported on the combustion characteristics of torrefied biomass [4,7,24,28–32]. Given the fact that the torrefaction process produces different type of torrefied materials based on the particle size, operating conditions (time and temperature), materials, type of reactors, and torrefaction media. It is therefore essential to examine the combustion behavior of the torrefied materials, which are produced from the rotary torrefier.

This study, thus, focuses on kinetic study of torrefaction process using superposition approach and investigation of the combustion behavior of torrefied poplar wood produced in a two-stage indirectly heated rotary torrefier [33]. For the former work, two biomass materials (Yellow poplar and sugarcane bagasse) and polymeric compositions (Hemicellulose, cellulose, and lignin) were torrefied in the different temperatures in the Quartz Wool Matrix reactor and determined the kinetic parameters. The validity of the superposition approach of reaction kinetics of torrefaction was also tested. For the latter work, the combustion behavior and the combustion kinetics of torrefied materials were analyzed.

## 4.2. Methodology

### *4.2.1. Materials*

Grounded Yellow poplar (YP) and sugarcane bagasse (SCB) were used to examine the torrefaction kinetics. Xylan, cellulose, and lignin powder were also torrefied to validate the superposition approach of the reaction kinetics. While proximate analysis was measured in a muffle furnace per the ASTM D1762-84 standard, the ultimate analysis was analyzed in the Elemental analyzer (Model EA1110). Higher heating value was determined using a bomb calorimeter (Parr 6100). Measurement procedure for the analysis of the polymeric compositions of biomass is reported by Granados et al. [33]. Material properties are shown in Table 4-1.

Table 4-1: Important fuel properties of yellow poplar (YP) and sugarcane bagasse (SCB)

| Sample | Proximate analysis (%, db) | | | Ultimate analysis (%, dab) | | | | HHV (MJ/kg, db) | Polymeric compositions (%) | | |
|---|---|---|---|---|---|---|---|---|---|---|---|
| | VM | FC | ASH | C | H | N | O | | He | Ce | Li |
| YP | 82.40 | 16.20 | 1.40 | 45.90 | 6.10 | 0.40 | 47.60 | 18.4 | 25.71 | 61.49 | 12.80 |
| SCB | 81.86 | 15.98 | 2.03 | 42.09 | 5.42 | 0.18 | 51.50 | 16.79 | 35.21 | 37.59 | 27.20 |

### *4.2.2. Experimental Procedures*

The Quartz Wool Matrix (QWM) reactor shown in Figure 4-1 was deployed to measure continuous mass loss and temperature during the torrefaction process. Mass (YP, SCB, xylan, cellulose, and lignin) of 0.25 gm was collected in a container and torrefied in the QWM reactor at different torrefaction temperatures (240, 260, 270, 280, and 300 ˚C). Data points for the mass and temperature were recorded in computer via a precision balance and K-type of thermocouple, respectively. Residence time was maintained for 60 minutes for all the tests.

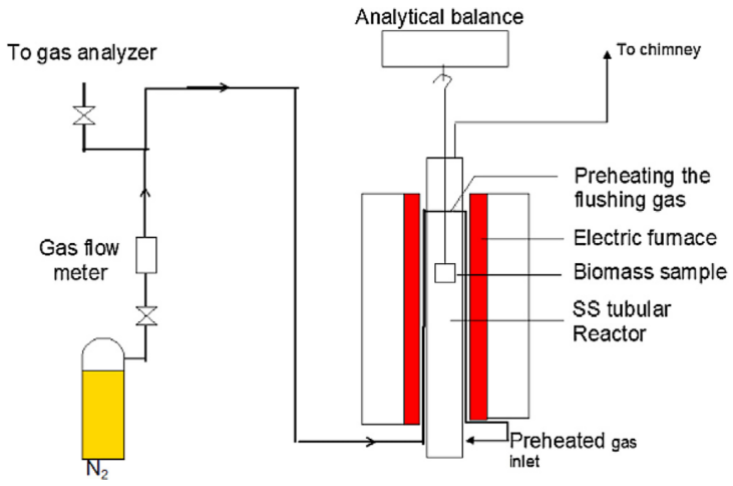


Figure 4-1. Schematic diagram of the experimental set-up

After torrefaction process, the torrefied poplar was subjected to pyrolysis process up to 800°C with heating rate of 10°C/min. The combustion tests were then carried out with torrefied bagasse and torrefied and pyrolyzed poplar. The combustion characteristics were investigated using a STA PT-1600 LINSEIS thermogravimetric analyzer using approximately 10mg of sample.

### *4.2.3. Torrefaction kinetics*

As reported by Repellin et al. [34], all reaction models including simple, Di Blazi-Lanzetta, and Rousset models could be used to predict the mass loss during torrefaction, this study has thus selected the simple model. The rate of reaction of biomass sample can be estimated as [4]:

$$\frac{d\alpha}{dt} = k(1-\alpha)^n \tag{4-1}$$

Where, $n$ is the order of reaction and $\alpha$ is the degree of conversion at a given time and is determined as:

$$\alpha = \frac{m_i - m}{m_i - m_f} \tag{4-2}$$

Where, $m$ is the mass of the biomass at time $t$, $m_i$ is the initial mass of the sample, and $m_f$ is the final weight of biomass sample. The initial mass of sample is the dried material at 105 ˚C, and the final mass of the torrefied biomass at the end of test.

The order of reactions for biomass and the polymeric compositions were determined graphically. Different graphs were plotted for different order of reactions and the order of reaction of was selected at which the $R^2$ value is maximum. To plot the graph, following equations derived by integrating Eq. (4-1) were used [4].

$$\ln\left(\frac{1-\alpha_0}{1-\alpha}\right) = k(t-t_0) \tag{4-3}$$

$$(1-\alpha)^{1-n} - (1-\alpha_0)^{1-n} = k(n-1)(t-t_0) \tag{4-4}$$

$\alpha_0$ is the degree of conversion at the beginning of torrefaction at time $t_0$. The reaction kinetic of the first order reaction and non-first order reaction can be determined by plotting Eq. (4-3) and Eq. (4-4), respectively. This can be repeated to different temperatures to determine the reaction kinetics of sample at a given temperature.

The temperature dependent reaction kinetic can also be expressed using Arrhenius law as:

$$k = A_0 \exp\left(-\frac{E_a}{RT}\right) \tag{4-5}$$

Where, $R$ is the universal gas constant (8.3146 J mol$^{-1}$ K$^{-1}$), $A_0$ is the pre-exponential factor, and $E_a$ is the activation energy of material. Eq. (4-5) can be simplified as:

$$\ln(k) = \ln(A_0) - \frac{E_a}{RT} \tag{4-6}$$

The reaction rate constant determined at a temperature could be then used to plot Eq. (4-6). The plot between ln($k$) and $1/T$ gives a straight line with the slope $-E_a/R$, and the y-intercept ln($A_0$). The pre-exponential factor and the activation energy can be then determined for different materials (yellow poplar – $k_{yp}$, sugarcane bagasse – $k_{scb}$, xylan - $k_{he}$, cellulose - $k_{ce}$, and lignin - $k_{li}$.

The superposition approach was then validated using the xylan, cellulose, and lignin fraction in raw yellow poplar and sugarcane bagasse as:

$$\alpha_{biomass} = \alpha_{he} + \alpha_{ce} + \alpha_{li} \tag{4-7}$$

$$\alpha_{biomass} = X_{he}k_{he} + X_{ce}k_{ce} + X_{li}k_{li} \tag{4-8}$$

Where $\alpha_i$ and $X_i$ stands for the conversion and proportion respectively of hemicellulose, cellulose and lignin during the process.

### *4.2.4. Combustion behavior*

Samples were subjected to a combustion process in a STA PT-1600 LINSEIS thermogravimetric analyzer in order to assess the reactivities. Approximately 10 mg of material was burned under three different thermal conditions with heating rates of 5, 10, and 15°C/min until 900°C. Prior to the combustion process, a soft heating at a temperature of 105°C for around 30 minutes was developed in order to obtain a complete drying process of the sample. A second heating ramp was made from this temperature to 900°C with the considered heating rate. DTG curves were obtained

in order to find some differences between tested materials and to compare them. For this combustion reactivity testing, only samples torrefied to 280 and 300°C were tested. Kinetic parameters for combustion process were obtained following Ozawa's iso-conversional method [35], in which a distribution of activation energies was obtained for the entire combustion process. In addition, a reactivity index was used in order to measure the reactivity of each sample. This index was chosen to measure the temperature for a conversion of 25% of the sample.

## 4.3. Results and Discussion

### *4.3.1. Torrefaction kinetics*

Experimental tests were developed for temperatures 240, 260, 270, 280, and 300°C, 4 of them were used to determine the kinetic parameters, and one (270°C) for the validation. In Figure 4-2, the temperature and mass loss profiles are shown for experimental tests developed for all materials. In this figure, one can see that xylan is the most reactive polymer at low temperatures. For all temperatures evaluated keeping residence time of 89 minutes, the char formation was found around 40%.

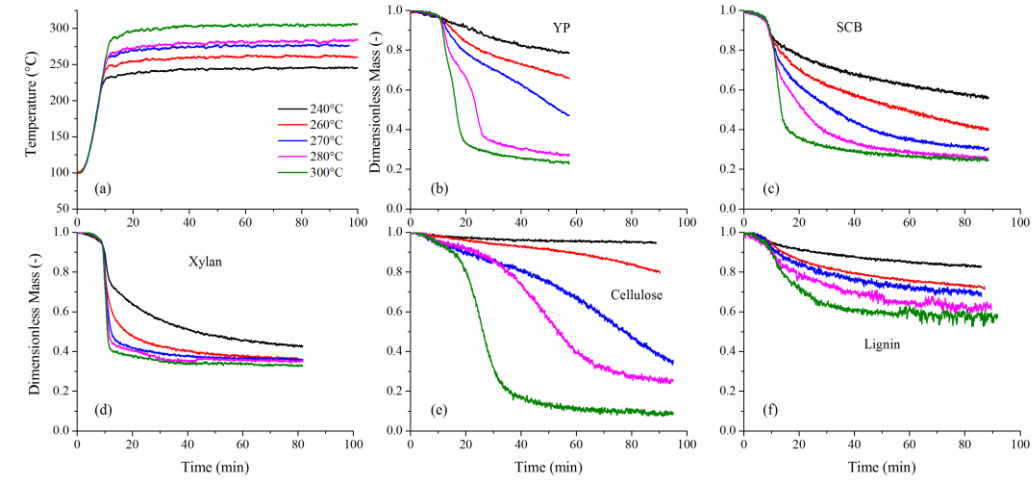


Figure 4-2. Torrefaction temperature (a) and dimensionless mass profiles (b-f) for samples during torrefaction process.

At low temperature, the mass degradation of the cellulose is almost imperceptible, around 5%, but with the increase in temperature, the devolatilization process becomes more prominent. Thus, the mass loss increases significantly at 300°C, resulting in only 8% the char. On the other hand, lignin is the most stable polymer showing a very low devolatilization in all temperature range evaluated in this study. The char yield (final mass) was found between 57-82%. This tells that the char yield in poplar or sugarcane bagasse at low temperatures is mostly due to lignin, follow by cellulose. But, when the torrefaction temperature increases, this char is mainly due to lignin and xylan.

From this experimental decomposition of each polymers of the biomass, a prediction of total biomass decomposition was made using fractions of hemicellulose, cellulose and lignin in the materials. This prediction was performed for temperatures of 240, 260, 280 and 300°C with a residence time of 80 minutes. The predictions made were then compared with the experimental results of each torrefied biomass for the same residence time and temperatures.

Errors for each predicted value are presented in the table attached to the Figure 4-3. One can see the good fit that can be obtained with this method. In this figure, lines have been drawn representing a deviation of 10% between the predicted and experimental values for each biomass.

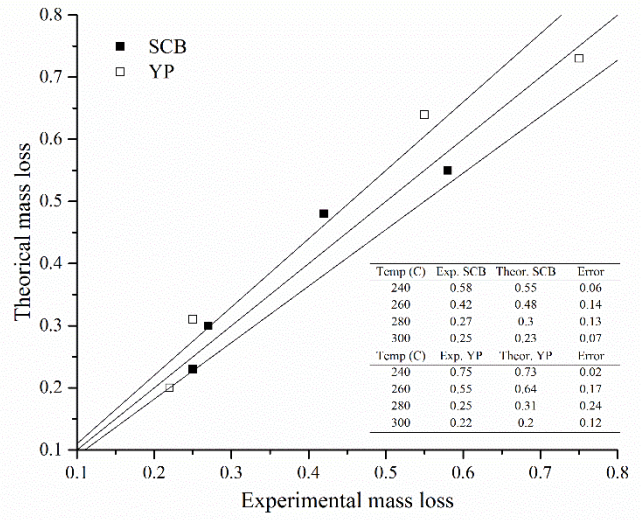


| Temp (C) | Exp. SCB | Theor. SCB | Error |
|---|---|---|---|
| 240 | 0.58 | 0.55 | 0.06 |
| 260 | 0.42 | 0.48 | 0.14 |
| 280 | 0.27 | 0.3 | 0.13 |
| 300 | 0.25 | 0.23 | 0.07 |
| Temp (C) | Exp. YP | Theor. YP | Error |
| 240 | 0.75 | 0.73 | 0.02 |
| 260 | 0.55 | 0.64 | 0.17 |
| 280 | 0.25 | 0.31 | 0.24 |
| 300 | 0.22 | 0.2 | 0.12 |

Figure 4-3. Adjust for experimental and predicted final mass loss for sugarcane bagasse (SCB) and poplar wood (YP).

For SCB, the average deviation was 10%, for YP it was 14%, suggesting a good prediction of the final mass yield. Thus, this method can be considered as an excellent option for predicting mass yield during a torrefaction process. This methodology, despite its simplicity, can only be applicable when the lignocellulosic contents are known.

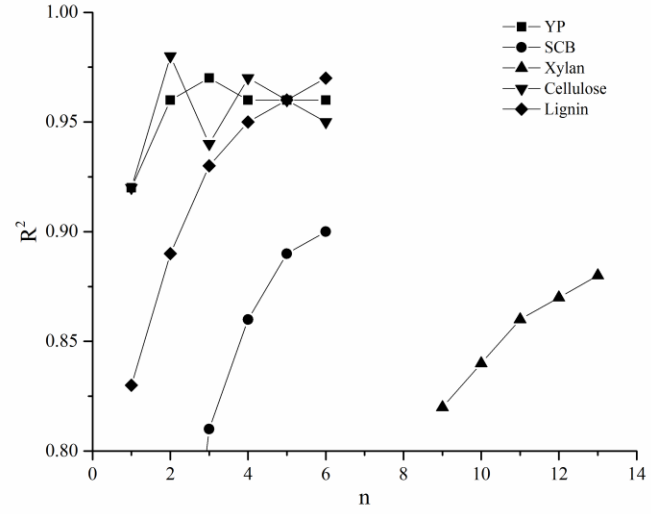


Figure 4-4. Adjust for different reaction orders of biomass and polymers.

For a better and complete prediction of the mass loss during the process, it is necessary to obtain temperature independent kinetic parameters that describe the thermal behavior of biomass during

the process. The rate of reaction can be expressed as in Eq. (5), which only requires a pre-exponential factor and an activation energy factor to estimate temperature dependent reaction rate.

Evaluations were developed for different reaction orders for each material, aiming tofind the best fit for experimental data. Figure 4-4 shows the variation of the coefficient of determination ($R^2$) with the reaction order. When the reaction order increases the $R^2$ value also increases for all materials, except for the cellulose. $R^2$ value for cellulose decreases after second order reaction.

The best reaction orders for better fitting were selected and are presented with their kinetic parameters in Table 4-2.

Table 4-2. Kinetic parameters for biomass and polymers studied

| Sample | n | $R^2$ | A($min^{-1}$) | $E_a$ (kJ/mole) |
|---|---|---|---|---|
| YP | 3 | 0.97 | 2.85E+13 | 154.45 |
| SCB | 6 | 0.9 | 3.64E+19 | 203.78 |
| Xylan | 11 | 0.86 | 2.02E+11 | 99.09 |
| Cellulose | 2 | 0.98 | 1.19E+23 | 258.57 |
| Lignin | 6 | 0.97 | 1.34E+08 | 103.65 |

The latter kinetic parameters found for the experimental tests performed at temperatures of 240, 260, 280 and 300°C were validated using the mass loss data obtained at temperature 270°C. This prediction can be performed using equation (4-4) because all reaction orders found are greater than one. The modified expression with which the conversion at each moment can be predicted is presented in equation (4-9), where *k* Is the Arrhenius parameter and $\alpha_0$ is the conversion of the sample to the beginning of the torrefaction process which is presented in Figure 4-5(a). Predicted results of conversion are shown in Figure 4-5 (b) with the respective adjustment errors for each sample.

$$\alpha = 1 - \left[k(t - t_0)(n-1) + (1-\alpha_0)^{1-n}\right]^{\frac{1}{1-n}} \quad (4\text{-}9)$$

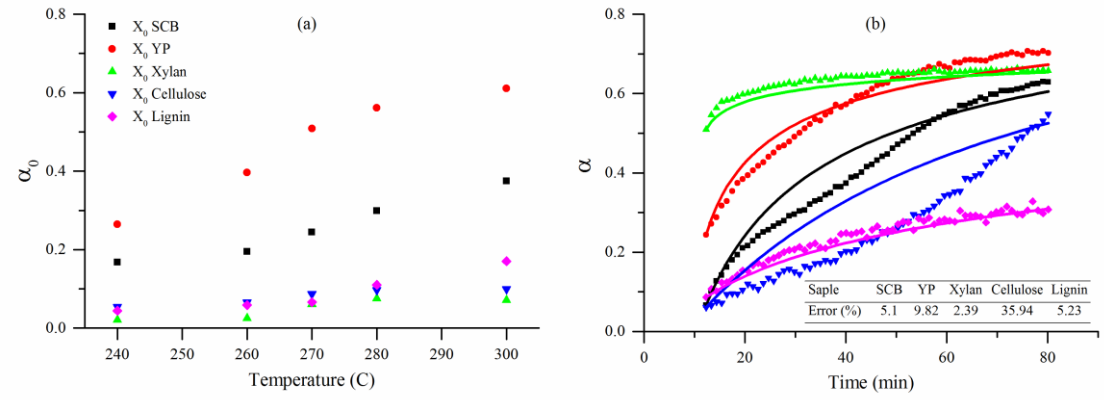


Figure 4-5. Initial conversion (a) and conversion comparison (b) between predictions (lines) and experiments (symbols) for biomasses and polymers in torrefaction at 270°C.

From Figure 4-5(b) it is possible to observe that the adjustments in the predictions made are quite good, except for cellulose which shows 35.94% in deviation. This indicates that the kinetic parameters obtained for reaction orders evaluated are adequate to represent the material decomposition in a torrefaction process.

### *4.3.2. Prediction of torrefaction process*

Once the kinetics were obtained for each of the materials, the superposition theory was evaluated according to equations (4-7) and (4-8), taking into account the proportion of hemicellulose, cellulose and lignin in the processed biomass according with Table 4-1. A comparison between predicted and experimental results for each tested biomass is shown in Figure 4-6.

As can be seen in Figure 4-6, predictions for decomposition of biomasses are not adequate, resulting in mean values of deviation of 21% and 17% for SCB and YP, respectively. At low temperatures deviations are much higher reaching values of 27% for both biomass. When the temperature increases, the adjustment improves ostensibly, with deviations of 6% for the SCB and 5% for the YP.

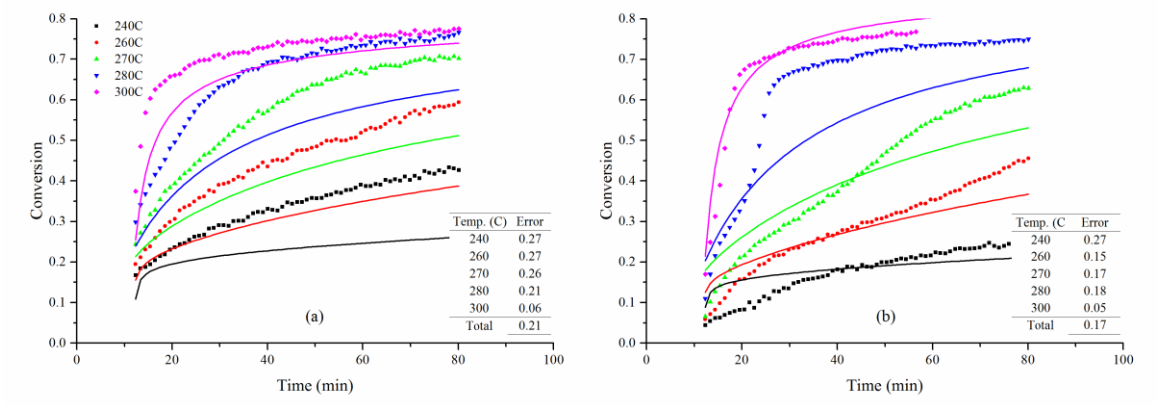


Figure 4-6. Experimental and modeled by superposition theory conversions for SCB (a) and YP (b).

One of the reasons for the difference in behavior among the evaluated biomass may be due to the difference in their compositions and type of biomass. The above indicates that there are differences in the nature of the polymers of each of the biomasses. Additionally, the evaluated polymers (xylan, cellulose and lignin) correspond to the extractions made to hardwoods and for this reason are not representative of biomasses such as sugarcane bagasse.

A correction to equation (4-8) used to predict the total conversion of the biomass was made in order to improve the predictive capacity of the method. The correction was based on the addition of exponents to the proportions of each polymer in the biomass, as shown in equation (4-10).

$$\alpha_{biomass} = X_{he}^{a} k_{he} + X_{ce}^{b} k_{ce} + X_{li}^{c} k_{li} \qquad (4\text{-}10)$$

As can be seen in equation 10, the correction in the expression was performed through additional parameters *a*, *b*, and *c*, associated with the concentration of hemicellulose, cellulose and lignin. These parameters take values of 0.004, 1.5 and 1.3 respectively and the results of the predictions with the addition of these correction factors are shown in Figure 3-6.

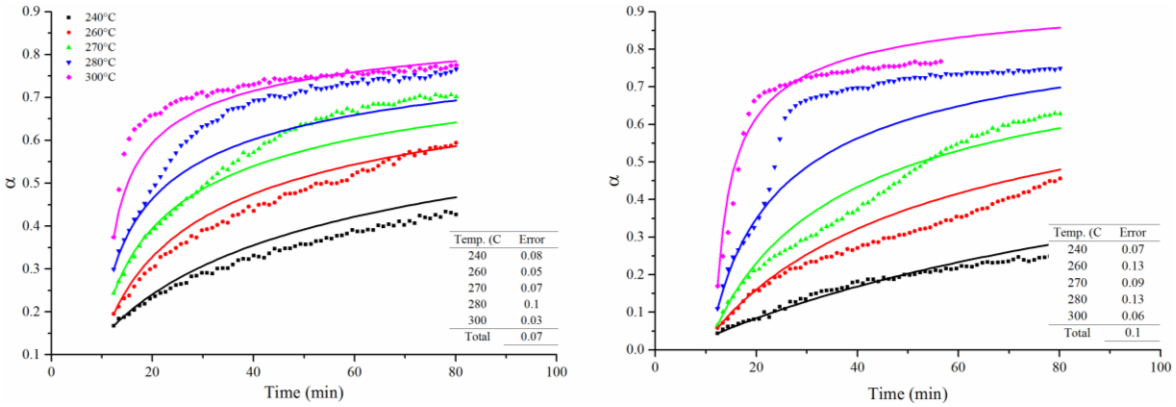


(a) (b)

Figure 4-7. Experimental and modeled by superposition theory conversions for SCB (a) and YP (b) with correction through parameter *a*.

From Figure 4-7 it is possible to observe the differences in the adjustments between experimental and predicted data when the correction parameters are involved. The deviations are reduced from 21% to 7% for SCB and from 17% to 10% for YP. It is possible to observe that from this superposition theory it is possible to make good predictions for biomass in a torrefaction process, from the proportion of each polymer in the biomass, and it becomes a predictive tool in simulations for reactors working in torrefaction conditions.

### *4.3.3. Combustion behavior*

Combustion reactivity of raw and torrefied biomass at 280 and 300°C for sugarcane bagasse and pyrolyzed raw and torrefied biomass at 280 and 300°C for yellow poplar was examined in TGA. Only torrefied samples at higher temperature were burned in oxygen media because the major changes due to the torrefaction process occur during these temperatures. The biomass samples were heated from room temperature to 900°C with three different heating rates of 5, 10, and 15°C/min. On the other hand, both raw and the torrefied yellow poplar were pyrolyzed at 800°C to evaluate and compare the effect of torrefaction and pyrolysis on the combustion process. In Figure 4-8, the TGA and DTG for combustion testing performed on all samples for the heating rate of 5°C/min are shown. Figure 4-8(a), shows that the mass loss of raw SCB starts earlier than in the other torrefied samples. This is due to presence of untreated polymeric structures and other light volatiles that require very less activation energy for the thermal degradation. As the polymeric his structures contain a large number of weak functional groups, such as C-H and O-H which are responsible for volatile material generation when the biomass is heated. This indicates that the activation energy required to decompose raw biomass is much smaller compared to the pretreated samples.

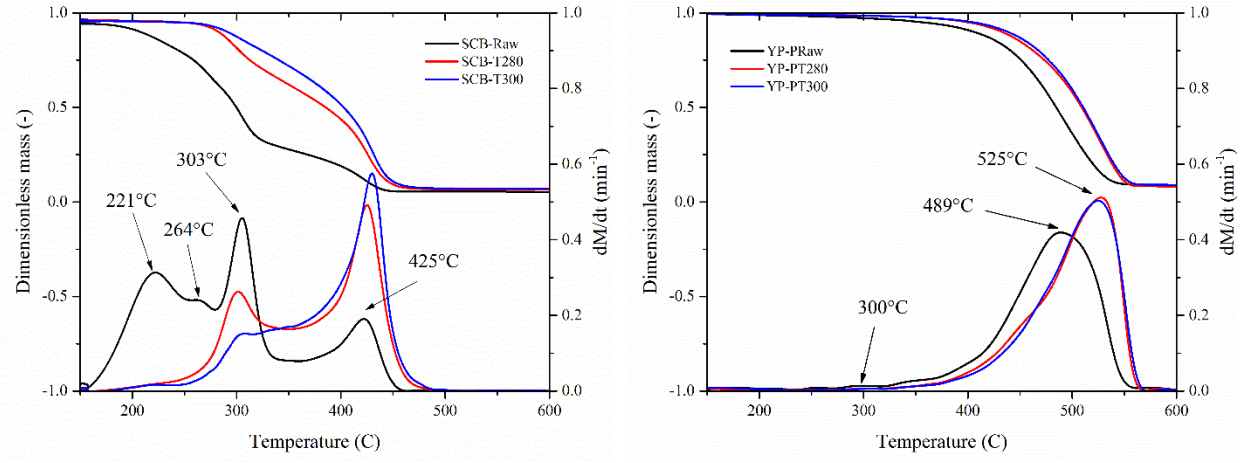


Figure 4-8. TGA and DTG for raw and torrefied samples (a), and pyrolyzed raw and torrefied samples (b) for a heating rate of 5°C/min.

The mass loss behavior of the torrefied samples, which was obtained after releasing such weak functional groups (e.g. C-H and O-H), moves towards higher temperature compared with that of raw biomass. For the torrefied sample at 280°C, hemicellulose and cellulose decompose partially and the remaining shares of corresponding polymeric components in the torrefied samples are only 2.80 and 4.97% respectively. Though the torrefied sample will consist of some unstable functional groups like $CH_3$, O-H, and C-OH, due to formation of other stable groups formed during the torrefaction process from the primary reactions like some aromatic compounds, the reactivity of torrefied sample is small in comparison to the raw biomass. The last material to begin its mass loss was that torrefied at 300°C, because the severely torrefied sample will not be having unstable polymers such as hemicellulose and cellulose in its structure, but it will be more like a stable lignified structure and aromatic groups established from the primary reactions during the torrefaction process.

In Figure 4-8(a), the DTG for raw biomass shows a large initial peak around 221°C, because of the large amount of hemicellulose in its structure compared to the torrefied samples. The same peak decreases in the other samples, indicating that the amount of hemicellulose in the torrefied materials decreased significantly. It completely stays flat to sample torrefied at 300°C. An unexpected behavior was presented in DTG curve at about 264°C for raw sample, because a small additional peak was observed. This could be attributed to the amorphous structure of the cellulose, less thermally stable than the crystalline cellulose, which begins its decomposition at this lower temperature and can be observed separated at a peak due to the low heating rate at which the process was conducted. This could be due to the very slow process of thermal degradation of amorphous cellulose that would be possible to track only at lower heating rate. However, this small intermediate peak was not observed at higher heating rate.

A peak presented at temperature around 303°C corresponds to the breakdown of cellulose. In the untreated material sample, this peak is shown larger because the amount of cellulose is 100% of

the original amount. When the material is treated at higher temperatures, the amount of cellulose is reduced, as it is evidenced at the peak of these two samples, which decreases considerably.

The final peak in DTG curves shown about at 425°C, is attributed to lignin and other carbonaceous materials produced in the primary reactions of cellulose and hemicellulose. In the untreated material, this peak is lower than those presented in the other samples. Due to decomposition of the less thermally stable polymers such as cellulose and hemicellulose, the proportion of lignin in the material increases considerably, which is clearly observed in the peaks of the torrefied materials at higher temperatures. In addition, this is consistent with the aforementioned and claimed by different authors [36,37], who found that the hemicellulose and cellulose polymers, because of their primary decomposition, decrease significantly and yield a char primarily formed by aromatic structures that increase the aromaticity in the material.

Figure 4-8(b) shows the TGA and DTG for torrefied and pyrolyzed yellow poplar. For the pyrolyzed char obtained from a raw poplar, no peaks at low temperatures were observed. The above indicates that those weak structures were completely removed from the biomass and is composed mainly of thermally stable carbonized material. A small peak was identified at 300°C, also observed in larger proportions in Figure 3-6(a) and which corresponded to the remaining cellulose in the biomass. The main peak observed in the DTG occurs between 489 and 525°C, corresponding to the combustion of the char formed in the torrefaction and subsequent pyrolysis processes and structures stables of lignin. Small differences can be observed in the DTGs of pyrolyzed biomasses, since they start their mass loss at temperatures of around 350°C, with a higher speed starting at 400°C.

A great difference found for the samples analyzed was the temperature at which the reaction ends. In the case of the samples in Figure 4-8(a), the final peak corresponding to the combustion of the most stable structures has its maximum point at 425°C and disappears at around 500°C. For the samples of Figure 4-8(b), this peak has its maximum around 525°C and disappears at 550°C. This clearly indicates that the char structures obtained with pyrolysis after torrefaction process are more stable. This behavior could be very useful in co-firing power plant, reducing the accumulation of coal in the combustor. In addition to this, the shift of combustion of biomass towards the higher temperature zone could also help to maintain the uniform heat distribution along the combustor.

The acceptable separation in the peaks for each material was observed at low heating rates because at high heating rates this behavior was avoided and the peaks of the cellulose and hemicellulose tend to overlap, such as it is shown in Figure 4-9. In this graph, it is possible to observe how for high heating rates the peaks are moved to the right at high temperature zone and the decomposition of each component in the process is difficult to differentiate.

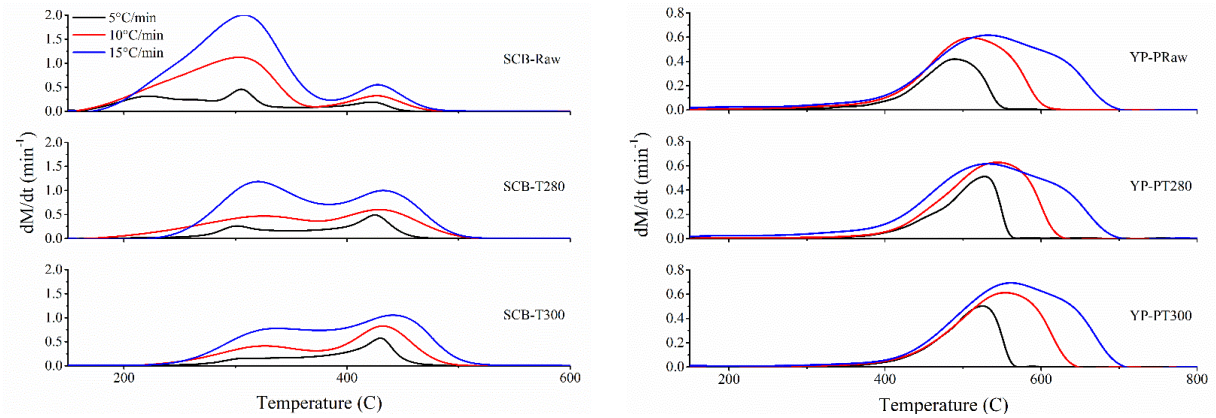


Figure 4-9. DTG for torrefied samples (a) and pyrolyzed samples (b) for all heating rates.

Activation energy describing the behavior of each material in the combustion process were obtained and are shown in Figure 4-10(a). The procedure was performed by the Ozawa iso-conversional method [35], by means of which a distribution of activation energies for the entire spectrum of conversion in the material can be obtained from the material conversion in each thermal condition of the tests.

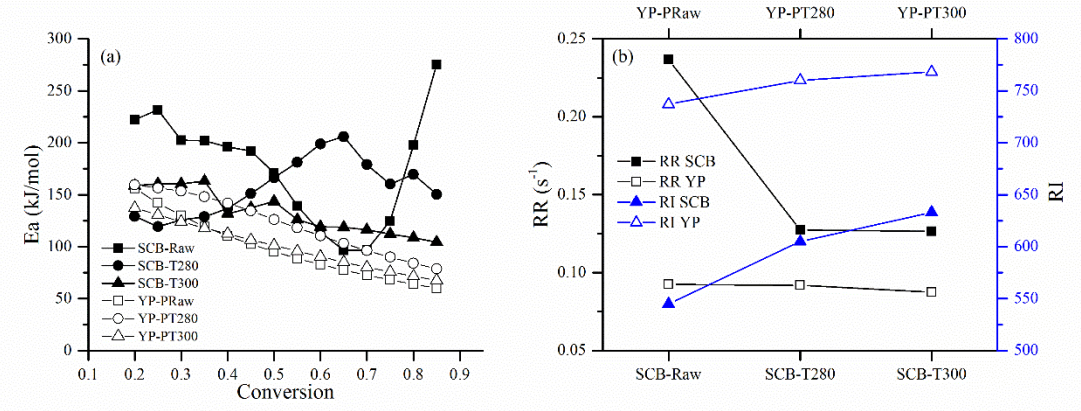


Figure 4-10. Activation energy distribution (a) and reaction rate (RR) and reactivity index (RI) (b) for samples tested in a combustion process.

Although many authors measure the reactivity of a material when the maximum speed of mass loss is reached in the process, in this work it was chosen to measure it at 25% of the conversion. In Figure 4-10(b), the variation of reactivity with the pre-treatment can be observed. This tendency was consistent with the above discussion, where the reactivity of the treated materials decreases with the torrefaction and much more with pyrolysis temperature due to decrease in the thermally unstable compounds after the process. As a result, more energy would be needed to obtain a similar conversion level in comparison with other untreated samples. The reactivity index indicated in Figure 4-10(b), corresponds to a temperature value where the decomposition reaches 25%. When the reactivity index is higher, the reactivity of material examined in this study were reduced.

## 4.4. Conclusions

Torrefaction kinetics and combustion reactivity of important Colombian and Canadian agricultural residue such as sugarcane bagasse and yellow poplar, respectively were examined. Thermal behavior of biomass and three major polymeric components (xylan, cellulose, and lignin) of biomass in the range of torrefaction process were determined in the QWM reactor. Superposition theory was verified and validated with experimental data from biomasses treated in torrefaction. Good results were found with deviations of 10% for yellow poplar and 7% for sugarcane bagasse, indicating the superposition approach can be used to predict the mass loss behavior during the torrefaction process. A slight modification of the superposition was made that can predict the thermal degradation of biomass more accurately. The modified expression for the superposition theory using corresponding fractions of polymeric compositions of biomass was found to be:

$$\alpha_{biomass} = {X_{He}}^{0.004} k_{He} + {X_{Ce}}^{1.5} k_{Ce} + {X_{Li}}^{1.3} k_{Li}$$

The combustion reaction rate of the char obtained from pyrolysis of raw SCB was found significantly higher compared with that to the char from pyrolysis of torrefied SCB. But only small changes in the reaction rate of YP was found between the char from raw YP and the char from torrefied YP.

## Acknowledgments

The experimental work was performed in the Biomass Conversion Laboratory at Dalhousie University under the guidance of Prof. Prabir Basu, who acknowledge the support of Natural Science & Engineering Council and from Greenfield Research Incorporated of Canada.

D.A. Granados wish to thank the Colombian Administrative Department of Science, Technology and Innovation (COLCIENCIAS) (Departamento Administrativo de Ciencia, Tecnología e Innovacion) for financial support.

## References

[1] Demirbaş A. Biomass resource facilities and biomass conversion processing for fuels and chemicals. Energy Convers Manag 2001;42:1357–78. doi:10.1016/S0196-8904(00)00137-0.

[2] Chen W, Peng J, Bi XT. A state-of-the-art review of biomass torrefaction , densi fi cation and applications. Renew Sustain Energy Rev 2015;44:847–66. doi:10.1016/j.rser.2014.12.039.

[3] Nhuchhen DR, Basu P, Acharya B. A Comprehensive Review on Biomass Torrefaction. Int J Renew Energy Biofuels 2014;2014:1–56. doi:10.5171/2014.506376.

[4] Chen WH, Kuo PC. Isothermal torrefaction kinetics of hemicellulose, cellulose, lignin and xylan using thermogravimetric analysis. Energy 2011;36:6451–60. doi:10.1016/j.energy.2011.09.022.

[5] Chen W-H, Kuo P-C. Isothermal torrefaction kinetics of hemicellulose, cellulose, lignin and xylan using thermogravimetric analysis. Energy 2011;36:6451–60.

doi:10.1016/j.energy.2011.09.022.

[6] Rousset P, Aguiar C, Labbé N, Commandré JM. Enhancing the combustible properties of bamboo by torrefaction. Bioresour Technol 2011;102:8225–31. doi:10.1016/j.biortech.2011.05.093.

[7] Broström M, Nordin A, Pommer L, Branca C, Di Blasi C. Influence of torrefaction on the devolatilization and oxidation kinetics of wood. J Anal Appl Pyrolysis 2012;96:100–9. doi:10.1016/j.jaap.2012.03.011.

[8] Park SW, Jang CH. Effects of pyrolysis temperature on changes in fuel characteristics of biomass char. Energy 2012;39:187–95. doi:10.1016/j.energy.2012.01.031.

[9] Shang L, Ahrenfeldt J, Holm JK, Barsberg S, Zhang R, Luo Y, et al. Intrinsic kinetics and devolatilization of wheat straw during torrefaction. J Anal Appl Pyrolysis 2013;100:145–52. doi:10.1016/j.jaap.2012.12.010.

[10] Sarvaramini a., Assima GP, Larachi F. Dry torrefaction of biomass – Torrefied products and torrefaction kinetics using the distributed activation energy model. Chem Eng J 2013;229:498–507. doi:10.1016/j.cej.2013.06.056.

[11] Wang C, Peng J, Li H, Bi XT, Legros R, Lim CJ, et al. Oxidative torrefaction of biomass residues and densification of torrefied sawdust to pellets. Bioresour Technol 2013;127:318–25. doi:10.1016/j.biortech.2012.09.092.

[12] Bates RB, Ghoniem AF. Biomass torrefaction: Modeling of reaction thermochemistry. Bioresour Technol 2013;134:331–40. doi:10.1016/j.biortech.2013.01.158.

[13] Klinger J, Bar-Ziv E, Shonnard D. Kinetic study of aspen during torrefaction. J Anal Appl Pyrolysis 2013;104:146–52. doi:10.1016/j.jaap.2013.08.010.

[14] Brachi P, Miccio F, Miccio M, Ruoppolo G. Isoconversional kinetic analysis of olive pomace decomposition under torrefaction operating conditions. Fuel Process Technol 2015;130:147–54. doi:10.1016/j.fuproc.2014.09.043.

[15] Klinger J, Bar-Ziv E, Shonnard D. Unified kinetic model for torrefaction-pyrolysis. Fuel Process Technol 2015;138:175–83. doi:10.1016/j.fuproc.2015.05.010.

[16] Doddapaneni TRKC, Konttinen J, Hukka TI, Moilanen A. Influence of torrefaction pretreatment on the pyrolysis of Eucalyptus clone: A study on kinetics, reaction mechanism and heat flow. Ind Crops Prod 2016;92:244–54. doi:10.1016/j.indcrop.2016.08.013.

[17] Martín-Lara MA, Blázquez G, Zamora MC, Calero M. Kinetic modelling of torrefaction of olive tree pruning. Appl Therm Eng 2017;113:1410–8. doi:10.1016/j.applthermaleng.2016.11.147.

[18] Prins MJ, Ptasinski KJ, Janssen FJJ. Torrefaction of wood. Part 1. Weight loss kinetics. J Anal Appl Pyrolysis 2006;77:28–34. doi:10.1016/j.jaap.2006.01.002.

[19] Papari S, Hawboldt K. A review on the pyrolysis of woody biomass to bio-oil: Focus on kinetic models. Renew Sustain Energy Rev 2015;52:1580–95. doi:10.1016/j.rser.2015.07.191.

[20] Kaushal P, Abedi J. Application of Monte-Carlo simulation to estimate the kinetic parameters for pyrolysis-Part I. Can J Chem Eng 2012;90:163–70. doi:10.1002/cjce.20529.

[21] Di Blasi C. Modeling chemical and physical processes of wood and biomass pyrolysis. Prog Energy Combust Sci 2008;34:47–90. doi:10.1016/j.pecs.2006.12.001.

[22] Turner I, Rousset P, Rémond R, Perré P. An experimental and theoretical investigation of the thermal treatment of wood (Fagus sylvatica L.) in the range 200–260°C. Int J Heat Mass Transf 2010;53:715–25. doi:10.1016/j.ijheatmasstransfer.2009.10.020.

[23] Repellin V, Govin A, Rolland M, Guyonnet R. Energy requirement for fine grinding of torrefied wood. Biomass and Bioenergy 2010;34:923–30. doi:10.1016/j.biombioe.2010.01.039.

[24] Jones JM, Bridgeman TG, Darvell LI, Gudka B, Saddawi a., Williams a. Combustion properties of torrefied willow compared with bituminous coals. Fuel Process Technol 2012;101:1–9. doi:10.1016/j.fuproc.2012.03.010.

[25] Costa FF, Wang G, Costa M. Combustion kinetics and particle fragmentation of raw and torrified pine shells and olive stones in a drop tube furnace. Proc Combust Inst 2014;35:3591–9. doi:10.1016/j.proci.2014.06.024.

[26] Nhuchhen DR, Basu P. Experimental investigation of mildly pressurized torrefaction in air and nitrogen. Energy and Fuels 2014;28:3110–21. doi:10.1021/ef4022202.

[27] Nhuchhen DR, Basu P, Acharya B. Torrefaction of poplar in continuous two- stage indirectly heated rotary torrefier. Energy & Fuels 2016;30:1027–38. doi:10.1021/acs.energyfuels.5b02288.

[28] Bridgeman TG, Jones JM, Shield I, Williams PT. Torrefaction of reed canary grass, wheat straw and willow to enhance solid fuel qualities and combustion properties. Fuel 2008;87:844–56. doi:10.1016/j.fuel.2007.05.041.

[29] Bach QV, Tran KQ, Skreiberg ??yvind. Comparative study on the thermal degradation of dry- and wet-torrefied woods. Appl Energy 2017;185:1051–8. doi:10.1016/j.apenergy.2016.01.079.

[30] Bach QV, Tran KQ. Wet Torrefaction of forest Residues-Combustion Kinetics. Energy Procedia 2015;75:168–73. doi:10.1016/j.egypro.2015.07.279.

[31] Zhang S, Chen T, Li W, Dong Q, Xiong Y. Physicochemical properties and combustion behavior of duckweed during wet torrefaction. Bioresour Technol 2016;218:1157–62. doi:10.1016/j.biortech.2016.07.086.

[32] Fisher EM, Dupont C, Darvell LI, Commandré J-M, Saddawi a, Jones JM, et al. Combustion and gasification characteristics of chars from raw and torrefied biomass. Bioresour Technol 2012;119:157–65. doi:10.1016/j.biortech.2012.05.109.

[33] Granados DA, Basu P, Chejne F, Nhuchhen DR. Detailed Investigation into Torrefaction of Wood in a Two-Stage Inclined Rotary Torrefier. Energy & Fuels 2016:acs.energyfuels.6b02524. doi:10.1021/acs.energyfuels.6b02524.

[34] Repellin V, Govin A, Rolland M, Guyonnet R. Modelling anhydrous weight loss of wood chips during torrefaction in a pilot kiln. Biomass and Bioenergy 2010;34:602–9. doi:10.1016/j.biombioe.2010.01.002.

[35] Ozawa T. A New Method of Analyzing Thermogravimetric Data. Bull Chem Soc Jpn 1965;38:1881–6. doi:10.1246/bcsj.38.1881.

[36] Pastorova I, Botto RE, Arisz PW, Boon JJ. Cellulose char structure: a combined analytical Py-GC-MS, FTIR, and NMR study. Carbohydr Res 1994;262:27–47. doi:10.1016/0008-6215(94)84003-2.

[37] McGrath TE, Chan WG, Hajaligol MR. Low temperature mechanism for the formation of polycyclic aromatic hydrocarbons from the pyrolysis of cellulose. J Anal Appl Pyrolysis 2003;66:51–70. doi:10.1016/S0165-2370(02)00105-5.

# Chapter 5. A Detailed Investigation into Torrefaction of Wood in a Two-Stage Inclined Rotary Torrefier

**(Paper published in Energy and Fuels Journal)**


## Abstract

A two-stage, inclined continuous rotary torrefier with novel flights has been developed in the Biomass Conversion Laboratory at Dalhousie University for improving biomass torrefaction process. Experimental work on torrefaction of fine Poplar wood particles (0.5-1.0 mm) in the torrefier was undertaken for a deeper understanding of the working of such torrefiers where the volatile gas released was used as the torrefaction medium instead of nitrogen. The rotary torrefier is operated under different operating conditions by varying its rotational speed, tilt angle and temperature. Measured chemical and physical properties of the torrefied products included ultimate and proximate analysis, polymeric analysis, energy density, mass yield, energy yield, and bulk density. A novel probe was developed to collect samples of biomass and measure temperature at different interior points along the length of the rotary reactor while the biomass was being progressively torrefied in it. Axial temperature distribution of the rotary torrefier showed a parabolic profile but the fixed carbon content, volatile and energy density of biomass undergoing torrefaction varied linearly along the length of the torrefier. Typical values of change in heating value, mass yield and energy yield of torrefied biomass was 40%, 34% and 48% respectively for 300°C and 5 RPM and 1° of tilt angle. Results showed that temperature is the most important parameter in the torrefaction process.


***Keywords:*** Biomass torrefaction, Rotary kiln, Volatiles atmosphere, Fine particles

## 5.1. Introduction

Owing to its negligible greenhouse gas emissions, abundance, low costs, and acceptable performance in thermal processes, biomass emerged as a promising energy alternative to fossil fuels. Biomass, however, suffers from a number of limitations such as its high moisture content, low mass density, low specific energy and rapid dry mass losses due to bacterial decompositions, which may discourage its use as an energy source. This, in turn, brings additional disadvantages in a production and supply chain including those in its transportation and handling [1].

Torrefaction is defined as a thermal pre-treatment between 200-300°C, at low heating rates (<20°C/min) in inert environments or with low oxygen concentrations [1]. During the process, the biomass undergoes different thermochemical transformation leading to mass and energy losses, which depend on torrefaction temperature and solid residence time. The thermochemical transformation during torrefaction offers with some attractive attributes. It produces torrefied biomass, a product like biochar with higher specific energy, hydrophobicity, brittleness requiring low grinding energy, and resistive to environmental degradation compared that to raw biomass.

Additionally, torrefaction provides a product of uniform qualities from a mixture of diverse feedstock [2–4]. Torrefaction process, thus, appears as a better solution for pretreating biomass, as it can improve chemical and physical properties, leaving behind some inherent problems of biomass.

Much experimental research on torrefaction has been carried out, where different types of biomasses are torrefied under different operational conditions [2,5–13]. In these works, the operating conditions are tested in order to find those that can produce the best final properties of bio-char. Most of these are carried out in a batch reactor or in the muffle furnace [11,14–20], but a limited number of studies have been made specifically in continuous reactors [11, 21–28]. Continuous systems offer many advantages in the torrefaction processes especially when they are considered for an industrial scale. These kinds of continuous reactors (fluidized beds, screw reactor, rotary kiln, etc.) offers great productive and energy advantages. They also offer great advantages during operation, like easy operation and a good control over some variables in the process such as residence time. Some of them, such as rotary reactors, avoid jamming of material by means of an enhancement of mixing and depending on their design can offer high levels of energy transfer from kiln walls to material such as in the case of rotary reactors with internal longitudinal flights.

Zheng et al. [11], used a screw type reactor for both drying and torrefaction to produce volatiles that was subsequently fed into another vertical fast pyrolysis reactor for evaluate bio-oil yield. In their work, the torrefaction and pyrolysis processes can be performed continuously. They found that the amount of bio-oil is reduced because in the pre-treatment process cross-linking reactions have already taken place in the biomass. The bio-oil from the torrefied biomass has higher HHV, lower acids, become a more viscous, and lower moisture compared that from the raw biomass.

Doassans-Carrère et al. [23] studied in a novel continuous reactor for biomass torrefaction called REVE, which is a vertical cylindrical chamber that was vibrated to enhance mixing. Four types of biomass were tested, and properties such as HHV, elemental analysis, and grindability of the torrefied biomass were measured. They also compared their results with the published works that use different reactors, considering aspects like solid mixing, heat transfer, and products uniformity.

Mei et al. [25] also worked in a continuous torrefaction process with a rotary drum with two different atmospheres (Nitrogen and flue gases). This system is somewhat similar to the one developed here, but unlike the present design it conducted both drying and torrefaction in the same reactor without any mixing flight. They studied properties like grindability, hydrophobicity, elemental and proximate analyses, and HHV of the torrefied biomass, but did not explore a deeper into the process by analyzing the progress of torrefaction as biomass moved along the reactor.

One can note that the above studies were for single-stage torrefiers. Few authors have worked in two-stage reactors [13,28] for biomass torrefaction. Nachenius et al. [28] evaluated a two-stage indirectly heated screw reactor by measuring grindability of the torrefied solid and some properties like HHV, elemental and proximate analyses. Nhuchhen et al. [13] used a two-stage indirectly heated rotary reactor to evaluate the overall performance of the torrefaction process for large particle size. They conducted a parametric study for the two-stage torrefier by characterizing properties of torrefied biomass and established an overall energy balance of the system. One

important feature of the reactor designed in this work was to split the drying section from the torrefaction section. Thus, the generated volatiles during torrefaction is not diluted by the moisture released during the drying process. This allows one to effectively burn and then provide partial energy requirement of the process. The present system also prevents the use of expensive nitrogen gas to provide an inert ambience in the torrefier. The volatiles released during torrefaction provides the required non-oxidizing atmosphere in the torrefier.

In the present work, authors aim to widen the parametric study of the two-stage torrefier developed by Nhuchhen et al. [13] using smaller particle size. Experimental tests were carried out to determine the combined and quantified effects of torrefaction temperature and residence time on a large selection of process responses and product properties of poplar wood, e.g. proximate analysis, ultimate analysis, polymeric compositions, higher heating value (HHV), mass yield (MY), energy yield (EY), oxidation reactivity, and porosity. In addition, biomass samplings were collected in different axial positions inside the torrefier to evaluate the conversion level in polymeric compositions of biomass along the reactor length. The samples were also tested to analyze reduction rate of volatile matter and gain rate of the carbon content of the torrefied biomass inside the rotary reactor.

## 5.2. Methods

### *5.2.1. Materials*

Poplar dowels were crushed in a grinder and the collected ground wood particles were then sieved to prepare the sample of fine particle size in the ranges of 0.5 -1 mm. The collected sieved fine wood samples were used for the experimental tests. Proximate and ultimate analyses of the raw sample are presented in Table 5-1.

Table 5-1. Properties of Poplar wood (wb–wet basis; db–dry basis; daf–dry ash free basis).

| Biomass size range 0.5-1 mm | | | | | |
|---|---|---|---|---|---|
| Proximate analysis (%w/w) | | Ultimate analysis (%w/w) | | Fiber analysis (%w/w) | |
| Moisture (wb) | 3.4 | Carbon (daf) | 45.97 | Extractives (db) | 8.2 |
| Volatiles (db) | 82.4 | Hydrogen (daf) | 6.1 | Hemicellulose (db) | 23.6 |
| Fixed carbon (db) | 16.2 | Nitrogen (daf) | 0.4 | Cellulose (db) | 56.5 |
| Ash (db) | 1.4 | Oxygen (daf) | 47.5 | Lignin (db) | 11.7 |
| HHV (db) (MJ/kg) | 18.4 | | | Ash (db) | 0.2 |

### *5.2.2. Torrefaction process*

Experiments were conducted in the two-stage indirectly heated rotary torrefier Figure 5-1(a). This system consists of two coupled rotary kilns, separating drying and devolalitilization reactions of a torrefaction process. Wet biomass enters to the first rotary drum of 64 mm ID and 610 mm length, where only drying process is permitted by maintaining the reactor temperature well below the thermal degradation point. Dried biomass, without coming out of the system, then drops into another rotary reactor of 100 mm ID and 762 mm length, where the reactor temperature is set at the designated torrefaction temperature. The first rotary reactor is termed as a dryer whereas the second one as a torrefier. No external inert gas is supplied to both the dryer and torrefier.

Both the rotary dryer and torrefier have axially inserted three flights placed 120° apart from each other on the inner wall of the rotating cylindrical drums. Both dryer and torrefier rotate inside two concentric fixed cylindrical shells, which are wrapped with the electric heaters and then tightly covered with insulation (Calcium-Magnesium-Silicate wool). Thermocouples (K-type) measure the surface temperatures of both the dryer and torrefier. Those thermocouples comfortably touch the outer wall of the very slowly rotating reactor. Due the high thermal conductivity of the thin steel wall, one expects only a small temperature difference between the solid inside and that recorded by this thermocouple for the external wall. This was verified by pilot tests.

A screw system feeds biomass at a desired rate to an upper drum for drying and then falls to the torrefier for the devolitilization. Fixed cylindrical heater shells of both kilns consist of three different materials: steel, electrical heaters, and external thermal insulation.

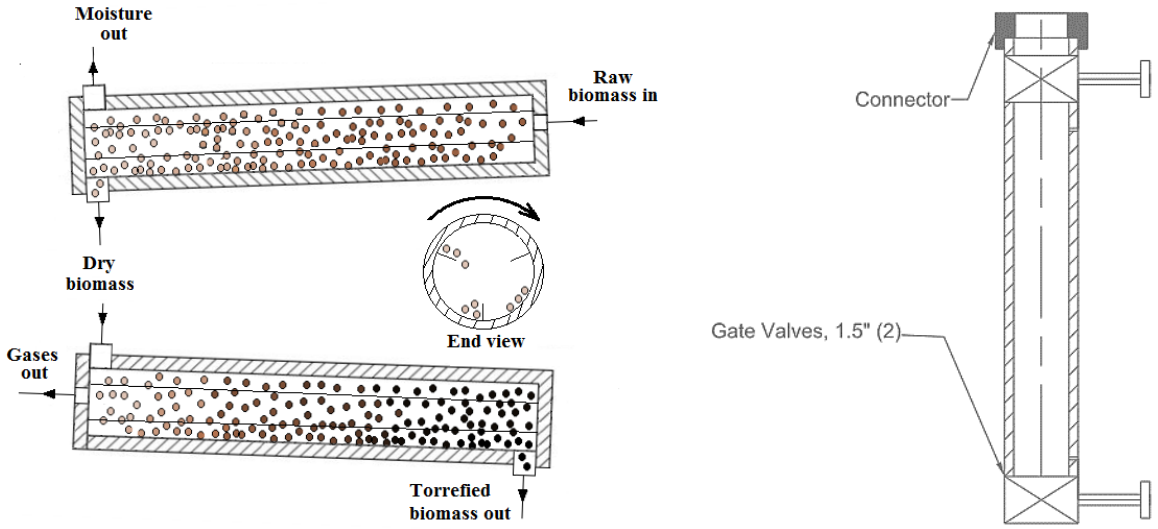


(a) (b)

Figure 5-1. Kiln layout and torrefied biomass collector [29].

Heat is supplied by electrical resistance heaters, which heats the static steel wall and in turn, the rotating steel drum is heated. There is an air gap between the rotating and static steel walls, which are heated by convection and conduction from the static wall and also exchanges energy with the rotary drum. The temperature in both processes (drying and torrefaction), is controlled by a thermocouple in contact with the electrical heater. The temperature on the rotary drum surface is monitored. Experiments do not begin until a steady temperature is achieved to ensures a correct temperature for the process.

The heat exchange between three items present inside the kiln (gas, solid, and walls) is basically as same as in the conventional kilns, but there will be additional heat transfers to the biomass falling from the flight from the gas phase and reactor walls respectively. This additional heating of biomass makes the heat transfer inside the kiln much effective [13,30,31].

### *5.2.3. Experimental design*

Preliminary tests were carried out to find the right operational condition of the dryer. It showed that at 3 RPM and 2° angle of inclination it is possible to obtain biomass dried with the moisture content smaller than 0.5%. For this reason, the operating condition of the dryer held constant at this during subsequent tests. The operating conditions of the torrefier reactor were, however, varied in order to observe differences in the characteristics of the torrefied biomass with operating conditions. Poplar wood was fed into the system with the screw conveyor at the rate of 4.2 g/min. Before tests, nitrogen was supplied to flush out of the system the oxygen that could initiate burning when the initial material starts to fall in the torrefier. This flow of nitrogen was stopped after 10 minutes when only volatiles released from torrefaction was enough to guarantee an inert atmosphere for the process. Approximately 1 kg of biomass was fed to the system, which was collected and weighed at the end of the process in order to determine the mass loss during the process.

Experiments were conducted in the torrefier with two different rotational speed of the reactor (5 and 7 RPM), three tilt angles (1º, 2º, and 3º) and three temperatures (260, 280, and 300°C). The tilt angle in the torrefier was measured using a Level Master Craft with an accuracy of 0.1°. With the above operational conditions, the residence time of biomass in the torrefier reactor ranges between 6 and 18 minutes. For the dryer, the residence time is around 18 minutes. Thus biomass has a total residence time in the system of between 24 and 36 minutes.

At the end of the torrefaction process, the biomass was collected in a container system that prevents air infiltration to the system. This system consists of two valves and a pipe as is shown in Figure 5-1(b). In this system, the upper valve is open throughout the process, while the lower valve is kept closed. Biomass falls into the cavity, and once it is filled the upper valve is closed while the bottom valve is opened to get the torrefied biomass. Once biomass is removed from the system, the lower valve is closed again and nitrogen is fed into the system for few minutes for purging out the oxygen entered during the collection of the torrefied biomass. The top valve is opened again and the procedure is repeated several times during the torrefaction process. This system is separated from the torrefier reactor by a thick piece of insulation to prevent heating. This system, therefore, remains cold that helps cooling the collected torrefied biomass.

### *5.2.4. Sample characterizations and torrefaction yields*

Raw and torrefied biomass were characterized by proximate analysis and elemental analysis, polymeric analysis, HHV, fuel ratio, MY, EY, oxidation reactivity, and surface area. Fuel ratio, mass yield, and energy yield are defined as follows.

$$FR = \frac{FC}{VM} \tag{5-1}$$

$$MY = \frac{M_{T,daf}}{M_{R,daf}} \tag{5-2}$$

$$EY = \frac{M_{T,daf}\ x\, HHV_T}{M_{R,daf}\ x\, HHV_R} \tag{5-3}$$

Proximate analysis for Poplar wood and torrefied biomass were carried out in the muffle furnace according to ASTM D1762-84. These analyses were carried out twice for repeatability. The torrefied biomass samples were stored in air-tight containers before analyses. Elemental analysis of Poplar wood and torrefied biomass were measured using an Elemental Analyzer (Organic Elemental Analyzer - Model EA1110), where tests were conducted in triplicate according to ASTM D5373-02. This test determined the amount of carbon, hydrogen, and nitrogen of the material, while the oxygen content is calculated by difference. L-Cystine was used as a standard reference before tests. Higher Heating Values (HHV) of Poplar and torrefied biomass were measured in duplicate by a bomb calorimeter (Parr 6100), following the ASTM D5865-04. All sieving of the biomass sample for tests had followed the ASTM C136-01.

Polymeric compositions (Fiber analysis) of both the raw and torrefied biomasses were determined by following the Vans Soest procedure. In this test, three steps with different liquid solutions (neutral and acids) were deployed. In the first step, the biomass is treated with a Neutral Detergent Solution (NDS) to find the amount of soluble material in it. This soluble material is called *extractives*. The residue of this test is called NDF that is made mainly of cellulose, hemicellulose, and lignin. In the second step, the NDF material is treated with Acid Detergent Solution (ADS) with sulphuric acid of concentration 1N. The soluble material in this solution is identified as hemicellulose. Insoluble material is called ADF and is made mainly of cellulose and lignin. In the last step, ADF is treated with a strong sulphuric acid solution with a concentration of 24N. In this step, the cellulose is washed out by the acid and the remaining solid residue is termed as lignin or ADL. The polymeric compositions of the biomass can be estimated as follows.

$$Extractives = NDF - ADF \tag{5-4}$$

$$Hemicellulose = NDF - ADF \tag{5-5}$$

$$Cellulose = ADF - ADL \tag{5-6}$$

$$Lignin = ADL \tag{5-7}$$

The pore surface area (BET), pore volumes, and average pore diameter measurements were carried out using a Micromeritics TriStar II PLUS surface area analyzer, with nitrogen gas as an adsorbate. Besides the BET analysis, the surface area of pores was also obtained using carbon dioxide gas as the adsorbate. BET analysis can quantify the surface area in the mesoporosity level, but not quantifies the microporosity of the material, therefore a second analysis with $CO_2$ was developed. Thus, information about micro and meso porosities for torrefied biomass were also examined. Both analyses were developed to torrefied samples at temperatures of 280°C and 300°C.

### *5.2.5. Biomass sampling*

A novel technique of sampling biomass while it is being torrefied inside the continuously rotating reactor was developed. The Figure 5-2 shows the designed devices used to collect the biomass in different axial positions and to measure the particle temperature inside the kiln. The scoop for biomass sampling shown in Figure 5-2(a), is introduced from one end of the kiln while all holes are covered by the external cylinder. Once the hole in position, the external cylinder is rotated to collect the torrefied sample at that position. After approximately 2 or 3 minutes, the holes are covered by the external cylinder and the scooper is removed from the reactor. In this sampling, material was taken at five different axial positions inside the reactor to estimate the conversion level while the process progresses. This degree of conversion is determined in two ways: by polymeric analysis where is possible to determine the decomposition of main components of biomass like hemicellulose, cellulose, and lignin; and by proximate analysis where volatiles and fixed carbon content can be determined.

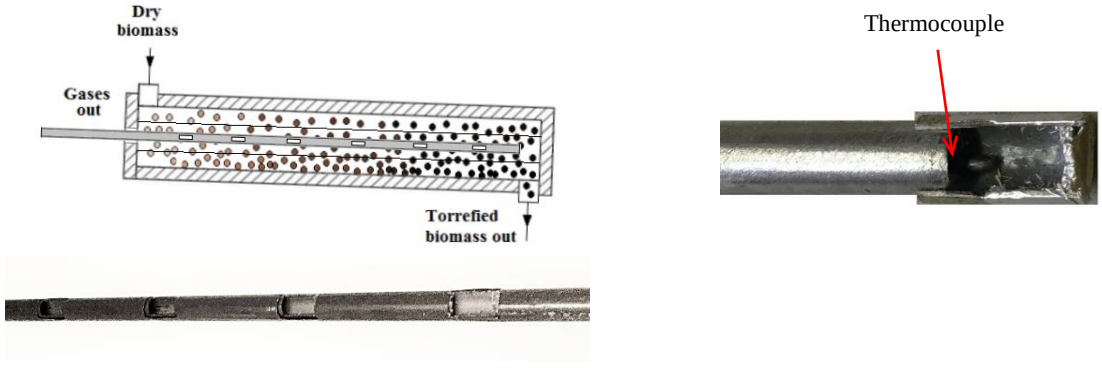


(a) (b)

Figure 5-2. Designed scoopers for biomass sampling (a); and temperature measurement (b).

The temperature of the biomass, while it is being torrefied inside the rotary torrefier, was also measured by a similar kind of scoop as used in the biomass sampling, but with only one hole and a thermocouple at its end which measures the temperature of biomass when is collected as is shown in Figure 5-2(b). The device can record the solid temperature in only one position by capturing the material inside the kiln. To prevent an additional heating of the thermocouple from gases and kiln walls, a protection was performed through of the capsule in which the biomass is housed, thus only the contact with the biomass heated the thermocouple. In this capsule, the biomass is collected and only the temperature of the material in contact with the thermocouple is recorded. The biomass is evacuated from the cavity by a device rotation the external cylinder of 180° and new biomass is then collected in the same position. This procedure is performed until the temperature measured by the thermocouple has no major variations to ensure that the measured temperature is that of the biomass or not. This procedure is performed as many times as temperatures are to be obtained for different points inside the furnace.

## 5.3. Results and discussion

### *5.3.1. Biomass temperatures during torrefaction in the system*

The reactor temperature is set with an external control system. This system is controlled with type K a thermocouple kept in contact with electrical heater wrapped peripherally on the cylindrical shell. The rotary reactor temperature is monitored by another k-type thermocouple kept in contact with the external wall surface. Values measured by this thermocouple is considered as the operating torrefaction temperature.

Before experiments, a pilot test was conducted to establish temperature variation along the length of the reactor. This was performed by inserting a thermocouple inside the heated stationery torrefier drum by means of a special probe, and made to touch the inner wall of the torrefier at different axial positions. Steady state values of the temperature were measured at the inner wall of the reactor for three different operating temperatures v (see Figure 5-3(a)–(c)). Simultaneous measurement of the outer wall shows this temperature is approximately 25 °C higher compared that measured on the inner wall. This test was performed without supplying biomass through the reactor and without rotating the reactor. During actual tests when biomass was flowing through the reactor temperature dropped only about 2 °C compared that without biomass flowing through. One of the reasons for this drop may be due to the wall to solid heat transfer. In Figure 5-3(a)–(c), the red dot indicates the torrefaction process temperature. It also shows the axial position for external thermocouple.

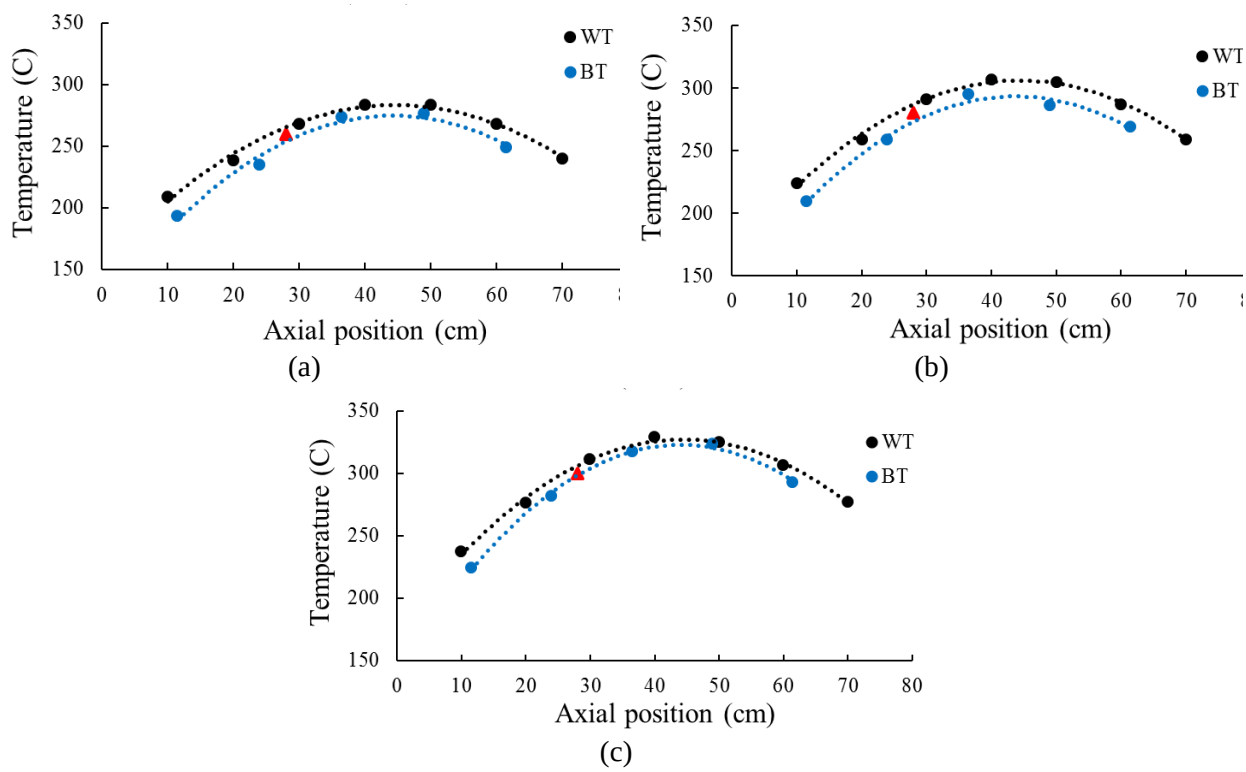


Figure 5-3. Axial kiln and biomass temperatures inside the kiln. Kiln wall temperatures measured in static conditions and biomass temperature measured at 5 RPM and 2° of inclination. (a) 260°C; (b) 280°C; (c) 300°C. (BT – biomass temperature; WT – Temperature on the inner wall of the torrefier)

The biomass temperature was measured with the special scooper shown in Figure 5-2(b). The measuring device has a cavity at its end where the K thermocouple type is housed. Biomass temperatures were recorded at five different points inside the reactor and for three different thermal operating conditions. These five points correspond to those points where the biomass was sampled and therefore these results can be accurately corroborated. In Figure 5-3(a)-(c) the results of axial temperature distribution are presented for torrefaction temperatures of 260 °C, 280 °C, and 300 °C respectively. All of them were for 5 RPM and 2° inclination of the reactor.

The axial temperature profile of biomass undergoing torrefaction through the reactor is similar to the temperature profile of the reactor walls. It is observed in Figure 5-3(a)–(c), that the biomass begins its heating process upon entering the reactor, and its temperature increases reaching closest to the wall temperature at around 40 centimeters. The peak temperature of biomass occurs is approximately in the center of the reactor, this because heat losses are considerable at both ends of the reactor due to thermal conduction to coupling with other systems. The process temperature was set according to the measurement at a central point inside of the reactor, but, as expected, the temperature distribution is not entirely homogeneous, which means that biomass was not torrefied in a constant temperature but within in a range of values.

### *5.3.2. Proximate analysis and High Heating Value*

Variation of product qualities with changes in severity of torrefaction was similar to that obtained in results of other researchers who used other types of torrefiers. Amongst the process variables, temperature was the most influencing parameter in the torrefaction process as observed from the Table 5-2.

Here, we note that the amount of volatile, fixed carbon, HHV and Fuel Ratio are strongly influenced by process temperature and the solid residence time. The percentages of volatile material in the torrefied product decrease with increases in temperature and residence times, while remaining properties like fixed carbon, HHV, and fuel ratio increase with the same increments of temperature and residence times.

Angular speed and tilt of the reactor directly influence the residence time. Higher inclination angle gives shorter residence time of solids in the reactor. Higher RPM of the rotor also provides shorter residence time as apparent from Table 5-2. It results in decreased in the devolatilization reactions. However, the severe change occurs when the temperature and residence time take their highest value. In the case of volatiles (Figure 5-4(a)), when the temperature is 260°C and the residence time is low (approximately 6 minutes), the percentage of volatiles decreased only 2.3%, but it decreased by 7.7% for high residence time (approximately 18 minutes) for the same temperature. In the case of a higher temperature of 300°C, when the residence time is low, the percentage of volatiles in the torrefied biomass decreases by 12.8%, but eventually at high residence, this value increases to 42.3%.

Table 5-2. Proximate (%wt), elemental analysis (%wt) and higher heating value (MJ/kg).

| Temperature (C) | RPM | Tilt angle | Residence time (RT) | VM* | FC* | FR | C** | H** | N** | O** | HHV* |
|---|---|---|---|---|---|---|---|---|---|---|---|
| Raw biomass | - | - | - | 82.4 | 16.2 | 0.19 | 45.9 | 6.1 | 0.4 | 47.5 | 18.4 |
| | | 1 | 16.4 | 73.4 | 25.8 | 0.35 | 49.5 | 5.4 | 0.0 | 45.1 | 19.6 |
| | | 2 | 9.6 | 76.6 | 22.7 | 0.30 | 49.1 | 5.7 | 0.0 | 45.3 | 18.7 |
| | | 3 | 7 | 76.7 | 22.5 | 0.29 | 49.0 | 5.2 | 0.0 | 45.9 | 18.5 |
| | | 1 | 11 | 75.6 | 23.1 | 0.31 | 48.1 | 5.5 | 0.0 | 46.4 | 19.1 |
| | | 2 | 6.6 | 76.8 | 22.5 | 0.29 | 48.5 | 5.4 | 0.0 | 46.1 | 19.2 |
| | | 3 | 5.2 | 77.8 | 21.7 | 0.28 | 49.1 | 5.1 | 0.0 | 45.8 | 19.2 |
| | | 1 | 16.4 | 59.1 | 39.6 | 0.67 | 53.6 | 4.9 | 0.0 | 41.5 | 22.5 |
| | | 2 | 9.6 | 71.6 | 27.4 | 0.38 | 49.0 | 5.2 | 0.1 | 45.8 | 20.4 |
| | | 3 | 7 | 74.9 | 24.1 | 0.32 | 50.0 | 5.3 | 0.0 | 44.6 | 19.8 |
| | | 1 | 11 | 70.6 | 28.6 | 0.41 | 48.5 | 4.8 | 0.1 | 46.6 | 21.5 |
| | | 2 | 6.6 | 73.4 | 25.5 | 0.35 | 50.0 | 5.2 | 0.3 | 44.6 | 19.8 |
| | | 3 | 5.2 | 74.9 | 24.5 | 0.33 | 48.1 | 5.0 | 0.3 | 46.6 | 19.6 |
| | | 1 | 16.4 | 45.9 | 52.7 | 1.15 | 58.5 | 3.6 | 0.5 | 37.5 | 25.8 |
| | | 2 | 9.6 | 57.7 | 41.2 | 0.71 | 53.4 | 4.6 | 0.6 | 41.4 | 23.7 |
| | | 3 | 7 | 64.9 | 33.6 | 0.52 | 56.7 | 3.7 | 0.9 | 38.7 | 21.1 |
| | | 1 | 11 | 52.6 | 46.1 | 0.87 | 52.2 | 4.6 | 0.8 | 42.4 | 23.9 |
| | | 2 | 6.6 | 61.1 | 37.9 | 0.62 | 53.1 | 4.4 | 0.6 | 41.9 | 21.8 |
| | | 3 | 5.2 | 69.4 | 29.4 | 0.42 | 50.6 | 4.8 | 0.7 | 43.9 | 20.0 |

* Analysis in dry basis.

** Analysis in dry and ash free basis

Fixed carbon content of the product (Figure 5-4(b)) exhibits a reverse behavior. When both temperature and residence time are high, the fixed carbon increases significantly from 15% in raw biomass to values of 52.7%, i.e., up to 237%. At the low residence time and torrefaction temperature fixed carbon is low 21.66%, which is still an increase of about 39% above that in the raw biomass. The large differences in the final values of the product yields are due to the difference in residence time when the tilt is switched from 2 degrees to 1 degree for the same RPM. This difference is about 5 minutes (Table 5-2), which is considerable because in this condition the polymeric changes in the biomass occur slowly. At 300°C, the structural changes occur very fast, the biomass is more reactive, therefore changes in final FC values due to changes in other operational parameters were more visible. This is attributed to degradation of cell wall due to depletion of middle lamellae at around 300 C.

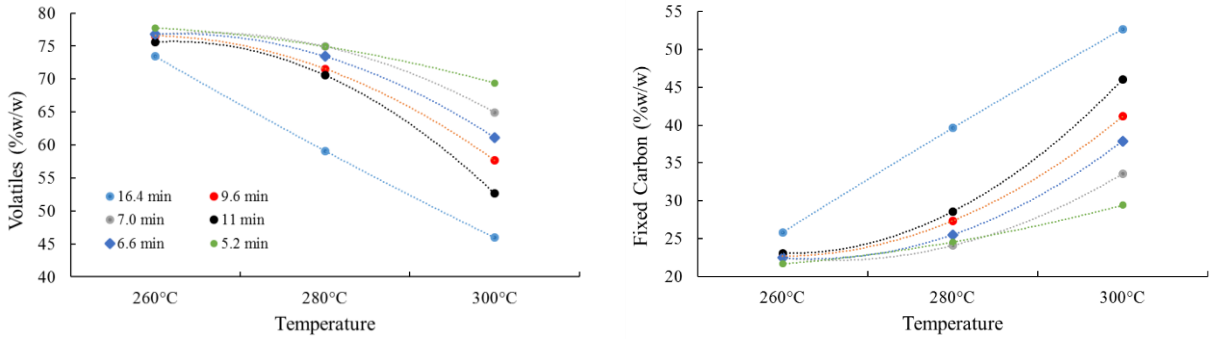


(a) (b)

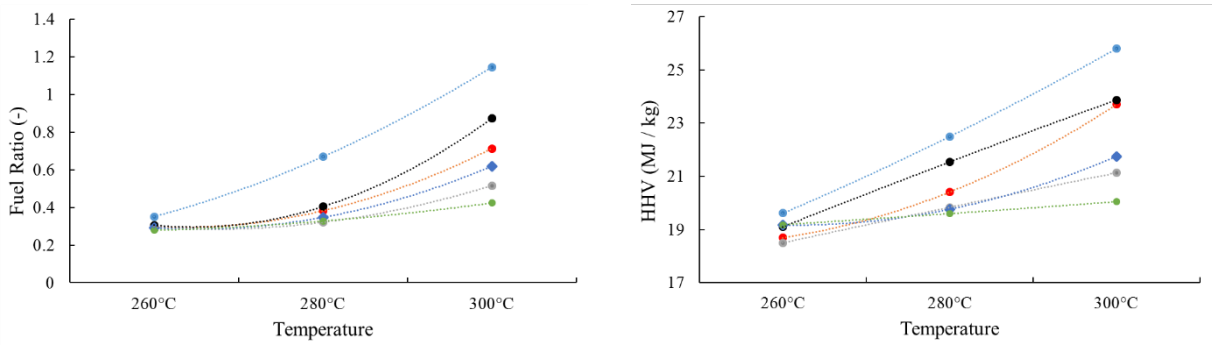


(c) (d)

Figure 5-4. Influence of process temperature and residence time in torrefied properties. (a) Volatiles, (b) Fixed Carbon, (c) Fuel Ratio, and (d) HHV.

Fuel Ratio (FR) is defined as the ratio of fixed carbon to volatile matter. Knowledge of this parameter is of great importance for a combustion processes because it indicates the combustion type that could occur in the process. Fuel Ratio increases with temperature and residence time (Figure 5-4(c)) producing a better quality solid fuel for co-combustional, reducing emissions compared that to the coal based combustion. Combustions of torrefied biomass with low Fuel Ratios may generate high more emissions of CO and hydrocarbons the blending ratio is higher. In contrast, combustion of torrefied biomass with high Fuel Ratios, reduces greenhouse gas emission and thus encourage mixing higher amounts of biomass with coal in a co-firing process. In the present study, the Fuel Ratio parameter starts with values of 0.19 for raw biomass, which increases to 0.28 at low temperature and residence time and to 1.15 at high temperature and residence time. This indicates that the developed torrefaction system could increase the Fuel Ratio from 42% to 485%. Such solid with the increased fuel ratio can have significant positive impacts on design and development of the co-fired power plant.

The Higher Heating Value (HHV), the most important property of a solid fuel, shows a behavior similar to those fixed carbon and fuel ratio (Figure 5-4(d)). It improves greatly when temperature and residence time of the process increase, but the mass yield decrease with HHV increases. The mass loss can reach a point where the torrefaction process may be unviable. This means that the torrefaction process finds products with better energy values at the expenses of mass loss due to devolatilization processes. The HHV of the raw biomass was 18.37 MJ/kg, which increases to values from 19.1 MJ/kg for mild torrefaction and to 25.8 MJ/kg when torrefaction severity is high. This indicates that the process can enhance the HHV of the biomass to 40.5%.

It is apparent from above only a small difference in the product qualities is noted at temperature of 260 C. As the process temperature and residence time increase larger variations in these values were observed. From Figure 5-4 it is also apparent that temperature has more impact on the final properties of torrefied biomass.

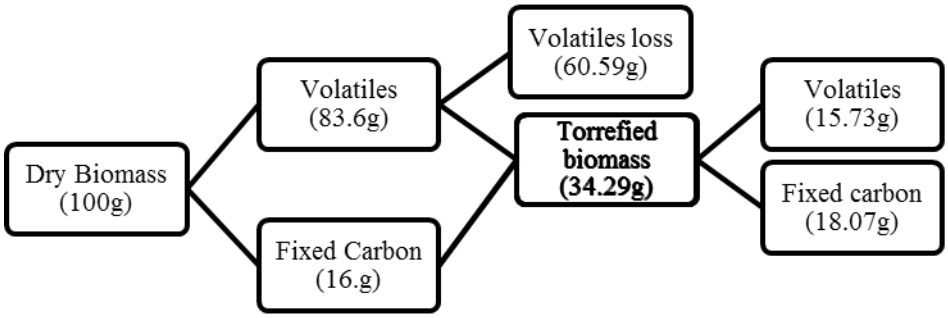


Figure 5-5. Mass balance for raw and torrefied biomass from proximate analysis for sample torrefied at T30051 (16.4 minutes of RT)

According to Figure 5-5, where mass balances for raw and torrefied biomass for the material T30051 is shown, it is possible see an interesting result in terms of the amount of solid linked with the fixed carbon. For raw material, the initial amount of fixed carbon obtained by proximate analysis is approximately 16.2 grams of an initial amount of 100 grams (16.2% Fixed Carbon w/w). During the torrefaction process the main polymeric compounds in the biomass partially is devolatilized, but, it would be expected that the amount of solid associated with fixed carbon before and after torrefaction should remain approximately constant. The amount of final solid of torrefied biomass linked to fixed carbon was about 18.06 grams from proximate analysis (52.68% Fixed carbon w/w). This result shows that there is an increase in the amount of fixed carbon by 11.5% (approx. 1.9 grams) in the torrefied biomass compared to the fixed carbon in raw material. This increase in the fixed carbon of the final material can be explained by the formation of new solid structures from reactions of carbonization, dehydration, and re-polymerization of glucose chains that generate reorganization in the solid. This formation of new solid from a liquid phase and volatiles has been observed by other authors [32–34].

The largest in fixed carbon content in torrefied biomass was detected in test T28051 (16.4 min of RT), which had an increase of 3.05 grams in solid per 100 grams of initial raw material. This is not surprising because several authors have found that reactions of re-polymerization, dehydration and restructuring of main biomass molecules have occurred greatly at around 280ºC. Above this temperature at around 300 °C, the devolatilization of condensed phases also increase, which can reduce the amount of secondary solid into the material [33,35].

### *5.3.3. Elemental analysis*

Table 5-2 also shows the variation in elemental analysis of biomass through torrefaction. An increase in the carbon content and a decrease in the hydrogen and oxygen contents were observed after torrefaction process. The decrease in hydrogen and oxygen contents are caused mainly by the removal of hydrogen and oxygen based compounds such as water vapor and carbon dioxide. At high torrefaction temperature, the decarboxylation reactions will be more, and the torrefied biomass becomes a more carbon dense product compared to that at a low temperature.

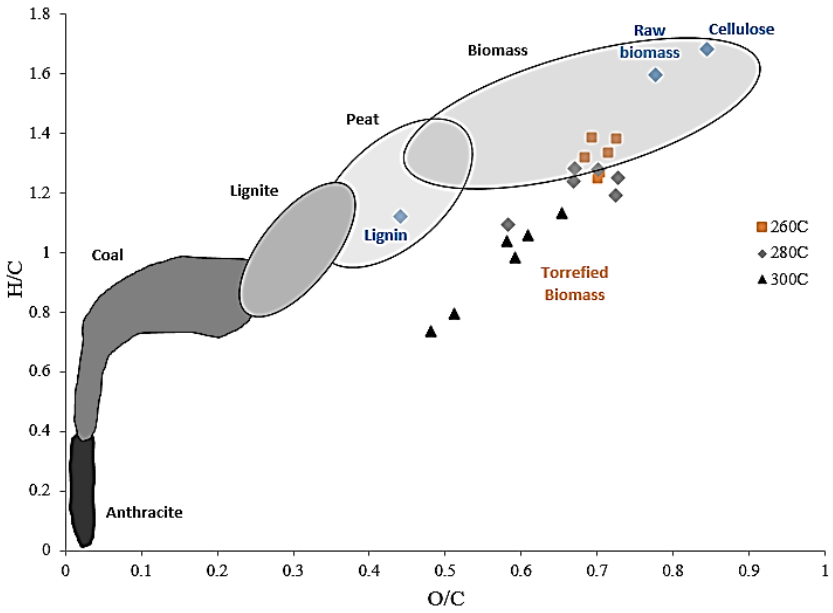


Figure 5-6. Van krevelen diagram for raw and torrefied biomass.

Both temperature and residence time affects the element compositions (Table 5-2). The carbon in the material increases with temperature and residence time, while the hydrogen and oxygen decrease with both operating parameters. This is a clear indication of the changes that take place in each of the major polymers in the biomass (hemicellulose, cellulose and lignin). At low temperatures, around 180 °C, decomposition is primarily hemicellulose, being exothermic [36] and mainly generates carbon monoxide and carbon dioxide through decarboxylation reactions of acid groups linked to hemicelluloses. Cellulose, meanwhile, strongly begins its process of endothermic decomposition around 280 °C [36], and generates small amounts of carbon dioxide. These two polymers are decomposed in greater amounts in the torrefaction process and are largely responsible for the changes in properties of the final solid.

Due to devolatilization, the value of biomass as fuel improves. Figure 5-6 shows that biomass is located towards the upper part bottom of the diagram, but torrefaction brings it close to medium range coals, as a result of the decline in relations O/C and H/C. It is clear that the temperature improves the quality of the material, and when the temperature increases to 300 °C, the product appears close to the lignin. This is because in torrefaction, the cellulose and hemicellulose are decomposed greatly and the proportion of lignin in the material increases, leaving a highly lignified material. For the product obtained at temperature of 260°C, we do not see much breakdown of the polymers and the release of oxygenates volatile in the process is very low. This makes that the fuel quality less improved and the product lies still in the area of biomass.

### *5.3.4. Product yield*

Parameters like Mass and Energy yields are similarly affected by temperature and residence time. From Figure 5-7(a) and Figure 5-7(b) it is apparent that the process temperature has a major impact on these two parameters. The largest mass loss occurred at temperature of 300 °C and at the high values of residence time. At temperature of 260 °C, the change in the tilt angle did not have much

variation in mass and energy yields. Differences of only 9% were observed between range of tilt angle studied and around 3% were found in studied range of RPM.

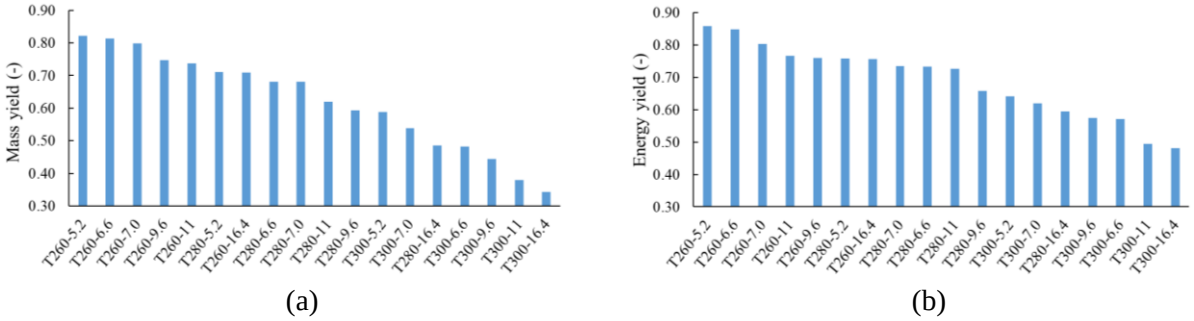


(a) (b)

Figure 5-7. Influence of process temperature in Mass yield (a) and energy yield (b) for all operational conditions evaluated in experiments. (TXXX-YY – torrefaction at XXX °C with YY residence time).

An interesting result is seen in tests T280-5.2 and T260-16.4, where both products showed the same values of mass and energy yield though temperature and residence time were different. This indicates that the torrefaction process is a conjugation between residence time and temperature, which means that, the same properties can be obtained at low temperature and high residence time or high temperature with low residence time. Similar behavior is observed between samples T280-9.6 and T300-5.2, and between T280-16.4 and T300-6.6, where the conjugation mentioned above can be checked. In Table 5-2, one observes the great similarity between the final properties of these pairs of materials mentioned above in the values of elemental carbon, fixed carbon and HHV.

For tests T280-5.2 and T260-16.4, the residence times of torrefaction were 5 and 16 minutes respectively, i.e., with adjusted temperature of 260°C and 280°C it is possible to obtain the same properties, but, the first one with an increase in residence time of 300%. This result is interesting in the context of economic evaluation of the torrefaction process because energy consumption could be quantified for a given amount of torrefied biomass.

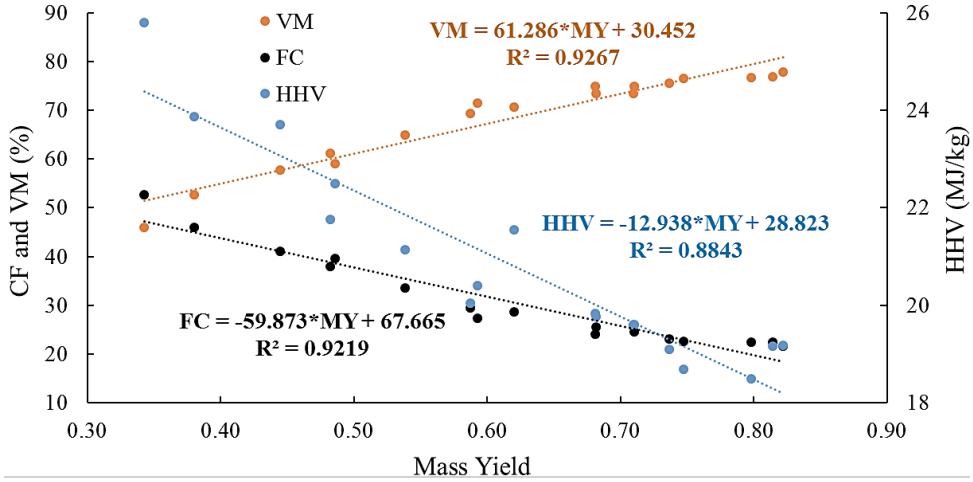


Figure 5-8. Relationship between Mass yield and HHV, FC, and VM.

Using data in Table 5-2 attempt was made to develop empirical correlation between temperature, residence time, mass yield for the given biomass, poplar wood. In the Figure 5-8, correlations for fixed carbon, volatiles, and HHV, from parameter Mass Yield are shown.

$$VM = 61.285 * MY + 30.452 \quad (5\text{-}8)$$

$$FC = -59.873 * MY + 67.665 \quad (5\text{-}9)$$

$$HHV(MJ/kg) = -12.938 * MY + 28.823 \quad (5\text{-}10)$$

In addition, using information shown in Figure 5-7, a predictive correlation for the mass yield for a given temperature and residence time, was obtained (Equation (5-11)). A double interpolation was done, aiming to find expressions as function of residence time and temperature. It is clear that this correlation applies only for the range of parameters studied, i.e., temperatures between 260°C and 300°C and residence times between 5 and 16 minutes for the poplar wood.

$$MY = a * RT + b \quad (5\text{-}11)$$

where *a*, and *b* are the slope and intercept respectively for the first interpolation. These both parameters are function of temperature as is shown in equations (5-12) and (5-13):

$$a = 0.00001T^2 - 0.005T + 0.83 \quad (5\text{-}12)$$

$$b = -0.0053T + 2.2702 \quad (5\text{-}13)$$

With the previous system of correlations, it is possible to predict from the residence time and process temperature, the final properties of the torrefied biomass as MY, HHV, Energy yield, fixed carbon, volatile and fuel ratio. These correlations are important tools for predicting properties in this type of biomass when it is subjected to torrefaction in a two-stage reactor.

Analysis of gaseous and condensable products generated during the process was also performed for three torrefaction tests. The selected conditions were T260-11, T280-11 and T300-11, the residence times were the same in all tests and only process temperature was varied. The volatiles generated inside the reactor exited and passed through a cold water bath at a temperature of about 5°C, in order to condense some of the major products generated in volatile product, as acetic and formic acids, furfural, methanol and water. After the cold water bath, the non-condensable gases were captured in sample bags and brought to a gas chromatography to analyze them. For the condensed phase, only the mass was measured. Liquid product characterization was not done. The total amount of non-condensable gases generated were obtained by difference.

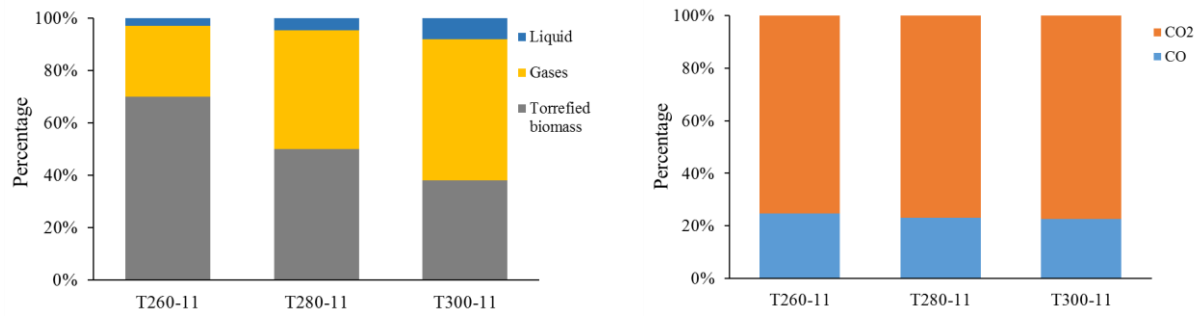


(a) (b)

Figure 5-9. Products distribution in the process for different temperatures and 7 RPM and 1° inclinations. (a) Product distribution in the process, (b) Product distribution in the gas phase. (TXXXYZ – torrefaction at XXX 0C, Y RPM and Z degree inclination of the torrefier)

As is shown in Figure 5-9(a), the production of both liquids and gasses in the process increases with torrefaction temperature. For 260°C, gasses and liquids were 3.1% and 27% respectively, while, for 300°C, it was 8% and 54%. The characterization of non-condensable gasses in the process showed only a small difference in the amounts of CO and $CO_2$ in the process when the operating condition was changed (Figure 5-9(b)). The solid mass losses due to torrefaction at 260 °C, 280 °C and 300 °C was 30%, 50% and 62% respectively. As the torrefaction temperature increases, devolatilization reactions become significant. At 260 °C the hemicellulose degradation starts along with primary char formation [35,36]. At this temperature the cellulose decomposition just begins, while lignin decomposes slowly with low mass loss [35,36]. When the temperature increases to 280 °C, the cellulose starts degradation of its amorphous structure, resulting in a significant mass loss. Lignin meanwhile continues its slow decomposition at this temperature without significant mass loss. When the temperature increases to 300 °C, the mass loss of cellulose becomes considerable, losing up to 40% of its initial mass, and hemicellulose is decomposed significantly, with a mass loss up to 60% of its initial mass [34]. Both polymers generate aromatic structures from structural rearrangements that generate primary char. Lignin meanwhile suffered minor structural modifications, a mass loss of about 15% of its initial mass can be found, and only mild devolatilization of some weak groups in their structure [34].

The chromatography of volatiles in the laboratory could measure only monoxide and dioxide of carbon (Figure 5-9(b)). It could not detect methane or other additional species. This is consistent with findings by several authors in the thermal range of the torrefaction process [9,35–37] who studied the decomposition hemicellulose, cellulose and lignin in order to characterize their products. They found only monoxide and dioxide carbon in analysis of non-condensable gases in the thermal ranges for torrefaction, also they found water (condensed in our work) and small amounts of methane, hydrogen, ethylene and ethane but above 400°C. The high amounts of carbon dioxide generated in volatile is explained by different authors as decarboxylation product of -COOH groups in glucuronic acid units [38], and cracking of C=O and -COOH [35], or by decarboxylation of O-acetyl groups attached to xylan normally in C2 position [39]. At temperatures lower than 280 °C, the carbon dioxide generated is due primarily to hemicellulose, and less to

lignin, but when the temperature increases, the contribution of the cellulose becomes considerable as observed by Yang et al. [35]. The formation of carbon monoxide in turn, is attributed to cracking of carbonyl groups (C-O-C) and carboxyl (C=O) [35], and secondary reactions of low molecular weight aldehydes [39,40]. Carbon monoxide has a similar behavior to carbon dioxide, since at lower temperatures, the contribution is mainly due to the hemicellulose in the range evaluated for torrefaction. From approximately 300 °C, the cellulose starts generating monoxide while hemicellulose decreases its formation [35]. Lignin meanwhile, has negligible monoxide generation from approximately 250°C and increases at high temperatures (>600 °C). This formation increases with temperature, while dioxide formation remains relatively constant for lignin.

Condensable volatiles were not characterized, but from previous works [34–36,39] we can assume it to contain what kind acidic compounds and aldehydes (C=O), alkenes (C-C), and ethers (C-O-C) and water when torrefied in the temperature range 200-400°C for hemicellulose [35], phenolic compounds (monomers or oligomers) to the case of lignin, and 5-HMF, HAA, HA and furfural in the case of cellulose [34].

In conclusion, at low temperatures, torrefaction primarily involves decomposition of hemicellulose, which exothermic [35,36] and mainly monoxide and dioxide carbon are generated through decarboxylation of acid groups attached to hemicelluloses. Condensable volatiles contain water, acid acetic, methanol, furfural, lactic acid, which are formed from the acethoxy group and methoxy monomers bound to hemicellulose during heating are detached by deacetylation and demethoxylation reactions [9,37]. Water is formed from the dehydration process of the polymers through the expulsion of hydroxyl groups [9,37].

### *5.3.5. Polymeric analysis*

Polymer content tests for selected torrefied biomasses were also performed to determine the final main polymeric compositions such as hemicellulose, cellulose and lignin. From Van Soest tests, the amount of Ash and Extractives can also be estimated., The selected torrefied biomasses used for these tests were produced at temperatures of 280 °C and 300 °C, 5 RPM and all inclinations. Results are presented in Figure 5-10 where one can note the effects of temperature and residence time on the final polymeric compositions. The figure shows the distribution of the mass of polymeric components in different torrefied biomasses and compared those compositions available in the 50 gm of raw biomass. This figure also shows the impact of torrefaction process on the final amount of hemicellulose, cellulose, and lignin of a biomass.

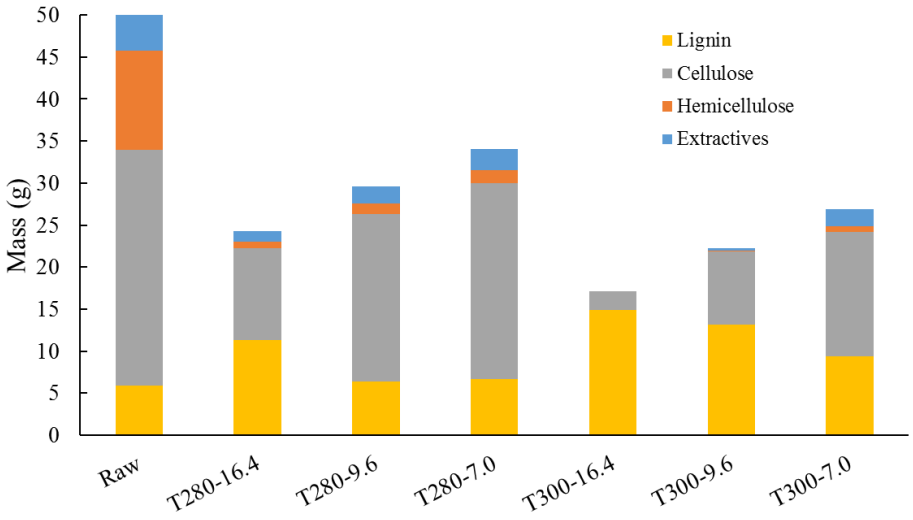


Figure 5-10. Polymeric test for some torrefied biomass. (TXXXYY – torrefaction at XXX °C with YY of residence times).

Effect of residence time on the extractive is shown in Figure 5-10. At 280°C, we note that the amount of extractives in the torrefied samples is reduced by as much as 40% from the raw biomass with minor dependence on the residence time. The amount of hemicellulose, in turn, is affected largely by the temperature Even at 280°C, hemicellulose content reduces from 23.5% in raw biomass (11.7 grams) to values of 4.6% (1.24 grams) and 3% (0.73 grams) for samples with high and low residence time, respectively. This was expected, because from previous works reported in the literature it was found that this polymer begins its further degradation around 260°C and accelerates as the temperature increases.

In this degradation process, volatiles generation such as $CO_2$, CO, $CH_4$, water, acetic acid are generated [9,34–37,39]. For shorter residence time, only a small decrease (5 grams) in cellulose content is observed. The raw biomass with 28 grams of cellulose is turned into the torrefied biomass with 23.3 grams after the torrefaction at 280ºC and with low residence time. For the other two residence times, a decrease in the amount is significantly high when residence time increases, going to only 20 and 11 grams. An interesting behavior is found when lignin was examined quantitatively. An increase in quantity can be observed as the temperature and residence time increases. This could be because of the formation of aromatic structures of benzene rings during the degradation of the hemicellulose and cellulose. These benzene rings are linked with aliphatic and oxygenated groups (hydroxyl and ether) [41,42], giving the cellulose char to a structure relatively close to the one of the lignin char. Addition of such char with aromatic structures generated from the primary reactions of hemicellulose and cellulose on the original lignin with similar aromatic structure may be one of the reasons that has resulted in increasing lignin content.

For torrefaction at temperature of 300 °C a similar behavior is found. The extractives the torrefied product decreases with increases of residence times (or increase in inclination). At very shorter residence time ($1^{\circ}$ inclination) extractives could not be detected in the product. Hemicellulose was as low as 0.7 grams even at the lowest residence time of 7 minutes. For all other residence times,

the hemicellulose completely disappears in the torrefied biomass. Cellulose is meanwhile decomposed, but left large percentage of it in the torrefied product (Figure 5-10). About 50% of the initial cellulose is still in the torrefied biomass at low residence time. On the other hand, lignin increases when the solid residence time increases. An increase of 253% in lignin was obtained for the T300-16.4 test. The reason for this behavior has already been discussed, but it is more noticeable when treatment conditions are severe.

### *5.3.6. BET analysis*

Tests on measurements of the pore area using nitrogen (BET) and $CO_2$ methods (Dubinin Radushkevich) were performed for samples torrefied at temperatures of 280 °C and 300 °C. Nitrogen adsorption gives surface areas of meso-pores (1-100 nm) while carbon dioxide adsorption gives surface areas of narrow micro-pores (< 1 nm). Measure values in Table 5-3 show that torrefaction improves the porosity and superficial area of the product when the temperature and residence time increases. Baud [43] in his tests noted that the surface area for raw poplar wood material is close to zero (~0.0098 $m^2$/gram). For this reason, the raw material was not characterized in this work. BET analysis was limited to torrefied poplar alone.

In the torrefied biomass increases its porosity with severity in the process because devolatilization reactions of polymers in the biomass leading to structures with space available in it. Table 5-3 shows that the surface area increases to 2 $m^2$/gram with BET analysis when poplar wood is torrefied at severe conditions. This BET surface area indicates the area of the meso-porous structure, i.e., where the pores are greater than 2nm.

Table 5-3. Superficial area with meso and micro-porosity for torrefied biomass.

| Sample | BET ($m^2$/g) | $CO_2$ ($m^2$/g) | Sample | BET ($m^2$/g) | $CO_2$ ($m^2$/g) |
|---|---|---|---|---|---|
| T280-16.4 | 0.67 | 108.69 | T300-16.4 | 1.14 | 125.59 |
| T280-9.6 | 0.92 | 60.28 | T300-9.6 | 2.11 | 142.35 |
| T280-7.0 | 0.76 | 53.30 | T300-7.0 | 1.46 | 97.14 |
| T280-11 | 0.51 | 79.31 | T300-11 | 1.70 | 141.16 |
| T280-6.6 | 0.68 | 50.11 | T300-6.6 | 0.48 | 81.02 |
| T280-5.2 | 0.48 | 50.40 | T300-5.2 | 0.66 | 68.32 |

Adsorption with $CO_2$, shows the surface area to be as high as 142 $m^2$ / gram, as a result of measurements of with pore sizes less than 2nm. This indicates that the devolatilization of the material generates largely micro-pores.

In Figure 5-11 the distributions of the pore surface area for each range of pores width in the torrefied biomasses with longer residence times. These biomasses developed more porosity in the process. The torrefaction temperature of 280°C with residence times of 16.4 minutes, no develops meso-porosity (Figure 5-11(b)) and only increases in micro-porosity was observed (Figure 5-11(a)). When the process temperature is increased to 300°C with the same residence time, a big amount of porosity is formed on the meso-scale, compared to 280°C, and the micro-porosity is favored by this temperature.

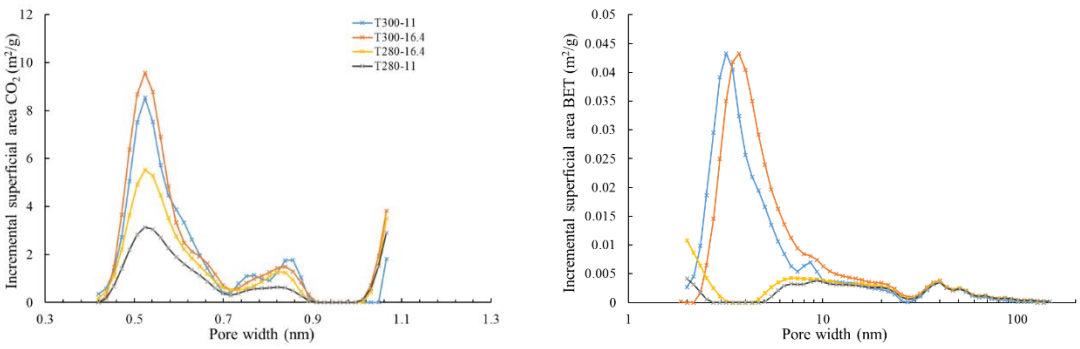


(a) (b)

Figure 5-11. Incremental superficial area analysis for samples with bigger residence time. CO2 analysis (a); BET analysis (b). (TXXXYZ – torrefaction at XXX °C, Y RPM and Z degree inclination of the torrefier).

In the meso-porosity, a pore formation around 3nm is observed, and in the micro-porosity, the formation of pores occurs in approximately 0.52nm and 0.8nm of pore sizing, being predominant pore formation in first size. This information is important for to establish an end-use product, because from pore sizes we could think of capturing certain compounds similar to these sizes

### *5.3.7. Characterization for biomass sampled inside kiln*

The biomass was sampled inside the rotary kiln while it was still being torrefied, and was characterized using fiber analysis and proximate analysis. This helped study changes in polymeric decomposition, and variations in volatiles and fixed carbon content during torrefaction.

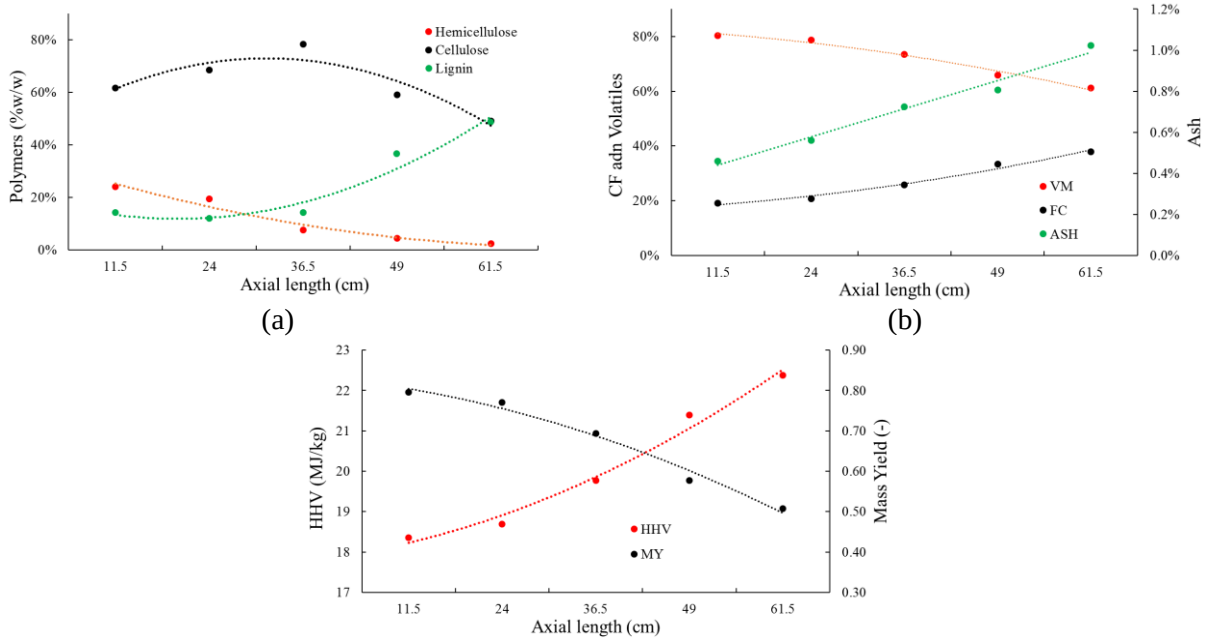


(a) (b)

(c)

Figure 5-12. Fiber analysis (a), proximate analysis (b), and predicted Mass yield and HHV with correlations shown in Figure 5-8 (c) for torrefied biomass taken inside kiln for 300C, 7 RPM and 1 grade of inclination.

The sampling of intermediate products was conducted for 7 RPM, 1° tilt angle with torrefaction temperature of 300°C. Five samples were obtained inside the kiln for different axial positions (Figure 5-12). The first sample (11.5 cm) was withdrawn from a point near the entrance of the rotary reactor while the last sample (61.5 cm) was captured near the reactor exit.

As seen in this Figure 5-12(a), hemicellulose contents of biomass decreased from 23.6% to 2.3% as biomass move from front to the end of the reactor. This means that the residence time in these operating conditions, were not sufficient to decompose this polymer entirely. It thus produced a less energy dense product because the hemicellulose is the most oxygenated component in the biomass. The lignin, increases its percentage share (not absolute amount) in the biomass as the torrefaction process progresses. This is due to primary reactions of hemicellulose and cellulose, which generate char with aromatic structures, which are very similar to those of lignin. Cellulose decomposes and decreases its amorphous structure, as mentioned above, but its slight increase in the middle of the reactor could be a result of higher temperature.

In addition to obtaining information on the structural changes of the material through knowledge of its polymeric compositions, a characterization was also performed by the proximate analysis in order to know the variations of the fixed carbon and volatile material along the reactor length as the process proceeds. This helps to estimate degree of torrefaction or degree of devolatilization of the torrefaction process.

As seen in Figure 5-12(b), the volatile matter decreases as it moves down the reactor or as the torrefaction process proceeds. Opposite behavior is noted for the fixed carbon as the biomass is torrefied. From this analysis, it is possible to obtain information about changes in FR during the process, which also increases. The Figure 5-12(c), also shows the values of HHV and MY predicted from correlation (Equations (5-8) and (5-10)). These correlations thus, allow one to obtain predictive product qualities for a given set of operating condition. This could help control and manipulation of the process.

This novel method of sampling inside the reactor and characterization the material being processed, is of great importance for continuously production processes, because through this sampling is possible to obtain information about the process and material properties in real time, in order to modify operational parameters and get final specific properties desired for the material without stopping the process.

### *5.3.8. Comparison with big particles*

Present results of small particles (0.5 - 1 mm ) were compared with those from previously work by Nhuchhen et al. [13] in the same two-stage rotary reactor but with large particles of about 5 mm. Evaluation was done for temperatures of 260°C, 290°C and 320°C. Results of two sizes of particles but under same process, same parameters are compared in Table 5-4.

Table 5-4. Comparison between a torrefaction process with poplar for big and small particles [13].

| Properties | Large particles (5 mm) [28] | | Small particles (0.5 – 1 mm) | |
|---|---|---|---|---|
| | T26051* | T32051* | T26051* | T30051* |
| HHV (% Increase) | 4.1% | 13.6% | 7.2% | 40.50% |
| FC (% Increase) | 6.1% | 73.7% | 59.5% | 225% |
| FR (% Increase) | 6.6% | 90.8% | 78.7% | 485% |
| VM (% Decrease) | 0.5% | 9.0% | 10.9% | 44% |
| MY | 94.3 | 82.9 | 71 | 34 |
| EY | 98 | 96.1 | 76 | 48 |

*TXXXYZ, where XXX is temperature in °C, Y is the RPM, and Z is the tilt angle.

From Table 5-4 it can be concluded that the torrefaction had a great impact on small particles. At 260 °C, the differences in results between two particle sizes is very prominent. Large particles were not torrefied to the same extent as small particles torrefied at this temperature. A small increase in HHV, fixed carbon and an almost imperceptible decrease in volatile material was noticed in large particles while small particles showed major changes in their final properties. Increases of up 59% in the fixed carbon and 7% in HHV was evidenced. The mass loss in small particles is considerable, approximately 29% compared with 5.7% in the large particles confirms the difference. This is because a thermal gradient between surface and core occurs in large particles, causing a delay in the heating of the material and in its devolatilization process. This means that, to obtain a similar conversion as in small particles large particles must be allowed a longer residence time under the same thermal conditions. This may also suggest that the thermal gradient in large particles may lead to non-uniform conversion at the outer and inner surfaces of large particles. This, however, requires further investigation at different particle sizes.

## 5.4. Conclusions

Torrefaction of fine particles of poplar wood in a continuous two-stage, indirectly heated rotary torrefier was investigated under different operating conditions. It investigated the effect of temperature and residence time on the properties of torrefied biomass. Compared to residence time torrefaction temperature has a stronger effect on all properties of the torrefied biomass. Axial temperature distribution of the rotary torrefier showed a parabolic profile due heat losses from two ends. Samples taken from within the reactor shows continuous degradation of the biomass as it moves along the reactor. With increases in temperature, HHV, fixed carbon, mass loss increases also, but with increase in RPM and tilt angle of the rotary reactor an opposite trend is observed because these provided shorter residence time of torrefaction. Important parameters such as HHV and fuel ratio (FR) increased when temperature and residence time were increased. Increments up to 40% for HHV and 485% for FR when temperature and residence time taken the maximum values. Results of different characteristics of the torrefied biomass and process parameters indicate that the torrefaction process in a volatile gases medium is possible to be developed.

A comparison of torrefaction of particles (5 mm approximately) with that of small particles in the same rotary reactor under same torrefaction condition showed that the torrefaction is much more effective for small particles, because for large particles, owing to thermal gradient within it do not

under go uniform degradation. For a similar conversion level, large particles need longer residence time or more severe torrefaction.

**Acknowledgments**

The work was performed in the Biomass Conversion Laboratory at Dalhousie University under the guidance of Prof. Prabir Basu, who acknowledge the support of Natural Science & Engineering Council and from Greenfield Research Incorporated of Canada. The first authors thank the Colombian Administrative Department of Science, Technology and Innovation (COLCIENCIAS) (Departamento Administrativo de Ciencia, Tecnología e Innovacion) for providing him with financial support.

**References**

[1] Basu P. Biomass Gasification, Pyrolysis and Torrefaction: Practical Design and Theory. 2013.

[2] Pentananunt R, Rahman ANMM, Bhattacharya SC. Upgrading of biomass by means of torrefaction. Energy 1990;15:1175–9. doi:10.1016/0360-5442(90)90109-F.

[3] Wattananoi W, Khumsak O, Worasuwannarak N. Upgrading of biomass by torrefaction and densification process. 2011 IEEE Conf Clean Energy Technol 2011:209–12. doi:10.1109/CET.2011.6041465.

[4] Medic D, Darr M, Shah a., Potter B, Zimmerman J. Effects of torrefaction process parameters on biomass feedstock upgrading. Fuel 2012;91:147–54. doi:10.1016/j.fuel.2011.07.019.

[5] Li J, Brzdekiewicz A, Yang W, Blasiak W. Co-firing based on biomass torrefaction in a pulverized coal boiler with aim of 100% fuel switching. Appl Energy 2012;99:344–54. doi:10.1016/j.apenergy.2012.05.046.

[6] Fisher EM, Dupont C, Darvell LI, Commandré J-M, Saddawi a, Jones JM, et al. Combustion and gasification characteristics of chars from raw and torrefied biomass. Bioresour Technol 2012;119:157–65. doi:10.1016/j.biortech.2012.05.109.

[7] Broström M, Nordin A, Pommer L, Branca C, Di Blasi C. Influence of torrefaction on the devolatilization and oxidation kinetics of wood. J Anal Appl Pyrolysis 2012;96:100–9. doi:10.1016/j.jaap.2012.03.011.

[8] Berrueco C, Recari J, Güell BM, Alamo G Del. Pressurized gasification of torrefied woody biomass in a lab scale fluidized bed. Energy 2014;70:68–78. doi:10.1016/j.energy.2014.03.087.

[9] Deng J, Wang G, Kuang J, Zhang Y, Luo Y. Pretreatment of agricultural residues for co-gasification via torrefaction. J Anal Appl Pyrolysis 2009;86:331–7. doi:10.1016/j.jaap.2009.08.006.

[10] Hassan E, Steele P, Ingram L. Characterization of fast pyrolysis bio-oils produced from pretreated pine wood. Appl Biochem Biotechnol 2009;154:182–92. doi:10.1007/s12010-008-8445-3.

[11] Zheng A, Zhao Z, Chang S, Huang Z, Wang X, He F, et al. Effect of torrefaction on structure

and fast pyrolysis behavior of corncobs. Bioresour Technol 2013;128:370–7. doi:10.1016/j.biortech.2012.10.067.

[12] Granados DA, Velásquez HI, Chejne F. Energetic and exergetic evaluation of residual biomass in a torrefaction process. Energy 2014;74:181–9. doi:10.1016/j.energy.2014.05.046.

[13] Nhuchhen DR, Basu P, Acharya B. Torrefaction of poplar in continuous two- stage indirectly heated rotary torrefier. Energy & Fuels 2016;30:1027–38. doi:10.1021/acs.energyfuels.5b02288.

[14] Huang YF, Chen WR, Chiueh PT, Kuan WH, Lo SL. Microwave torrefaction of rice straw and Pennisetum. Bioresour Technol 2012;123:1–7. doi:10.1016/j.biortech.2012.08.006.

[15] Ren S, Lei H, Wang L, Bu Q, Wei Y, Liang J, et al. Microwave Torrefaction of Douglas Fir Sawdust Pellets. Energy & Fuels 2012;26:5936–43. doi:10.1021/ef300633c.

[16] Satpathy SK, Tabil LG, Meda V, Naik SN, Prasad R. Torrefaction of wheat and barley straw after microwave heating. Fuel 2014;124:269–78. doi:10.1016/j.fuel.2014.01.102.

[17] Wang MJ, Huang YF, Chiueh PT, Kuan WH, Lo SL. Microwave-induced torrefaction of rice husk and sugarcane residues. Energy 2012;37:177–84. doi:10.1016/j.energy.2011.11.053.

[18] Li H, Liu X, Legros R, Bi XT, Lim CJ, Sokhansanj S. Torrefaction of sawdust in a fluidized bed reactor. Bioresour Technol 2012;103:453–8. doi:10.1016/j.biortech.2011.10.009.

[19] Wang C, Peng J, Li H, Bi XT, Legros R, Lim CJ, et al. Oxidative torrefaction of biomass residues and densification of torrefied sawdust to pellets. Bioresour Technol 2013;127:318–25. doi:10.1016/j.biortech.2012.09.092.

[20] Carrier M, Hugo T, Gorgens J, Knoetze H. Comparison of slow and vacuum pyrolysis of sugar cane bagasse. J Anal Appl Pyrolysis 2011;90:18–26. doi:10.1016/j.jaap.2010.10.001.

[21] Zajec L. Slow pyrolysis in a rotary kiln reactor : Optimization and experiment 2009:28–43.

[22] Colin B, Dirion JL, Arlabosse P, Salvador S. Experimental study of wood chips torrefaction in a pilot scale rotary kiln. Chem Eng Trans 2014;37:505–10. doi:10.3303/CET1437085.

[23] Doassans-Carrère N, Muller S, Mitzkat M. REVE - A new industrial technology for biomass torrefaction: Pilot studies. Fuel Process Technol 2014;126:155–62. doi:10.1016/j.fuproc.2014.04.026.

[24] Nachenius RW, van de Wardt TA, Ronsse F, Prins W. Torrefaction of pine in a bench-scale screw conveyor reactor. Biomass and Bioenergy 2014;79:96–104. doi:10.1016/j.biombioe.2015.03.027.

[25] Mei Y, Liu R, Yang Q, Yang H, Shao J, Draper C, et al. Torrefaction of cedarwood in a pilot scale rotary kiln and the influence of industrial flue gas. Bioresour Technol 2015;177:355–60. doi:10.1016/j.biortech.2014.10.113.

[26] Strandberg M, Olofsson I, Pommer L, Wiklund-Lindström S, Åberg K, Nordin A. Effects of temperature and residence time on continuous torrefaction of spruce wood. Fuel Process Technol 2015;134:387–98. doi:10.1016/j.fuproc.2015.02.021.

[27] Nanou P, Carbo MC, Kiel JHA. Detailed mapping of the mass and energy balance of a

continuous biomass torrefaction plant. Biomass and Bioenergy 2016. doi:10.1016/j.biombioe.2016.02.012.

[28] Nachenius RW, Van De Wardt TA, Ronsse F, Prins W. Residence time distributions of coarse biomass particles in a screw conveyor reactor. Fuel Process Technol 2015;130:87–95. doi:10.1016/j.fuproc.2014.09.039.

[29] Nhuchhen DR. Studies on Advanced Means of Biomass Torrefaction. Dalhousie University, 2016. doi:10.1017/CBO9781107415324.004.

[30] Piton M, Huchet F, Le Corre O, Le Guen L, Cazacliu B. A coupled thermal-granular model in flights rotary kiln: Industrial validation and process design. Appl Therm Eng 2015;75:1011–21. doi:10.1016/j.applthermaleng.2014.10.052.

[31] Pan JP, Wang TJ, Yao JJ, Jin Y. Granule transport and mean residence time in horizontal drum with inclined flights. Powder Technol 2006;162:50–8. doi:10.1016/j.powtec.2005.12.004.

[32] Wang Z, Pecha B, Westerhof RJM, Kersten SR a, Li CZ, McDonald AG, et al. Effect of cellulose crystallinity on solid/liquid phase reactions responsible for the formation of carbonaceous residues during pyrolysis. Ind Eng Chem Res 2014;53:2940–55. doi:10.1021/ie4014259.

[33] Pelaez-Samaniego MR, Yadama V, Garcia-Perez M, Lowell E, McDonald AG. Effect of temperature during wood torrefaction on the formation of lignin liquid intermediates. J Anal Appl Pyrolysis 2014;109:222–33. doi:10.1016/j.jaap.2014.06.008.

[34] Collard FX, Blin J. A review on pyrolysis of biomass constituents: Mechanisms and composition of the products obtained from the conversion of cellulose, hemicelluloses and lignin. Renew Sustain Energy Rev 2014;38:594–608. doi:10.1016/j.rser.2014.06.013.

[35] Yang H, Yan R, Chen H, Lee DH, Zheng C. Characteristics of hemicellulose, cellulose and lignin pyrolysis. Fuel 2007;86:1781–8. doi:10.1016/j.fuel.2006.12.013.

[36] Werner K, Pommer L, Broström M. Thermal decomposition of hemicelluloses. J Anal Appl Pyrolysis 2014;110:130–7. doi:10.1016/j.jaap.2014.08.013.

[37] Wang G, Luo Y, Deng J, Kuang J, Zhang Y. Pretreatment of biomass by torrefaction. Chinese Sci Bull 2011;56:1442–8. doi:10.1007/s11434-010-4143-y.

[38] Patwardhan PR, Brown RC, Shanks BH. Product distribution from the fast pyrolysis of hemicellulose. ChemSusChem 2011;4:636–43. doi:10.1002/cssc.201000425.

[39] Shen DK, Gu S, Bridgwater a. V. The thermal performance of the polysaccharides extracted from hardwood: Cellulose and hemicellulose. Carbohydr Polym 2010;82:39–45. doi:10.1016/j.carbpol.2010.04.018.

[40] Hosoya T, Kawamoto H, Saka S. Pyrolysis behaviors of wood and its constituent polymers at gasification temperature. J Anal Appl Pyrolysis 2007;78:328–36. doi:10.1016/j.jaap.2006.08.008.

[41] Pastorova I, Botto RE, Arisz PW, Boon JJ. Cellulose char structure: a combined analytical Py-GC-MS, FTIR, and NMR study. Carbohydr Res 1994;262:27–47. doi:10.1016/0008-6215(94)84003-2.

[42] McGrath TE, Chan WG, Hajaligol MR. Low temperature mechanism for the formation of polycyclic aromatic hydrocarbons from the pyrolysis of cellulose. J Anal Appl Pyrolysis 2003;66:51–70. doi:10.1016/S0165-2370(02)00105-5.

[43] Raut MK. Studies Into the Effect of Torrefaction on Gasification of Biomass. Dalhousie University, 2014.

# Chapter 6. Torrefaction of Large Biomass Particles in a Custom Designed Thermo-gravimetric Unit

**(Paper to be submitted to JAAP)**


## Abstract

Sugarcane bagasse with different particle sizes was evaluated in torrefaction process by TGA and a custom thermo-gravimetric unit designed for big particles evaluation. Big particles of 2.5x2.5x5cm, constructed with different particles sizes of sugarcane bagasse (small, big, and bagasse without crushing) were torrefied to evaluate the devolatilization process. The designed and constructed reactor allows to measure the mass and temperature of the particle, and capture condensable volatiles through a condensation unit which is maintained at -12°C during torrefaction. Final products of the process (liquids, solids and gases) were measured and characterized to understand and analyze the processes occurring in the biomass during torrefaction. From tests in TGA, a two-step kinetic model was fitted to experimental data to get the kinetic parameters for dynamic and isothermal process. Results of experimental tests for big particles show an incidence of particle size in the process of decomposition of the material, since the material without crushing has the lowest mass loss of that evaluated particles. torrefaction process shows a big thermal impact for fine particles, having highest core temperatures, devolatilization, and aromaticity.


***Keywords:*** Biomass torrefaction, particle size, kinetic model, product yield, mass balance

## 6.1. Introduction

Torrefaction process has been recently known as a pretreatment that improves the biomass, improving some properties such as equilibrium moisture absorption, fragility, heterogeneity, and some other properties such as calorific value, reactivity, etc. Some authors have worked torrefaction in the experimental field with the objective of evaluating the operational parameters, such as atmosphere [1–6], particle sizes [7–12], temperature [13–16], residence time [17–20] and heating rate [17,21–24], and to find the optimal combination that generate the best properties in the final solid. Some of them have quantified and characterized the products of the process by different experimental techniques such as GC-MS, FTIR, HPLC, and others, in order to understand the decomposition process occurring during the torrefaction in the biomass.

Torrefaction test have been developed in several technologies such as TGA [15,25–31], fluidized and fix beds [21,22,31,32], rotary reactors [32–39], microwave [40–46], and others. Through them, authors have tried to obtain more effective and simplified methods for carrying out the torrefaction process. The final torrefied solid has been evaluated in subsequent thermal processes such as combustion, gasification, pyrolysis, crushing and pelletizing [47–59], with excellent results in these thermal and physical processes, demonstrating characteristics very close to those of low-grade coals, in terms of grindability and reactivity.

New kind of reactors have been designed in order to find new options and facilitate the obtaining of products in a continuous operating, and their characterization. Some of them have been two-stage rotary reactors [16,32–34,60], designed to separate drying from devolatilization and have a gas with less moisture and higher calorific values. Screw reactors [35,61–65] are other kind of new

developed technology with which it is easy to control parameters such as residence time, but come up with difficulties with big particle sizes. Microwaves [40–46] are used to reduce the processing time due to the rapid heating rates with the associated problems of different temperatures inside the solid which generates heterogeneous torrefied solid.

In recent works [7,22,66], the effect of material amount over decomposition has been studied. After having studied the decomposition of the material through small amounts of material generally carried out in TGA to obtaining their kinetics and other kind of studies, several studies have been carried out in which the decomposition in large particles is analyzed in order to obtain information about secondary reactions in heterogeneous phase, if any, and the effect of decomposition when volatiles release become difficult, increasing pressure and diffusivity in the solid.

In this work, the torrefaction in TGA of particles of size 0.075mm under kinetic control has been studied to obtain kinetic information of the process. In addition, to study particles of larger size, a thermo-gravimetric reactor has been designed and built with which valuable information can be obtained from particles up to 9cm in diameter and 15cm in length. With this reactor is possible to separate condensable from non-condensable volatiles by a condensation unit which is maintained at -12°C throughout the process and captures most of condensable products. In this way, it is possible to obtain the main products of the torrefaction to carry out their respective characterizations. Tests with approximately 6 grams of sugarcane bagasse have been made with three different particle sizes called fines, large and complete bagasse without crushing. Characterizations were performed to each product obtained in the process, and great information was obtained about differences in decomposition for each studied material.

## 6.2. Methods

### *6.2.1. Biomass sample*

Sugarcane bagasse with four different particle size denominated powder, fines, coarse and bagasse without crushing were used in these torrefaction tests. The powder material with a particle size of 0.075mm was used for the experimental tests in TGA. In Table 6-1 the results of characterizations are presented for elemental, proximate, HHV and polymer analysis.

Table 6-1. Proximate, and elemental analysis, HHV, and lignocellulosic composition for raw biomass (dry and ash free basis)

| Proximate analysis (%w/w) | | Ultimate analysis (%w/w) | | Polymeric analysis (%w/w) | |
|---|---|---|---|---|---|
| Moisture (wb) | 5.4 | Carbon (daf) | 45.9 | Cellulose | 25.2 |
| Volatiles (db) | 82.4 | Hydrogen (daf) | 6.1 | Hemicellulose | 26.4 |
| Fixed carbon (db) | 16.2 | Nitrogen (daf) | 0.4 | Lignin | 20.4 |
| Ash (db) | 1.4 | Oxygen (daf) | 47.6 | | |
| HHV (db)(MJ/kg) | 18.3 | | | | |

The remaining three particle sizes were used to construct particles of 2.5x2.5x5cm and torrefied with the custom thermo-gravimetric reactor designed for big particles. An image of the materials used is presented in Figure 6-1.

(a) (b) (c)

Figure 6-1. Material used for big particles building. Fine (a), coarse (b), and sugarcane bagasse without crushing (c).

### *6.2.2. Experimental*

Torrefaction tests with different temperatures between 200 and 300°C were performed on a TGA STA PT-1600 LINSEIS with samples of approximately 9 mg. Different heating rates between 5-20°C/min were evaluated with a residence time of 60 minutes. It was observed that during crushing process the material tends to divide between particles of belong to marrow and cortex, with more marrow material found in finer particles. To solve this problem, these two materials were separated from the bagasse and the weight ratio of these two materials was determined experimentally. They were then crushed separately until the desired particle size and then mixed in the same experimentally measured proportions.

The experimental setup for big particles consists of a custom-designed thermo-gravimetric reactor with 100mm in diameter and 35cm in long. Energy supply is through electrical heaters surrounding the stainless-steel tube with a capacity to heat it up to 900°C. Approximately, 7 grams of biomass is packed in a special basket built with a stainless-steel mesh with 2.5x2.5x5cm. This basket is suspended inside the reactor from the bottom of a digital balance (Figure 6-2) placed at the top of reactor. The balance sensitivity is 0.1mg, and records the sample mass continuously to the computer. The reactor is continuously flushed by Nitrogen at 0.5 liters per minute (lpm). The temperature of reactor is measured and controlled by a thermocouple placed in its center whose data is also logged in a computer.

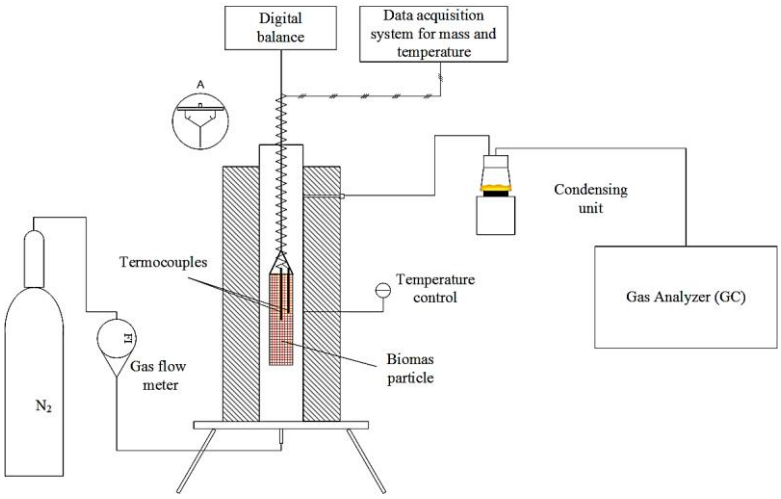


Figure 6-2. Schematic diagram of the experimental set-up

The sample is heated by two heating ramps, from room temperature to 105°C with a heating rate of 10°C/min for 3 hours, to remove all surface water from sample and not interfere with mass loss later. The sample is then heated from this temperature to the selected process temperature between 200-300°C at 10°C/min for 5 hours. Before test, nitrogen is passed for 20 minutes in order to ensure inert atmosphere and to remove any amount of oxygen into the reactor. The mass loss is monitored continuously in all process. A thermocouple is placed in the center of the particle to measure its temperature and records continuously to the computer. All tests are performed with two different configurations to characterize all torrefaction products. With the first configuration is possible to obtain information about the mass loss of the particle and its core temperature during process (Figure 6-2). With the second configuration, the reactor is sealed and the digital balance is decoupled from reactor. The sample is fastened from the reactor cover as is shown in detail A from Figure 6-2. With this configuration, volatiles are addressed to condenser unit and, condensable and non-condensable volatiles are separated and then both products are characterized separately. These tests give a complete information about products such as solids, liquids and gases.

### *6.2.3. Products characterization*

The main products captured during torrefaction process were characterized. Gas was characterized and quantified by GC where the main expected species such as $CO_2$, CO, $H_2$ and $CH_4$ were detected. Gas measurements were made during sample heating and the isothermal period and it was possible to obtain the entire yield profile of each species in the process to be quantified. Liquids, on the other hand, were captured with the condensation unit during process, and only at the end was weighted and characterized by GC-MS. For this characterization calibrations were made with standard species such as water, formic acid, acetic acid, furan, phenol, 5HMF, 5-Methyl-2-furaldehyde, LVG, and oleic acid. These species were diluted in methanol to form a standard solution and then were performed dilutions of 5, 25, 50, 75 and 100% to obtain enough points to quantify in GC-MS. The torrefied solid obtained was characterized by the ultimate and elemental analysis, HHV, and FTIR, to elucidate some differences in the decomposition process of the main functional groups.

### *6.2.4. Kinetics*

For TGA tests, the kinetic parameters were obtained according to fitting model method, which consists in adjusting a mathematical model to experimental data from an objective function. this function minimizes the expression shown in equation (6-1).

$$F = \sum_i \left( \left( \frac{M_t}{M_0} \right)_{\exp,i} - \left( \frac{M_t}{M_0} \right)_{theor,i} \right)^2 \tag{6-1}$$

The kinetic model selected to be fitted to the experimental data is that proposed by Di Blasi et al. [67] is presented in Figure 6-3.

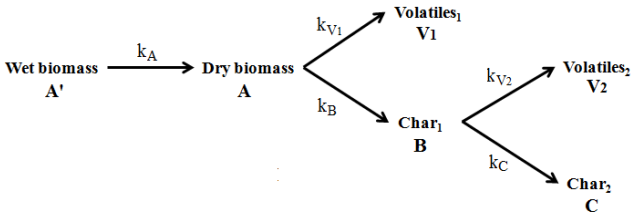


Figure 6-3. Kinetic model used in the biomass torrefaction model.

In this kinetic model, the torrefaction process is described starting from a wet biomass and later, a decomposition process of two stages, starting from a dry biomass. According to the previous model, the mass of each of the species can be expressed as follows:

$$\frac{d[A']}{dt} = -k_A[A'] \tag{6-2}$$

$$\frac{d[A]}{dt} = k_A[A'] - \left(k_B + k_{v_1}\right)[A] \tag{6-3}$$

$$\frac{d[B]}{dt} = k_B[A] - \left(k_C + k_{v_2}\right)[B] \tag{6-4}$$

$$\frac{d[C]}{dt} = k_C[B] \tag{6-5}$$

In this kinetic model, biomass is considered composed of organic and inorganic materials, and kinetic values were obtained from the biomass without any kind of extraction. This means that catalytic effects in relation with ash or with some other compound formed as acids, are all captured in these kinetic values. According with this, final char is composed of devolatilized organic material and inorganic material equal to that in the initial biomass, because it remained unchanged throughout the process. All kinetic constants from Figure 6-3, are the generation/destruction rate of different phases and are defined by the Arrhenius equation (eq. (6-6)).

$$k_i = A_i exp\left(-E_i/RT\right) \tag{6-6}$$

As shown in Figure 6-3, torrefaction process includes a drying process of a wet biomass with low moisture content. Moisture is removed in the first drying step and a completely dry biomass is obtained by reaction $k_{A'}$. Once the temperature increases, biomass devolatilization starts through $k_{v1}$ and $k_B$ reactions and produce condensable and non-condensable volatiles and a solid respectively. After that, a secondary step is present through $k_{v2}$ and $k_C$ where more volatiles and a new solid are yielded.

For the fitting of kinetic model to the experimental data, reactions will be considered only from dry biomass, that is from the reactions $K_{v1}$ and $K_B$ because the data will be taken from 150°C, as different authors have used in previous works [68–72].

The kinetic model used in this work does not differentiate between polymeric constituents (cellulose, hemicellulose, and lignin), but from experimental evidence found in the literature [73–76], it is possible to determine the decomposition of each polymer through DTG graphics of the process. Below 250°C, the decomposition rate of hemicellulose is high and dominates the torrefaction process, but above 250°C, cellulose and lignin also start decomposition but to a lesser extent.

## 6.3. Results and discussion

### *6.3.1. Torrefaction in TGA*

As mentioned in previous sections, experimental tests in TGA were carried out in order to obtain information about the kinetic parameters in primary reactions of sugarcane bagasse in the range of torrefaction temperatures. These tests were performed with particles with a diameter of 0.075 mm and under conditions of kinetic control. These tests were performed in two stages, the first stage a heating ramp is performed at 10°C/min from room temperature to 105°C with for 15 minutes where the material is completely dried. The biomass is then heated to 10°C/min to process temperature in the range of (220-300°C) and held during 60 minutes in this temperature. Four temperatures were tested, 220, 250, 280 and 300°C. Results of experimental tests and temperature profiles are shown in Figure 6-4.

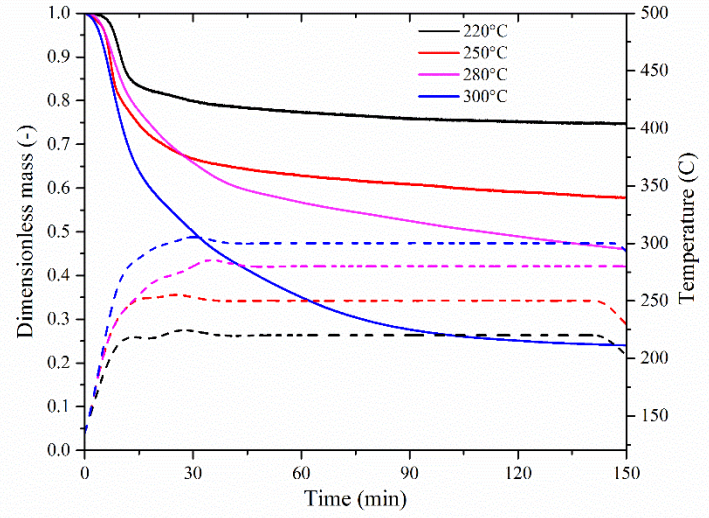


Figure 6-4. Mass and temperature for torrefaction test in TGA

From results obtained in TGA tests, the kinetic parameters for the kinetic model presented in Figure 6-3 were obtained. Non-isothermal and isothermal periods were fitted in order to obtain all the information about the process. The kinetic model adjust was done using the fitting model methodology, in which the theoretical mass presented in equation (6-7) [77], is adjusted to the experimental mass minimizing the objective function presented in equation (6-1) and solved in MATLAB.

$$\frac{M_t}{M_0} = \left(1 + \left[\frac{k_1K_1 - k_1k_2}{K_1(K_2 - K_1)}\right]\right)e^{-K_1t} + \left[\frac{-k_1K_2 + k_1k_2}{K_2(K_2 - K_1)}\right]e^{-K_2t} + \frac{k_1k_2}{K_1K_2}, \quad (6\text{-}7)$$

Where

$$K_1 = k_1 + k_{v1} \tag{6-8}$$

$$K_2 = k_2 + k_{v2} \tag{6-9}$$

As was said before, kinetic study starts from the dry biomass, taking its initial mass at a temperature of 150°C. Accordingly, differential equations (6-3)-(6-5) were solved without incorporating the drying of the biomass. Through chain rule, the expressions for the dynamic process were obtained considering the heating rate. Some expressions for the theoretical mass for each phase can be observed in previous works [21,76]. According to Prins et al. [76], below 250°C, biomass decomposition does not exhibit a two-stage behavior, and only linear decomposition can be observed. The two-stage model must therefore be applied for torrefaction temperatures above 250°C. The adjustment performed for the non-isothermal process is presented in Figure 6-5(a) for each of the evaluated temperatures and for a heating rate of 10°C/min.

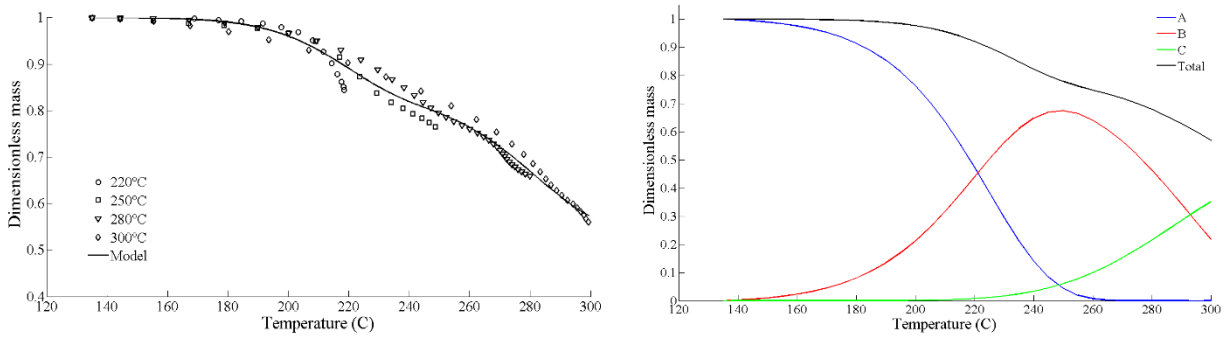


(a) (b)

Figure 6-5. Fitting of kinetic model for the heating period in TGA (a), and mass of each phase during non-isothermal process (b).

With the obtained kinetic parameters from the dynamic adjustment, it is possible to obtain the evolution of each intermediate phase as a function of temperature, as is shown in Figure 6-5(b). With these dynamic parameters and the fractions of each component at the end of this period, the process of obtaining the kinetic parameters for the isothermal period is started, and again the objective function is minimized in MATLAB. The results of the obtained adjustment are presented in Figure 6-6.

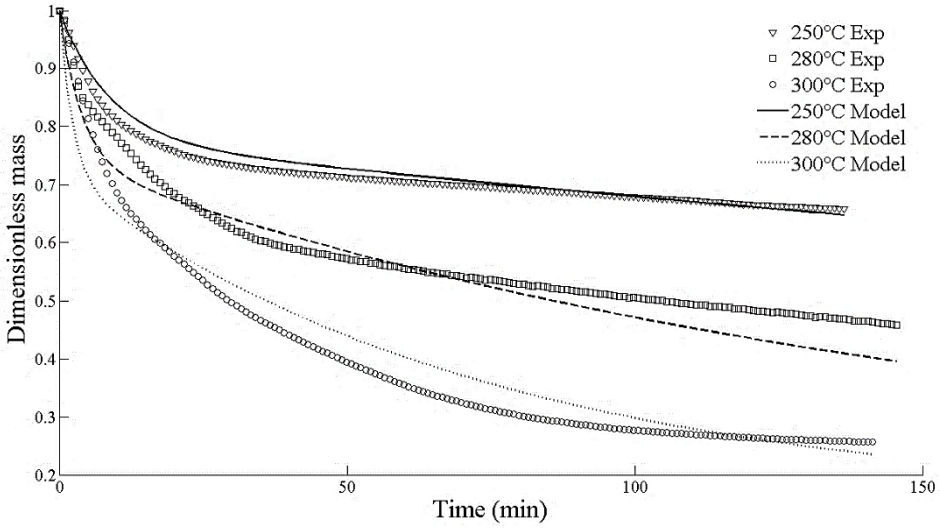


Figure 6-6. Fitting of kinetic model with experimental data in TGA.

From the fitting performed for the isothermal process with the objective function, the values of the kinetic parameters presented in equations (6-10)-(6-13) were obtained.

$$k_B = 2.141 x 10^4 \exp\left(\frac{-61691}{RT}\right) \quad (6\text{-}10)$$

$$k_{v_1} = 2.88 x 10^9 \exp\left(\frac{-115455}{RT}\right) \quad (6\text{-}11)$$

$$k_C = 1.759 x 10^3 \exp\left(\frac{-62698}{RT}\right) \quad (6\text{-}12)$$

$$k_{v_2} = 3.518 x 10^6 \exp\left(\frac{-98115}{RT}\right) \quad (6\text{-}13)$$

Where $k$ is the kinetic rate ($s^{-1}$), $T$ is the temperature (K), and $R$ is the constant of gases ($J\ mol^{-1}\ k^{-1}$).

### *6.3.2. Experimental tests for different particle sizes*

As explained in previous sections, the torrefaction tests were carried out with particles of 2.5x2.5x5cm of sugarcane bagasse conformed with 3 different materials, fine, large and bagasse without crushing. In these tests, four different temperatures were evaluated 220, 250, 280 and 300°C with a single heating rate of 10°C/min. During these experimental tests, the material was inserted into the cold reactor and then heated from room temperature with two heating programs. In the first, the material is dried at 105°C with a residence time of 3 hours. In the second program, the biomass is heated from 105°C to process temperature for about 5 hours. A thermocouple was located in the center of the material to monitor its temperature during the process. The mass was also monitored during the process and this information was stored in the processing unit. The results of the loss of mass and temperature of the particles are presented in Figure 6-7.

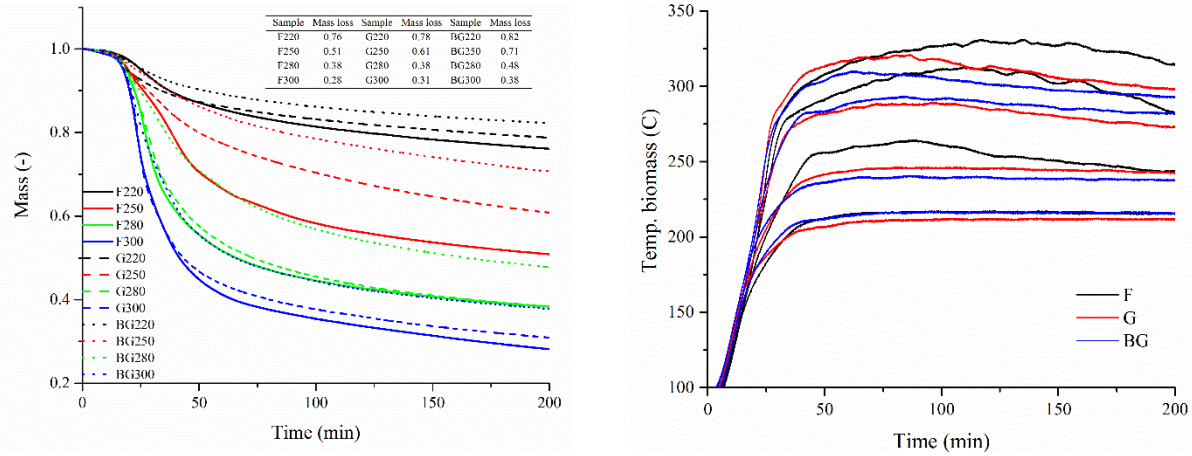


(a) (b)

Figure 6-7. Mass loss (a) and temperature in central point (b) for all particle sizes during torrefaction tests.

Figure 6-7(a) shows the mass loss for each particle, starting at 135°C, which include heating from this temperature and the isothermal period at process temperature. The mass loss of the fine particles is the lowest, and in turn, the mass loss of the whole bagasse is the smallest. This could indicate that particle size has a considerable impact over the decomposition of the material, maybe through some retention effects of yielded volatiles. This generated restriction can be highly related to the internal structure of the material, because with larger particle sizes, the cellular structures have less destruction, and so, greater restriction in the exit of yielded volatiles. This, in turn, could lead to greater internal pressures in the material, raising boiling points of molten phases, which, according to some authors [23,78], could favor secondary reactions to solids through repolymerization, and dehydration.

Figure 6-7(b) shows the core temperature of the particle during the process. During the heating period, it can be observed that the core particle is heated at the same speed, indicating that the average conductivity does not have a great impact when the material is changed. In addition, an exothermic behavior in fine particles can be seen, and the increase in temperature (overshoot) in its core is greater than others. This increase occurs above 250°C, which could indicate a considerable start of secondary reactions. In addition, it is observed that when the temperature increases, this overshoot in temperature is maintained for a longer time. At 250 ° C, the core of the particle reaches values of approximately 264°C, 15°C of overshoot, but around 100 minutes the temperature decreases. For the process at 280°C, the core reaches a temperature of approximately 311°C, 31°C of overshoot, but decreases from 125 minutes. For the case of 300°C, the maximum temperature is 331°C, also 31°C of overshoot, and is reduced only to the end of the process in approximately 150 minutes. This might suggest that at higher temperatures, more solid takes place in the secondary char formation.

These excesses of temperature have been commonly observed by different authors in their works [8,9,11,22,79–83] when they have performed torrefaction tests with big particles and measured the temperature of the material constantly during the process. These overshooting in temperature becomes in disadvantages in large particles as they generate heterogeneous structures due to differences in the thermal conditions in the solid.

During torrefaction of sugarcane bagasse particles, condensable and non-condensable volatiles were divided through the condensation unit of the custom designed reactor, which works at -12°C, and non-condensable yielded volatiles were characterized by gas chromatography (GC). Sampling of these gases started when the reactor temperature reached 150°C, and from this moment a sampling was performed every 5 minutes during the heating period and every 10 minutes for the isothermal process. The evolution of main permanent gases for all particle sizes evaluated is shown in Figure 6-8 for a temperature of 300°C.

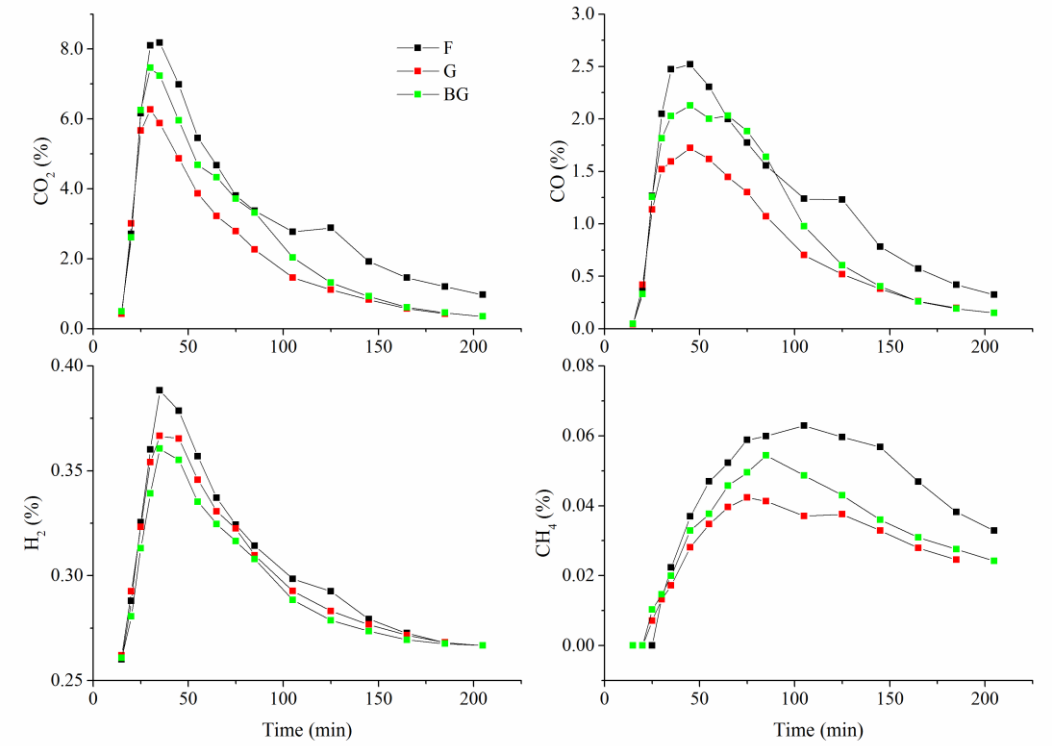


Figure 6-8. Profiles of species in non-condensable volatiles for all particles during torrefaction test at 300°C.

In this figure, you can see that the species $CO_2$ and CO have predominant production. This was expected because in the range of torrefaction temperatures, the decomposition of hemicellulose and amorphous cellulose are strong and generate these two species when decarboxylation reactions of acid groups attached to the polymer chains occur. In addition to these species, small amounts of $CH_4$ and $H_2$ were detected. Some authors have performed similar tests and have not reported these compounds on their detected volatiles [24,84–88], perhaps because of very low concentrations. These species are indicative of lignin reactions, and are generally found in higher concentrations at higher temperatures [88]. Lignin start its decomposition at low temperature, but becomes considerable at temperatures around 350-400°C [88,89]. The recorded concentrations of these two species reach about 2% of the total gas volume at higher temperatures (Figure 6-9(a)).

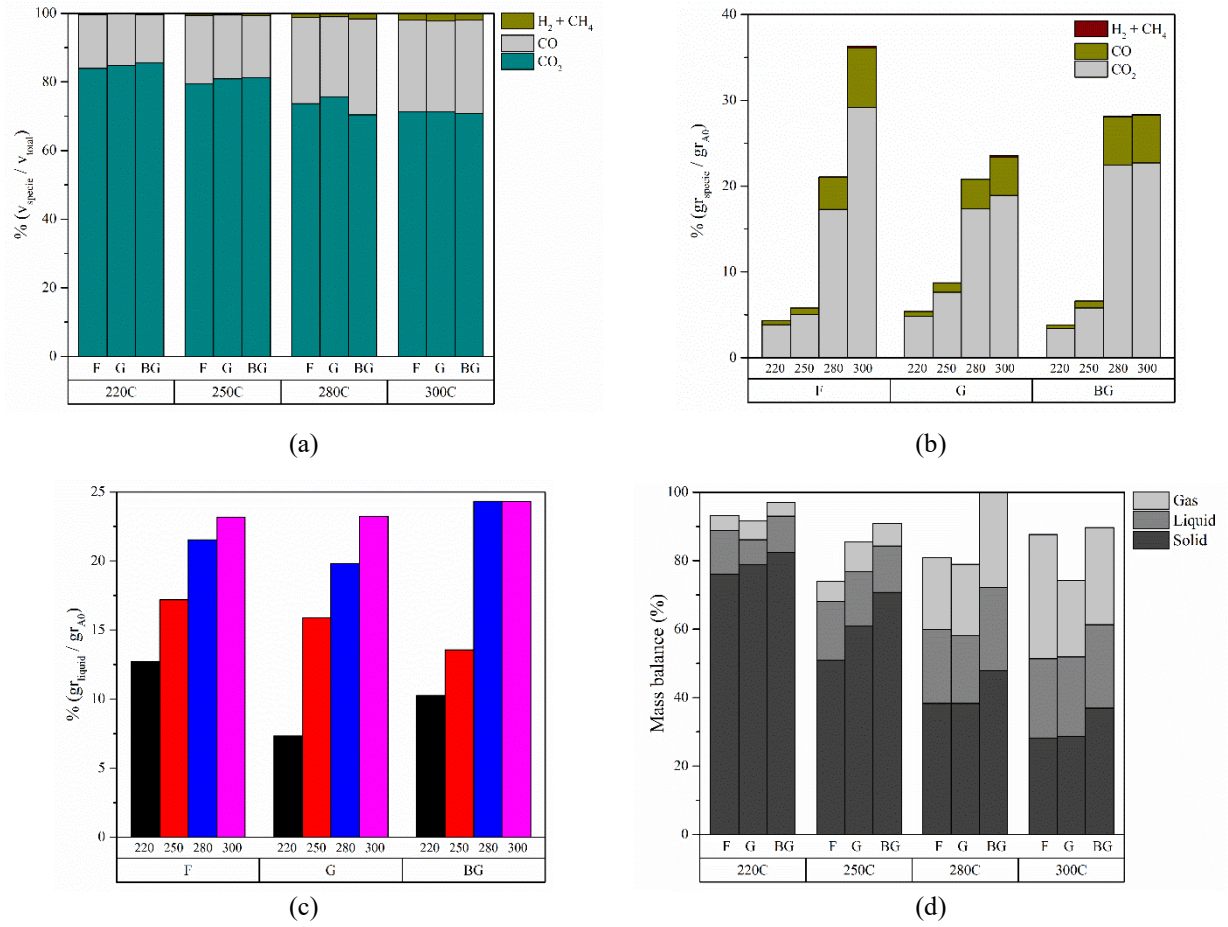


Figure 6-9. Species inside non-condensable gases phase (a), percentage of each species from initial biomass (b), percentage of final liquid from initial biomass (c), and mass balances for torrefaction products (d).

Figure 6-9(a) shows the distribution of the species detected in the gases, and the dominance of $CO_2$ and CO is clear. The proportion of $CO_2$ in the gas in the tests performed remains almost constant ranging between approximately 70-80% and 20-30% for CO.

Figure 6-9(b) shows the percentage of mass of each species based on the initial mass of raw material. This figure clearly shows the difference in decomposition of each material when the process temperature increases. Below 250°C, the differences are minimal in gas production for all particles, being about 4% for CO and 7% for $CO_2$. Differences become important when the temperature increases, the fine particles produce more gases due to the ease escape of the volatiles from its structure and the greater temperature inside (Figure 6-7(b)). The large particles and the complete bagasse on the other hand, strongly increase their decomposition when the temperature exceeds 250°C, but does not undergo great changes between 280 and 300°C because its gas yield is considerably similar.

Figure 6-9(c) shows the percentage of mass liquid captured at the end of each process. In contrast to the previous figure, the behavior of all evaluated particles is similar. For fine and large particles, the formation of liquids always increases with temperature, up to 23% of the initial mass of the

material. For the whole bagasse, a higher formation of this liquid was obtained, but for temperatures of 280 and 300°C the amounts are similar, in agreement with the yielded gases.

Figure 6-9(d) shows the final mass balances of products in each torrefaction test performed. Most of the mass balances performed are far from 100%, which was to be expected in this type of tests. Some reasons for this could be that the generated volatiles condense in the inner walls of the reactor and in the stainless-steel pipes that directing them towards the condenser, which was experimentally evidenced by the presence of a solid adhered to the reactor cover. This cover and ducts are at lower temperature than the center of the reactor during process. Although the reactor leakages were evaluated and sealed before starting the tests, the arising of some of them due to deterioration of the rubber seal of the cover is not discarded. This rubber seal was replaced every 4 tests. In addition, the experimental errors in all sampling measurements of products will always be unavoidable.

An analysis of species in the condensable volatiles was performed by means of GC-MS. In this analysis, the water, formic acid, acetic acid, furan, phenol, 5HMF, 5M-2F species were detected and the results are presented in Figure 6-10(a) and (b). Formic acid, followed by water and then acetic acid were the predominant compounds in the condensable volatiles, indicating an evident dehydration of the polymeric structure. The behavior presented by acetic acid was like reported in the literature [90–92], increasing with temperature since acetoxy acid groups break more easily. The trend of water also behaves similarly with the increase in temperature, as the dehydration reactions intensify. For the case of formic acid, trends similar to those presented in the literature [90–92] were obtained, with the particular result of being found in greater quantity than the water in the condensates, which had already been found by Patwardhan et al. [90] in a previous work.

As the particle size increases, the acetic acid and water yields remain almost similar, but the formic acid decrease as the particle size increases. This generation of formic acid comes from hemicellulose and to a lesser extent from cellulose [84,86,93,92]. Formic acid decomposes thermally and yields $H_2$, which could justify its decrease since the amount of H2 is increased as can be verified in the formation of this compound in the permanent gas. Patwardhan et al. [90] stated that the increase in the light acid groups as formic acid could be linked to decreases in the formation of phenols, 5M-2F and 5HMF, since the latter decomposes to form it. This behavior was evidenced in fine particles from 280°C to 300°C, when 5HMF was reduced and formic acid was increased. For large particles and the whole bagasse, the formic acid showed a decrease while the 5HMF showed a slight increase in the same temperatures. The phenol in turn is a product of the decomposition of lignin, and as expected was increased when the temperature also did.

The tendency in the production of the other species for all evaluated particles was similar. The production of acetic acid was very constant for all particles, while the formic acid generation was higher for the fine particles with 14.3%, followed by the large particles with 11.5% and the whole bagasse with 11%. This maximum value was reached in the fine particles at the highest temperature while for the others it was reached at 280°C and then decreased at 300°C. An important detail was the non-detection of LVG, despite having been considered in the calibration for its characterization. It is important to remember that the particle sizes evaluated are large, as was the reactor, which

clearly indicates that this compound had the appropriate conditions to decompose, dehydrate and form gaseous species such as $CO_2$ and CO and some monomers.

Figure 6-10(c) shows the fraction of condensable volatiles that was not characterized in GC-MS. For liquids obtained at low temperatures there is a greater fraction that could not be characterized with the selected species. This indicates that there is a greater formation of different species than those quantified for torrefaction at low temperatures. One of the species that may have been produced and not quantified in this study was methanol since it was used for the dilution of the condensates and thus not quantified. Another species that could be formed and not quantified was formaldehyde, since it is highly volatile with a boiling point of -19°C, so it is very likely that it has not been condensed in our condensation unit, and continued in the gaseous stream, and neither detected in the CG. It is noteworthy that as the particle size increases, the percentage of uncharacterized increases, indicating the generation of more species not considered in this work for quantification. In conclusion, as the large number of undetected species are at low temperatures, they could come from the decomposition of hemicellulose.

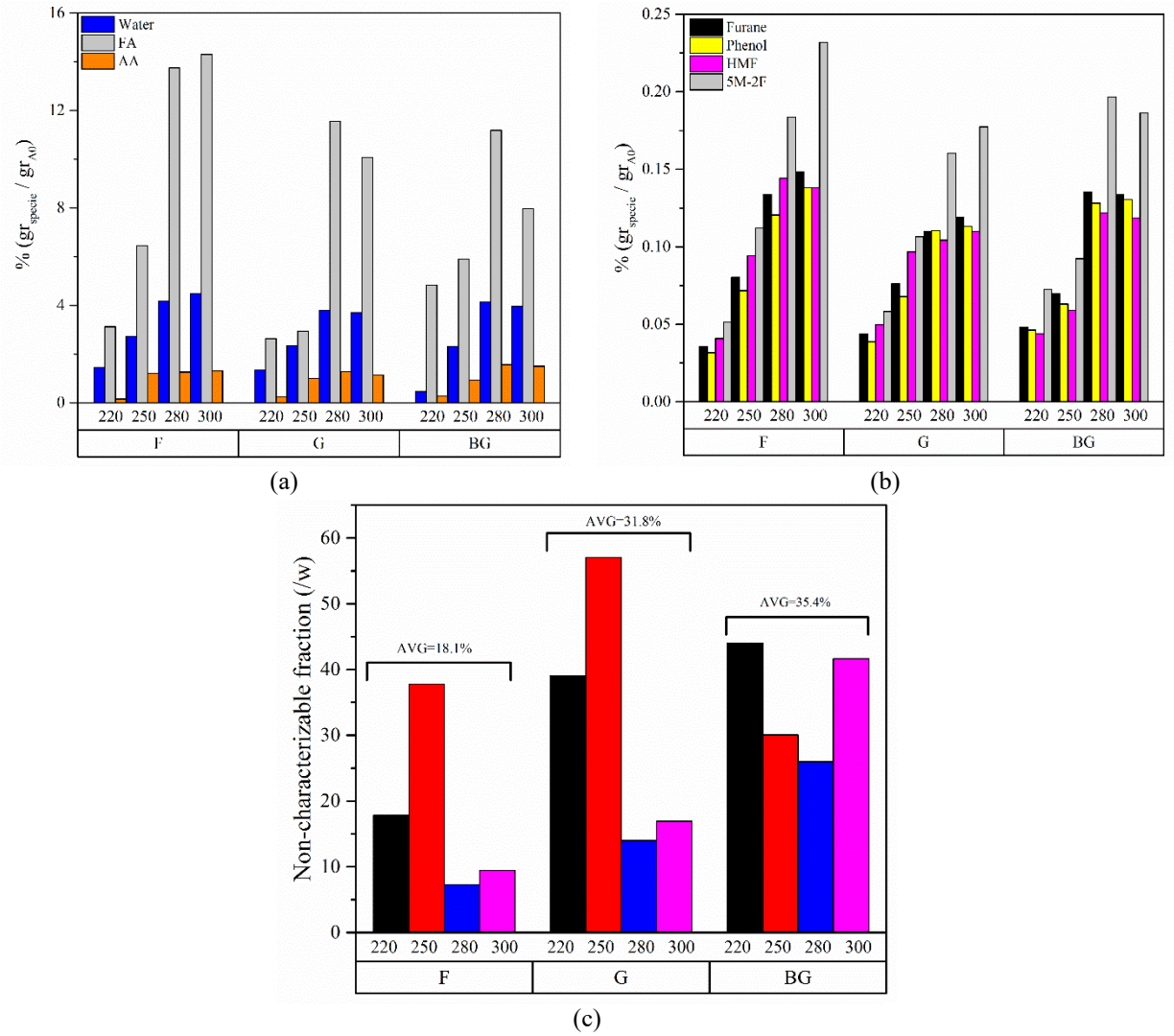


Figure 6-10. Mass of characterized species by GC-MS (a) and (b), and non-characterized fraction in the liquid (c).

The yielded char in each test was characterized by FTIR and results are shown Figure 6-11. In addition, Table 3-2 shown in Chapter 3 the information about main groups that can be identified by FTIR. This table was constructed for each polymer in the biomass. Clear concordances can be observed in shown results when are contrasted with productions of volatiles of each sample.

In these figures, you can show the spectrum of raw and torrefied biomasses. Similar behavior was presented in the particle formed with fine material and that presented in Figure 3-4 for the process developed with small sample in kinetic control in TGA. A very small difference can be observed in the peaks between 2850-3000cm$^{-1}$ since in the large particle a remnant of these compounds contrary to torrefied material in TGA. Some important region in this figure are between 2850-3000cm$^{-1}$ and 1200-1300cm$^{-1}$, where aliphatic hydrocarbons such as alkanes and alkenes, and where C-C and C-O stretching in aromatics are located respectively. The peaks at 1600cm$^{-1}$ and 1712 cm$^{-1}$ were assigned to C=O and COOH/C=O aromatic stretching, both from lignin. These bands showed great intensity in samples, which are characterizations of highly condensed aromatic structure in char [94]. The width and intensity of the bands between 1000-1100cm$^{-1}$ is dependent on presence of any sugars in the sample, while the bands for the hydroxyl group above 3000cm$^{-1}$ are due to alcoholic or phenolic components [95]. Additional bands observed between 700-900cm$^{-1}$ are characteristics of aromatic C-H out-of-plane bending vibrations. According with Yan et al. [96], the signal of peaks between 1400 and 1600 cm$^{-1}$ is attributed to complicated lignin existed but became weak as temperature increased, which implied that lignin was not completely decomposed and some fragrant and intermediate structure from lignin remained in torrefied biomass.

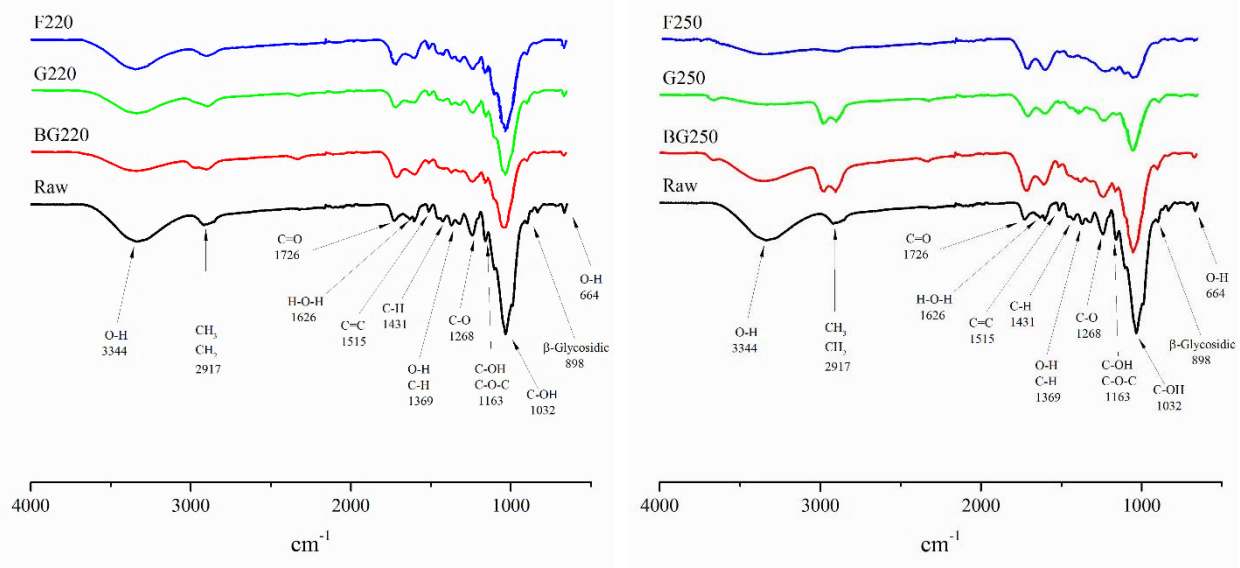

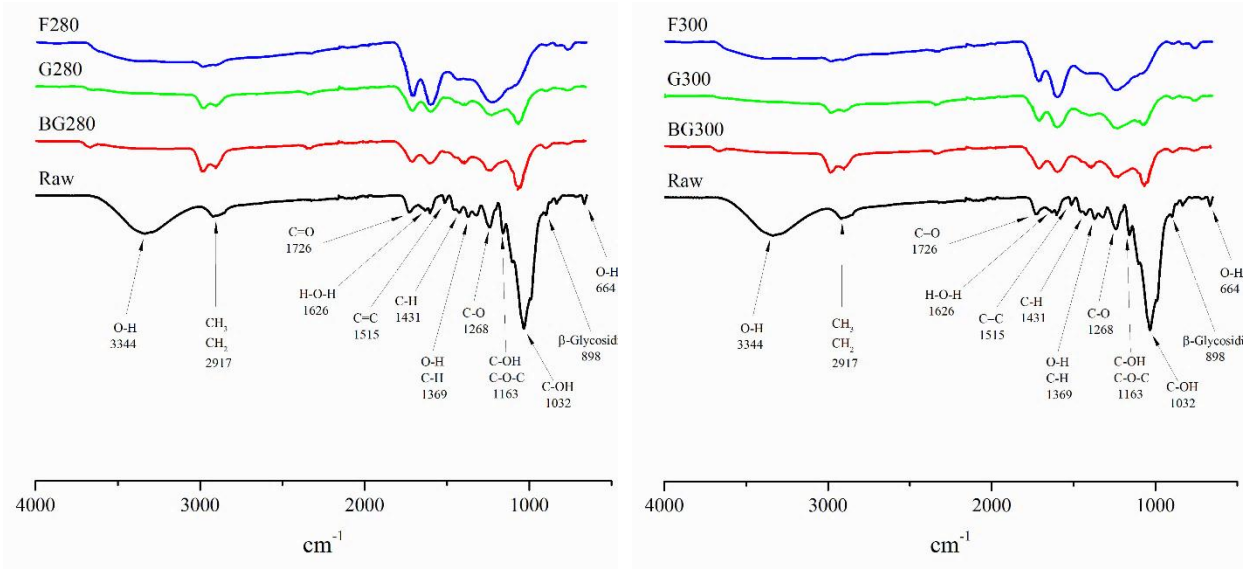


Figure 6-11. FTIR spectrum for torrefied biomass with different particle sizes.

In a previous work, Zheng et al. [63], detected the peak in 1160cm$^{-1}$ because of C–O–C vibration, could be attributed to the formation of cross-linking during cellulose torrefaction. Cross-linking of cellulose is probably a bimolecular nucleophilic substitution reaction in which a hydroxyl group of one cellulose chain is protonated first, then the protonated hydroxyl group is attacked by a second cellulose chain as a nucleophile to form ethers and water. In our work, this peak at 1160cm$^{-1}$ was not clearly identified. A peak was identified by Sharma et al. [95] above 3600cm$^{-1}$ which was attributed to free OH stretching vibrations to phenols, grew slowly with temperature, which could be due to increased carbonization of the sample. However, the intensity of the free OH stretch was much smaller than that of the bonded OH stretch

According to the afore mentioned peaks, the aromatic groups are mostly concentrated in the particle formed with the fine material, since the peak at 1600, 1712 and 12668cm$^{-1}$ are predominant in this material. In this way, a material with higher aromaticity can be obtained with fine particles. For the case of the particles formed with the whole bagasse, an appearance of phenolic groups according to the peak above 3600cm$^{-1}$ is detected. As mentioned above, this may be indicative of an increase in carbonization of the sample. Another additional peak for the larger samples, presented after torrefaction was due to phosphorus acids and esters P-H bond between 2340-2377cm$^{-1}$ according to Khare et al. [97] and also gives a sharp absorption peak which implies the presence of ketone group -(C=O)- [98].

For 220°C you can note for the large material and complete bagasse, the appearance of different bands between 2850cm$^{-1}$ and 2950cm$^{-1}$. The rest of the spectrum remains very similar. These same bands become more intense as the torrefaction temperature increases, and at 250°C these bands increase their area and become more intense. It can also be observed that for the whole bagasse, the band at 1032cm$^{-1}$ remains almost constant unlike other materials, in which its decrease is observed. As the temperature increases to 280 and 300°C, it can be clearly seen how, in the fine particles, the band disappeared completely in 1032 and 3344cm$^{-1}$, because of dehydroxylation and demethylation reactions when the methoxy and hydroxy groups were released of polymers chains.

The same occurs with the large material, but with the whole bagasse a remnant of this compounds are yet in the material.

## 6.4. Conclusions

A torrefaction study of sugarcane bagasse with different particle sizes was carried out in TGA and in a custom thermo-gravimetric reactor specially designed to torrefier large particles. In TGA were torrefied the particles with 0.075mm under kinetic control, and in the designed and built reactor were torrefied the particles of 2.5x2.5x5cm conformed with fine, big and and bagasse without crushing. The products from torrefaction were analyzed and characterized in order to find differences in devolatilization processes as a consequence of the used materials.

From characterizations, a more exothermic behavior could be evidenced in the particle of fine material, which causes a greater generation of volatiles (condensable and non-condensable), and in turn, a greater devolatilization in the solid through reactions of repolimerización, dehydration, and charring. This was evidenced in its mainly aromatic structure unlike the other particles studied. For particles formed with big material, it was evidenced a smaller decomposition in the material, generating less volatiles and smaller mass loss. This was evidenced in the FTIR results where a lower decomposition of the polymers of the material was observed.

## Acknowledgments

The authors wish to thank the Colombian Administrative Department of Science, Technology and Innovation (COLCIENCIAS) (Departamento Administrativo de Ciencia, Tecnología e Innovacion) for financial support.

D.A. Granados would like to thank COLCIENCIAS for the Ph.D scholarship.

## References

[1] Chen WH, Zhuang YQ, Liu SH, Juang TT, Tsai CM. Product characteristics from the torrefaction of oil palm fiber pellets in inert and oxidative atmospheres. Bioresour Technol 2016;199:367–74. doi:10.1016/j.biortech.2015.08.066.

[2] Sellappah V, Uemura Y, Hassan S, Sulaiman MH, Lam MK. Torrefaction of Empty Fruit Bunch in the Presence of Combustion Gas. Procedia Eng 2016;148:750–7. doi:10.1016/j.proeng.2016.06.608.

[3] Bach QV, Trinh TN, Tran KQ, Thi NBD. Pyrolysis characteristics and kinetics of biomass torrefied in various atmospheres. Energy Convers Manag 2016. doi:10.1016/j.enconman.2016.04.097.

[4] Rodriguez Alonso E, Dupont C, Heux L, Da Silva Perez D, Commandre JM, Gourdon C. Study of solid chemical evolution in torrefaction of different biomasses through solid-state 13C cross-polarization/magic angle spinning NMR (nuclear magnetic resonance) and TGA (thermogravimetric analysis). Energy 2016;97:381–90. doi:10.1016/j.energy.2015.12.120.

[5] Uemura Y, Saadon S, Osman N, Mansor N, Tanoue KI. Torrefaction of oil palm kernel shell in the presence of oxygen and carbon dioxide. Fuel 2015;144:171–9.

doi:10.1016/j.fuel.2014.12.050.

[6] Li M-F, Li X, Bian J, Xu J-K, Yang S, Sun R-C. Influence of temperature on bamboo torrefaction under carbon dioxide atmosphere. Ind Crops Prod 2015;76:149–57. doi:10.1016/j.indcrop.2015.04.060.

[7] Soponpongpipat N, Sae-Ueng U. The effect of biomass bulk arrangements on the decomposition pathways in the torrefaction process. Renew Energy 2015;81:679–84. doi:10.1016/j.renene.2015.03.060.

[8] Basu P, Rao S, Dhungana A. An investigation into the effect of biomass particle size on its torrefaction. Can J Chem Eng 2013;91:466–74. doi:10.1002/cjce.21710.

[9] Granados DA, Chejne F, Basu P. A two dimensional model for torrefaction of large biomass particles. J Anal Appl Pyrolysis 2016;120:1–14. doi:10.1016/j.jaap.2016.02.016.

[10] Jones JM, Bridgeman TG, Darvell LI, Gudka B, Saddawi a., Williams a. Combustion properties of torrefied willow compared with bituminous coals. Fuel Process Technol 2012;101:1–9. doi:10.1016/j.fuproc.2012.03.010.

[11] Pierre F, Almeida G, Brito J, Perré P. Influence of torrefaction on some chemical and energy properties of maritime pine and pedunculate oak. Bioresources 2011;6:1204–18.

[12] Bridgeman TG, Darvell LI, Jones JM, Williams PT, Fahmi R, Bridgwater a. V, et al. Influence of particle size on the analytical and chemical properties of two energy crops. Fuel 2007;86:60–72. doi:10.1016/j.fuel.2006.06.022.

[13] Wang C, Peng J, Li H, Bi XT, Legros R, Lim CJ, et al. Oxidative torrefaction of biomass residues and densification of torrefied sawdust to pellets. Bioresour Technol 2013;127:318–25. doi:10.1016/j.biortech.2012.09.092.

[14] Medic D, Darr M, Shah a., Potter B, Zimmerman J. Effects of torrefaction process parameters on biomass feedstock upgrading. Fuel 2012;91:147–54. doi:10.1016/j.fuel.2011.07.019.

[15] Granados DA, Velásquez HI, Chejne F. Energetic and exergetic evaluation of residual biomass in a torrefaction process. Energy 2014;74:181–9. doi:10.1016/j.energy.2014.05.046.

[16] Granados DA, Basu P, Chejne F, Nhuchhen DR. Detailed Investigation into Torrefaction of Wood in a Two-Stage Inclined Rotary Torrefier. Energy & Fuels 2016:acs.energyfuels.6b02524. doi:10.1021/acs.energyfuels.6b02524.

[17] Broström M, Nordin A, Pommer L, Branca C, Di Blasi C. Influence of torrefaction on the devolatilization and oxidation kinetics of wood. J Anal Appl Pyrolysis 2012;96:100–9. doi:10.1016/j.jaap.2012.03.011.

[18] Dhungana A, Dutta A, Basu P. Torrefaction of non -lignocellulose biomass waste. Can J Chem Eng 2012;90:186–95. doi:10.1002/cjce.20527.

[19] Shang L, Ahrenfeldt J, Holm JK, Sanadi AR, Barsberg S, Thomsen T, et al. Changes of chemical and mechanical behavior of torrefied wheat straw. Biomass and Bioenergy 2012;40:63–70. doi:10.1016/j.biombioe.2012.01.049.

[20] Chen W-H, Lu K-M, Tsai C-M. An experimental analysis on property and structure

variations of agricultural wastes undergoing torrefaction. Appl Energy 2012;100:318–25. doi:10.1016/j.apenergy.2012.05.056.

[21] Shang L, Ahrenfeldt J, Holm JK, Barsberg S, Zhang R, Luo Y, et al. Intrinsic kinetics and devolatilization of wheat straw during torrefaction. J Anal Appl Pyrolysis 2013;100:145–52. doi:10.1016/j.jaap.2012.12.010.

[22] Basu P, Sadhukhan AK, Gupta P, Rao S, Dhungana A, Acharya B. An experimental and theoretical investigation on torrefaction of a large wet wood particle. Bioresour Technol 2014;159:215–22. doi:10.1016/j.biortech.2014.02.105.

[23] Carrier M, Hugo T, Gorgens J, Knoetze H. Comparison of slow and vacuum pyrolysis of sugar cane bagasse. J Anal Appl Pyrolysis 2011;90:18–26. doi:10.1016/j.jaap.2010.10.001.

[24] Peng Y, Wu S. The structural and thermal characteristics of wheat straw hemicellulose. J Anal Appl Pyrolysis 2010;88:134–9. doi:10.1016/j.jaap.2010.03.006.

[25] Zhang S, Dong Q, Zhang L, Xiong Y. Effects of water washing and torrefaction on the pyrolysis behavior and kinetics of rice husk through TGA and Py-GC/MS. Bioresour Technol 2016;199:352–61. doi:10.1016/j.biortech.2015.08.110.

[26] Chen YC, Chen WH, Lin BJ, Chang JS, Ong HC. Impact of torrefaction on the composition, structure and reactivity of a microalga residue. Appl Energy 2016;181:110–9. doi:10.1016/j.apenergy.2016.07.130.

[27] Wilk M, Magdziarz A, Kalemba I. Characterisation of renewable fuels' torrefaction process with different instrumental techniques. Energy 2015;87:259–69. doi:10.1016/j.energy.2015.04.073.

[28] Pushkin SA, Kozlova L V., Makarov AA, Grachev AN, Gorshkova TA. Cell wall components in torrefied softwood and hardwood samples. J Anal Appl Pyrolysis 2015;116:102–13. doi:10.1016/j.jaap.2015.09.020.

[29] Kihedu J. Torrefaction and Combustion of Ligno-Cellulosic Biomass. Energy Procedia 2015;75:162–7. doi:10.1016/j.egypro.2015.07.273.

[30] Ren S, Lei H, Wang L, Bu Q, Chen S, Wu J. Thermal behaviour and kinetic study for woody biomass torrefaction and torrefied biomass pyrolysis by TGA. Biosyst Eng 2013;116:420–6. doi:10.1016/j.biosystemseng.2013.10.003.

[31] Burhenne L, Messmer J, Aicher T, Laborie M-P. The effect of the biomass components lignin, cellulose and hemicellulose on TGA and fixed bed pyrolysis. J Anal Appl Pyrolysis 2013:1–8. doi:10.1016/j.jaap.2013.01.012.

[32] Nhuchhen DR, Basu P. Experimental investigation of mildly pressurized torrefaction in air and nitrogen. Energy and Fuels 2014;28:3110–21. doi:10.1021/ef4022202.

[33] Nhuchhen DR, Basu P, Acharya B. Investigation into overall heat transfer coefficient in indirectly heated rotary torrefier. Int J Heat Mass Transf 2016;102:64–76. doi:10.1016/j.ijheatmasstransfer.2016.06.011.

[34] Nhuchhen DR, Basu P, Acharya B. Torrefaction of poplar in continuous two- stage indirectly heated rotary torrefier. Energy & Fuels 2016;30:1027–38. doi:10.1021/acs.energyfuels.5b02288.

[35] Strandberg M, Olofsson I, Pommer L, Wiklund-Lindström S, Åberg K, Nordin A. Effects of temperature and residence time on continuous torrefaction of spruce wood. Fuel Process Technol 2015;134:387–98. doi:10.1016/j.fuproc.2015.02.021.

[36] Mei Y, Liu R, Yang Q, Yang H, Shao J, Draper C, et al. Torrefaction of cedarwood in a pilot scale rotary kiln and the influence of industrial flue gas. Bioresour Technol 2015;177:355–60. doi:10.1016/j.biortech.2014.10.113.

[37] Piton M, Huchet F, Le Corre O, Le Guen L, Cazacliu B. A coupled thermal-granular model in flights rotary kiln: Industrial validation and process design. Appl Therm Eng 2015;75:1011–21. doi:10.1016/j.applthermaleng.2014.10.052.

[38] Colin B, Dirion J-L, Arlabosse P, Salvador S. Wood chips flow in a rotary kiln: experiments and modeling. Chem Eng Res Des 2015;98:179–87. doi:10.1016/j.cherd.2015.04.017.

[39] Sanginés P, Domínguez MP, Sánchez F, San Miguel G. Slow pyrolysis of olive stones in a rotary kiln: Chemical and energy characterization of solid, gas, and condensable products. J Renew Sustain Energy 2015;7. doi:http://dx.doi.org/10.1063/1.4923442.

[40] Huang Y-F, Sung H-T, Chiueh P-T, Lo S-L. Microwave torrefaction of sewage sludge and leucaena. J Taiwan Inst Chem Eng 2017;70:236–43. doi:10.1016/j.jtice.2016.10.056.

[41] Huang Y-F, Cheng P-H, Chiueh P-T, Lo S-L. Leucaena biochar produced by microwave torrefaction: Fuel properties and energy efficiency. Appl Energy 2017. doi:10.1016/j.apenergy.2017.03.007.

[42] Bach QV, Chen WH, Lin SC, Sheen HK, Chang JS. Wet torrefaction of microalga Chlorella vulgaris ESP-31 with microwave-assisted heating. Energy Convers Manag 2016. doi:10.1016/j.enconman.2016.07.035.

[43] Huang YF, Sung H Te, Chiueh P Te, Lo SL. Co-torrefaction of sewage sludge and leucaena by using microwave heating. Energy 2016;116:1–7. doi:10.1016/j.energy.2016.09.102.

[44] Ren S, Lei H, Wang L, Yadavalli G, Liu Y, Julson J. The integrated process of microwave torrefaction and pyrolysis of corn stover for biofuel production. J Anal Appl Pyrolysis 2014;108:248–53. doi:10.1016/j.jaap.2014.04.008.

[45] Satpathy SK, Tabil LG, Meda V, Naik SN, Prasad R. Torrefaction of wheat and barley straw after microwave heating. Fuel 2014;124:269–78. doi:10.1016/j.fuel.2014.01.102.

[46] Santaniello R, Galgano A, Di Blasi C. Coupling transport phenomena and tar cracking in the modeling of microwave-induced pyrolysis of wood. Fuel 2012;96:355–73. doi:10.1016/j.fuel.2012.01.040.

[47] Lasek JA, Kopczyński M, Janusz M, Iluk A, Zuwała J. Combustion properties of torrefied biomass obtained from flue gas-enhanced reactor. Energy 2017;119:362–8. doi:10.1016/j.energy.2016.12.079.

[48] Valix M, Katyal S, Cheung WH. Combustion of thermochemically torrefied sugar cane bagasse. Bioresour Technol 2017;223:202–9. doi:10.1016/j.biortech.2016.10.053.

[49] Arteaga-Pérez LE, Grandón H, Flores M, Segura C, Kelley SS. Steam torrefaction of Eucalyptus globulus for producing black pellets: A pilot-scale experience. Bioresour Technol 2017;238:194–204. doi:10.1016/j.biortech.2017.04.037.

[50] Bai X, Wang G, Gong C, Yu Y, Liu W, Wang D. Co-pelletizing characteristics of torrefied wheat straw with peanut shell. Bioresour Technol 2017;233:373–81. doi:10.1016/j.biortech.2017.02.091.

[51] Rudolfsson M, Borén E, Pommer L, Nordin A, Lestander TA. Combined effects of torrefaction and pelletization parameters on the quality of pellets produced from torrefied biomass. Appl Energy 2017;191:414–24. doi:10.1016/j.apenergy.2017.01.035.

[52] Chen D, Cen K, Jing X, Gao J, Li C, Ma Z. An approach for upgrading biomass and pyrolysis product quality using a combination of aqueous phase bio-oil washing and torrefaction pretreatment. Bioresour Technol 2017;233:150–8. doi:10.1016/j.biortech.2017.02.120.

[53] Manatura K, Lu JH, Wu KT, Hsu H Te. Exergy analysis on torrefied rice husk pellet in fluidized bed gasification. Appl Therm Eng 2017;111:1016–24. doi:10.1016/j.applthermaleng.2016.09.135.

[54] Chen H, Chen X, Qin Y, Wei J, Liu H. Effect of torrefaction on the properties of rice straw high temperature pyrolysis char: Pore structure, aromaticity and gasification activity. Bioresour Technol 2017;228:241–9. doi:10.1016/j.biortech.2016.12.074.

[55] Gogoi D, Bordoloi N, Goswami R, Narzari R, Saikia R, Sut D, et al. Effect of torrefaction on yield and quality of pyrolytic products of arecanut husk: An agro-processing wastes. Bioresour Technol 2017. doi:10.1016/j.biortech.2017.03.169.

[56] Ku X, Jin H, Lin J. Comparison of gasification performances between raw and torrefied biomasses in an air-blown fluidized-bed gasifier. Chem Eng Sci 2017. doi:10.1016/j.ces.2017.04.050.

[57] Woytiuk K, Campbell W, Gerspacher R, Evitts RW, Phoenix A. The effect of torrefaction on syngas quality metrics from fluidized bed gasification of SRC willow. Renew Energy 2017;101:409–16. doi:10.1016/j.renene.2016.08.071.

[58] Kopczyński M, Lasek JA, Iluk A, Zuwała J. The co-combustion of hard coal with raw and torrefied biomasses (willow (Salix viminalis), olive oil residue and waste wood from furniture manufacturing). Energy 2017:1–10. doi:10.1016/j.energy.2017.04.036.

[59] Colin B, Dirion J-L, Arlabosse P, Salvador S. Quantification of the torrefaction effects on the grindability and the hygroscopicity of wood chips. Fuel 2017;197:232–9. doi:10.1016/j.fuel.2017.02.028.

[60] Granados DA, Basu P, Chejne F. Biomass Torrefaction in a Two-Stage Rotary Reactor: Modeling and Experimental Validation. Energy & Fuels 2017:acs.energyfuels.7b00653. doi:10.1021/acs.energyfuels.7b00653.

[61] Nachenius RW, van de Wardt TA, Ronsse F, Prins W. Torrefaction of pine in a bench-scale screw conveyor reactor. Biomass and Bioenergy 2014;79:96–104. doi:10.1016/j.biombioe.2015.03.027.

[62] Nachenius RW, Van De Wardt TA, Ronsse F, Prins W. Residence time distributions of coarse biomass particles in a screw conveyor reactor. Fuel Process Technol 2015;130:87–95. doi:10.1016/j.fuproc.2014.09.039.

[63] Zheng A, Zhao Z, Chang S, Huang Z, Wang X, He F, et al. Effect of torrefaction on structure and fast pyrolysis behavior of corncobs. Bioresour Technol 2013;128:370–7.

doi:10.1016/j.biortech.2012.10.067.

[64] Hilten RN, Speir R a., Kastner JR, Mani S, Das KC. Effect of torrefaction on bio-oil upgrading over HZSM-5. Part 2: Byproduct formation and catalyst properties and function. Energy and Fuels 2013;27:844–56. doi:10.1021/ef301695c.

[65] Chang S, Zhao Z, Zheng A, He F, Huang Z, Li H. Characterization of products from torrefaction of sprucewood and bagasse in an auger reactor. Energy and Fuels, vol. 26, American Chemical Society; 2012, p. 7009–17. doi:10.1021/ef301048a.

[66] Granados DA, Chejne F, Basu P. A two dimensional model for torrefaction of large biomass particles. J Anal Appl Pyrolysis 2016. doi:10.1016/j.jaap.2016.02.016.

[67] Di Blasi C, Lanzetta M. Intrinsic kinetics of isothermal xylan degradation in inert atmosphere. J Anal Appl Pyrolysis 1997;40–41:287–303. doi:10.1016/S0165-2370(97)00028-4.

[68] Di Blasi C, Branca C. Kinetics of Primary Product Formation from Wood Pyrolysis. Ind Eng Chem Res 2001;40:5547–56. doi:10.1021/ie000997e.

[69] Rogers F., Ohlemiller T. Cellulosic Insulation Material I. Overall Degradation Kinetics and Reaction Heats. Combust Sci Technol 1980;24:129–37.

[70] Thurner F, Mann U. Kinetic Investigation of Wood Pyrolysis. Ind Eng Chem Process Des Dev 1981;20:482–8.

[71] Ward SM, Braslaw J. Experimental weight loss kinetics of wood pyrolysis under vacuum. Combust Flame 1985;61:261–9. doi:10.1016/0010-2180(85)90107-5.

[72] Shafizadeh F, Chin PPS. Thermal Deterioration of Wood. ACS Symp. Ser., Washington: 1977, p. 57–81.

[73] Chen W-H, Kuo P-C. Isothermal torrefaction kinetics of hemicellulose, cellulose, lignin and xylan using thermogravimetric analysis. Energy 2011;36:6451–60. doi:10.1016/j.energy.2011.09.022.

[74] Varhegyi G, Antal J, Szekely T, Szabo P. Kinetics of the thermal decomposition of cellulose, hemicellulose, and sugarcane bagasse. Energy & Fuels 1989;3:329–35.

[75] Peng J, Bi XT, Lim J, Sokhansanj S. Development of Torrefaction Kinetics for British Columbia Softwoods. Int J Chem React Eng 2012;10. doi:10.1515/1542-6580.2878.

[76] Prins MJ, Ptasinski KJ, Janssen FJJ. Torrefaction of wood. Part 1. Weight loss kinetics. J Anal Appl Pyrolysis 2006;77:28–34. doi:10.1016/j.jaap.2006.01.002.

[77] Prins MJ, Ptasinski KJ, Janssen FJJG. Torrefaction of wood. Part 1. Weight loss kinetics. J Anal Appl Pyrolysis 2006;77:28–34. doi:10.1016/j.jaap.2006.01.002.

[78] Carrier M, Hardie AG, Uras Ü, Görgens J, Knoetze J. Production of char from vacuum pyrolysis of South-African sugar cane bagasse and its characterization as activated carbon and biochar. J Anal Appl Pyrolysis 2012;96:24–32. doi:10.1016/j.jaap.2012.02.016.

[79] Nhuchhen DR, Basu P, Acharya B. A Comprehensive Review on Biomass Torrefaction. Int J Renew Energy Biofuels 2014;2014:1–56. doi:10.5171/2014.506376.

[80] Perré P, Rémond R, Turner I. A comprehensive dual-scale wood torrefaction model:

Application to the analysis of thermal run-away in industrial heat treatment processes. Int J Heat Mass Transf 2013;64:838–49. doi:10.1016/j.ijheatmasstransfer.2013.03.066.

[81] Sand U, Sandberg J, Larfeldt J, Bel Fdhila R. Numerical prediction of the transport and pyrolysis in the interior and surrounding of dry and wet wood log. Appl Energy 2008;85:1208–24. doi:10.1016/j.apenergy.2008.03.001.

[82] Bates RB, Ghoniem AF. Modeling kinetics-transport interactions during biomass torrefaction: The effects of temperature, particle size, and moisture content. Fuel 2014;137:216–29. doi:10.1016/j.fuel.2014.07.047.

[83] Shi X, Ronsse F, Pieters JG. Space-time integral method for simplifying the modeling of torrefaction of a centimeter-sized biomass particle. J Anal Appl Pyrolysis 2017;124:486–98. doi:10.1016/j.jaap.2017.02.009.

[84] Nocquet T, Dupont C, Commandre JM, Grateau M, Thiery S, Salvador S. Volatile species release during torrefaction of biomass and its macromolecular constituents: Part 2 - Modeling study. Energy 2014;72:188–94. doi:10.1016/j.energy.2014.05.023.

[85] Nocquet T, Dupont C, Commandre JM, Grateau M, Thiery S, Salvador S. Volatile species release during torrefaction of wood and its macromolecular constituents: Part 1 - Experimental study. Energy 2014;72:180–7. doi:10.1016/j.energy.2014.02.061.

[86] Klinger J, Bar-Ziv E, Shonnard D. Unified kinetic model for torrefaction-pyrolysis. Fuel Process Technol 2015;138:175–83. doi:10.1016/j.fuproc.2015.05.010.

[87] Wang G, Luo Y, Deng J, Kuang J, Zhang Y. Pretreatment of biomass by torrefaction. Chinese Sci Bull 2011;56:1442–8. doi:10.1007/s11434-010-4143-y.

[88] Yang H, Yan R, Chen H, Lee DH, Zheng C. Characteristics of hemicellulose, cellulose and lignin pyrolysis. Fuel 2007;86:1781–8. doi:10.1016/j.fuel.2006.12.013.

[89] Basu P. Biomass Gasification, Pyrolysis and Torrefaction. Elsevier; 2013. doi:10.1016/B978-0-12-396488-5.00004-6.

[90] Patwardhan PR, Dalluge DL, Shanks BH, Brown RC. Distinguishing primary and secondary reactions of cellulose pyrolysis. Bioresour Technol 2011;102:5265–9. doi:10.1016/j.biortech.2011.02.018.

[91] Patwardhan PR, Brown RC, Shanks BH. Product distribution from the fast pyrolysis of hemicellulose. ChemSusChem 2011;4:636–43. doi:10.1002/cssc.201000425.

[92] Shen DK, Gu S, Bridgwater AV. Study on the pyrolytic behaviour of xylan-based hemicellulose using TG–FTIR and Py–GC–FTIR. J Anal Appl Pyrolysis 2010;87:199–206. doi:10.1016/j.jaap.2009.12.001.

[93] Patwardhan PR, Satrio JA, Brown RC, Shanks BH. Influence of inorganic salts on the primary pyrolysis products of cellulose. Bioresour Technol 2010;101:4646–55. doi:10.1016/j.biortech.2010.01.112.

[94] Xue Y, Zhou S, Brown RC, Kelkar A, Bai X. Fast pyrolysis of biomass and waste plastic in a fluidized bed reactor. Fuel 2015;156:40–6. doi:10.1016/j.fuel.2015.04.033.

[95] Sharma RK, Wooten JB, Baliga VL, Lin X, Chan WG, Hajaligol MR. Characterization of chars from pyrolysis of lignin. Fuel 2004;83:1469–82. doi:10.1016/j.fuel.2003.11.015.

[96] Yan W, Perez S, Sheng K. Upgrading fuel quality of moso bamboo via low temperature thermochemical treatments: Dry torrefaction and hydrothermal carbonization. Fuel 2017;196:473–80. doi:10.1016/j.fuel.2017.02.015.

[97] Khare P, Goyal DK. Effect of high and low rank char on soil quality and carbon sequestration. Ecol Eng 2013;52:161–6. doi:10.1016/j.ecoleng.2012.12.101.

[98] Tripathi M, Sahu JN, Ganesan P, Monash P, Dey TK. Effect of microwave frequency on dielectric properties of oil palm shell (OPS) and OPS char synthesized by microwave pyrolysis of OPS. J Anal Appl Pyrolysis 2015;112:306–12. doi:10.1016/j.jaap.2015.01.007.

# Chapter 7. Biomass Torrefaction in a Two-Stage Rotary Reactor: Modeling and Experimental validation

**(Paper published in Energy and Fuels)**


## Abstract

Torrefaction is a thermal pre-treatment process performed in the temperature range between 200-300°C with low heating rates (<20°C/min) in inert environments. A phenomenological model of the torrefaction process in rotary reactor was developed in this work. Mass and energy balances were coupled to a kinetic model, which considers the progressive decomposition of biomass into volatiles and char released simultaneously from the raw biomass. Mathematical expressions for residence time, heat transfer coefficient, and bed height inside the kiln were taken from literature for model calculations. The gaseous phase is composed of a mixture of condensable and non-condensable gases, and the solid phase comprises a mixture of raw and torrefied biomass. The model can predict different output parameters of torrefaction in a rotary continuous torrefier like final amounts of solids and gas yields, temperatures for different operational conditions. Properties for torrefied solid such as volatile matter, fixed carbon and high heating value, can also be predicted by the model through mathematical correlations obtained in a previous experimental work. Results obtained in the model were compared with experimental data and a good agreement was found.


***Keywords:*** Biomass torrefaction, Rotary reactor, 1D model, Kinetic model.

## 7.1. Introduction

Biomass is emerging as a promising energy alternative to fossil fuels due to its abundance, low greenhouse gas emissions and renewable feature. Also, it has acceptable thermal performance. Biomass has, however, several disadvantages such as high moisture content, low density, irregular shape, malleable nature that discourage its use as an energy source. Transportation and handling become difficult for these shortcomings of biomass [1].

Torrefaction is a thermal pre-treatment process that takes place between 200-300°C at low heating rates (<20°C/min) in inert or with low oxygen environments [1]. In this process biomass undergoes mass-energy losses, and polymeric changes that depend on the temperature and residence time of torrefaction. These changes result in a higher energy density, brittle nature requiring low energy for grinding, and hydrophobicity. The hydrophobic property attained increases its resistance to environmental degradation. Additionally, torrefaction of non-homogenous feedstock also provides a product uniform in quality [2–4].

Many experimental research work on torrefaction have been carried out where different kinds of biomass are torrefied under different operational conditions [2,5–13]. These works tried to find operating conditions that produce best final properties of bio-char. Some studies on different types

of reactors have been made [11,14–20]. It shows that torrefaction in rotary reactors enjoys benefits like the ease of control of residence time, biomass mixing, and continuity of the process. Work on rotary reactors is rather limited [7,13,21–29]. Some works found in literature develops the torrefaction process in two steps reactors [13,30]. Nachenius et al [30] develops the torrefaction process with two screw feeders, where drying and initial torrefaction steps are performed in the first screw reactor and then the final steps of torrefaction are performed in the second screw reactor. The reactor studied by Nhuchhen et al. [13] is also a two-step reactor. In that system, drying and torrefaction process are performed separately. There is an additional advantage of the system in two stages like moisture-free volatiles recovery in the second step, making it easy to burn volatiles and make an auto-thermal process. The present work studied a two-step reactor that is inclined.

Information on predictive models of torrefaction is presently limited. Among those available [31–36], some models consider the influence of physical phenomena, such as heat transfer between phases, and global kinetics are used for chemical reaction in decomposition [37–40]. Some models also consider the decomposition of individual components of biomass like hemicellulose, cellulose and lignin [41–44]. Most of these kinetic models, however, do not consider secondary reaction in condensable volatiles generated in the devolatilization process [40,43,45–47]. Models for torrefaction in rotary inclined reactor are even more scarce.

This work developed a phenomenological model for torrefaction in a rotary reactor. It uses a kinetic model developed earlier by Basu et al. [34] considering only primary reactions. Mass and energy balance of phases in the system: solid and gas were developed. Mathematical expressions for biomass residence times, heat transfer coefficient and bed height developed by Nhuchhen et al. [28,29] for the same system were incorporated in the model. In addition, experimental correlations for solid properties such as volatile matter, fixed carbon and high heating value developed in a previous work [48] were included. An important feature of the model is to predict the progress of torrefaction of biomass particles as it travels along the length of rotary reactor. It examines the progressive change in solid conversion, gas yield and temperature for gas and solid along the reactor.

## 7.2. Experimental Methods

### *7.2.1. Materials*

Finely crushed dowels of poplar wood were used in this work. It was sieved to collect particles in size range of (250–500 μm) used for this study. Proximate and ultimate analyses of the samples were conducted, and results are shown in Table 7-1.

### *7.2.2. Torrefaction process*

Experiments are done on a two-step rotary reactor system as shown in Figure 7-1. This system consists of two in-series inclined rotary drums for continuous drying and torrefaction stages of the biomass. Wet biomass enters the first rotary drum of 64 mm in diameter and 610 mm long through a screw feeder placed in the left side of the drum. In this step, only drying process occurs. Water vapors from drying are expelled from a hole at top of the far right end of the drum. The dried biomass comes out of this drum and drop directly into inlet of the next rotary inclined drum which

is 100 mm in diameter and 762 mm in length. This reactor is operated such that the torrefaction process completes in it. Residence times on it are controlled through variation of RPM and tilt angles. The biomass travels along the length of the inclined drum as it torrefies. No inert gas is supplied to either dryer or torrefier.

Table 7-1. Properties of Poplar wood fines (wb–wet basis; db–dry basis; daf–dry ash free basis).

| Biomass size range 0.5 - 1 mm | | | |
|---|---|---|---|
| Proximate analysis (%w/w) | | Ultimate analysis (%w/w) | |
| Moisture (wb) | 5.4 | Carbon (daf) | 45.90 |
| Volatiles (db) | 82.4 | Hydrogen (daf) | 6.1 |
| Fixed carbon (db) | 16.2 | Nitrogen (daf) | 0.4 |
| Ash (db) | 1.4 | Oxygen (daf) | 47.6 |
| HHV (db)(MJ/kg) | 18.3 | | |

The rotary drum does not use any spiral as done in some rotary reactors. It has instead a novel set of axial inserts to facilitate mixing inside the drums. Three flights are axially inserted 120° apart from each other are placed on the inner walls of both dryer and torrefier (Figure 7-1). Both dryer and torrefier rotate inside co-centric fixed cylindrical shells, which are wrapped with electric heaters and then tightly covered with insulation (Calcium-Magnesium-Silicate wool). Thermocouples (K-type), as shown in Figure 7-1, measure surface temperatures of both dryer and torrefier. A screw feeder at one end of the dryer feeds biomass at the desired rate. Fixed cylindrical shells of the reactors comprise of 3 different materials: steel, electrical heaters and finally, external thermal insulation.

Power is supplied to electrical resistance wrapped around the external static steel wall that in turn heat the rotating steel shell (Figure 7-2). There is an air gap between the rotating reactor and the static steel tube. This air is heated by convection and conduction from static heater wall and transfer the heat to the rotary drum. The temperature of both processes (drying and torrefaction), is controlled by a thermocouple in contact with electrical heater. In order to control power supply to each system and to ensure the correct temperature inside the rotating drum in contact with the biomass, the temperature inside rotary drum was measured by another long K-type thermocouple inserted from one end and placed in the same axial position as that of the external thermocouple (Figure 7-1). This temperature is monitored until the desired stable temperature is reached, and then the experiment is started. This ensures a correct temperature for the process. External insulation on the stationery drum reduces heat loss from the electrical heaters to the environment.

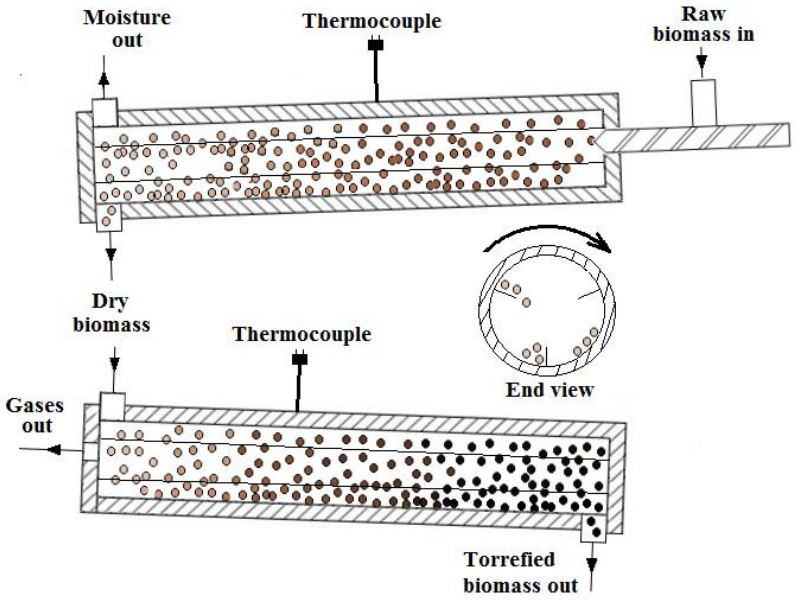


Figure 7-1. Schematic of the rotary dryer and torrefier.

At the end of the torrefaction process, the torrefied biomass was collected in a container that prevents air infiltration to the system and thereby consequent ignition of the torrefied product. More details about this two-step rotary reactor is given elsewhere [49].

### *7.2.3. Experimental design*

The operating condition of the dryer is generally held constant at 3 rpm and 2° inclination of the reactor because with these parameters it was possible to obtain biomass dried with a moisture content less than 0.5%. The other operating conditions of the torrefier reactor were, however, varied.

Poplar wood was fed into the system with a screw conveyor at the rate of 4.2 g/min. Before beginning the tests, nitrogen was supplied to flush out any oxygen out of the system and thereby avoid any burning of dried biomass when it starts to fall out of the torrefier. The flow of nitrogen was stopped before start of the process as gas products of the process provided the required inert environment required torrefaction in this system.

Approximately 1.0 kg of biomass was fed to the system. All solids in the system was collected and weighed at the end of the process in order to determine the mass loss during the process. Though bulk of the tests was for a fixed rpm and tilt angle, experiments were conducted in the torrefier with two different rotational speeds of the reactor (5 and 7 rpm), three tilt angles (1°,2°, and 3°) and three temperatures (260, 280, and 300 °C). Table 7-2 shows the residence times for operational conditions evaluated in the present work.

The tilt angle in the torrefier was measured using a digital level with an accuracy of 0.1°. With the above operational conditions, the residence time of biomass in the torrefier reactor ranges between 5.2 and 16.4 minutes. For the dryer, the residence time is around 18 minutes. Thus, the biomass

has a total residence time in the system of around 23.2 to 34.4 minutes. Each test will be referred to as TXXX-YY, where XXX refers to the process temperature and YY to residence time.

Table 7-2. Residence times for different operational conditions.

| RPM | Tilt angle | Mean residence time (min) |
|---|---|---|
| | 1 | 16.4 |
| | 2 | 9.6 |
| | 3 | 7.0 |
| | 1 | 11.0 |
| | 2 | 6.6 |
| | 3 | 5.2 |

The temperature of the biomass, while it is being torrefied inside the rotary torrefier, was measured by a novel probe with one thermocouple at its end which measures the temperature of biomass [48]. The device can record the solid temperature and collect sample at a specified position inside the rotating torrefier. To prevent additional heating of the thermocouple from gases and kiln walls, a protection was provided through of the capsule in which the biomass is housed. Thus, only the contact with the biomass heated the thermocouple. In this capsule, the sample of biomass being torrefied is collected and the temperature of the sample in contact with the thermocouple is recorded. The sample is withdrawn from the reactor by rotating the probe 180°, and new biomass is then collected in the same position. This procedure is repeated until the temperature measured by the thermocouple showed no major variations. This procedure is repeated many times to measure temperatures and collect samples from different points inside the torrefier.

## 7.3. Model

The model is a one-dimensional simulation of the torrefaction process in a two-stage rotary reactor. Inside the rotary reactor three clearly distinguishable phases can be observed: gas phase, generated by devolatilization of biomass being torrefied, a solid phase located at the bottom forming a bed, and a second solid phase generated by solid particles that fall from longitudinal reactor flights (Figure 7-2).

The first two phases of gas and solid can be modeled as continuous phases, but the third phase is clearly a discrete phase due to scattering and raining down of particles generated by the flights. First two continuous phases are commonly found in models of traditional rotary reactors [22,50–54], but the third phase, is only present in rotary reactors with mixing flights [55,56].

Heat transfer between rotating and fixed reactor walls is shown in Figure 7-2. Conduction is the dominant heat transfer mode, except for the radiation transfer occurring between rotary and fixed steel walls, but some conduction and convection occurs. Energy transfer between phases present inside the reactor (gas, solid, and walls) is essentially the same as that in conventional reactors. Additional energy transfer between biomass falling from the flights and gas phase and reactor walls take place by convection and radiation, respectively. This additional heating, though of a small

fraction of biomass, could make important contribution to the energy transfer to the biomass inside the reactor [13,55,56].

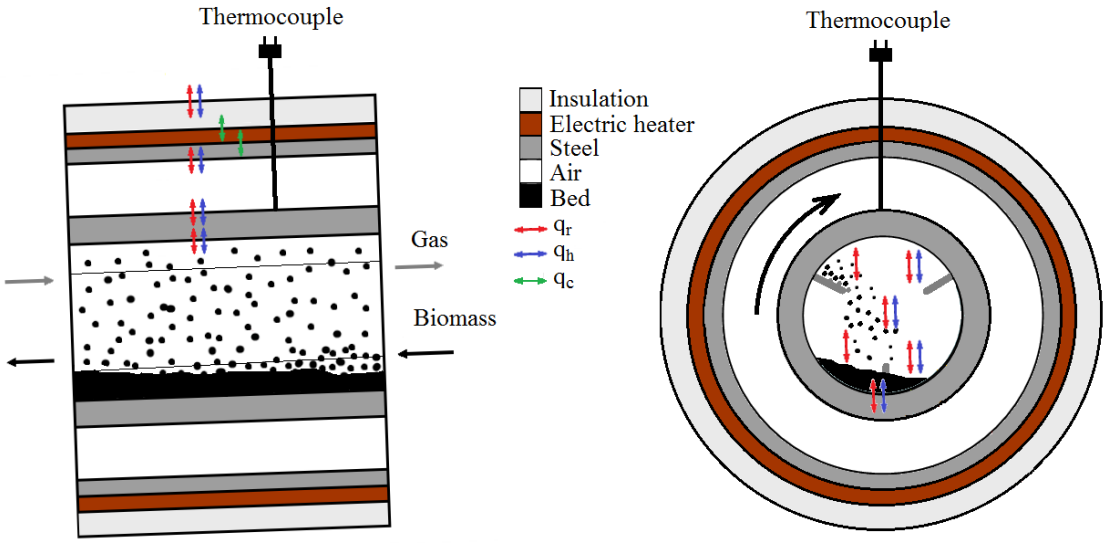


Figure 7-2. Solid and heat transfer between considered phases of rotary drums in a differential element of the torrefied is shown here. The symbol q stands for energy transfer and subscripts r, h and c stand for radiation, convections and conduction respectively.

Modelling the dispersed phase in the reactor according to the Lagrangian equations is computationally very expensive. For this reason, we have taken expressions developed by Nhuchhen et al. [28] for heat transfer between solid and systems, that considers all thermal effects inside reactor. Thus, only two continuum phases are modeled in this work. In addition, we also used correlations developed by Nhuchhen et al. [29] for solid residence time and filling factor. All the above expressions were developed for the same two-stage rotary reactor that is modeled in the present work.

### *7.3.1. Governing equations*

Mass and energy balance equations were developed for solid, gases, and reactor wall, in order to follow changes at each time step during the torrefaction process. These mass balances must be associated with a kinetic model, which describes the decomposition and generation of each phase inside reactor. The kinetic model used is presented in Figure 7-3.

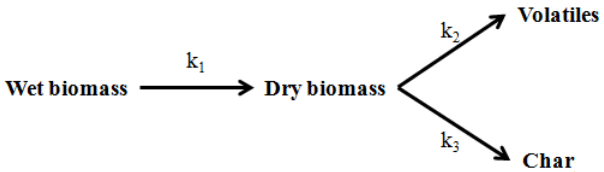


Figure 7-3. Kinetic model used in the biomass torrefaction model [34].

In this model, $k_1$, $k_2$ and $k_3$ were obtained for kinetic control conditions without secondary reactions in TGA. In this kinetic model biomass is considered to be made of both organic and inorganic

materials. The main reason is that the kinetic parameters were obtained from the biomass without any kind of extraction. Catalytic effects in relation with inorganic compounds in the biomass or some compounds formed in the process like acids are all captured in the values of the global kinetic constants. The total final char yield is thus made up of both organic and inorganic materials. Inorganic part in the biomass remains unchanged as that in the initial biomass, because it is assumed not to undergo any reaction during torrefaction. Secondary reactions inside particles were not considered in the kinetic model because the small biomass particle size, and small bed heght inside kiln.

Kinetic constants $k_1$, $k_2$ and $k_3$ are for the generation/destruction of the phases, and are defined by the Arrhenius equation (eq. (7-1)).

$$k_i = A_i \exp\left(\frac{-E_i}{RT}\right) \tag{7-1}$$

The kinetic parameters for kinetic model shown in Figure 7-3 are shown in the Table 7-3.

Table 7-3. Kinetic parameters [34]

| $k_i$ | $A_0(s^{-1})$ | $E_a(kJ/mol)$ |
|---|---|---|
| $k_1$ | 7.11 | 23.7 |
| $k_2$ | $1.45x10^{12}$ | 156 |
| $k_3$ | $6.58x10^{6}$ | 106.4 |

The activation energy for volatiles, $k_2$ is greater than that for char, indicating that the formation of volatiles is more susceptible to changes with temperature and therefore, at low temperatures the char formation is higher than the volatiles release.

Two phases are considered in the model: solid phase (biomass) and gas phase formed by condensable and non-condensable volatiles generated in the torrefaction process. It includes $CO_2$, CO, water, acetic acid, formic acid, methanol, furfural and others [9,57–61]. In the model, we calculate the gas properties (thermal conductivity, heat capacity, density, emissivity, viscosity) as a function of the amount of each specie in the mixture of gases. Based on previous experimental works developed in this reactor [13,48] we assume that the gas phase (volatiles) is formed mainly by a mixture of $CO_2$ and CO.

***Solid phase:*** Mass balance for species in the solid phase (biomass) is expressed as follows:

$$\frac{\partial \rho_{s,i}}{\partial t} + \frac{\partial\left(\rho_{s,i} v_s\right)}{\partial x} = \dot{r}_{s,i} \tag{7-2}$$

Where $\rho$ is density, $v$ is velocity of the solids along $x$, which is the length of the reactor, $\dot{r}$ is the reaction rate. Subscripts $s$ and $i$ stands for solid phase and $i^{th}$ species in the phase (water, biomass and char), respectively.

Energy balance in the solid phase is:

$$\rho_s c_{p_s} \frac{\partial T_s}{\partial t} + \frac{\partial \left(\rho_s c_{p_s} v_s T_s\right)}{\partial x} = \frac{\partial}{\partial x}\left(\lambda_s \frac{\partial T_s}{\partial x}\right) + \dot{q}'''_{conv} + \dot{q}'''_{rad} + \dot{S}_g \tag{7-3}$$

Where $c_p$ represents the heat capacity, $v$ the velocity, $\lambda$ the thermal conductivity, $T$ the temperature. Here, $\dot{q}'''_{conv}$ represents the energy transfer by convection, $\dot{q}'''_{rad}$ represents the energy transfer by radiation, and $\dot{S}_g$ represents the energy source/sink due to the chemical reactions.

***Gas Phase*.** The mass balance transport equation for species in the phase gas may be written as:

$$\frac{\partial \rho_{g,i}}{\partial t} + \frac{\partial \left(\rho_{g,i} v_{g,i}\right)}{\partial x} = \dot{r}_{g,i} \tag{7-4}$$

Where the subscript *g* stands for gas phase. Diffusional effects in Equation (7-4) were neglected because the Peclet number is much higher than 1.0.

Energy balance of the gas phase is:

$$\rho_g c_{p_g} \frac{\partial T_g}{\partial t} + \frac{\partial \left(\rho_g c_{p_g} v_g T_g\right)}{\partial x} = \dot{q}'''_{conv} + \dot{q}'''_{rad} + \dot{S}_g \tag{7-5}$$

Where $\dot{q}'''_{conv}$ represents the energy transfer by convection and $\dot{q}'''_{rad}$ represents the energy transfer by radiation. In our system, there are no external gas streams entering to the reactor, only that generated by the biomass devolatilization. So, analyze the thermal behavior of the gas is not important, and that results are not presented for the gas in future sections.

The reactor wall also was modeled in 2D in order to obtain a temperature distribution during process. The energy transport equation for the wall is given by:

$$\rho_w c_{p_w} \frac{\partial T_w}{\partial t} = \frac{\partial}{\partial x}\left(\lambda_{w,x} \frac{\partial T_w}{\partial x}\right) + \frac{1}{r}\frac{\partial}{\partial r}\left(\lambda_{w,r} \frac{\partial T_w}{\partial r}\right) \tag{7-6}$$

Where the subscript *w* stands for wall, *x* and *r* stands for geometrical axial and radial axis. With the above equation it is possible to evaluate the thermal behavior of kiln walls, such as energy transfer and thermal losses with the environment or in its ends. For our case, the internal wall temperature was defined according to experimental measurements, so this expression does not take great importance in our system.

The properties of gas and solids used in the model are shown in Table 7-4. Average values of solid density, gas density, total conductivity and heat capacity are calculated based on temperature and fractions of each phase in the solid.

Table 7-4. Property values.

| Property | Value |
|---|---|
| $\rho_s$ | 250 kg/m$^3$ |
| $\rho_c$ | 200 kg/m$^3$ |
| $\rho_{H2O}$ | 1000 kg/m$^3$ |
| $Cp_s$ | (1112.3 + 4.85*Tsol)/1000 kJ/kg K [62] |
| $Cp_c$ | (1003.2 + 2.09*Tsol)/1000 kJ/kg K [62] |
| $Cp_{H2O}$ | 4.1 kJ/kg K |
| $Cp_g$ | 1 kJ/kg K |
| $k_s$ | (0.13 + 0.0003*Tsol)/1000 kW/mK [62] |
| $k_{H2O}$ | 0.5*10$^{-3}$ kW/mK |
| $k_g$ | 2*10$^{-5}$ kW/mK |
| $k_c$ | (0.08 - 0.0001*Tsol)/1000 kW/mK [62] |
| $\mu$ | 2.75*10$^{-5}$ Pa s |

***Analytical expressions and experimental correlations:*** The mechanism of energy transfer inside the two-step rotary reactor was studied by Nhuchhen et al. [28], who obtained expressions for heat transfer coefficients between wall-gas ($h_{wf}$), and wall-solid ($h_{ewb}$) as shown in equations (7-7) and (7-8).

$$h_{wf} = \frac{k_f}{D}\left(0.60 + \frac{0.387\,Ra_D^{1/16}}{\left(1+\left(\frac{0.559}{\mathrm{Pr}_f}\right)^{9/16}\right)^{8/27}}\right)^2 \tag{7-7}$$

$$h_{ewb} = \frac{1}{\frac{d_p}{10k_f} + \left(\frac{\pi t_c}{4k_{bs}C_{pbs}\rho_{bs}}\right)^{0.5}} \tag{7-8}$$

Where, $k_f$, $D$, $Ra_D$, and $Pr_f$ stand for thermal conductivity of gas, reactor diameter, Rayleigh number, and Prandtl number, respectively. $t_c$ stands for the average solid contact time with hot surface per cascaded cycle.

The overall heat transfer coefficient of indirectly heated rotary reactor can be expressed as:

$$h_0 = \delta h_{ewb} + (1-\delta)h_{wf} \tag{7-9}$$

Where $\delta$ stand for the fraction of cylindrical wall area covered by solids, defined as the ratio of surface area of reactor covered by particle bed per unit length to total lateral surface area of reactor per unit length.

### *7.3.2. Initial and boundary conditions*

Initial boundary conditions for biomass, gas, and walls are defined as follows:

$$\left.\begin{aligned} T_g &= T_{g_0} \\ T_s &= T_{s_0} \\ \dot{m}_s &= \dot{m}_{s_0} \\ \dot{m}_g &= 0 \\ T_w &= T_{w_0} \end{aligned}\right\}_{t=0} \tag{7-10}$$

Boundary conditions for modeled phases are defined as follows:

$$-\frac{k_w dT_w}{dr} = Q_{w-g} + Q_{w-s} \Big\}_{x=[0,L];\, r=r_{in_w}} \tag{7-11}$$

$$T_w = cte \}_{x=[0,L_{dryer}];\, r=r_{in_w}} \tag{7-12}$$

$$T_w = f(x) \}_{x=[L_{dryer},L_{torreefier}];\, r=r_{in_w}} \tag{7-13}$$

For equation (7-13), *f(x)* was obtained from experimentally measured temperatures from a previous work by Granados et al. [48]. In this work, the actual temperature profile inside rotary torrefier was measured. The temperature inside rotary dryer was not measured, for this reason it was considered constant.

### *7.3.3. Numerical solution*

In order to solve the system of above partial differential equations, a discretization of the modeled system is performed by means of finite volumes elements [63]. The system was solved using a FORTRAN program with the Gear method linked to DIVPAG subroutine [64,65] which in turn is linked with IMSL libraries of Visual Numerics. Tolerance for the Gear method was defined in $1x10^{-6}$ that indicate the difference between iterations for calculate and control the error. Time step in the model iterations was defined by the Courant number which was set to 0.8 to ensure numerical stability.

### *7.3.4. Mesh independence tests*

A test study of mesh independence for the model developed was done in order to evaluate the impact of the mesh size over the numerical solution of equation system. It allows the selection of a mesh that provides good numerical resolution at a reasonable computational time. Five different meshes were evaluated with 20, 30, 40, 50, and 60 nodes and results are shown in Figure 7-4.

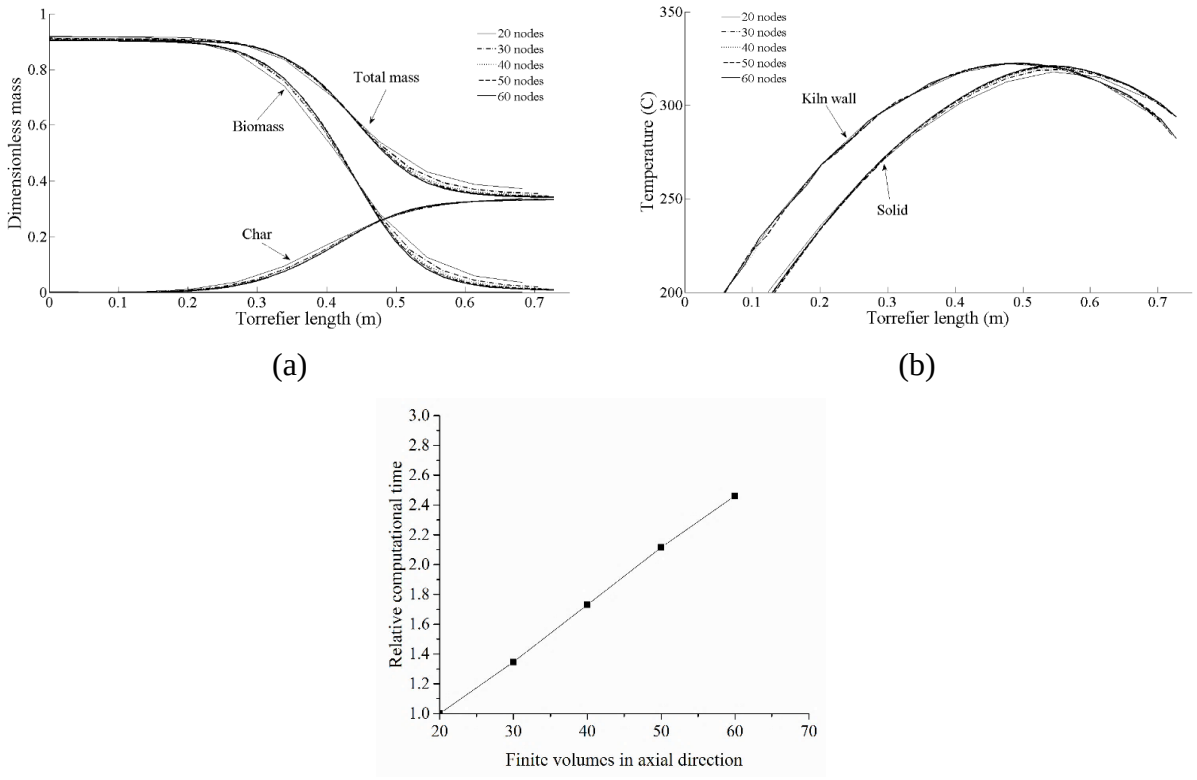


Figure 7-4. Dimensionless mass for phases in the solid (a), temperatures (b), and relative computational time for different mesh densities.

It is apparent from Figure 7-4(a) and Figure 7-4(b) for mass of the phases and solid temperature, that the mesh with 20 and 30 nodes differ slightly from the others, which means that these meshes are not dense enough to generate acceptable results despite a low computational effort observed in Figure 7-4(c). The other meshes have similar results, which seems to indicate that, although the mesh density increases, the results could not change much compared to those delivered with these denser meshes. For this reason, it was decided to perform all simulations with a mesh with 50 nodes as it generates reliable results with a reasonable computational effort.

## 7.4. Model results and validation

Experiments were conducted in the Biomass conversion laboratory at Dalhousie University, Canada, in order to validate the model developed. Temperatures, final conversions and different properties for torrefied biomass were measured and compared with theoretical values.

### *7.4.1. Final conversions and properties of biomass*

For all tests described in previous section, the torrefied biomass was collected and weighted for its final mass. After this, elemental and proximate analysis, and HHV were measured in order to characterize the final solid product. With the modeled MY, and experimental correlations mentioned in previous section taken from Granados et al. [48], was possible to find the modeled properties. A comparison between measured and predicted values of MY, HHV, FC, and VM are shown in Figure 7-5.

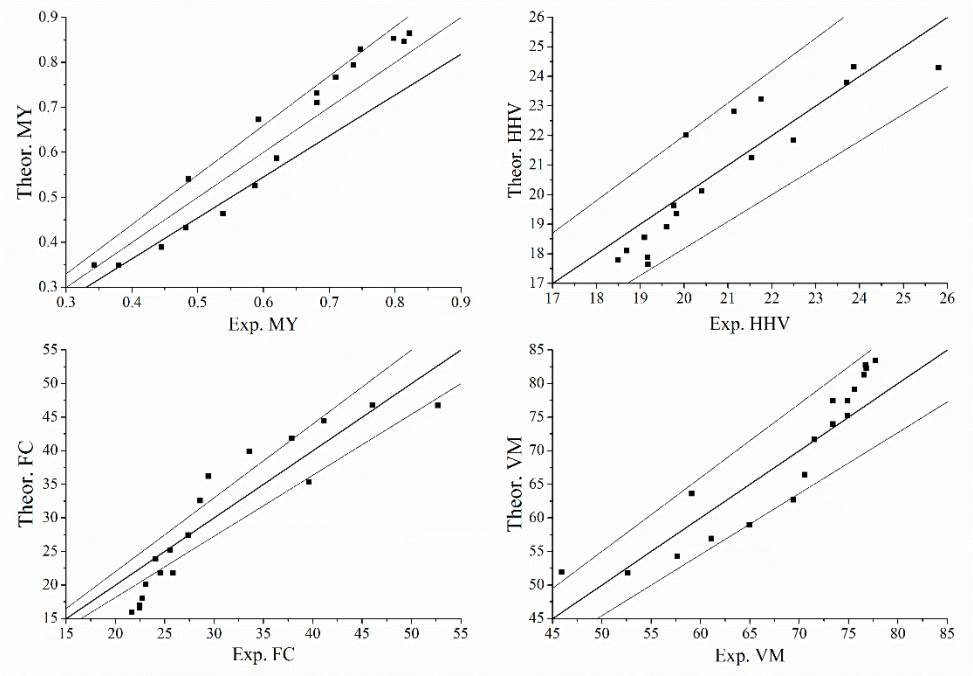


Figure 7-5. Comparison between experimental and theoretical properties for torrefied biomass.

Table 7-5. Comparison between experimental and predicted properties in the torrefied biomass.

| | MY | | | HHV (MJ/kg) | | | FC (%) | | | VM (%) | | |
|---|---|---|---|---|---|---|---|---|---|---|---|---|
| Samples | Theor. | Exp. | Dev (%) | Theor. | Exp. | Dev (%) | Theor. | Exp. | Dev (%) | Theor. | Exp. | Dev (%) |
| T260-16.4 | 0.77 | 0.71 | 8.0 | 18.9 | 19.6 | 3.6 | 21.8 | 25.8 | 15.8 | 77.4 | 73.4 | 5.4 |
| T280-16.4 | 0.54 | 0.49 | 11.1 | 21.8 | 22.5 | 2.9 | 35.3 | 39.6 | 10.8 | 63.6 | 59.1 | 7.5 |
| T300-16.4 | 0.35 | 0.34 | 2.0 | 24.3 | 25.8 | 5.8 | 46.7 | 52.7 | 11.3 | 51.9 | 45.9 | 12.9 |
| T260-9.6 | 0.83 | 0.75 | 10.9 | 18.1 | 18.7 | 3.2 | 18.0 | 22.7 | 20.6 | 81.3 | 76.6 | 6.1 |
| T280-9.6 | 0.67 | 0.59 | 13.4 | 20.1 | 20.4 | 1.4 | 27.4 | 27.4 | 0.1 | 71.7 | 71.6 | 0.1 |
| T300-9.6 | 0.39 | 0.44 | 12.6 | 23.8 | 23.7 | 0.4 | 44.4 | 41.2 | 7.9 | 54.3 | 57.7 | 5.9 |
| T260-7.0 | 0.85 | 0.80 | 6.9 | 17.8 | 18.5 | 3.8 | 16.6 | 22.5 | 26.1 | 82.7 | 76.7 | 7.8 |
| T280-7.0 | 0.73 | 0.68 | 7.3 | 19.4 | 19.8 | 2.4 | 23.9 | 24.1 | 0.9 | 75.3 | 74.9 | 0.5 |
| T300-7.0 | 0.46 | 0.54 | 13.8 | 22.8 | 21.1 | 8.0 | 39.9 | 33.6 | 18.8 | 58.9 | 64.9 | 9.3 |
| T260-11.0 | 0.79 | 0.74 | 7.8 | 18.5 | 19.1 | 2.9 | 20.1 | 23.1 | 12.9 | 79.1 | 75.6 | 4.6 |
| T280-11.0 | 0.59 | 0.62 | 5.4 | 21.2 | 21.5 | 1.4 | 32.5 | 28.6 | 13.8 | 66.4 | 70.6 | 5.9 |
| T300-11.0 | 0.35 | 0.38 | 8.3 | 24.3 | 23.9 | 1.8 | 46.8 | 46.1 | 1.6 | 51.8 | 52.6 | 1.6 |
| T260-6.6 | 0.85 | 0.81 | 3.9 | 17.9 | 19.2 | 6.7 | 17.0 | 22.5 | 24.2 | 82.3 | 76.8 | 7.1 |
| T280-6.6 | 0.71 | 0.68 | 4.2 | 19.6 | 19.8 | 0.6 | 25.1 | 25.5 | 1.5 | 74.0 | 73.4 | 0.7 |
| T300-6.6 | 0.43 | 0.48 | 10.5 | 23.2 | 21.8 | 6.8 | 41.8 | 37.9 | 10.3 | 56.9 | 61.1 | 6.9 |
| T260-5.2 | 0.9 | 0.8 | 5.2 | 17.6 | 19.2 | 8.0 | 15.9 | 21.7 | 26.6 | 83.4 | 77.8 | 7.3 |
| T280-5.2 | 0.8 | 0.7 | 7.9 | 18.9 | 19.6 | 3.5 | 21.8 | 24.5 | 11.4 | 77.4 | 74.9 | 3.4 |
| T300-5.2 | 0.5 | 0.6 | 10.5 | 22.0 | 20.0 | 9.9 | 36.2 | 29.4 | 23.0 | 62.7 | 69.4 | 9.7 |
| | Total dev. | | 8.3 | Total dev. | | 4.1 | Total dev. | | 13.2 | Total dev. | | 5.7 |

Figure 7-5 shows that the model predictions have good agreement with the experimental data obtained in the laboratory. It is also possible to observe stripes that indicate a deviation of 5%. An overestimation of the loss of mass in the lower temperatures contrasts with an underestimation at high temperatures. The differences are not considerable, it does not appear to have set pattern. So, this small difference may be attributed to choice of the kinetic model employed. Comparisons with experimental data are also shown in Table 7-5, which also presents the deviations for each experimental test performed with different experimental conditions, such was mentioned in the Experimental design section. For each of these evaluated parameters, it is possible to observe that the model presents a good fit with deviations of 8.3% for MY, 13.21% for MV, 5.72% for HR and 4.07% for HHV.

### *7.4.2. Solid temperatures*

Measurements of the solid temperature while it advances through the reactor were performed to validate the model developed. In these experiments, the biomass temperature was measured at 5 different points along the length and inside the torrefier and for three different experimental conditions. Comparisons of these measurements and those obtained with the model are presented below in Figure 7-6.

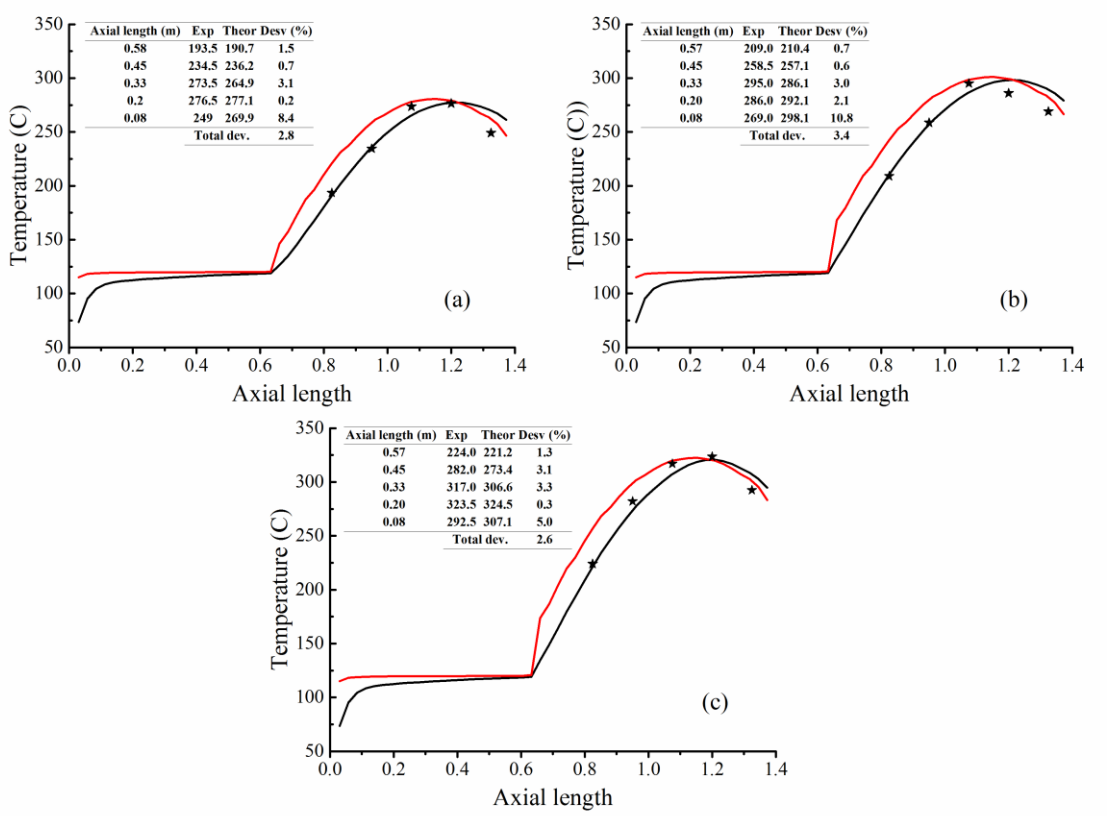


Figure 7-6. Comparison between theoretical and experimental temperatures for biomass during torrefaction with residence time of 16.4 minutes. (a) 260°C, (b) 280°C, and (c) 300°C. Red line: theoretical wall temperature; black line: theoretical biomass temperature; stars: experimental biomass temperature

Deviations between experimental and theoretical data are presented in the attached table in each figure. As can be observed, the model predictions fit well with experimental data in each of the experimental condition evaluated. The greatest deviation is presented for the data obtained at 280 °C with a value of 3.4%, and the lowest is presented for the data of 300 °C with a value of 2.6%.

### *7.4.3. Transient temperature of the solid*

As stated in model description the model is transient in nature, and it can simulate this transient behavior of the torrefaction process for a given initial conditions. From simulations carried, the temporal evolution of solid temperature was obtained at three different points inside the torrefaction reactor and are presented in Figure 7-7. These three points were located near to the entrance of the reactor, in the central point, and near to the exit of the torrefied biomass.

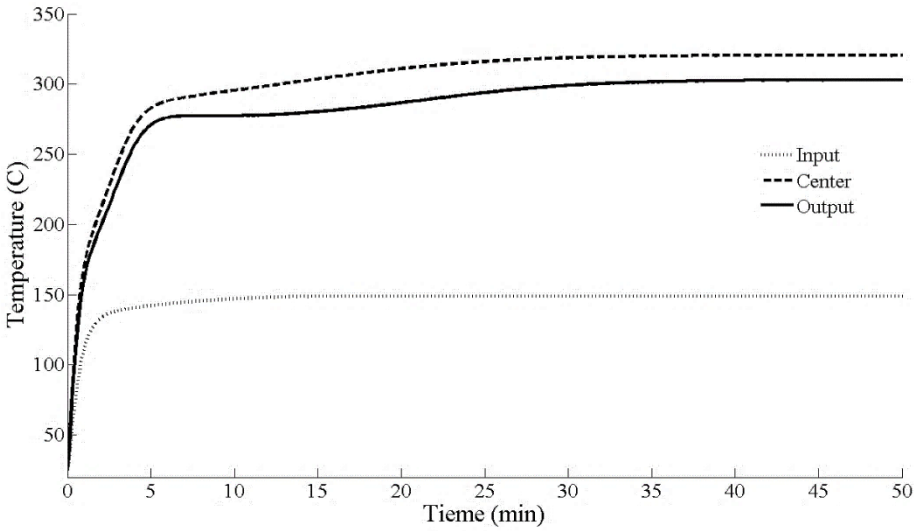


Figure 7-7. Evolution of solid temperature for different positions inside torrefier.

According to simulations performed for the torrefaction reactor, the solid takes around 40 minutes to reach its stable steady state in the central and outlet points. The above considering that, at the beginning of the process, the biomass is inside of the reactor at room temperature in its length, and the reactor walls are at the process temperature, according to experimental measurements. The biomass in the inlet zone reaches its steady state in less than 20 minutes approximately.

### *7.4.4. Axial profiles of properties*

After obtaining the minimum simulation time, in which the steady state is obtained in the system, several operating conditions were defined in order to obtain profiles of some important properties inside the torrefier reactor. One of the profiles that can be obtained with the developed model and presented in Figure 7-8, is the yield/loss of each phases considered in the torrefied biomass such as water, raw biomass and char.

In these profiles, it is possible to observe that the biomass does not completely decompose when the operating temperature are 260 and 280 °C. For the temperature of 260 °C, a small char formation is observed, as well as a small devolatilization. Both formations of these phases increase when the temperature increases to 280 °C, but when the temperature increases to 300 °C, the

biomass decompose completely, generating the maximum char formation found in the evaluated operational conditions in simulations. In the same way, the formation of volatiles increases, and the total mass loss increases.

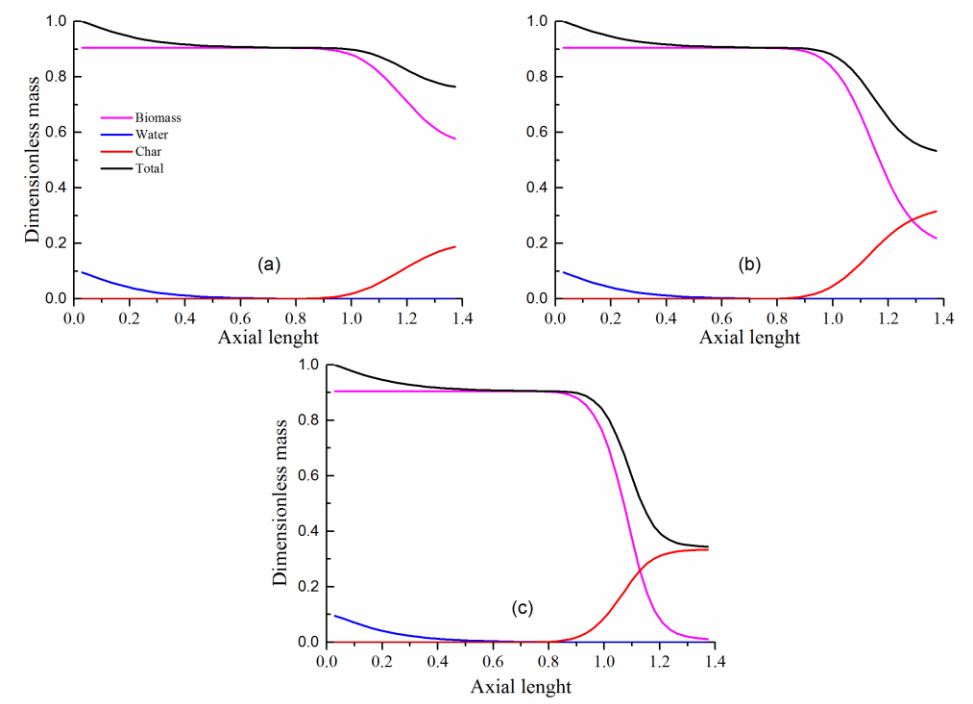


Figure 7-8. Products yield during torrefaction process for tests with residence time of 16.4 min. (a) 260°C, (a) 280°C and (a) 300°C.

The model simulations show that the drying takes place in a fraction of the dryer, approximately in the first 0.5 m, after which, the biomass is only transported in the reactor without undergoing any conversion. This could indicate that the drying reactor could operate with lower residence times, or with less demanding thermal conditions. This present model is thus an excellent tool to evaluate the behavior of reactors, or to develop optimal designs of new reactors.

For the case of the torrefaction reactor, there is a length of about 0.15 m where the biomass is warmed up from drying temperature to the torrefaction temperature. After that, the torrefaction occurs over the remainder length of the reactor until it exits. According to this result, the torrefaction reactor has an optimum length to complete the process for a set of conditions evaluated. Additionally, from previous results, it is possible to conclude that the kinetics parameters used in the model are adequate to predict the biomass behavior in the thermal process.

Additionally, it also possible to obtained variation in property values like HHV, FC, and VM for the biomass along the length of the torrefier. These profiles are presented only for the torrefaction reactor, as is shown in Figure 7-9. These profiles give valuable information in predicting properties of the final product after the process. According to the information shown in Figure 7-9, the devolatilization starts from 0.9 m approximately when the biomass reaches temperatures above 180°C. The decrease of VM in the biomass, goes from 86% to 51.5%. Meanwhile, the CF in the

material increases from 13.3% to 47%. One of the most important properties when evaluating the torrefied biomass as a potential solid fuel, is HHV, which increases from 17 MJ/kg up to 24.4 MJ/kg. As previously mentioned, the model developed in this work, besides allowing to visualize the properties of the solid being torrefied, allows to evaluate the behavior of the oven in operation and its dimensions.

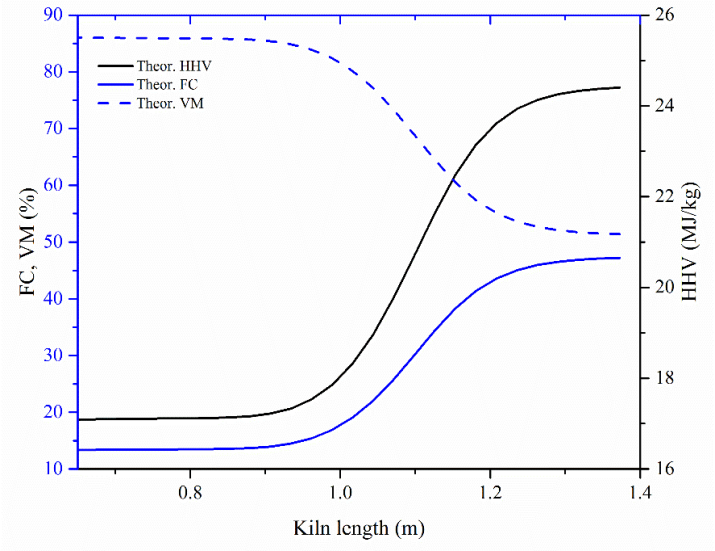


Figure 7-9. Properties profiles for torrefied biomass inside torrefier reactor for test T300-9.6.

In addition to the above simulations, the model becomes a powerful tool for these types of rotary reactors, and similar ones, that could be evaluated, or designed from functional furnace simulations.

## 7.5. Conclusions

A one-dimensional model for simulation of the torrefaction process and prediction of its thermal behavior in a two-stage rotary reactor was developed. It can be used to predict gas and solid temperature, mass yield, higher heating value, and other important properties of the final torrefied solid. This model can also be used to evaluate torrefier's performance under different operating conditions, for different reactor dimensions. Performance for different biomass types can be evaluated only by changing some parameters of kinetic constants. Additionally, the model allows implementation of advanced control methods by predicting the dynamic performance of the torrefier. The mathematical model was validated against experimental data obtained by the authors.

The model shows that torrefaction brings about a considerable improvement in biomass properties like high HHV, high FC, and low VM which is an indicator of higher reactivity. As a result, from these simulations, the conversion process with high temperature occurs in smaller lengths inside the kiln. Therefore, with base on data from model, it is possible to state that torrefier rotary reactor can be redesigned for having smaller dimensions and to develop the thermal process with high temperature.

**Acknowledgments**

The experimental work was performed in the Biomass Conversion Laboratory at Dalhousie University under the guidance of Prof. Prabir Basu, who acknowledge the support of Natural Science & Engineering Council and from Greenfield Research Incorporated of Canada.

D.A Granados wish to thank the Colombian Administrative Department of Science, Technology and Innovation (COLCIENCIAS) (Departamento Administrativo de Ciencia, Tecnología e Innovacion) for financial support.

**References**

[1] Basu P. Biomass Gasification, Pyrolysis and Torrefaction: Practical Design and Theory. 2013.

[2] Pentananunt R, Rahman ANMM, Bhattacharya SC. Upgrading of biomass by means of torrefaction. Energy 1990;15:1175–9. doi:10.1016/0360-5442(90)90109-F.

[3] Wattananoi W, Khumsak O, Worasuwannarak N. Upgrading of biomass by torrefaction and densification process. 2011 IEEE Conf Clean Energy Technol 2011:209–12. doi:10.1109/CET.2011.6041465.

[4] Medic D, Darr M, Shah a., Potter B, Zimmerman J. Effects of torrefaction process parameters on biomass feedstock upgrading. Fuel 2012;91:147–54. doi:10.1016/j.fuel.2011.07.019.

[5] Li J, Brzdekiewicz A, Yang W, Blasiak W. Co-firing based on biomass torrefaction in a pulverized coal boiler with aim of 100% fuel switching. Appl Energy 2012;99:344–54. doi:10.1016/j.apenergy.2012.05.046.

[6] Fisher EM, Dupont C, Darvell LI, Commandré J-M, Saddawi a, Jones JM, et al. Combustion and gasification characteristics of chars from raw and torrefied biomass. Bioresour Technol 2012;119:157–65. doi:10.1016/j.biortech.2012.05.109.

[7] Broström M, Nordin A, Pommer L, Branca C, Di Blasi C. Influence of torrefaction on the devolatilization and oxidation kinetics of wood. J Anal Appl Pyrolysis 2012;96:100–9. doi:10.1016/j.jaap.2012.03.011.

[8] Berrueco C, Recari J, Güell BM, Alamo G Del. Pressurized gasification of torrefied woody biomass in a lab scale fluidized bed. Energy 2014;70:68–78. doi:10.1016/j.energy.2014.03.087.

[9] Deng J, Wang G, Kuang J, Zhang Y, Luo Y. Pretreatment of agricultural residues for co-gasification via torrefaction. J Anal Appl Pyrolysis 2009;86:331–7. doi:10.1016/j.jaap.2009.08.006.

[10] Hassan E, Steele P, Ingram L. Characterization of fast pyrolysis bio-oils produced from pretreated pine wood. Appl Biochem Biotechnol 2009;154:182–92. doi:10.1007/s12010-008-8445-3.

[11] Zheng A, Zhao Z, Chang S, Huang Z, Wang X, He F, et al. Effect of torrefaction on structure and fast pyrolysis behavior of corncobs. Bioresour Technol 2013;128:370–7. doi:10.1016/j.biortech.2012.10.067.

[12] Granados DA, Velásquez HI, Chejne F. Energetic and exergetic evaluation of residual biomass in a torrefaction process. Energy 2014;74:181–9. doi:10.1016/j.energy.2014.05.046.

[13] Nhuchhen DR, Basu P, Acharya B. Torrefaction of poplar in continuous two- stage indirectly heated rotary torrefier. Energy & Fuels 2016;30:1027–38. doi:10.1021/acs.energyfuels.5b02288.

[14] Huang YF, Chen WR, Chiueh PT, Kuan WH, Lo SL. Microwave torrefaction of rice straw and Pennisetum. Bioresour Technol 2012;123:1–7. doi:10.1016/j.biortech.2012.08.006.

[15] Ren S, Lei H, Wang L, Bu Q, Wei Y, Liang J, et al. Microwave Torrefaction of Douglas Fir Sawdust Pellets. Energy & Fuels 2012;26:5936–43. doi:10.1021/ef300633c.

[16] Satpathy SK, Tabil LG, Meda V, Naik SN, Prasad R. Torrefaction of wheat and barley straw after microwave heating. Fuel 2014;124:269–78. doi:10.1016/j.fuel.2014.01.102.

[17] Wang MJ, Huang YF, Chiueh PT, Kuan WH, Lo SL. Microwave-induced torrefaction of rice husk and sugarcane residues. Energy 2012;37:177–84. doi:10.1016/j.energy.2011.11.053.

[18] Li H, Liu X, Legros R, Bi XT, Lim CJ, Sokhansanj S. Torrefaction of sawdust in a fluidized bed reactor. Bioresour Technol 2012;103:453–8. doi:10.1016/j.biortech.2011.10.009.

[19] Wang C, Peng J, Li H, Bi XT, Legros R, Lim CJ, et al. Oxidative torrefaction of biomass residues and densification of torrefied sawdust to pellets. Bioresour Technol 2013;127:318–25. doi:10.1016/j.biortech.2012.09.092.

[20] Carrier M, Hugo T, Gorgens J, Knoetze H. Comparison of slow and vacuum pyrolysis of sugar cane bagasse. J Anal Appl Pyrolysis 2011;90:18–26. doi:10.1016/j.jaap.2010.10.001.

[21] Carrasco JC, Oporto GS, Zondlo J, Wang J. com Observed Kinetic Parameters during the Torrefaction of Red Oak ( Quercus rubra ) in a Pilot Rotary Kiln Reactor 2014;9:5417–37.

[22] Colin B, Dirion J-L, Arlabosse P, Salvador S. Wood chips flow in a rotary kiln: experiments and modeling. Chem Eng Res Des 2015;98:179–87. doi:10.1016/j.cherd.2015.04.017.

[23] Colin B, Dirion JL, Arlabosse P, Salvador S. Experimental study of wood chips torrefaction in a pilot scale rotary kiln. Chem Eng Trans 2014;37:505–10. doi:10.3303/CET1437085.

[24] Hilten RN, Speir R a., Kastner JR, Mani S, Das KC. Effect of torrefaction on bio-oil upgrading over HZSM-5. Part 2: Byproduct formation and catalyst properties and function. Energy and Fuels 2013;27:844–56. doi:10.1021/ef301695c.

[25] Repellin V, Govin A, Rolland M, Guyonnet R. Modelling anhydrous weight loss of wood chips during torrefaction in a pilot kiln. Biomass and Bioenergy 2010;34:602–9. doi:10.1016/j.biombioe.2010.01.002.

[26] Saleh SB, Hansen BB, Jensen PA, Dam-Johansen K. Efficient fuel pretreatment: Simultaneous torrefaction and grinding of biomass. Energy and Fuels 2013;27:7531–40. doi:10.1021/ef401787q.

[27] Zajec L. Slow pyrolysis in a rotary kiln reactor : Optimization and experiment. University of Iceland, University of Akureyri, 2009.

[28] Nhuchhen DR, Basu P, Acharya B. Investigation into overall heat transfer coefficient in

indirectly heated rotary torrefier. Int J Heat Mass Transf 2016;102:64–76. doi:10.1016/j.ijheatmasstransfer.2016.06.011.

[29] Nhuchhen DR, Basu P, Acharya B. Investigation into mean residence time and filling factor in flighted rotary torrefier. Can J Chem Eng 2016;94:1448–56. doi:10.1002/cjce.22520.

[30] Nachenius RW, van de Wardt TA, Ronsse F, Prins W. Torrefaction of pine in a bench-scale screw conveyor reactor. Biomass and Bioenergy 2014;79:96–104. doi:10.1016/j.biombioe.2015.03.027.

[31] Ratte J, Fardet E, Mateos D, Héry J-S. Mathematical modelling of a continuous biomass torrefaction reactor: TORSPYD$^{TM}$ column. Biomass and Bioenergy 2011;35:3481–95. doi:10.1016/j.biombioe.2011.04.045.

[32] Bates RB, Ghoniem AF. Biomass torrefaction: modeling of volatile and solid product evolution kinetics. Bioresour Technol 2012;124:460–9. doi:10.1016/j.biortech.2012.07.018.

[33] Felfli FF, Luengo CA, Suárez JA, Beatón PA. Wood briquette torrefaction. Energy Sustain Dev 2005;9:19–22. doi:10.1016/S0973-0826(08)60519-0.

[34] Basu P, Sadhukhan AK, Gupta P, Rao S, Dhungana A, Acharya B. An experimental and theoretical investigation on torrefaction of a large wet wood particle. Bioresour Technol 2014;159:215–22. doi:10.1016/j.biortech.2014.02.105.

[35] Perré P, Rémond R, Turner I. A comprehensive dual-scale wood torrefaction model: Application to the analysis of thermal run-away in industrial heat treatment processes. Int J Heat Mass Transf 2013;64:838–49. doi:10.1016/j.ijheatmasstransfer.2013.03.066.

[36] Ratte J, Marias F, Vaxelaire J, Bernada P. Mathematical modelling of slow pyrolysis of a particle of treated wood waste. J Hazard Mater 2009;170:1023–40. doi:10.1016/j.jhazmat.2009.05.077.

[37] Di Blasi C. Modeling chemical and physical processes of wood and biomass pyrolysis. Prog Energy Combust Sci 2008;34:47–90. doi:10.1016/j.pecs.2006.12.001.

[38] Bradbury AGW, Sakai Y, Shafizadeh F. A kinetic model for Pyrolysis of Cellulose. J Appl Polym Sci 1979;23:3271–80. doi:10.1002/app.1979.070231112.

[39] Di Blasi C, Lanzetta M. Intrinsic kinetics of isothermal xylan degradation in inert atmosphere. J Anal Appl Pyrolysis 1997;40–41:287–303. doi:10.1016/S0165-2370(97)00028-4.

[40] Prins MJ, Ptasinski KJ, Janssen FJJ. Torrefaction of wood. Part 1. Weight loss kinetics. J Anal Appl Pyrolysis 2006;77:28–34. doi:10.1016/j.jaap.2006.01.002.

[41] Chen W-H, Kuo P-C. Torrefaction and co-torrefaction characterization of hemicellulose, cellulose and lignin as well as torrefaction of some basic constituents in biomass. Energy 2011;36:803–11. doi:10.1016/j.energy.2010.12.036.

[42] Rousset P, Turner I, Donnot A, Perré P. Choix d'un modèle de pyrolyse ménagée du bois à l'échelle de la microparticule en vue de la modélisation macroscopique. Ann For Sci 2006;63:213–29. doi:10.1051/forest.

[43] Turner I, Rousset P, Rémond R, Perré P. An experimental and theoretical investigation of the thermal treatment of wood (Fagus sylvatica L.) in the range 200–260°C. Int J Heat Mass

Transf 2010;53:715–25. doi:10.1016/j.ijheatmasstransfer.2009.10.020.

[44] Sarvaramini a., Assima GP, Larachi F. Dry torrefaction of biomass – Torrefied products and torrefaction kinetics using the distributed activation energy model. Chem Eng J 2013;229:498–507. doi:10.1016/j.cej.2013.06.056.

[45] Gronli MG, Melaaen MC, Grønli M, Melaaen MC. Mathematical model for wood pyrolysis - Comparison of experimental measurements with model predictions. Energy & Fuels 2000;14:791–800. doi:10.1021/ef990176q.

[46] Ren S, Lei H, Wang L, Bu Q, Chen S, Wu J. Thermal behaviour and kinetic study for woody biomass torrefaction and torrefied biomass pyrolysis by TGA. Biosyst Eng 2013;116:420–6. doi:10.1016/j.biosystemseng.2013.10.003.

[47] Park C, Zahid U, Lee S, Han C. Effect of process operating conditions in the biomass torrefaction: A simulation study using one-dimensional reactor and process model. Energy 2015;79:127–39. doi:10.1016/j.energy.2014.10.085.

[48] Granados DA, Basu P, Chejne F, Nhuchhen DR. A Detailed Investigation into Torrefaction of Wood in a Two-Stage Inclined Rotary Torrefier. Energy & Fuels 2016:acs.energyfuels.6b02524. doi:10.1021/acs.energyfuels.6b02524.

[49] Nhuchhen DR. Studies on Advanced Means of Biomass Torrefaction. Dalhousie University, 2016. doi:10.1017/CBO9781107415324.004.

[50] Mujumdar K, Ranade V. Simulation of Rotary Cement Kilns Using a One-Dimensional Model. Chem Eng Res Des 2006;84:165–77. doi:10.1205/cherd.04193.

[51] Tscheng S. Convective heat transfer in a rotary kiln. The University of British Columbia, 1978.

[52] Tscheng S., Watkinson A. Convective Heat Transfer in a Rotary Kiln. Can J Chem Eng 1979;57:433–43.

[53] Watkinson A., Brimacombe J. Limestone Calcination in a Rotary Kiln. Metall Trans B 1982;13:369–78.

[54] Heydenrych MD, Greeff P, Heesink a. BM, Versteeg GF. Mass transfer in rolling rotary kilns: A novel approach. Chem Eng Sci 2002;57:3851–9. doi:10.1016/S0009-2509(02)00312-3.

[55] Piton M, Huchet F, Le Corre O, Le Guen L, Cazacliu B. A coupled thermal-granular model in flights rotary kiln: Industrial validation and process design. Appl Therm Eng 2015;75:1011–21. doi:10.1016/j.applthermaleng.2014.10.052.

[56] Pan JP, Wang TJ, Yao JJ, Jin Y. Granule transport and mean residence time in horizontal drum with inclined flights. Powder Technol 2006;162:50–8. doi:10.1016/j.powtec.2005.12.004.

[57] Yang H, Yan R, Chen H, Lee DH, Zheng C. Characteristics of hemicellulose, cellulose and lignin pyrolysis. Fuel 2007;86:1781–8. doi:10.1016/j.fuel.2006.12.013.

[58] Werner K, Pommer L, Broström M. Thermal decomposition of hemicelluloses. J Anal Appl Pyrolysis 2014;110:130–7. doi:10.1016/j.jaap.2014.08.013.

[59] Wang G, Luo Y, Deng J, Kuang J, Zhang Y. Pretreatment of biomass by torrefaction.

Chinese Sci Bull 2011;56:1442–8. doi:10.1007/s11434-010-4143-y.

[60] Collard FX, Blin J. A review on pyrolysis of biomass constituents: Mechanisms and composition of the products obtained from the conversion of cellulose, hemicelluloses and lignin. Renew Sustain Energy Rev 2014;38:594–608. doi:10.1016/j.rser.2014.06.013.

[61] Shen DK, Gu S, Bridgwater a. V. The thermal performance of the polysaccharides extracted from hardwood: Cellulose and hemicellulose. Carbohydr Polym 2010;82:39–45. doi:10.1016/j.carbpol.2010.04.018.

[62] Babu BV, Chaurasia a. S. Pyrolysis of biomass: improved models for simultaneous kinetics and transport of heat, mass and momentum. Energy Convers Manag 2004;45:1297–327. doi:10.1016/j.enconman.2003.09.013.

[63] Versteeg HK, Malalasekera W. An Introduction to Computational Fluid Dynamics, the Finite Volume Method. London: 1996.

[64] Gear CW. Numerical Initial Value Problems in Ordinary Differential Equations. PRENTICE-H. Englewood Cliffs, N.J.: 1971.

[65] Gear CW, Petzold LR. ODE Methods for the Solution of Differential/Algebraic Systems. SIAM J Numer Anal 1984;21:716–28. doi:10.1137/0721048.

# Chapter 8. A Two Dimensional Model for Torrefaction of Large Biomass Particles

**(Paper published in Journal of Analytical and Applied Pyrolysis)**


## Abstract

Torrefaction is defined as a thermal pre-treatment process performed within a temperature range of 200-300°C, at low-heating rates (<20°C/min) and for residence times between 15-60 minutes in inert environments. A phenomenological model of the torrefaction process of large biomass particles is developed in this work. Mass and energy balance coupled to a kinetic model take into account two steps of the biomass decomposition. First of the two steps, considers simultaneous production of vapor and solids from raw biomass. The vapor phase comprises a mixture of condensable and non-condensable gases, while the solid phase consists of torrefied biomass. The second step involves decomposition of volatiles into gases and secondary char. The model analyzes torrefaction behavior of both large and small biomass particles, predicting their final solid and gas yields, temperatures distribution, internal pressure and velocity of the gas phase within the particles. The model also predicts maximum conversions for given particle sizes and temperatures during the process. For given set of conditions small particles showed higher (~77%) than that (~52%) for large particles. Maximum interstitial gas velocities inside the large particle (25mm in diameter and 65mm in length) was about 1.2 mm/s and pressure gradients of about 2000 kPa and it occurred after 20 minutes in the process.


***Keywords:*** Biomass torrefaction, 2-D model, Kinetic model, Heat transfer

## 8.1. Introduction

Biomass is a promising source of solid fuels that could compete with fossil fuels like oil and coal because of its low emissions of greenhouse gases and their acceptable performance in thermal processes. Despite the benefits of using biomass in thermal processes, its implementation is hindered due to high moisture content and low energy density of biomass. The projects feasibility is compromised due to the cost associated with transport and handling of large volumes of biomass. Therefore only small and medium scale projects may provide an option for obtaining economic benefits of the biomass thermal transformation.

The torrefaction process, defined as a thermal pre-treatment performed in the temperature range of 200-300°C, with low heating rates (<20°C/min), and over residence times ranging from 15-60 minutes in inert environments or with low oxygen concentrations [1]. During the torrefaction process, the biomass undergoes a mass loss of up to about 40% and an energy loss of 10-15%, resulting in a biomass with higher specific energy, of brittle nature requiring low energy for grinding process, and hydrophobic (the amounts of moisture absorbed after the process can be around 3%). Additionally, it provides a product uniform in quality, with higher energy density and resistant to decomposition by exposure to the environment [2–4].

The lignocellulose biomass is composed mostly of hemicellulose, cellulose, and lignin, which, during the thermal process degrades, generating gases, tars and a torrefied solid. Hemicellulose decomposes thermally in the temperature range of 150-350°C, cellulose is decomposed in the temperature range of 275-350°C, and lignin decomposes in the temperature range of 250 -500°C [1]. Much of the hemicellulose structure is broken down during the torrefaction process, while cellulose and lignin suffer a minor decomposition depending on the treatment conditions performed [5].

Many research works on torrefaction have been carried out in the experimental field, where different kinds of biomass are torrefied under different operational conditions [2,6–13]. In these experimental works, the operating conditions of the torrefaction process are proposed intuitively in order to find those that can produce the best final properties of torrefied biomass. A phenomenological model can describe the chemical and physical phenomena occurring in the process and thereby provide the optimum operating condition for the best final properties of the torrefied biomass.

Currently in the literature, the information about predictive models in the field of torrefaction is rather limited [14–19]. These models consider the influence of physical phenomena, such as heat transfer between phases, and chemical reactions studied through global kinetics for biomass decomposition [20–23]. Some [24,25] also consider decomposition of individual components like hemicellulose, cellulose, and lignin. Most of these kinetic models, however, did not consider the formation of secondary char from condensable volatiles generated in the devolatilization process [26]. The initial steps of torrefaction could involve pyrolysis and gasification. These processes are extensively studied in the context of combustion of coal resulting in an accurate description of the kinetics and complete models of different kinds of coals. Latter studies on torrefaction process have taken advantage of much of the knowledge and advances developed in the field of pyrolysis [27–36] for structuring models and describe the torrefaction process in a biomass.

Chan et al. [28] developed a model for a biomass particles subjected to heating in an inert atmosphere. The model considered drying of the particle, volatiles generation and its secondary reactions. Conduction and convection processes inside the particle and variation of properties with temperature are considered. A decomposition model that considers solid formation, gas, tar and secondary tar decomposition was included in the model. This torrefaction model predicted the compositions of the final products.

Generally, biomass particles are considered an isotropic solid with properties varying in the thermal process. Di Blasi et al. [37] modeled a biomass particle in two dimensions which is heated in an inert atmosphere at a controlled heating rate. In this model, conduction and convection heat transfer within the particle and convection and radiation with external systems outside of the particle were considered. They used a kinetic decomposition model for biomass without considering secondary reactions between tar and solid. This model can predict temperature profiles, speed of gas and char production. Results were compared with simulations of one-dimensional models and found comparable results [38–40].

Felfi et al. [41] developed a phenomenological one-dimensional transient model applied to the torrefaction of a wood pellet. This model considered that the volatiles and steam generated in the

process are in thermal equilibrium with the solid. Geometrical changes of the solid and pressure gradients during the torrefaction process are considered negligible due to the high permeability of the solid. The kinetic model used in this model was proposed by Shafizadeh et al. [42] which considers that biomass is decomposed by three competitive reactions to gas, tar, and char. This model reproduced the process of drying, and heating of the particles, and volatile production. This model is, however, not sufficiently explicit about the phenomena occurring inside the particle.

Ratte et al. [19] proposed a phenomenological one-dimensional transient model for the slow pyrolysis of spherical wood particles. In this model the average volume simplification proposed by Whitaker [43] was used. Mass and energy balances were performed for the particles considering the kinetic model proposed by Shafizadeh et al. [42]. With this model, it is possible to reproduce the temperature distribution inside the particle, moisture content and pressure increase due to the generation of volatiles over time. This model was more rigorous than that considered by Felfi et al. [41], but the kinetic model still did not consider the secondary char formation from heterogeneous reactions between volatiles and char.

Turner et al. [44] modeled the torrefaction process of wood using a two-dimensional phenomenological transient model. In this model chemical and physical phenomena are coupled using the "Transpore" model developed earlier by Perré et al. [45] that describes the drying process in a porous medium. The kinetic model used is centered on the hypothesis that decomposition of biomass can be described as decomposition of each component (cellulose, hemicellulose and lignin). Again, in this “Transpore” model, the secondary char formation from volatiles was not considered.

Pétrissans et al. [46] modeled the thermal degradation of wood particles with a one-dimensional transient model. This model neglected energy transfer by convection between the solid and the volatiles generated inside the particle. The decomposition of wood was represented by two simultaneous reactions which generate gas and char. The main focus this work was the formation of primary char. It did not provide any information about formation of other products.

Ratte et al. [14] developed one of the few models found in the literature applied for a continuous torrefaction reactor. Two phases were considered inside the reactor: a particles phase composed of biomass and a continuous phase composed of 11 species present in the gases entering the reactor and generated in the process. The kinetic model considers only the formation of volatile and char without considering the secondary reactions in the heterogeneous phase. Eight reactions were considered to represent the secondary reactions in the homogeneous phase during the torrefaction process.

According to the above literature review of modeling of torrefaction process, it is clear that the available information about secondary reactions describing the secondary formation of a solid or char is scarce. Despite the low production of secondary char in the torrefaction process, it plays an important role, and understanding its formation is an ongoing challenge. The present work attempts to develop a phenomenological model of the torrefaction process with a kinetic model presented by Basu et al. [17] that considers the formation of secondary char and condensable and non-condensable volatiles. The model is able to predict the behavior of a biomass particle in kinetic control conditions and large particles in a torrefaction process.

## 8.2. Model description

This section presents a transient 2D model for the torrefaction process of a biomass particle. This model is applied over the system shown in Figure 8-1 for a vertical biomass particle. The model considers the drying and devolatilization stages of the biomass occurring in the sequence shown in Figure 8-2.

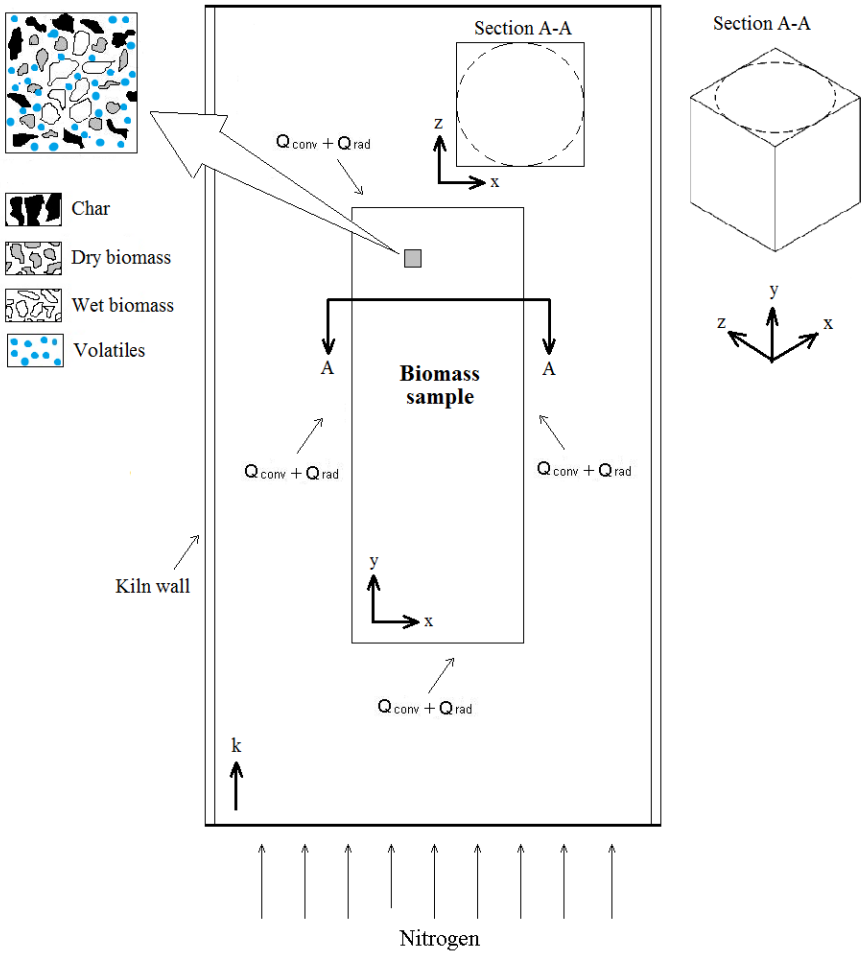


Figure 8-1. System scheme and energy transfer between biomass particle and external system.

This model predicts the behavior of the biomass sample undergoing torrefaction in an heated vertical kiln type reactor. Particle heating is through radiation from the kiln walls in which the sample is torrefied. During the initial heating stage, drying of the particle occurs, and thereafter the devolatilization process starts at temperatures of about 180°C with hemicellulose decomposition (Figure 8-2). The biomass particle is heated at a rate below 20°C/min from room temperature to the torrefaction temperature, which lies between 200 and 300°C. Biomass residence time varies between 15 and 60 minutes after it has reached the torrefaction temperature. Figure 8-2 illustrates the processes that occur in the biomass, which assumes that the residence time is such that the biomass fully transforms into char.

Depending on the particle size and heating rate, both drying and devolatilization processes may occur simultaneously inside the particle and thus one could expect wet biomass, dry biomass and char at the same time. This is observed in case of large particles within which large temperature gradients are present, but for very small particles such gradients are unlikely, and in such cases only one of these phases can be found inside the particle.

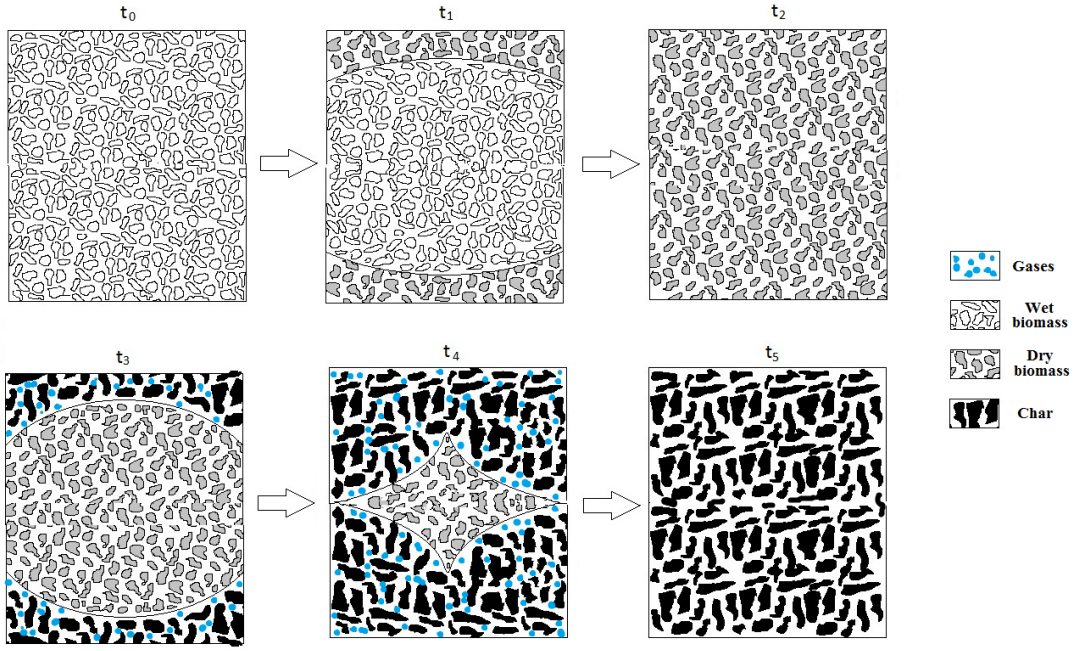


Figure 8-2. Sequence of torrefaction process. $t_0$ = start of the process from room temperature; $t_1$ = start of drying process; $t_2$ = end of drying process; $t_3$ = start of devolatilization process; $t_4$ = decomposition in the particle; $t_5$ = end of decomposition.

For each phase in Figure 8-2, mass and energy balances were developed in order to follow its generation/destruction in each time step during the torrefaction process. These balances are associated with kinetic model, which describes the decomposition and generation of each phase in the biomass. The kinetic model used follows that in reference [17] and is presented in Figure 8-3.

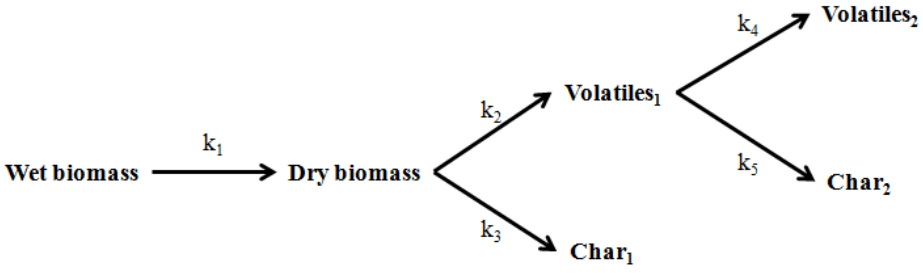


Figure 8-3. Kinetic model used in the biomass torrefaction model.

As shown in Figure 8-3, the torrefaction process includes a drying process. Here, the process starts with a wet biomass with low moisture content. Moisture is removed in the first drying step and a

completely dry biomass is obtained by reaction $k_1$. Once the temperature increases, biomass devolatilization starts through $k_2$ and $k_3$ reactions and produces condensable and non-condensable volatiles and a solid remnant.

At any point of time the biomass could contain varied amounts of the above four phases as shown in Figure 8-2. Simultaneous treatment of all four phases has not been recognized and treated in earlier models. No effort is made here for further subdivision of the dry biomass or char into individual polymeric constituents like hemicellulose, cellulose and lignin. We take an overall kinetic rate of breakdown of the dry biomass into char and volatiles as has been done by numerous pervious researchers [42,47–50].

This solid phase consists of a combination of unreacted biomass and biomass with different levels of decomposition. Although, the kinetic model does not differentiate between polymeric constituents, from experimental evidence found in the literature [23,51–53], it is possible to determine decomposition of which of the components is dominant during the process. At low temperature, the rate of hemicellulose decomposition is high, and it dominates throughout the torrefaction process. Only at high temperature, some cellulose and lignin also start decomposition but to a lesser extent. Secondary reactions are present after primary devolatilization through $k_4$ and $k_5$ where the produced condensable volatiles can react and form new solids and new volatiles.

In this model, $k_1$, $k_2$ and $k_3$ were obtained in a TGA operated under kinetic control conditions without secondary reactions. The values of $k_4$ and $k_5$ were obtained from experiments with coarse particles, and the results were fitted in the present kinetic model. In this kinetic model, biomass is considered to be made of organic and inorganic materials mainly because the kinetic values were obtained from the biomass without any kind of extraction. Catalytic effects in relation with ash or with some others compounds formed as acids, are captured in the values of the kinetic constants. In this way, final char is composed of organic material and inorganic material. The inorganic material is equal to that in the initial biomass because it remained unchanged throughout the process. Kinetic constants $k_1$, $k_2$, $k_3$, $k_4$ and $k_5$ are the generation/destruction rate of different phases shown in Figure 8-3, and are defined by the Arrhenius equation (eq. (8-1)).

$$k_i = A_i exp\left(-E_i/_{RT}\right) \tag{8-1}$$

The kinetic parameters for equation (8-1) are shown in the Table 8-1.

Table 8-1. Kinetic parameters [17].

| $k_i$ | $A_0(s^{-1})$ | $E_a(kJ/mol)$ |
|---|---|---|
| $k_1$ | 7.11 | 23.7 |
| $k_2$ | $1.45x10^{12}$ | 156 |
| $k_3$ | $6.58x10^{6}$ | 106.4 |
| $k_4$ | $6.17x10^{12}$ | 184 |
| $k_5$ | $4.69x10^{12}$ | 184 |

The activation energy for volatiles, $k_2$ is greater than that for char, $k_3$ indicating that the formation of volatiles is more susceptible to changes in temperature and therefore, at low temperatures the

char formation is higher than the volatile release. Equations for each phase are presented in the next section. This model includes wet biomass, dry biomass, volatiles (involving condensable and non-condensable gases generated in the primary and secondary devolatilization reactions), and char (which includes the solid formed in the primary and secondary reactions).

### *8.2.1. Mass balances*

Mass balance for each of the phases of the kinetic model as illustrated in Figure 8-3 is presented below. The methodology based on volume average was used like that by other workers [19,54] about volume average. Following Withaker [43] each phase balance equation is expressed as volume fraction into a differential element.

*Wet biomass*

The next balance is based on the initial amount of moisture in the biomass after being dried in atmospheric conditions. This drying process is modeled like a chemical process (Figure 8-3) through Arrhenius equation as is shown in equation (8-1). Moisture mass loss during the drying process in the biomass can be expressed as follows:

$$\frac{\partial m_w}{\partial t} = -\rho_w V_w k_1 \tag{8-2}$$

Where, $m$ represents the mass, $\rho$ the density, $V$ the volume and $k_1$ the reaction rate in the dry process. The subscript $w$ represents the water or moisture. To simplify the equation (8-2), a new parameter $\epsilon_i$ is defined, which relates the volume of the phase and initial solid volume as can be seen in the next equation:

$$\in_i = \frac{V_i}{V_p} \tag{8-3}$$

where, the subscript $i$ and $p$ represents the phases in the model and the original biomass particle respectively. The equation (8-2) may now be written as follows:

$$\rho_w \frac{\partial \in_w}{\partial t} = -\rho_w \in_w k_1 \tag{8-4}$$

This expression can give the water volumetric fraction in each time step, $t$. The evaporated water leaves the particle before the devolatilization process start and depends largely on particle size.

*Dry biomass*

Dry biomass resulting from the drying process is determined by the reaction rate $k_1$. This dried biomass then decomposes into volatiles (condensable and non-condensable gases) and solid char. Kinetic parameter $k_2$ governs the gases yield through the devolatilization process while $k_3$ determines the char formation. These reactions typically start at about 180°C. Mass balance of dry biomass is given by equation (8-5). The first term shows the rate of new dry biomass formation

through drying, and the second term shows the mass loss by decomposition reactions of the dried biomass.

$$\frac{\partial m_b}{\partial t} = \rho_w V_w k_1 - \rho_b V_b (k_2 + k_3) \tag{8-5}$$

where subscript *b* represents the dry biomass. Here $k_2$ *and* $k_3$ represents volatiles and primary char yield. Dry biomass is represented according to equation (8-3) by their volumetric fraction, and equation (8-5) becomes the following expression:

$$\rho_b \frac{\partial \in_b}{\partial t} = \rho_w \in_w k_1 - \rho_b \in_b (k_2 + k_3) \tag{8-6}$$

With the last equation, the volumetric fraction of biomass can be obtained in each zone of the particle. The density of the biomass is assumed constant, but total density of the solid is calculated by an average of all phases in each zone of the particle.

*Char*

Char is generated in the process by means of two reactions: from dry biomass by primary devolatilization, $k_3$, and from decomposition of volatiles by secondary reactions, $k_5$. The following balance can express the total char formation.

$$\frac{\partial m_c}{\partial t} = \rho_b V_b k_3 + \rho_v V_v k_5 \tag{8-7}$$

The subscripts *c* and *v* represent char and volatile respectively. Volumetric char fraction is expressed according to equation (8-3), and the equation (8-7) becomes the following expression:

$$\rho_c \frac{\partial \in_c}{\partial t} = \rho_b \in_b k_3 + \rho_v \in_v k_5 \tag{8-8}$$

Thus, the char volume fraction is obtained in each zone of the particle. Similar to the biomass phase, char density is considered constant, but total density of the solid is calculated by an average of all phases in each zone of the particle.

*Volatile*

As mentioned previously, the volatiles consist of moisture, condensable gases, and non-condensable gases. The main species for of these gases are water, acetic acid, formic acid, methanol, carbon dioxide and carbon monoxide. For simplicity, the volatile phase was studied and analyzed as a single species, and only one mass balance for the volatile phase was done. The volatiles released within the biomass travels at a finite speed, *v*, through the biomass pores. Only one species was considered (formed by the mixture of species mentioned). The flow of volatiles is through the pores created adjacent small particles. Only convection through the pores is considered in the transport equation. Following Bates et al. [55], the diffusive term is neglected here. Taking this into account the mass balance is written as:

$$\frac{\partial \in_v \rho_v}{\partial t} = -div\left(\in_v \rho_v \vec{v}_v\right) + \rho_w \in_w k_1 + \rho_b \in_b k_2 - \rho_g \in_g k_5 \tag{8-9}$$

where the subscript *v* represent the volatiles, and $\tilde{v}$ represents the velocity vector of gases inside of biomass. The sum of all volume fractions inside the particle must be unity. The volumetric fraction of volatiles in the biomass particle is expressed as follow:

$$\in_v = \frac{V_v}{V_p} = 1 - \in_w + \in_b + \in_c \tag{8-10}$$

This expression can be interpreted as solid porosity. Gas flow through pores generally follows Darcy's law. So, the velocity of gases in each axis of the biomass is modeled by Darcy Law, as follow:

$$v_x = -\frac{B_x}{\mu}\frac{\partial P}{\partial x} \qquad v_y = -\frac{B_y}{\mu}\frac{\partial P}{\partial y} \tag{8-11}$$

Where, *B* represents the biomass permeability, *P* the pressure and $\mu$ the viscosity. The subscripts *x* and *y* represent both dimensions used in the model. Biomass permeability in both directions is assumed different but constant. The gas phase is assumed with ideal gas behavior, and therefore can be described by ideal gas law.

### *8.2.2. Energy balances*

The amount of gas through fine pores is very small. We assume that the gas temperature reaches the solid temperature nearly instantaneously and it is possible assume that the gas and solid are in thermal equilibrium. Considering the above, a single equation is proposed for the solid.

$$\left(\in_b \rho_b c_{p_b} + \in_c \rho_c c_{p_c} + \in_v \rho_v c_{p_v}\right)\frac{\partial T}{\partial t} + div\left(\in_v \rho_v c_{p_v} \vec{v}_v T\right) = div\left(\lambda_{eff} \nabla T\right) + \dot{Q}_{reactions} \tag{8-12}$$

Where, $c_p$ represents the heat capacity, $\lambda_{eff}$ the solid effective thermal conductivity that depends on volumetric fractions (char, dry biomass and volatiles) and temperature. $Q_{reactions}$ represents the energy consumption/generation in the biomass due to drying and devolatilization reactions, as is shown in the next expression:

$$\dot{Q}_{reactions} = \sum_{i=1}^{5} \Delta H_{rxn_i} \rho_i \in_i k_i \tag{8-13}$$

Where, $\Delta H_{rxn}$ denote the enthalpy for each reaction in the kinetic model shown in the Figure 8-3.

### *8.2.3. Energy balance for gas (Nitrogen) outside the particle*

An energy balance for the external gas (nitrogen) which exchanges energy with biomass particles and internal walls of the kiln was developed. In a typical vertical torrefier, the inert gas enters from bottom, is heating through energy transfer with kiln walls and then exchanges energy with the biomass particle. Thus, the energy transfer between the particle surface and the external gas, change in longitudinal dimension.

The energy balance for this gas is as follows:

$$c_{p_{eg}} \rho_{eg} \frac{\partial T_{eg}}{\partial t} = -\frac{\partial}{\partial k}\left(c_{p_{eg}} \rho_{eg} v_{eg} T_{eg}\right) + \sum Q_{eg-\alpha} \tag{8-14}$$

Where, $Q$ represents the loss/gain energy in the gas, due to interactions with other systems. The subscripts $eg$ y $\alpha$ denote external gas and other systems (kiln walls and the biomass particle), respectively. $k$ denotes the axis for external gas.

To get around difficulty in getting reliable expressions for convection coefficients for the horizontal and vertical faces of the particle, we take help of CFD (Computational Fluid Dynamics) and calculate the energy transfer. To find the convective heat transfer in this area, the system shown in Figure 8-1 was simulated through FLUENT software. In this system, an external gas flow around the biomass particle is considered. The gas is pre-heated in the external surface of the kiln. In CFD simulation, reactions in the biomass were not considered, therefore, gases do not leave the particle. Correlations for the vertical and horizontal energy transfer coefficients were found and used in the global FORTRAN model. The CFD model was evaluated with a volumetric flow of nitrogen being 3 litre/min. The correlations found in CFD simulations are presented in equations (8-15) to (8-17).

$$h_y = 43.761\mathrm{y}^4 - 104.97\mathrm{y}^3 + 87.661\mathrm{y}^2 - 30.891\mathrm{y} + 5.5918 \tag{8-15}$$

$$h_{x_1} = 7.5975\mathrm{x}^2 - 7.2117\mathrm{x} + 5.0367 \tag{8-16}$$

$$h_{x_2} = 2.2039\mathrm{x}^2 - 2.3015\mathrm{x} + 0.8404 \tag{8-17}$$

Where, $h_y$, $h_{x1}$ and $h_{x2}$ stand for convective heat transfer coefficients in the vertical and horizontal surfaces of the particle respectively. $h_{x1}$ and $h_{x2}$ stands for the surfaces in bottom and top side respectively. For simplicity, the dimension $x$ and $y$ in correlations in equations (8-15) to (8-17) are dimensionless (between 0 and 1), where 1 is the maximum dimension in each axis from core of the particle. This values found in CFD simulations are concordant with results of Bates et al. [55]. Properties of all phases used in the model are shown in Table 8-2.

Table 8-2. Property values.

| Property | Value |
|---|---|
| $\rho_s$ | 250 kg/m$^3$ |
| $\rho_c$ | 200 kg/m$^3$ |
| $\rho_{eg}$ | 1.25 kg/m$^3$ |
| $c_{ps}$ | (1112.3 + 4.85*$T_{sol}$)/1000 kJ/kg K [57] |
| $c_{pc}$ | (1003.2 + 2.09*$T_{sol}$)/1000 kJ/kg K [57] |
| $c_{pg}$ | 1 kJ/kg K |
| $c_{peg}$ | 1 kJ/kg K |
| $k_s$ | (0.13 + 0.0003*$T_{sol}$)/1000 kW/mK [57] |
| $k_g$ | 2x10$^{-5}$ kW/mK |
| $k_c$ | (0.08 - 0.0001*$T_{sol}$)/1000 kW/mK [57] |
| $k_{eg}$ | 2x10$^{-5}$ kW/mK |
| $B_s$ | 4x10$^{-13}$ m$^2$ |
| $B_c$ | 1x10$^{-12}$ m$^2$ |
| $\mu$ | 2.75x10$^{-5}$ Pa s |

These properties are based on values found in literature. Total conductivity and heat capacity, are calculated based on temperature and volume fractions of each phase in the solid by means of an average value. In this work, the particle was considered isotropic, and properties in both directions were considered equal but changing with temperature and volumetric fractions of phases.

### *8.2.4. Initials and boundary conditions*

Biomass is heated primarily by the radiation from the kiln walls. A slight convective exchange occurs due to the nitrogen flowing over the particle. Initial conditions in the model for the biomass particle and external gas are shown in expression (8-18).

$$\left.\begin{aligned} &\epsilon_b = \epsilon_{b_0} \\ &\epsilon_w = \epsilon_{w_0} \\ &\epsilon_c = 0 \\ &\epsilon_v = 0 \\ &T_b = T_g = T_0 \\ &T_{ge} = T_{ge_0} \end{aligned}\right| ; t = 0 \qquad (8\text{-}18)$$

The boundary conditions for mass balances in both modeled axes (x and y) are shown in expressions (8-19) and (8-20).

$$\rho_v v_x|_{x=0, x=L} = h_m\left(\rho_{vs} - \rho_\infty\right) \qquad (8\text{-}19)$$

$$\rho_v v_y\Big|_{y=0,\,y=H} = h_m\left(\rho_{vs} - \rho_\infty\right) \tag{8-20}$$

Where, $h_m$ is the mass transfer coefficient, and the subscripts $s$ and $\infty$ represents the surface of the biomass particle and surroundings respectively. The density of the surrounding area is considered equal to the density of nitrogen. Density in surface of biomass is calculated with the mathematical function DZREAL from IMSL Fortran libraries. This function calculates the value of density that satisfies the mathematical expression.

The boundary conditions for energy balances are shown in expressions (8-21) to (8-23).

$$-\lambda_{eff}\frac{\partial T}{\partial y}\Big|_{y=H} = h_{x_2}\left(T_g - T_s\right) + \sigma\varepsilon\left(T_\infty^4 - T_s^4\right) \tag{8-21}$$

$$-\lambda_{eff}\frac{\partial T}{\partial y}\Big|_{y=0} = h_{x_1}\left(T_g - T_s\right) + \sigma\varepsilon\left(T_\infty^4 - T_s^4\right) \tag{8-22}$$

$$-\lambda_{eff}\frac{\partial T}{\partial x}\Big|_{x=0,x=L} = h_y\left(T_g - T_s\right) + \sigma\varepsilon\left(T_\infty^4 - T_s^4\right) \tag{8-23}$$

Where, $h$ represents the convective heat transfer coefficient, $\sigma$ the Boltzmann constant and $\varepsilon$ the emissivity. In the boundary condition (8-23), it is assumed that the thermal conditions in both vertical surfaces of the particle are equal. The surface temperatures are found with the DZREAL function of IMSL Fortran libraries.

The $k$ axis shown in Figure 8-1, is in the same direction as the $y$ axis, but they take different values because $k$ axis applies for the external gas and $y$ axis for the biomass particle. In order to distinguish both axis were named in different ways. Boundary condition for external gas is as follows:

$$-\lambda_{ge}\frac{\partial T_{ge}}{\partial k}\Big|_{k=0} = 0 \tag{8-24}$$

Where, $\lambda_{ge}$ represents the thermal conductivity of the nitrogen that flows around the biomass particle.

### *8.2.5. Model solution and Independence test*

In order to solve the partial differential equations system, a discretization by means of finite volumes in both dimensions was performed. The system was solved using FORTRAN program with the Gear method linked to DIVPAG subroutine, which in turn is linked with IMSL libraries of Visual Numerics. Tolerance for the Gear method was defined in $1x10^{-6}$ that indicate the difference between iterations for calculate and control the error. The time step for iterations was defined by the Courant number, which was set to 0.8 to ensure numerical stability.

A mesh independence study was performed in order to determine the optimum number of finite volumes that guarantee convergence with minimal computational time and minimal error. A

biomass particle with dimensions of 25mm in diameter and 153.4mm in length was used. The meshes used were from 30 to 60 finite volumes on each dimension of the particle (x and y).

Results in these test shows little differences in temperature between dense meshes, but noticeable difference in those less dense meshes. A mesh with 20 finite volumes can be used in this model because it guarantees the minimum computational time with a low error.

## 8.3. Experiments

Experiments were conducted in the Biomass conversion laboratory at Dalhousie University, Canada to measure the temperature change inside the biomass, and its mass loss during the course of torrefaction.

### *8.3.1. Biomass sample and methods*

Cylindrical poplar dowels, 152.4 mm long and 25.4 mm in diameter are used as large biomass samples. Proximate and ultimate analyses of the sample are shown elsewhere [17]. The experiments are conducted in a custom-designed thermo-gravimetric unit. It comprises a 42 mm diameter and 1.2 m long stainless steel tube that serves as a reactor. It is heated by a set of 2.4 kW annular electric heaters surrounding it with a capacity to heat it up to 900°C. The biomass sample is packed in a quartz wool matrix typically in a lump of 0.25 gm for fine biomass particles. It is kept in a perforated basket, which is suspended from the mass balance inside the reactor (Figure 8-4). For large biomass samples as in the present case the sample is directly attached to a fine thermocouple, which is attached to mass balance meter. The mass balance with least count of 0.1 mg records the mass of the biomass continuously to the computer.

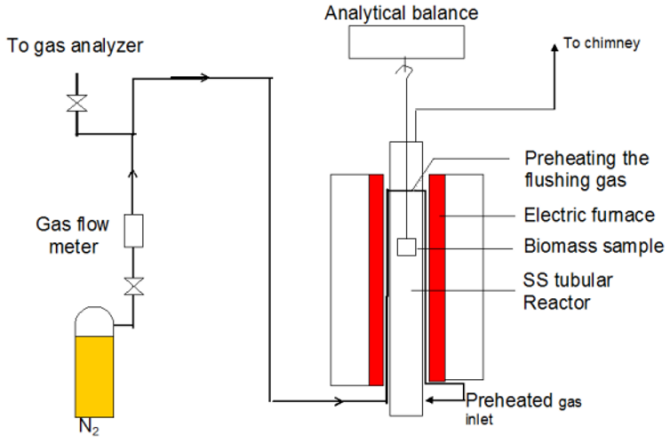


Figure 8-4. Schematic diagram of the experimental set-up

The unit is continuously flushed by Nitrogen at a flow rate of 3 lt/min. Before the gas is released at the bottom of the reactor, it is preheated through a tube coiling around the outside surface of the reactor but inside the heating furnace. A fine hole is drilled reaching down to the center in the biomass cylinder and a fine sheathed Chromel–Alumel thermocouple is inserted to measure its core or center point temperature. Another thermocouple is fixed at half the radial distance from the

centre. Both the thermocouples are plugged by iron-cement so as to ensure uniform reaction conditions. Output from this thermocouple is also logged in a computer.

Before starting the experiment, the reactor is preheated to the desired temperature for 30 minutes. Then the sample is lowered into the reactor and suspended from the bottom of the mass balance. The data logger in the computer continuously measures both mass and the temperatures. The reaction time (or residence time) is recorded once the biomass is loaded in the reactor. The mass loss data of the biomass stored in the computer is plotted and fed as an input to the model. Similarly, the wood cylinder is wrapped around by fine nichrome wires, acting as a cage, and is tied to a wire hanging from the balance. The sample is introduced into the reactor in presence of nitrogen gas flow. The mass-loss is monitored continuously at reactor temperature of 200-300$^0$C.

An important consideration was made in this work, the model despite being in Cartesian coordinates x and y, was validated with experimental tests applied on a particle in axisymmetric cylindrical coordinates. The particle was assumed in Cartesian coordinates of square cross section with each side of equal dimension to the diameter of the cylindrical particle. The geometrical differences mentioned may seem substantial, but by analyzing the ratio of surface areas which receive radiation is only 0.78. This means that the particle in cartesian coordinates has 20% more area for which can receive radiation. This fact can be analyzed in greater depth in a future work.

### *8.3.2. Model validation*

The model validation was performed by comparing the model results with the experimental data from experiments described above. The initial step of this validation process was a comparison of the core temperature of the particle when the particle is subjected to torrefaction at 240°C. A small difference between model and experimental setup was the particle geometry. In the model, particle was a rectangular parallelepiped, but in the experimental tests was a cylinder. This difference can contribute with small differences in validation procedure shown in Figure 8-5.

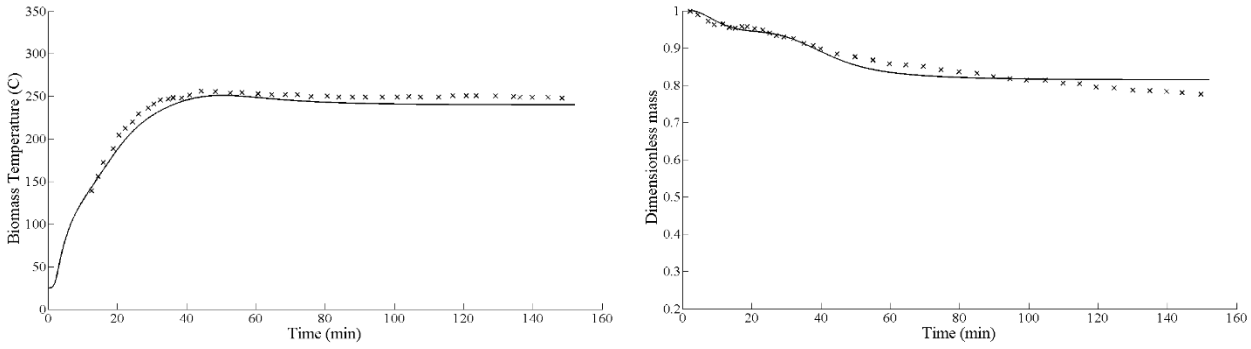


Figure 8-5. Model validation. Comparison of measured core temperature (a) and mass loss (b) of the particle with those predicted from the model for torrefaction at 240°C. Solid lines: Model results, (x): Experimental data from basu et al. [17]

Figure 8-5 shows an excellent agreement between time and core temperature and mass loss during drying and torrefaction process for theoretical and experimental data. Temperature increase in the

core of the particle was also detected in large number of other experiments conducted by Basu [17] and others [57,58]. This validation verified the essential correctness of the model in spite of some simplifying assumptions.

Additional simulations of the torrefaction process about core temperatures were also performed. In these tests, the maximum core temperature were extracted in order to compare with experimental data obtained in the work of Basu et al [59] and Stelt et al. [58], where particles of different sizes were torrefied at different temperatures. Comparison between simulation and experimental data is shown in Figure 8-6.

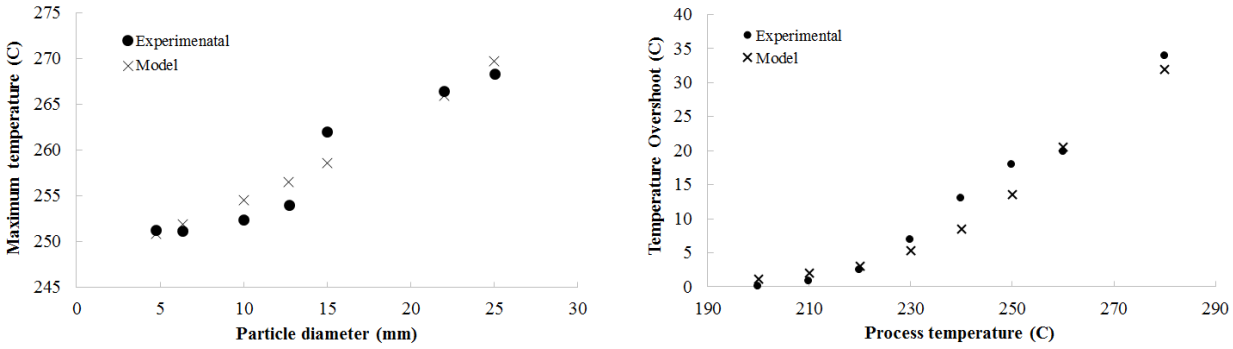


Figure 8-6. Model validation. Comparison of measured core temperatures for different particle diameter and 65 mm in length for 250°C (a). Experimental data from Basu et al. [59]. Comparison of kiln temperature with centerline temperature overshoot for a particle size of 28mm in diameter and 100mm in length (b). Experimental data from Stelt [58].

Figure 8-6(a) shows the agreement between model and experimental data. The temperature increases are until 30°C when the particle has a diameter of 25 mm. For small particles, the temperature increase is lower, about 1°C. The generated heat by exothermic reactions in big particles could not release from the particle resulting in higher core temperatures. For this reason, for a given kiln temperature, the rise in the core temperature was higher for larger diameter samples. This situation can promote non-homogeneous characteristics or properties in the torrefied biomass, becoming an important parameter to be controlled in the process. A similar performance was seen in Figure 8-6(b), but still maintaining the particle size and varying the temperature. When the kiln temperature increases, the temperature at the core of the particle also increases reaching values upto 35°C and at low kiln temperatures, increases only 2°C.

## 8.4. Simulation results

Simulations were performed with large particle with process temperatures in the range of 200 to 300°C. In addition to predicting the temperature, mass loss and internal pressure in the biomass particle, the model can also predict the yield/loss of each phase and the speed of the gas phase when is exits the particle. The model can predict both time resolved and space resolved changes in thermal properties and decomposition state in points of interest inside the particle. We can thus obtain spatial profiles of all properties in two dimensions using this model. Thus, the model can provide valuable information in optimizing the torrefaction process for a given geometry and

properties of the biomass. Results shown in next sections are the simulation results of experimental setup shown in Figure 8-4 for the same operational conditions.

### *8.4.1. Temperature inside the particle*

When studying torrefaction of a large a biomass particle the knowledge of temperature inside the particle is of vital importance as it affects both physical and chemical changes during the process. Chemical effects reflected in the re-polymerization, cross-linking and charring of secondary reaction generate increases in temperature due to the exothermic nature of these reactions of dehydration [60]. In turn, the physical effects for this particle sizes generate delay in thermal information to center of the particle causing that the central region be the last to achieve complete conversion. Model results for different temperatures between 200-300°C in the central point of the particle are presented in Figure 8-7 for a poplar cylinder of 25 mm diameter and 153.4 mm long.

Some authors [18,61–63] have founded this increase in core temperature in torrefaction tests in similar way as shown in Figure 8-7. As shown above, the kinetic model used in this work was a global model. It includes the combined effect of each of the polymeric components of the biomass (cellulose, hemicellulose and lignin). Thus, the analysis does not need to consider reactivity of each individual component. Some authors [51,52,57,64,65] have conducted experiments on torrefaction of cellulose, hemicellulose and lignin separately and tried to link all this information to a overall global model to elucidate the contribution of each component in the overall behavior of biomass. From these studies is possible conclude that this thermal over shooting in core particle is largely triggered by the first reactions of decomposition of hemicellulose, and to a lesser extent, by some dehydration reactions of the biomass. As the torrefaction temperature increases, these dehydration reactions are more significant and thereby increasing the temperature over-shoot higher [60].

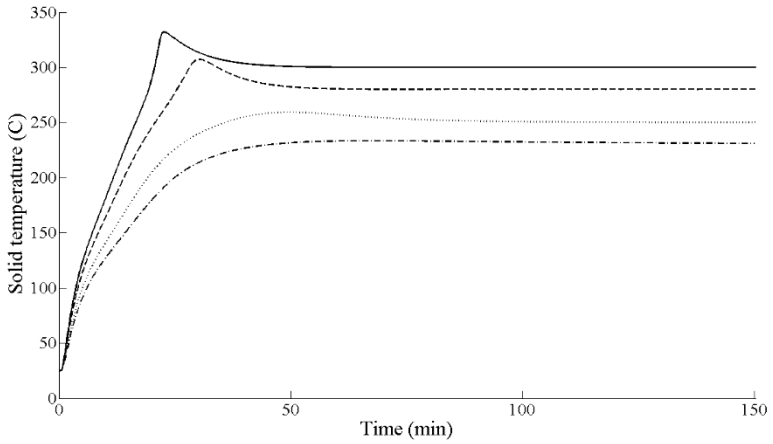


Figure 8-7. Temperature in the central point of the particle for a particle size of 25mm diameter and 153.4mm length. Dashed-dotted line: 230C; Dotted line: 250C; Dashed line: 280C; Solid line: 300C.

As said before, the particle is heated by radiative heat transfer from the furnace outside at the same time that could lose heat by side surfaces due to the nitrogen gas sweeping over the biomass particle. In this way, heating is similar in all surfaces of the particle.

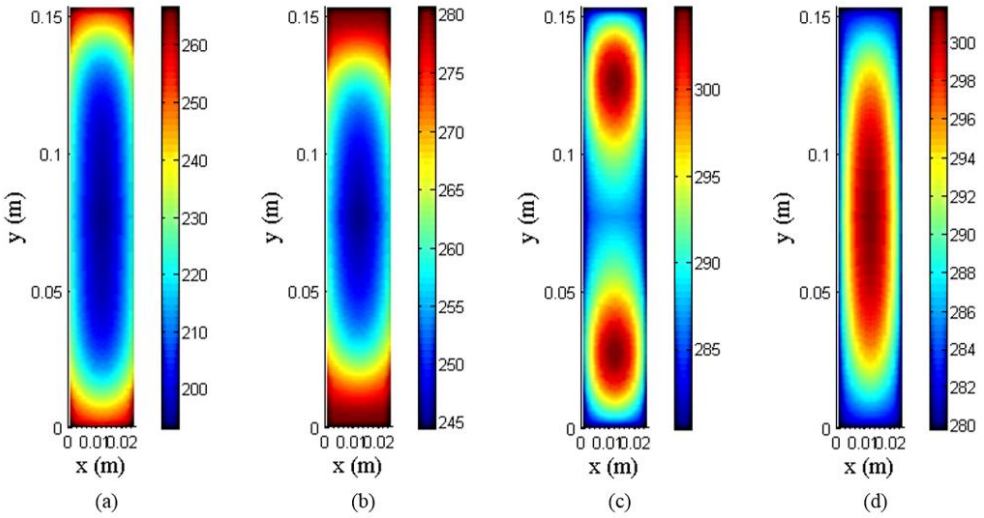


Figure 8-8. Temperature distribution inside the particle for different times in the process at 280°C for a particle size of 25mm in diameter and 153.4mm length. 13 min (a); 20 min (b); 26 min (c); 33 min (d)..

Figure 8-8 shows temperature contours for a particle size of 25 mm in diameter and 153.4mm in length. This figure also shows the thermal gradient between surface and core or central position of about 60°C in Figure 8-8(a) and about 35 °C in Figure 8-8(b). A curious behavior can be seen in Figure 8-8(c). The lower and upper ends of the simulated particle undergo a temperature increase above its temperature in the central part. During heating of the particle, their ends are heated more quickly than their core, because they receive heat from horizontal surface and two vertical surfaces. This rapid heating of the ends of the particle causes the secondary reactions of the kinetic scheme shown in Figure 8-3 to continue. These secondary reactions generate energy in its entire volume due to exothermic reaction. The temperature is higher in the two halves of the sample (bottom and top half portion) as consequence of exothermic reactions and the symmetry in boundary conditions for x-axis. Finally, the heat is dissipated to the central part of the sample where the secondary reactions are initiated and the temperature increases above the rest of the particle as is shown in Figure 8-8(d). Due to the exothermic reactions of mechanism biomass decomposition, core temperature is increased about 10°C in all process above kiln temperature. In this case, is difficult obtain a homogeneous torrefied biomass, because maximum temperatures in each side of the particle are different.

### *8.4.2. Volumetric fractions and mass of phases*

The model gives the volumetric fractions of each component in different positions within the particle during the torrefaction process. Through this 2D model it is possible to determine the areas where each phase and specially the final char are located in biomass structure. Using this information it is possible to analyze the conditions that favored the primary and secondary char yield on biomass particle.

The model developed here is based on volume fractions of each phase and Figure 8-9 shows production/decomposition history of each phase during torrefaction. During initial step, until around of 10 minutes, drying occurs in the particle and devolatilization is just starting inside

particle with a low gas production. When the decomposition temperature for the particle (around 190°C for hemicellulose) is reached, competing formation of char and volatile starts. According to values of the kinetic parameters shown in Table 8-1, low temperatures favor char formation rather than gases, but higher temperatures favor gas formation. In the Figure 8-9 one can see the variation in volume fraction inside particle in time. In this figure one can note that at all times the sum of these fractions is unity. Because of latter, mass lost caused by the escape of gases generated during the drying and devolatilization is not evidenced in Figure 8-9.

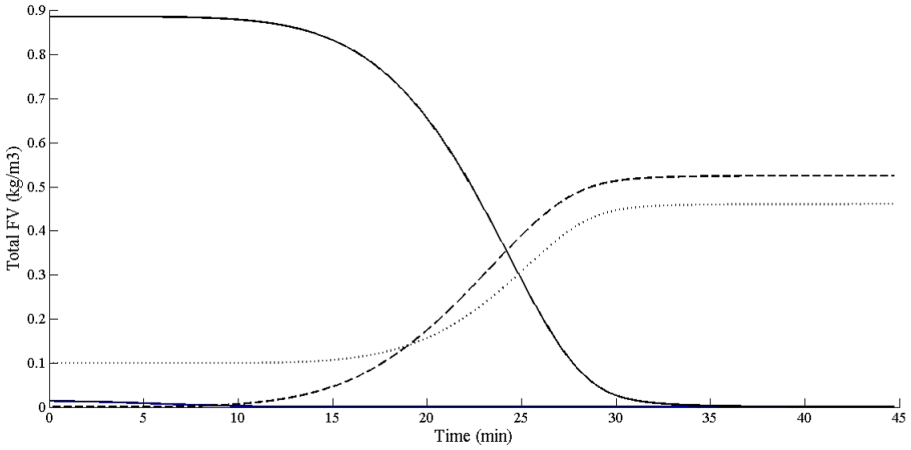


Figure 8-9. Products yield inside the particle at 280°C for a particle size of 25mm in diameter and 153.4mm length. Solid line: FV Biomass; dashed line: FV char; dotted line: FV gases; blue solid line; FV Water.

Figure 8-10 shows the iso-contours of volumetric fraction of char in heating process. In this figure, one can note that the greatest amount of char is formed in the corners because in this places, due to fast heating, the char is formed quickly and permits the contact with gases that are leaving from the particle and secondary reactions take place. (see Figure 8-8).

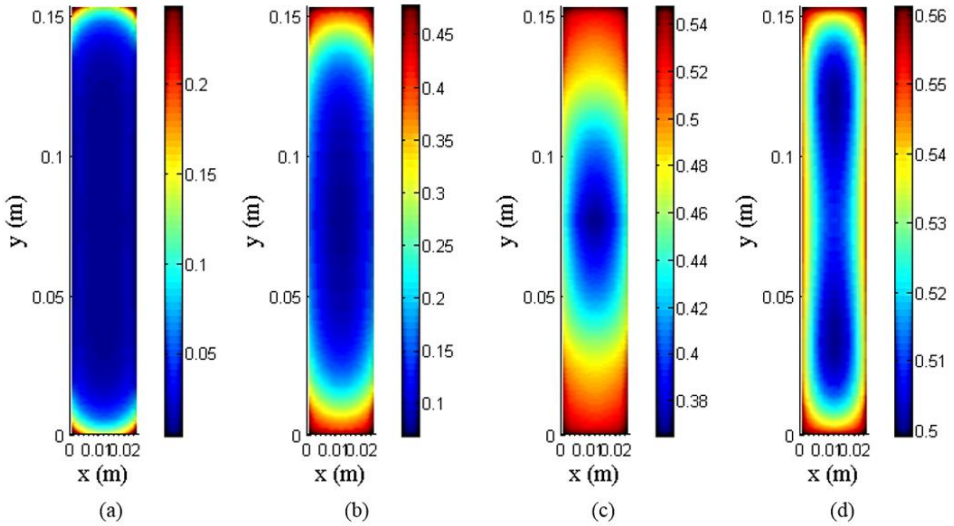


Figure 8-10. Distribution of volumetric fraction of char inside the particle for different times in the process to 280°C for a particle size of 25mm in diameter and 153.4mm length. 13 min (a); 20 min (b); 26 min (c); 33 min (d).

According to the work of Medic et al. [4], for a required conversion the initial amount of water in the biomass particle has an important effect on the residence time and temperature for the torrefaction process. Figure 8-9 shows that for 280°C and a particle size of 25mmx153.4mm, from 35 minutes, biomass not lose more mass.

### *8.4.3. Internal pressure*

The present model can predict the internal pressures developed during drying and devolatilization processes in the biomass particles as a function of the temperature. This is done through incorporation of the equation of state for gases or volatiles generated. The pressures reached during these two processes depend on the heating rate at which the biomass is subjected to. At low heating rate, in the initial stage of drying, water evaporation is slow, allowing time for the generated steam to leave of the particle. This naturally involves marginal increase in pressure. It typically happens during the devolatilization stage, when volatiles produced find ways to the particle exterior without any major increase in pressure.

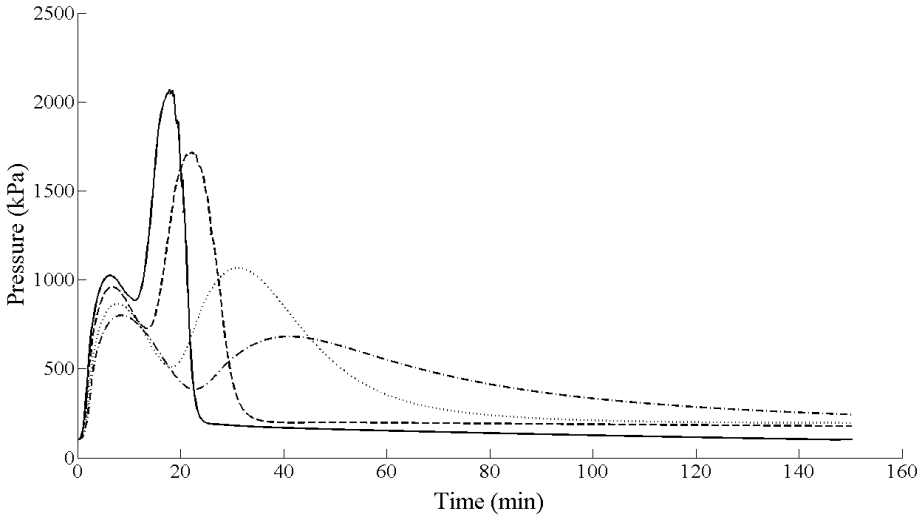


Figure 8-11. Internal pressure during torrefaction for a particle size of 25mm in diameter and 153.4mm length. Dotted-dashed line: 230°C; Dotted line: 250°C; Dashed line; 280°C; Solid line: 300°C

Opposite case occurs when the heating rate is high, the volatiles are released faster than they can exit from the biomass interior. Therefore, the internal pressure increases in the biomass particle. In some extreme cases the high pressure may even causes particle breakdown or fragmentation. Maximum level of pressure is reached when process temperature is high because a higher amount of volatiles are produced (see Figure 8-11). In the case of low temperatures, heating in the center of the particle is slower than that for higher temperatures and gas flow from the center of particle is slower, having lowest velocity than that for highest temperatures. This value of internal pressure is dependent on biomass properties like permeability and its size. For example, larger particles will have higher internal pressure.

Information on the internal pressure of the material is important because it could help predict if there is a fracture or not in the material. It is also important because, as was found by Wannapeera

et al. [66], pressure has an effect on the formation of char in the torrefaction process, because an increase in internal pressure of 1 MPa to 4 MPa produces an increase in char forming up to 50%.

### *8.4.4. Gas velocity (speed)*

The velocity of volatiles in biomass pores can be predicted with this model and, in addition, the model predicts the gas speed at each point of the particle. These speeds can be calculated by incorporating the Darcy law in the model. The speed of gas through the biomass interior depends on the properties of biomass such as permeability and porosity and the heating rate. The model prediction shows that when particle properties remain constant, but its size is increased, the gas velocity is higher due to higher pressures at its core where the devolatilization process starts. Same situation is observed when particle dimensions are constants but process temperatures is varied between 200 and 300 °C. Highest velocities are reached when the peak pressure is reached due to gas release from the center of the particle.

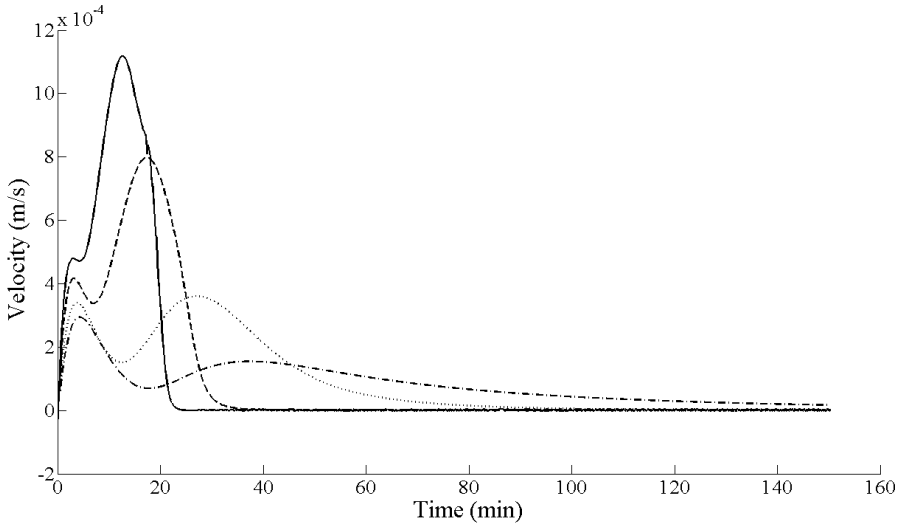


Figure 8-12. Velocities inside the particle for different temperatures for a particle size of 25mm in diameter and 153.4mm length. Dotted-dashed line: 230°C; Dotted line: 250°C; Dashed line; 280°C; Solid line: 300°C

Figure 8-12 shows the velocity of the gas phase during the process when the torrefaction temperature is varied. Clearly, when the process temperature is low, decomposition of the material is low, which creates low pressure in the particle resulting in low speeds of the gas. This is consistent with Figure 8-11. When the temperature is increased, the generation of volatiles in the biomass is higher which increases the internal pressure. This increased pressure causes faster release of gas and shows the maximum speed of the gas phase in accordance with the maximum internal pressure in the biomass. At this time a rapid release of volatiles generated in the center of the particle occurs. Volatiles come out of the particle through paths which offer less resistance. Since the properties of the solid were assumed constant in both directions (isotropic particle), volatiles come out equally by the vertical and horizontal surfaces of the particle.

This information about gas velocity is very important because, as some authors found in their works, low gas velocities means longer residence times, and secondary reactions like cross-linking

and dehydration reactions can be happen over intermediates compounds and increase the char formation [67,68].

### *8.4.5. Particle size*

The impact of particle size on the internal pressure and total conversion of biomass for a residence time of 60 minutes was evaluated. The residence time did not include the time of drying and heating of the particle. The material properties were kept same for all particle sizes evaluated. This analysis was carried out for temperatures of 220, 250, 280 and 300 °C and particle sizes of 1.0, 5.0, 10, 20, 50 and 100 mm in diameter and 153.4mm in length in order to determine the maximum pressure and conversion of the particle when operational conditions in the torrefaction process vary. In Figure 8-13 the maximum pressures of the particle are presented.

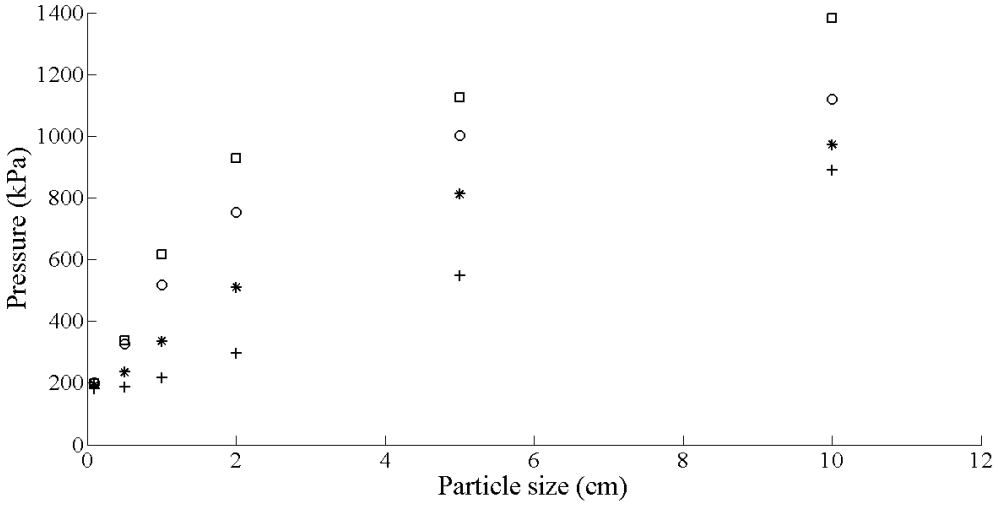


Figure 8-13. Maximum pressure for different sizes particles and temperatures. (+): 220°C; (*): 250°C; (o): 280°C; (□): 300°C.

Figure 8-13 also shows that the maximum internal pressure of the particles increase as a function of the process temperature and their size. This increase of pressure inside the particle can promote the secondary reactions and the formation of char, but in turn can break or destroy the material if they exceed the limits of their strength.

One of the author (Basu et al. [59]) experimentally measured biomass conversion to torrefied mass for a range of particle size and torrefaction temperature. They noted that as the diameter of a cylindrical biomass sample of fixed length increased the mass yield decreased, but when the biomass length increased for a fixed diameter the mass yield increased. The mass yield decreases with torrefaction temperature, and they found a close correlation between core temperature and mass yield. Larger diameter cylinder showed higher core temperature and lower mass yield. This being an interesting effect, an effort is made here to explore if the present model can simulate these experimental observations.

The present model can give the maximum conversion achieved for each particle size and at each evaluated temperature. Figure 8-14 shows that the conversion increases with torrefaction

temperature. This increase is more marked for smaller particles where 30% conversion is obtained at 220°C and 78% at 300 °C which is shows that conversion is tripled. For large particles, the increase is not as pronounced because it is 19% at 220 °C until 53% at 300 °C. An interesting effect is found when small particles are treated at high temperatures. The difference in maximum conversion in this temperatures is low; small changes in conversion are obtained for temperatures of 280 °C and 300 °C because conversions of 72% and 78% respectively were obtained. The same applies to large particles but at lower temperatures; small changes are achieved when going from 220 °C to 250 °C reaching conversions of 19% and 23% respectively.

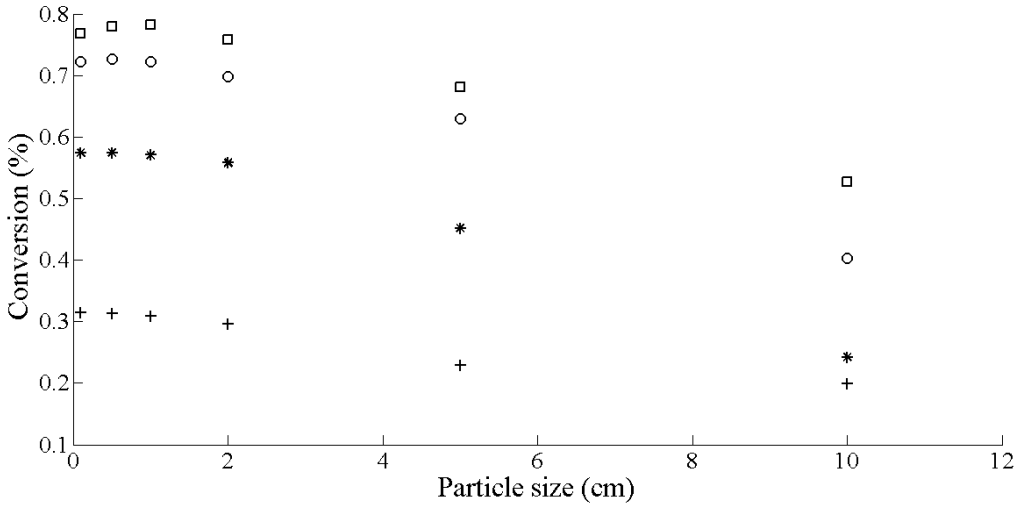


Figure 8-14. Biomass conversions in torrefaction process. (+): 220°C; (*): 250°C; (o): 280°C; (□): 300°C.

With particle size of 10 cm a small difference in maximum conversion it is possible to obtain for evaluated temperatures (around 30%). This could indicate that working with particles bigger than 10 cm require large residence times to achieve complete conversion of the material, which in practice would make the process unworkable.

## 8.5. Conclusions

A transient 2D model was developed to analyze the torrefaction process in biomass particles. This model predicts the temperature, composition of each component, overall conversion of biomass, internal pressure and speed of the gas phase within the particle. This model showed good agreement with experimental data and successfully simulated effects of secondary reactions within the particle noted by experimentally observed temperature rise in the center of it.

The effect of particle size and temperature on torrefaction was successfully predicted by the model. Biomass conversion was found to be a function of particle size. At a given residence time lower conversions are obtained when the particle size increases due to slower heat conduction into the particle.

With this present 2D model, it is possible to obtain the optimum values of temperature and residence time for maximum conversion of biomass for any particle size. This analysis also shows

that there is an optimal particle size to promote char formation without having large residence times.

**Acknowledgments**

The authors wish to thank the Colombian Administrative Department of Science, Technology and Innovation (COLCIENCIAS) (Departamento Administrativo de Ciencia, Tecnología e Innovacion) for financial support.

D.A. Granados would like to thank COLCIENCIAS for the Ph.D scholarship.

**References**

[1] Basu P. Biomass Gasification, Pyrolysis and Torrefaction: Practical Design and Theory. 2013.

[2] Pentananunt R, Rahman ANMM, Bhattacharya SC. Upgrading of biomass by means of torrefaction. Energy 1990;15:1175–9. doi:10.1016/0360-5442(90)90109-F.

[3] Wattananoi W, Khumsak O, Worasuwannarak N. Upgrading of biomass by torrefaction and densification process. 2011 IEEE Conf Clean Energy Technol 2011:209–12. doi:10.1109/CET.2011.6041465.

[4] Medic D, Darr M, Shah a., Potter B, Zimmerman J. Effects of torrefaction process parameters on biomass feedstock upgrading. Fuel 2012;91:147–54. doi:10.1016/j.fuel.2011.07.019.

[5] Bourgois J, Guyonnet R. Characterization and analysis of torrefied wood. Wood Sci Technol 1988;22:143–55. doi:10.1007/BF00355850.

[6] Li J, Brzdekiewicz A, Yang W, Blasiak W. Co-firing based on biomass torrefaction in a pulverized coal boiler with aim of 100% fuel switching. Appl Energy 2012;99:344–54. doi:10.1016/j.apenergy.2012.05.046.

[7] Fisher EM, Dupont C, Darvell LI, Commandré J-M, Saddawi a, Jones JM, et al. Combustion and gasification characteristics of chars from raw and torrefied biomass. Bioresour Technol 2012;119:157–65. doi:10.1016/j.biortech.2012.05.109.

[8] Broström M, Nordin A, Pommer L, Branca C, Di Blasi C. Influence of torrefaction on the devolatilization and oxidation kinetics of wood. J Anal Appl Pyrolysis 2012;96:100–9. doi:10.1016/j.jaap.2012.03.011.

[9] Berrueco C, Recari J, Güell BM, Alamo G Del. Pressurized gasification of torrefied woody biomass in a lab scale fluidized bed. Energy 2014;70:68–78. doi:10.1016/j.energy.2014.03.087.

[10] Deng J, Wang G, Kuang J, Zhang Y, Luo Y. Pretreatment of agricultural residues for co-gasification via torrefaction. J Anal Appl Pyrolysis 2009;86:331–7. doi:10.1016/j.jaap.2009.08.006.

[11] Hassan E, Steele P, Ingram L. Characterization of fast pyrolysis bio-oils produced from pretreated pine wood. Appl Biochem Biotechnol 2009;154:182–92. doi:10.1007/s12010-008-8445-3.

[12] Zheng A, Zhao Z, Chang S, Huang Z, Wang X, He F, et al. Effect of torrefaction on structure and fast pyrolysis behavior of corncobs. Bioresour Technol 2013;128:370–7. doi:10.1016/j.biortech.2012.10.067.

[13] Granados DA, Velásquez HI, Chejne F. Energetic and exergetic evaluation of residual biomass in a torrefaction process. Energy 2014;74:181–9. doi:10.1016/j.energy.2014.05.046.

[14] Ratte J, Fardet E, Mateos D, Héry J-S. Mathematical modelling of a continuous biomass torrefaction reactor: TORSPYD$^{TM}$ column. Biomass and Bioenergy 2011;35:3481–95. doi:10.1016/j.biombioe.2011.04.045.

[15] Bates RB, Ghoniem AF. Biomass torrefaction: modeling of volatile and solid product evolution kinetics. Bioresour Technol 2012;124:460–9. doi:10.1016/j.biortech.2012.07.018.

[16] Felfli FF, Luengo CA, Suárez JA, Beatón PA. Wood briquette torrefaction. Energy Sustain Dev 2005;9:19–22. doi:10.1016/S0973-0826(08)60519-0.

[17] Basu P, Sadhukhan AK, Gupta P, Rao S, Dhungana A, Acharya B. An experimental and theoretical investigation on torrefaction of a large wet wood particle. Bioresour Technol 2014;159:215–22. doi:10.1016/j.biortech.2014.02.105.

[18] Perré P, Rémond R, Turner I. A comprehensive dual-scale wood torrefaction model: Application to the analysis of thermal run-away in industrial heat treatment processes. Int J Heat Mass Transf 2013;64:838–49. doi:10.1016/j.ijheatmasstransfer.2013.03.066.

[19] Ratte J, Marias F, Vaxelaire J, Bernada P. Mathematical modelling of slow pyrolysis of a particle of treated wood waste. J Hazard Mater 2009;170:1023–40. doi:10.1016/j.jhazmat.2009.05.077.

[20] Di Blasi C. Modeling chemical and physical processes of wood and biomass pyrolysis. Prog Energy Combust Sci 2008;34:47–90. doi:10.1016/j.pecs.2006.12.001.

[21] Bradbury AGW, Sakai Y, Shafizadeh F. A kinetic model for Pyrolysis of Cellulose. J Appl Polym Sci 1979;23:3271–80. doi:10.1002/app.1979.070231112.

[22] Di Blasi C, Lanzetta M. Intrinsic kinetics of isothermal xylan degradation in inert atmosphere. J Anal Appl Pyrolysis 1997;40-41:287–303. doi:10.1016/S0165-2370(97)00028-4.

[23] Prins MJ, Ptasinski KJ, Janssen FJJ. Torrefaction of wood. Part 1. Weight loss kinetics. J Anal Appl Pyrolysis 2006;77:28–34. doi:10.1016/j.jaap.2006.01.002.

[24] Chen W-H, Kuo P-C. Torrefaction and co-torrefaction characterization of hemicellulose, cellulose and lignin as well as torrefaction of some basic constituents in biomass. Energy 2011;36:803–11. doi:10.1016/j.energy.2010.12.036.

[25] Rousset P, Turner I, Donnot A, Perré P. Choix d'un modèle de pyrolyse ménagée du bois à l'échelle de la microparticule en vue de la modélisation macroscopique. Ann For Sci 2006;63:213–29. doi:10.1051/forest.

[26] Di Blasi C. Heat, Momentum and Mass Transport Through a Shrinking Biomass Particle Exposed to Thermal Radiation. Chem Eng Sci 1996;51:1121–32.

[27] Antal J. Mathematical modelling of biomass pyrolysis phenomena. Fuel 1985;64:1483–6.

[28] Chan WC., Kelbon M, Krieger BB. Modelling and experimental verification of physical and chemical processes during pyrolysis of a large biomass particle. Fuel 1985;64:1505–13.

[29] Koufopanos C., Papayannakos N, Maschio G, Lucchesi A. Modelling of the pyrolysis of biomass particles. Studies on kinetics, thermal and heat transfer effects. Can J Chem Eng 1991;69:907–15. doi:10.1002/cjce.5450690413.

[30] Mousquès P, Dirion J, Grouset D. Modeling of solid particles pyrolysis. J Anal Appl Pyrolysis 2001;59:733–45.

[31] Park WC, Atreya A, Baum HR. Experimental and theoretical investigation of heat and mass transfer processes during wood pyrolysis. Combust Flame 2010;157:481–94. doi:10.1016/j.combustflame.2009.10.006.

[32] Dufour A, Ouartassi B, Bounaceur R, Zoulalian A. Modelling intra-particle phenomena of biomass pyrolysis. Chem Eng Res Des 2011;89:2136–46. doi:10.1016/j.cherd.2011.01.005.

[33] Peters B. Validation of a numerical approach to model pyrolysis of biomass and assessment of kinetic data. Fuel 2011;90:2301–14. doi:10.1016/j.fuel.2011.02.003.

[34] Haseli Y, van Oijen J a., de Goey LPH. Modeling biomass particle pyrolysis with temperature-dependent heat of reactions. J Anal Appl Pyrolysis 2011;90:140–54. doi:10.1016/j.jaap.2010.11.006.

[35] Lam KL, Oyedun AO, Hui CW. Experimental and Modelling Studies of Biomass Pyrolysis. Chinese J Chem Eng 2012;20:543–50. doi:10.1016/S1004-9541(11)60217-6.

[36] Mehrabian R, Scharler R, Obernberger I. Effects of pyrolysis conditions on the heating rate in biomass particles and applicability of TGA kinetic parameters in particle thermal conversion modelling. Fuel 2012;93:567–75. doi:10.1016/j.fuel.2011.09.054.

[37] Blasi C Di. Physico-chemical processes occurring inside a degrading two-dimensional anisotropic porous medium. Int J Heat Mass Transf 1998;41:4139–50. doi:10.1016/S0017-9310(98)00142-2.

[38] Di Blasi C. Numerical Simulation of Cellulose Pyrolysis. Biomass and Bioenergy 1994;7:87–98.

[39] Di Blasi C. Kinetic and Heat Transfer Control in the Slow and Flash Pyrolysis of Solids. Ind Eng Chem Res 1996;35:37–46. doi:10.1021/ie950243d.

[40] Di Blasi C. Influences of model assumptions on the predictions of cellulose pyrolysis in the heat transfer controlled regime. Fuel 1996;75:58–66. doi:10.1016/0016-2361(95)00203-0.

[41] Felfli F, Luengo C, Soler P, Rocha J. Mathematical modelling of wood and briquettes torrefaction. Procedings 5th Encontro Energ. no Meio Rural, Campinas: 2004, p. 1–9.

[42] Shafizadeh F, Chin PPS. Thermal Deterioration of Wood. ACS Symp. Ser., Washington: 1977, p. 57–81.

[43] Withaker S. Simultaneous heat, mass and momentum transfer in porous media. A theory of drying porous media. Adv Heat Transf 1977;13:119–203.

[44] Turner I, Rousset P, Rémond R, Perré P. An experimental and theoretical investigation of the thermal treatment of wood (Fagus sylvatica L.) in the range 200–260°C. Int J Heat Mass Transf 2010;53:715–25. doi:10.1016/j.ijheatmasstransfer.2009.10.020.

[45] Perré P, Turner I. A 3-D version of TransPore: a comprehensive heat and mass transfer computational model for simulating the drying of porous media. Int J Heat Mass Transf 1999;42:4501–21.

[46] Pétrissans a., Younsi R, Chaouch M, Gérardin P, Pétrissans M. Experimental and numerical analysis of wood thermodegradation. J Therm Anal Calorim 2011;109:907–14. doi:10.1007/s10973-011-1805-1.

[47] Di Blasi C, Branca C. Kinetics of Primary Product Formation from Wood Pyrolysis. Ind Eng Chem Res 2001;40:5547–56. doi:10.1021/ie000997e.

[48] Rogers F., Ohlemiller T. Cellulosic Insulation Material I. Overall Degradation Kinetics and Reaction Heats. Combust Sci Technol 1980;24:129–37.

[49] Thurner F, Mann U. Kinetic Investigation of Wood Pyrolysis. Ind Eng Chem Process Des Dev 1981;20:482–8.

[50] Ward SM, Braslaw J. Experimental weight loss kinetics of wood pyrolysis under vacuum. Combust Flame 1985;61:261–9. doi:10.1016/0010-2180(85)90107-5.

[51] Chen W-H, Kuo P-C. Isothermal torrefaction kinetics of hemicellulose, cellulose, lignin and xylan using thermogravimetric analysis. Energy 2011;36:6451–60. doi:10.1016/j.energy.2011.09.022.

[52] Varhegyi G, Antal J, Szekely T, Szabo P. Kinetics of the thermal decomposition of cellulose, hemicellulose, and sugarcane bagasse. Energy & Fuels 1989;3:329–35.

[53] Peng J, Bi XT, Lim J, Sokhansanj S. Development of Torrefaction Kinetics for British Columbia Softwoods. Int J Chem React Eng 2012;10. doi:10.1515/1542-6580.2878.

[54] Marias F, Santacreu SD. Modelling of pyrolysis in a high capacity thermo balance. Can J Chem Eng 2015;93:261–75. doi:10.1002/cjce.22084.

[55] Bates RB, Ghoniem AF. Modeling kinetics-transport interactions during biomass torrefaction: The effects of temperature, particle size, and moisture content. Fuel 2014;137:216–29. doi:10.1016/j.fuel.2014.07.047.

[56] Nowak W, Stachel A. Convective Heat Transfer in Air Flow Around a Cylinder at Low Reynolds Numbers. J Eng Phys Thermophys 2005;78:1214–21.

[57] Corbetta M, Frassoldati A, Bennadji H, Smith K, Serapiglia MJ, Gauthier G, et al. Pyrolysis of centimeter-scale woody biomass particles: Kinetic modeling and experimental validation. Energy and Fuels 2014;28:3884–98. doi:10.1021/ef500525v.

[58] Stelt MJC Van Der. Chemistry and reaction kinetics of biowaste torrefaction. 2010. doi:978-90-386-2435-8.

[59] Basu P, Rao S, Dhungana A. An investigation into the effect of biomass particle size on its torrefaction. Can J Chem Eng 2013;91:466–74. doi:10.1002/cjce.21710.

[60] Milosavljevic I, Oja V, Suuberg EM. Thermal Effects in Cellulose Pyrolysis: Relationship to Char Formation Processes. Ind Eng Chem Res 1996;35:653–62. doi:10.1021/ie950438l.

[61] Yang H, Yan R, Chen H, Lee DH, Zheng C. Characteristics of hemicellulose, cellulose and lignin pyrolysis. Fuel 2007;86:1781–8. doi:10.1016/j.fuel.2006.12.013.

[62] Pierre F, Almeida G, Brito J, Perré P. Influence of torrefaction on some chemical and energy properties of maritime pine and pedunculate oak. Bioresources 2011;6:1204–18.

[63] Bates RB, Ghoniem AF. Biomass torrefaction: Modeling of reaction thermochemistry. Bioresour Technol 2013;134:331–40. doi:10.1016/j.biortech.2013.01.158.

[64] Corbetta M, Pierucci S, Ranzi E, Bennadji H, Fisher EM. Multistep Kinetic Model of Biomass Pyrolysis. XXXVI Meet. Ital. Sect. Combust. Inst., 2013, p. 4–9.

[65] Ranzi E, Cuoci A, Faravelli T, Frassoldati A, Migliavacca G, Pierucci S, et al. Chemical Kinetics of Biomass Pyrolysis. Energy & Fuels 2008;22:4292–300.

[66] Wannapeera J, Worasuwannarak N. Upgrading of woody biomass by torrefaction under pressure. J Anal Appl Pyrolysis 2012;96:173–80. doi:10.1016/j.jaap.2012.04.002.

[67] Wang Z, McDonald AG, Westerhof RJM, Kersten SR a, Cuba-Torres CM, Ha S, et al. Effect of cellulose crystallinity on the formation of a liquid intermediate and on product distribution during pyrolysis. J Anal Appl Pyrolysis 2013;100:56–66. doi:10.1016/j.jaap.2012.11.017.

[68] Pelaez-Samaniego MR, Yadama V, Garcia-Perez M, Lowell E, McDonald AG. Effect of temperature during wood torrefaction on the formation of lignin liquid intermediates. J Anal Appl Pyrolysis 2014;109:222–33. doi:10.1016/j.jaap.2014.06.008.

# Chapter 9. Conclusions

Torrefaction process was evaluated for two different biomasses such as sugarcane bagasse and poplar wood. The torrefaction process was performed in different equipment in order to obtain different information for the process. Some conclusions found in this research work are those numbered below.

1. A methodology was developed for evaluation and selection of a biomass in a torrefaction process. This methodology was based on mass, energy, and exergy balance to the torrefaction process and evaluation of exergetic efficiencies as a biomass selection tool with better behavior in the process.
2. Tests for sugarcane bagasse in TGA were developed to perform an experimental verification of the kinetic control condition and then obtaining kinetics for the material. In these tests, a methodology was proposed by varying the bed height and particle sizes to find the optimum ones for obtain the kinetic control condition and to be able to reliably obtain the kinetics of the material during the torrefactin process.
3. A thermogravimetric reactor was designed and built, which records continuously mass and temperature of a sample during torrefaction process. This reactor conducts the yielded volatiles to a condensing unit which is maintained at -12 ° C with capacity to condense most of condensable volatiles. Through this reactor, it is possible to characterize of all yielded products (gas, liquid and solid) and to obtain great information of the material decomposition during torrefaction.
4. The QWM reactor (Quartz Wool Matrix), belonging to the biomass conversion laboratory of the Dalhousie University in Canada, was used to carry out studies on poplar wood kinetics and its char combustion reactivity produced from torrefaction and pyrolysis. With this reactor it is possible to follow the temperature and mass for all process. These tests were performed with particle sizes of 0.5mm in diameter.
5. Tests in a two-step rotary reactor were performed with particles of 0.5mm diameter of poplar wood. In this reactor, the material is dried in the first stage of the process and then is torrefied in the second stage. The yielded volatiles in the second stage of the process do not contain moisture from initial biomass, so they can be easily used in a recirculation process or as an energy source in low energy processes. This reactor was continuously operated until the stabilization, and then, material temperatures and sampling from inside of reactor were developed in order to capture the chemical and structural changes of the biomass during the process.
6. Two transient phenomenological models for particle (2D) and rotary reactor (1D) were constructed in this research to simulate the torrefaction process of a biomass. The reactor model reproduces well the torrefaction of poplar wood particles in a two-stage rotary reactor. This model is able to predict global decomposition and some properties such as HHV and fixed carbon of the material. In addition, according to the selected kinetic model, can predicts the char and volatile production profiles in the reactor and temperature profiles of the material throughout the process. The 2D particle model is able to simulate the torrefaction of a biomass particle of any size. This model predicts char and volatiles yields. In addition, can predict

HHV, volatile output velocities and internal pressures. Due to the 2D character of the model, the X-Y profiles for each parameter can be obtained in any plane of the particle. Both models were succesfully validated.

## 9.1. Future works

1. To investigate secondary reactions in big particles through yielded liquid phases from polymers and heterogeneous reactions inside particle.
2. To investigate the effect of the biomass torrefaction process on the performance of subsequent processes such as gasification, pyrolysis, combustion, and pelletization.
3. Re-validate the 2D particle model with experimental tests from the built thermogravimetric reactor, simulating the behavior of different sizes of particles subjected to torrefaction.
4. Include to the particle model (2D) the kinetics for the yielded gaseous species during devolatilization with experimental data obtained with built thermogravimetric reactor and expressions for particle breakage.
5. Improve the rotary reactor (1D) model implementing gas recirculation in the second stage of the process.
6. To study the reactivity of torrefied sugarcane bagasse with different particle sizes.

# Appendix

**Appendix A. (Chapter 3, 4, 6)**

A.1. Particle sizes for kinetic control test

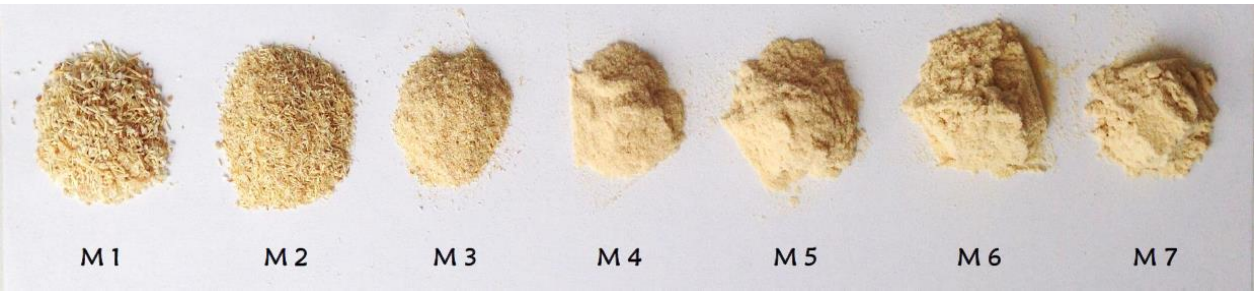


| Sample | Retained | Passing | Particles size (mm) |
|---|---|---|---|
| M1 | | 35 | 0.5 |
| M2 | 35 | 45 | 0.5 - 0.35 |
| M3 | 45 | 170 | 0.35 - 0.09 |
| M4 | 170 | 200 | 0.09 - 0.075 |
| M5 | 200 | 230 | 0.075 - 0.063 |
| M6 | 230 | 270 | 0.063 - 0.053 |
| M7 | 270 | 400 | 0.053 - 0.038 |

A2. Bed height for kinetic control tests

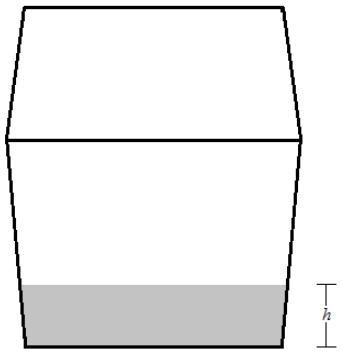


| Bed height (mm) | | |
|---|---|---|
| $h_1$ | $h_2$ | $h_3$ |
| 2 | 3.5 | 5 |

Appendix

A3. Torrefied biomass in kinetic control test

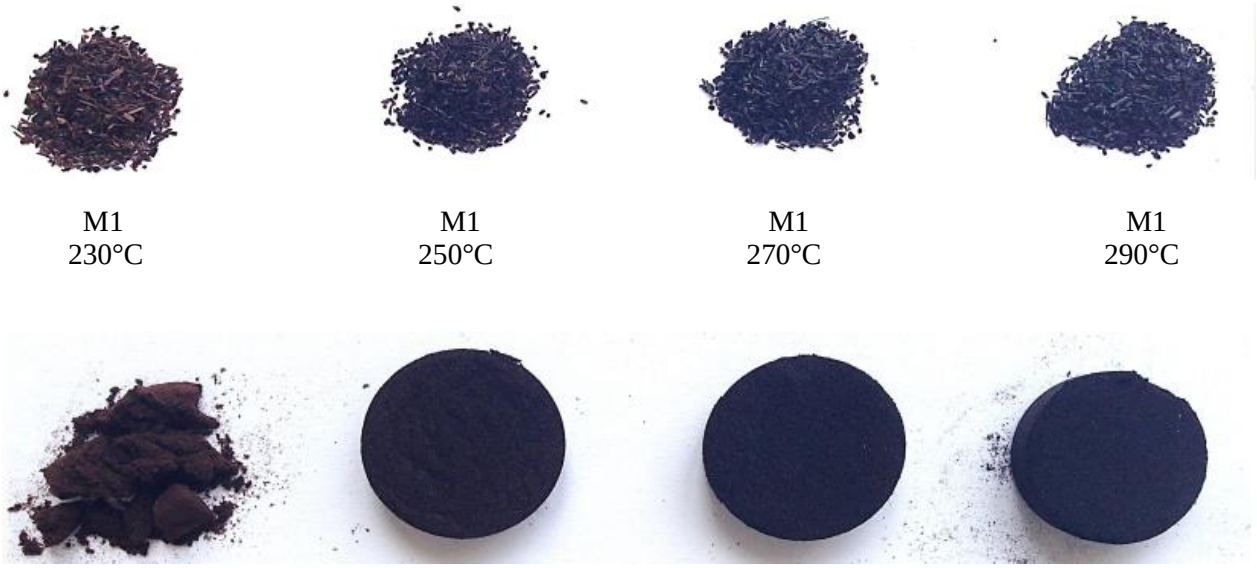

M1 230°C | M1 250°C | M1 270°C | M1 290°C

M7 230°C | M7 250°C | M7 270°C | M7 290°C

A4. Experimental validation for bed heights in torrefied biomass used in kinetic control test

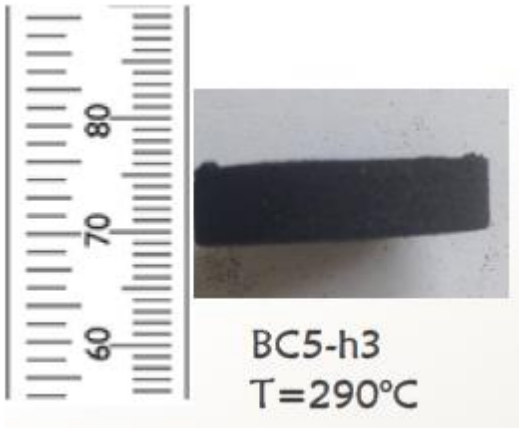


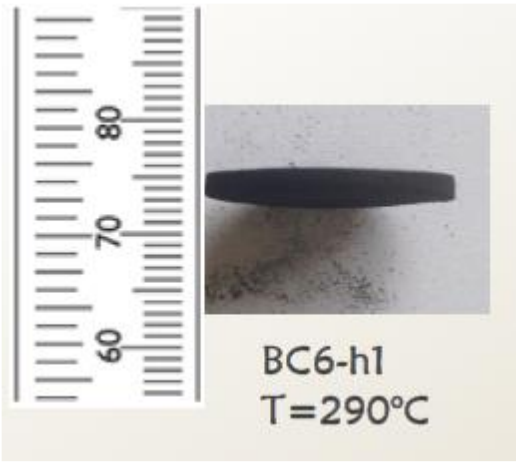

A5. Experimental results for kinetic control test (a), and theoretical Py'and Biot numbers for kinetic control.

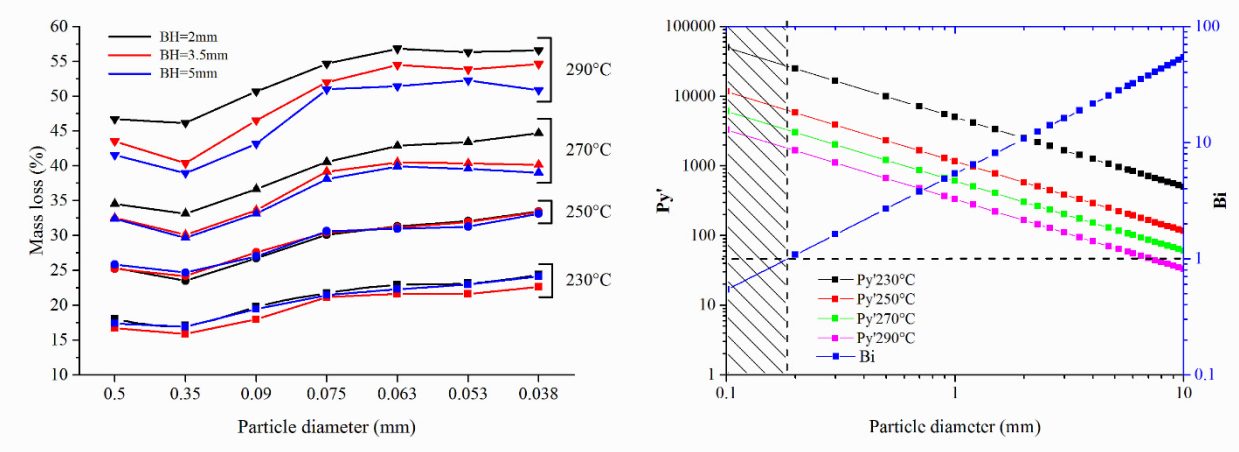


(a) (b)

## Appendix B. (Chapter 4)

B1. QWM reactor

**Appendix C. (Chapter 5)**

C1. Experimental setup for volatiles condensation in a two-stage rotary torrefier and condensates.


C2. Designed scooper and collected samples insode rotary torrefier.

C3. Designed scooper and collected samples insode rotary torrefier.

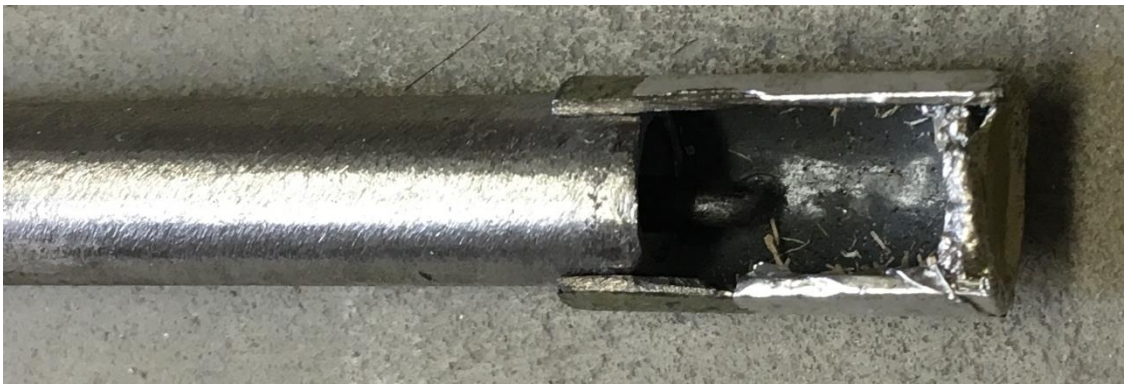

**Appendix D. (Chapter 6)**

D1. Material sizes used for building big particles (F, G, BG).

D2. Mesh for esperimental test, particle built with fine material and torrefied parrticle.

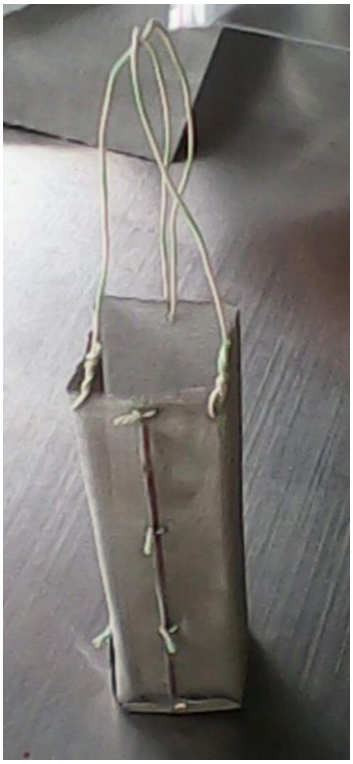

D3. Torrefied particles built with all materials.

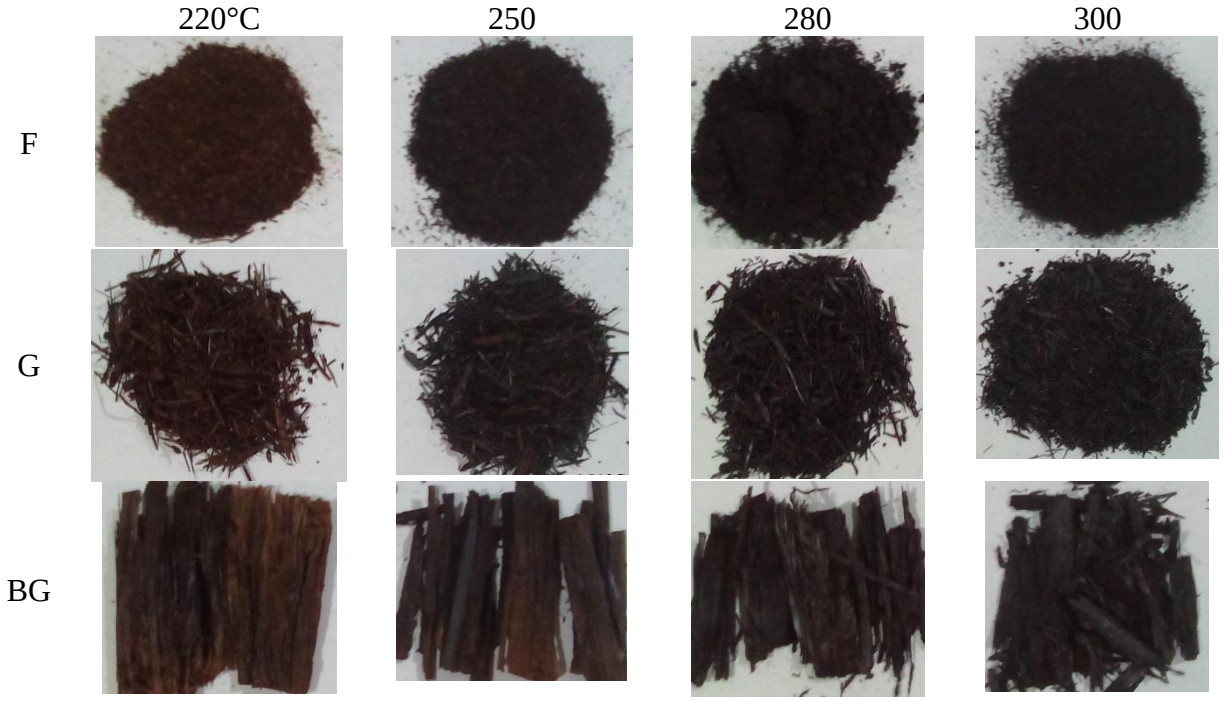

D4. Condensated volatiles in all tests

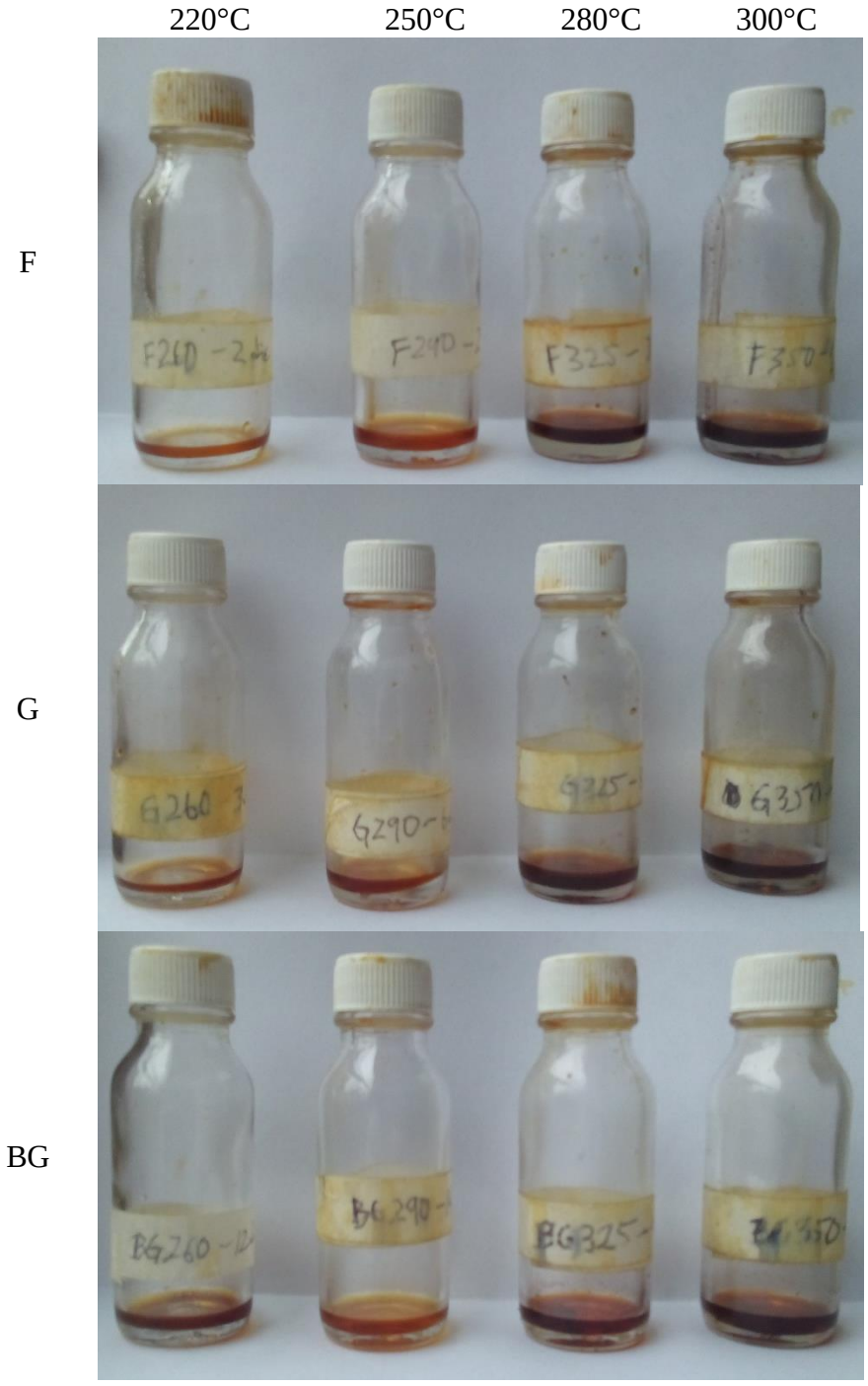

## Appendix E. Equipments photographs

E1. Bomb Calorimeter: Parr 6100


E2. SRI 8610C Gas Chromatograph

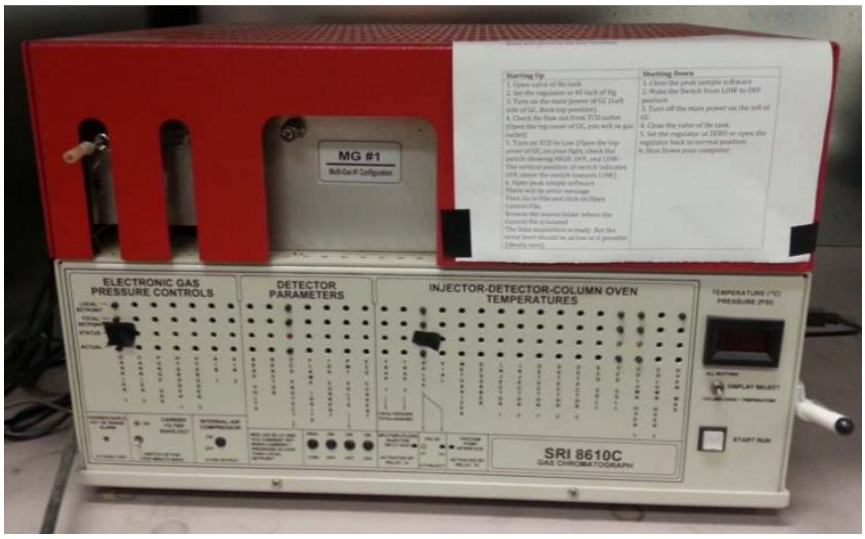

E3. Muffle furnace


E4. Two-step rotary reactor